UNIVERSITA' DEGLI STUDI DI
SASSARI
FACOLTA' DI AGRARIA

Dottorato di Ricerca in Agrometeorologia ed Ecofisiologia dei Sistemi Agrari e Forestali
XX Ciclo

EVALUATION OF THE "ADVANCED CANOPY-ATMOSPHERE-SOIL ALGORITHM" (ACASA) MODEL PERFORMANCE USING MICROMETEOROLOGICAL TECHNIQUES

Coordinatore:
Chiar.mo Prof. Pietro Deidda

Docenti Guida:
Prof.ssa Donatella Spano
Dr. Pierpaolo Duce

Dottorando:
Dott.ssa Serena Marras

Anno Accademico 2006-2007

A mia madre

con immenso affetto

"Nulla di grande si può compiere senza entusiasmo"

- R. Schumann

INDEX

ABSTRACT

In recent years, climate change and global warming are important topics. By adopting the Kyoto Protocol, each country committed to reduce anthropogenic gas emissions by 5% by the end of 2010. Conference participants agreed that the addition of carbon dioxide to the atmosphere by fossil fuel emissions, the removal of carbon dioxide by crops and natural ecosystems, and the effect of deforestation on carbon balance require future monitoring. This research was conducted as part of that effort.

Prentice et al. (2000) reported that atmospheric CO_2 concentration was about 280 part per million (ppm) in the pre-industrial era and increased at a rate of about 1.5 ppm per year (IPCC, 2001) to near 380 ppm in 2006. These increases will have an effect on natural and agricultural ecosystems that can alter their distribution and functionality.

Because the interaction and dynamic between ecosystems and atmosphere affect the global carbon cycle, there is the need to understand and quantify ecosystems capacity to absorb atmospheric carbon for planning long-term political action and sustainable development. The standard micrometeorological technique for estimating energy and CO_2 flux is the *Eddy Covariance* (EC) method used in the global monitoring network (FLUXNET). This research project used EC measurements to monitor sensible heat (*H*), latent heat (*LE*), soil heat (*G*), and CO_2 fluxes in two different ecosystems: a natural ecosystem (Mediterranean maquis) and an agricultural ecosystem (wine grape vineyard).

Although FLUXNET is widespread and provides useful information, most of the Earth's land surface is not monitored due to high costs and labour requirements. Consequently, models are sometimes used to quantify energy and mass fluxes on micro and regional scales. Several models are used to study ecosystem functioning and its response to environmental characteristics. Lagrangian, K-Theory, and Higher-Order Closure models are the most common. Models of the first two categories are not able to estimate the local turbulent transport within the canopy, while it is possible with higher-order closure models. Therefore, for this research we used one of the more elaborate higher-order

closure models for flux modelling: the Advanced Canopy-Atmosphere-Soil Algorithm (ACASA) model. The model predicts vegetation conditions and changes with time due to plant responses to environmental variables. The ACASA model divides the atmosphere into 20 layers with ten above and ten layers within the canopy. The soil is partitioned into fifteen layers of variable thickness.

ACASA model flux outputs were compared with field measurements from three consecutive years (2004-2006) over Mediterranean maquis in Northwestern Sardinia, and for two different seven-day periods (2005) and about one month (2006) over a wine grape vineyard in Tuscany, near Montalcino, Italy.

Flux exchanges between the vegetation and atmosphere and the factors affecting fluxes (e.g., air temperature and available water) were studied. In addition, seasonal and annual carbon balances were calculated to evaluate if the ecosystem acted as a carbon *sink* or *source*. The analysis showed that both maquis and grapevine acted as a carbon *sink*.

ACASA simulations were compared with measured fluxes of net radiation (*Rn*), sensible heat (*H*), latent heat (*LE*), soil heat (*G*), and CO_2 fluxes. Comparisons between simulated and measured values were evaluated using linear regression, the root mean squared error (RMSE), mean absolute error (RA), and mean bias error (MBE). In general, the model output matched well the observations. The use of ACASA model to predict energy and mass fluxes between the vegetation and atmosphere is promising. After some refinements to the input parameters and model code, the ACASA model could greatly improve our ability to estimate fluxes for use in carbon balance studies.

RIASSUNTO

Negli ultimi anni il dibattito sui cambiamenti climatici e sul riscaldamento globale ha assunto un'importanza crescente. Con l'adozione del Protocollo di Kyoto le nazioni firmatarie si sono impegnate a ridurre le emissioni di gas serra del 5% entro il 2010. Le perdite di anidride carbonica, a causa delle emissioni di combustibile fossile, della rimozione di CO_2 da colture agrarie e da ecosistemi naturali, e gli effetti della deforestazione sul bilancio del carbonio, richiedono un costante e futuro monitoraggio. Questa ricerca è stata condotta come parte di questo impegno.

Prentice et al. (2000) hanno riportato che la concentrazione atmosferica di CO_2 era circa 280 parti per milione (ppm) nell'era pre-industriale ed è aumentata a quasi 380 ppm nel 2006, con un tasso di circa 1.5 ppm per anno (IPCC, 2001). Questi cambiamenti climatici avranno chiaramente effetti sugli ecosistemi, naturali e agricoli, alterando la loro distribuzione e funzionalità. Siccome le interazioni tra gli ecosistemi e l'atmosfera influenzano il ciclo del carbonio, c'è la necessità di capire e quantificare la capacità degli ecosistemi nell'assorbire carbonio atmosferico, in modo da pianificare azioni politiche e attività sostenibili a lungo termine.

La tecnica micrometerologica standard, usata in tutte le reti di monitoraggio nazionali e internazionali (riunite nella rete globale FLUXNET) è *l'Eddy Covariance* (EC). Questo progetto di ricerca ha utilizzato la tecnica EC per monitorare i flussi di calore sensibile (*H*), calore latente (*LE*), calore del suolo (*G*), quantità di moto, e flusso di CO_2, in due ecosistemi differenti: un ecosistema naturale (macchia mediterranea) e uno agricolo (vigneto). I dati sono stati raccolti per tre anni consecutivi (2004-2006) sulla macchia mediterranea nella Sardegna Nord-Occidentale e durante due campagne sperimentali di misura di circa sette giorni ciascuna nel 2005 e di una campagna di misura di circa un mese (2006) nell'ecosistema vigneto in Toscana, vicino a Montalcino, Italia.

Oltre alla quantificazione degli scambi di energia e materia tra la vegetazione e l'atmosfera, l'analisi di questa ricerca si è concentrata anche sullo studio dei principali fattori che influenzano la dinamica di questi flussi (ad es.

temperatura dell'aria e acqua disponibile) e sul calcolo del bilancio stagionale e annuale di carbonio, in modo da valutare il comportamento da *sink* o *source* degli ecosistemi in esame. L'analisi ha evidenziato che sia la macchia mediterranea sia il vigneto hanno agito da *sink* nei confronti del carbonio durante i periodi di misura.

Sebbene FLUXNET è ampiamente diffusa e fornisce utili informazioni, la maggior parte della superficie terrestre non è monitorata. Perciò, per quantificare i flussi, vengono utilizzati anche dei modelli. Diversi modelli sono utilizzati per studiare la funzionalità degli ecosistemi e la loro risposta alle condizioni ambientali. I modelli possono essere di diversi tipi: Lagrangiani, K-Theory, e Higher-Order Closure. I modelli delle prime due categorie non riescono a stimare il trasporto turbolento locale che avviene dentro la canopy, mentre ciò è possibile con i modelli higher-order closure. Per questa ricerca, quindi, è stato utilizzato uno dei più sofisticati modelli higher order closure: il modello Advanced Canopy-Atmosphere-Soil Algorithm (ACASA), che fornisce flussi sia a scala regionale che più piccola. Il modello ACASA è stato utilizzato in questa ricerca per simulare i flussi sia sull'ecosistema a macchia mediterranea sia su vigneto. Il modello è anche in grado di stimare le condizioni della vegetazione e i cambiamenti nel tempo dovuti alle risposte delle piante alle variabili ambientali. ACASA utilizza equazioni differenziali di terzo ordine per stimare i flussi di calore, vapore e quantità di moto dentro e sopra la canopy. In particolare, il modello separa il dominio della canopy in 20 strati atmosferici (10 dentro la canopy e 10 sopra). Il suolo è, invece, suddiviso in 15 strati di profondità variabile nell'ordine di pochi cm ciascuno.

I risultati delle simulazioni sono stati confrontati con i dati dei flussi di radiazione netta (*Rn*), calore sensibile (*H*), calore latente (*LE*), calore nel suolo (*G*), e flusso di CO_2 misurati direttamente in campo. L'accuratezza del modello è stata valutata attraverso l'analisi statistica. In particolare, sono state calcolate le equazioni delle rette di regressione tra valori simulati e osservati e le differenze sono risultate significative alla probabilità del 99%. Alcuni indici statistici sono stati calcolati quali il root mean squared error (RMSE), l'errore assoluto medio (RA) e il mean bias error (MBE). In generale, il modello è in accordo con i dati

osservati. L'utilizzo del modello ACASA per la previsione dei flussi di energia e di massa tra la vegetazione e l'atmosfera è risultato promettente. Dopo l'apporto di qualche modifica nei parametri di input e nel codice del modello, il modello ACASA potrà migliorare grandemente la nostra abilità nello stimare i flussi negli studi sul bilancio del carbonio.

INTRODUCTION

In recent years, climate change and global warming are important topics. The United Nations Conference on Environment and Development (UNCED) took place in Rio de Janeiro in 1992, and interest in these topics increased. Since that conference, Earth's "global warming" and "greenhouse effect", on a global scale, have become a priority for research and action to reduce the anthropogenic impact. The conference led to several directives that were designed to reduce climate change by limiting greenhouse gas emission, planning for sustainable land use, and prevention of environment damage.

In 1997, national governments of several countries agreed to adopt the Kyoto Protocol to the United Nation Framework Convention on Climate Change as a legally binding framework to reduce emissions of greenhouse gases (GHG). By adopting the Kyoto Protocol, each country committed to reduce anthropogenic gas emissions by 5% by the end of 2010. Conference participants agreed that losses of carbon dioxide by fossil fuel emissions and deforestation require future monitoring.

Prentice et al. (2000) reported that atmospheric CO_2 concentration was about 280 part per million (ppm) in the pre-industrial era and increased at a rate of about 1.5 ppm per year (IPCC, 2001) to near 380 ppm today (IPCC, 2006). Global mean CO_2 levels are expected to continue rising to somewhere between 600 and 1000 ppm by 2100 (Friedlingstein et al., 2003; Fung et al., 2005). Because CO_2 is a long waveband radiation absorbing greenhouse gas, a direct effect of increased atmospheric CO_2 is a warmer climate (Manabe and Wetherald, 1975). The global average surface temperature, in fact, has increased by 0.6°C and the predictions for future warming over the period 1990-2100 range between 1.4-5.8°C (IPCC, 2001).

These increases will have an effect on natural and agricultural ecosystems that can alter their distribution and functionality. Ecosystems are, in fact, both carbon *sources* and *sinks*. They are a *sink* when they absorb more CO_2 through the photosynthesis than they respire, and they are a *source* when more CO_2 is released through respiration than is absorbed by photosynthesis. In some cases, ecosystems are temporary *sinks* for absorption of fossil fuel emissions, but they can also be *sources* depending on hydrologic and weather conditions. Therefore, carbon

exchanges between vegetation and atmosphere are a key component for prediction of global climate change, and there is a need to better understand the exchange mechanisms.

Because the interaction and dynamics between ecosystems and atmosphere affect the global carbon cycle, there is a need to understand and quantify the ecosystems' capacity to absorb atmospheric carbon for planning long-term political action and sustainable development. Micrometeorological techniques offer a means to obtain long-term measurements of energy (e.g., sensible heat), CO_2 and other trace gases, and mass (water vapour) exchanges between the vegetation and atmosphere. Continuous measurement of these fluxes provide direct information on the CO_2 exchange between the atmosphere and vegetation (Baldocchi, 2003) and on net ecosystem production. Therefore, CO_2 flux information is essential to understand how human activities impact on atmospheric CO_2 concentration through fossil fuel emissions and deforestation.

In recent decades, various extensive international projects to monitor energy and mass fluxes over a range of ecosystems and climates (e.g., CARBOEUROFLUX, AMERIFLUX, ASIAFLUX, FLUXNET-CANADA and CARBOEUROPE) were established. Together, these projects form a global network of micrometeorological measurements called FLUXNET (Baldocchi et al., 2001). The networks all use the *Eddy Covariance* (EC) method to measure carbon and energy fluxes. The research presented in this thesis used data from a CARBOEUROPE station, which was located in a natural Mediterranean maquis site in north-western Sardinia. In addition, data from a grape vineyard in north-central Italy were collected using EC technique to study both energy and mass fluxes from an agricultural site.

EC technique is explained in more detail in the following chapters. Most of the micrometeorological literature discussed measurements taken over forest, and few papers showed energy and mass exchanges between agricultural crops and the atmosphere. Therefore, fluxes were measured over a commercial grape vineyard to investigate exchanges over an agricultural crop.

Data from grape vineyard were collected within a national project "PRIN: *"Ecophysiological, healthful and molecular studies for the qualitative*

valorization and the environmental protection, in viticultural systems" funded by the "Ministry of Education, University and Research" in collaboration with other Italian Universities. Data were collected during the summer for two consecutive years.

Energy and mass fluxes from Mediterranean maquis ecosystems are rarely studied, so this research is one of the first attempts to quantify and understand fluxes from this important ecosystem. The CARBOEUROPE project is, therefore, important to understand and quantify the present terrestrial carbon balance of Europe and the associated uncertainty at local, regional and continental scale. The goals of the project are to (1) determine the European carbon balance with its spatial and temporal patterns, (2) understand the controlling processes and mechanisms of carbon cycling in European ecosystems, (3) know how these are affected by climate change and human management, and (4) develop an observation system to detect changes in atmospheric CO_2 concentrations and ecosystem carbon stocks related to the European commitments under the Kyoto Protocol.

Although FLUXNET is widespread and provides useful information, most of the Earth's land surface is not monitored due to high costs and labour requirements. Consequently, models are sometimes used to quantify energy and mass fluxes on micro- and regional scales. One of the more elaborate models for flux modelling is the Advanced Canopy-Atmosphere-Soil Algorithm (ACASA) model (Pyles et al., 2000b), which provides micro-scale as well as regional-scale fluxes when imbedded in a meso-scale meteorological model (e.g., MM5 or WRF). In this thesis, the ACASA model flux outputs are compared with field measurements over Mediterranean maquis and grape vineyard. The model predicts vegetation conditions and changes with time due to plant responses to environment variables. ACASA model separates canopy domain into twenty atmospheric layers. The atmosphere is divided into ten layers within the canopy and ten layers above the canopy. The soil is partitioned into fifteen layers of variable thickness. Model results were compared with EC flux data to evaluate ACASA accuracy and sensitivity.

1. ECOSYSTEMS MONITORING

1.1 Concepts

Odum (1959) defined an ecosystem as "any area of nature that includes living organisms and non-living substances that interact to produce an exchange of materials between the living and non-living parts." Thus, all living organisms in an ecosystem interact among themselves within the environment in which they live (i.e., soil, climate, water, and light), and an ecosystem involves a complex set of relationships between the living organisms (e.g., plants, animals, fish, birds, micro-organisms, water, soil, and people) and the habitat of an area.

An ecosystem does not have precise boundaries, and it can be as small as a pond or a dead tree or as large as the Earth itself. Ecosystem boundaries can be natural (e.g., based on vegetation) or established by man. An ecosystem can also be defined in terms of its vegetation, animal species, or type of relief. Ecosystems vary in size and in components, where each part is functioning unit of nature. Everything that lives in an ecosystem is dependent on the other species and components that are part of that ecological community. If one part of ecosystem is damaged or disappears, it has an impact on what remains. These interactions between organisms lead to changes in the abiotic environment and the organisms through functional processes.

All ecosystems are "open" systems in the sense that energy and matter are transferred in and out. Healt and Dighton (1986) defined ecosystems as "open dissipative thermodynamic systems whose energy flow is controlled by interactions and feedback mechanisms, selected to maintain biomass and minimize effects of fluctuation in environmental factors."

When all elements live in balance and are capable of reproducing themselves it said that the ecosystem is sustainable. Ecosystems consist of four components:

1. **Abiotic substances,** basic inorganic and organic compounds of the environment.
2. **Producers,** autotrophic organisms manufacturing food from simple inorganic substances.
3. **Consumers,** heterotrophic organisms consuming other organisms or particulate organic matter.
4. **Decomposers,** heterotrophic organisms breaking down the complex compounds of dead protoplasm and releasing simple substances useable by producers.

Each organism requires energy to live and provides energy for other organisms. Therefore, a continuous passage of energy between each trophic level is needed to sustain life. Physiological processes are related to environment characteristics and climate, so changes in atmospheric composition and climate change (i.e., increase in atmospheric CO_2 concentration and surface temperature, and variation in precipitation) can alter these mechanisms and lead to the destruction of the ecosystem (Bullock and Le Houérou, 1996). Studying energy and mass fluxes within an ecosystem, therefore, offers the possibility to better understand ecophysiological processes and protect ecosystems from alteration.

1.2 Ecosystem production

Creation of organic compounds from atmospheric or aquatic carbon dioxide -principally through photosynthesis process- is called "Primary Production." Organisms responsible for primary production are known as primary *producers* or autotrophs, which are autotrophic organisms that are able to fix energy (from the sun) into chemical bounds of organic molecules. These compounds are used by the other organisms to assimilate energy through various levels of the food chain. In terrestrial ecosystems, *producers* are mainly plants, while in aquatic ecosystems producers are mostly algae.

We define *gross photosynthesis* as the rate of carbon fixation by the producers (e.g., plants). The *Gross Primary Production* (GPP) is the accumulation

or sum of the carbon fixation. We define *Net Primary Production* (NPP) as the difference between carbon fixed by photosynthesis and carbon lost by autotrophic respiration (Woodwell and Whittaker 1968). The NPP corresponds at the rate at which new biomass accrues in an ecosystem. Some NPP contributes to growth and reproduction of primary producers, while some is consumed by herbivores and omnivore animals that contribute litter to the soil, which creates soil organic matter that can be lost through respiration. Both gross and net primary production has the unit mass area^{-1} time^{-1}. In terrestrial ecosystems, the unit kg of carbon m^{-2} year^{-1} is commonly used.

We define *Net Ecosystem Production* (NEP) as the difference between gross primary production and total ecosystem respiration, which is the sum of autotrophic and heterotrophic respiration (Woodwell and Whittaker 1968). It represents the total amount of organic carbon in an ecosystem available for storage, export as organic carbon, or non-biological oxidation to carbon dioxide through fire or ultraviolet oxidation. If the sign of NEP is positive the ecosystem is autotrophic (e.g., a typical forest or grassland). If NEP is negative, the ecosystem is heterotrophic as in cities and many lakes and rivers (Lovett et al., 2006).

In recent literature, NEP has been redefined as the rate of carbon accumulation in an ecosystem (Lichter 1998; Caspersen et al., 2000; Randerson et al., 2002; Chapin et al., 2002), but this definition is incorrect. The original definition maintains the conceptual coherence between NEP and NPP, and it is congruous with the widely accepted definitions of ecosystem autotrophy and heterotrophy. NEP may be a good approximation of the organic C accumulation rate within the system if inputs and outputs of organic C are negligible, but it is incorrect to assume that NEP and organic C accumulation are always equivalent (Lovett et al., 2006).

We can also define *Net Biome Productivity* (NBP) that accounts for carbon loss during episodic disturbance, which is equivalent to NEP at regional or global scale. The NBP allows a direct comparison of NEP estimates made at all temporal and spatial scales. Measurements of NEP are difficult, especially in terrestrial ecosystems, and they typically have high uncertainties. Micrometeorological

techniques (e.g., Eddy Covariance) have been used frequently to estimate NEP. In particular, EC directly measures the *Net Ecosystem Exchange* (NEE), which is conceptually identical to NEP except for a reverse in sign notation, so that fluxes into the ecosystem are negative (-NEE = +NEP). In reality, net ecosystem exchange is equal to NEP plus *sources* and *sinks* for CO_2 that do not involve conversion to or from organic C as shown in the following equation

$$-NEE = NEP + inorganic\ CO_2\ sinks - inorganic\ CO_2\ sources \quad (1.1)$$

Inorganic *sources* and *sinks* result from weathering reactions, precipitation or dissolution of carbonates, and atmosphere–water equilibrations (Lovett et al., 2006).

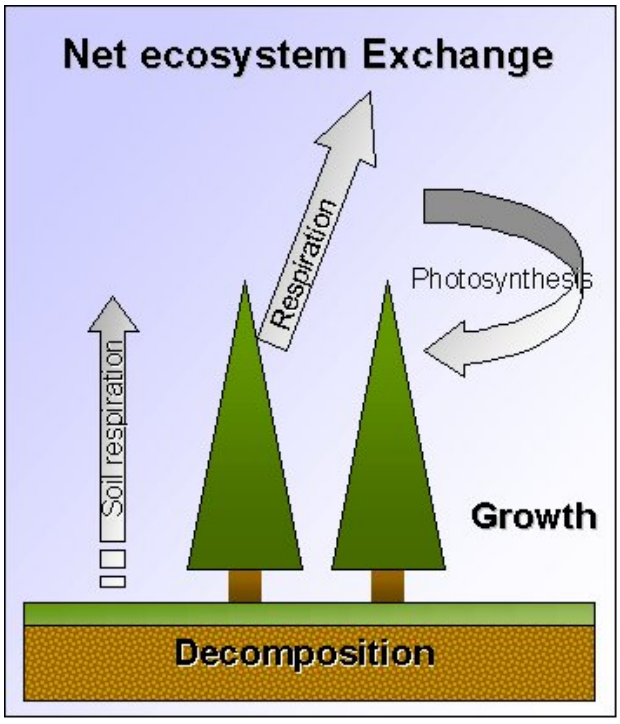

Figure.1 Fluxes contributing to net ecosystem exchange (NEE).

Net CO_2 flux is considered as the difference between two large terms: (1) photosynthetic uptake of CO_2 by foliage and (2) emission of CO_2 by soil respiration and plants (Figure 1). Changes in climatic conditions influence both terms, and one can monitor ecosystem exchanges using EC measurements to directly obtain NEE without disturbing ecosystem functioning.

1.3 Micrometeorological techniques and models

Ecology is the study of interrelationships between organisms' physical functioning and their environment. Ecophysiology is the study of plants in their natural environment and their relationships with environmental factors (e.g., radiation, temperature, vapour deficit pressure, etc.). In each environmental system, there is a complex network of relationships between system components and the external environment. These relationships include energy and mass fluxes that are not random because several mechanisms of regulation, organization, and control exist within the ecosystem.

Micrometeorological techniques are employed to estimate energy and mass fluxes and EC method is commonly used to obtain direct measurements of CO_2, water vapour, heat, and radiation exchanges between the vegetation and atmosphere. Knowing and describing the relationships between vegetation and its environment provides information that is useful for ecosystem management. In fact, knowing these relationships helps one to understand plant effects on temperature, humidity, carbon dioxide concentration, and radiation interception. Thus, plants can affect climate, which is important for scientists who are studying energy and mass fluxes over ecosystems.

It is important to understand the fate of anthropogenic CO_2 (Goulden et al., 1996) to know if ecosystems are a *source* or *sink* of carbon by monitoring the daily, annual, and inter-annual changes in CO_2 fixed and released. This allows a better understanding of the relationships between global change and CO_2 variability (Baldocchi et al., 1996). It is also important to know how energy fluxes vary in an ecosystem depending on climate. So, with micrometeorological field studies, it is possible to collect information on the ecosystem response to climate change and to predict *feedback* mechanisms. Having direct measurements is also important to understand the periodicity of biological activity in an ecosystem, related to climate periodicity, to biomass production and to phenological phases.

Using direct micrometeorological measurements provides the means to evaluate extreme meteorological event effects and, therefore, protect ecosystems from alteration processes. Measurements provide flux estimates over relatively

wide surfaces, and data can be collected for long time periods. Short term measurements can lead to data misinterpretation and incorrect global and seasonal flux estimates. Another advantage is that micrometeorological measurements are non-destructive to the vegetation since data are collected *in situ* (Baldocchi et al., 1988).

Models are also used to understand plant behaviour in regards to environmental factors, and they can operate at different spatial-temporal scales. Models connect plant factors (e.g., photosynthesis, growth, development, etc.) with environmental factors (e.g., energy and mass exchange). Therefore, models with these characteristics help to predict carbon budgets at different scales to better understand the role of CO_2 and to achieve the Kyoto Protocol objectives.

Kyoto Protocol mainly focuses on the role of forests in carbon sequestration, but there is broad agreement in the scientific community on the need to understand the whole carbon cycle (e.g., terrestrial, ocean, and atmosphere) and use these components in complementary and synergistic ways (Falkowski et al., 2000). In addition to forestry, there is need for satellite and *in situ* observational data, for land uses such as cropland and grazing land, wetlands, and coastal areas to obtain information needed for national, regional, and global carbon budgets (FAO, 2002a, b, 2003).

The inter-comparison of a number of global ecosystem models indicates that approximately 55 petagrams of carbon (PgC) are generated each year in the form of net primary production (NPP) in terrestrial ecosystems (Gaim, 1998). The area consists of forests and woodland, croplands, grasslands, and other ecosystems. An estimated 3.5 PgC are annually produced just by agricultural crops, accounting for about 7 percent of total NPP in terrestrial ecosystems. Of this amount approximately one-third represents the harvested product of which about half is used for direct human consumption and half for animal consumption (Goudrian, 2001).

Despite the importance of agricultural ecosystems in the global carbon cycle, most of investigations have been made on forests with few studies on exchanges of energy and mass in agricultural ecosystems. In particular, fluxes over grape vineyards and annual and seasonal variation of NEE are unknown. The

same deficiency of information exists for Mediterranean maquis. In fact, it is more difficult to estimate fluxes over sparse canopies than over dense canopies (e.g., forests). Micrometeorological techniques, however, can be used to monitor these kinds of ecosystems. These techniques are based on turbulence and boundary layer theory. Another important concept for using micrometeorological techniques is the energy budget. Before describing the EC technique and the ACASA model used in this research, it will be useful to describe micrometeorological concepts that will allow the understanding of theory behind their application.

2. MICROMETEOROLOGICAL CONCEPTS

2.1 Micrometeorology and Boundary layer

Phenomena with space scales smaller than 3 km and time scales shorter than one hour are classified as *microscale*. Stull, (1988) defined micrometeorology as the study of such small-scale phenomena occurring within the atmospheric layer, affected by the Earth's surface. Surface's roughness affects fluid motion above it, so at a certain height from the ground, the fluid motion varies from a laminar motion (regular and constant that is away from surface) to a turbulent motion (near the surface). Turbulence is, therefore, considered a microscale phenomena.

The troposphere may be divided into two parts, the *atmospheric boundary laye*r (ABL), close to the Earth's surface, and the *free atmosphere* above it (Rosenberg et al., 1983; Stull, 1988; Kaimal and Finnigan, 1994; Ceccon and Borin, 1995). Troposphere's extension goes up from the ground to about 11 km, but only the lowest couple kilometers are directly affected by the underlying surface. So, the **atmospheric boundary layer** is defined by Stull (1988) as "the part of the troposphere that is directly influenced by the presence of the Earth's surface, and responds to surface forcings with a timescale of about one hour or less."

In agricultural meteorology, micrometeorology focalizes on air layer really close to the canopy, affected by canopy themselves. Surface can decrease the wind speed or alter the air temperature and relative humidity in the air immediately above it. Other forcings include evaporation and transpiration, frictional drag, heat transfer, and terrain that induce flow modification. These latest surface forcings (friction and heating) induce vertical mixing of the horizontal flow, resulting in a three-dimensional swirling motion on different size scales that effectively mixes the air in the ABL. These swirls are often called turbulent *eddies*. In the free atmosphere, turbulence is absence or it is significantly weaker than ABL.

Boundary layer thickness varies depending on vegetation characteristics. It changes in time and space, ranging from hundreds of meters to few kilometers or millimeters (e.g., the leaf surface). Boundary layer thickness also depends on atmospheric stability (Stull, 1988; Kaimal and Finnigan, 1994). During summer days, solar radiation heats the surface and the boundary layer is unstable. There is a vigorous convection mixing the air and, in such conditions, the ABL height is typically 1-2 km. On the other hand, during the night (and the winter) the surface is cold and the ABL becomes stable, suppressing the turbulence. In this situation, only a weak turbulence can be created by wind shear.

Within the ABL can exist three categories of wind: mean wind, turbulence, and waves (Stull, 1988). Heat, moisture, momentum, and pollutants transport is dominated by the mean wind in the horizontal, and by the turbulence in the vertical. *Mean wind* is responsible for rapid horizontal transport, or advection; *waves* transport little heat, humidity, and pollutants, but are also responsible for transport of momentum and energy; *turbulence* has a high frequency near the ground, and it consists of many different size eddies. Large eddies have sizes roughly equal to the depth of the boundary layer, from 100 to 3000 m in diameter; small eddies are on the order of few millimeters in size, and they are weak because of the dissipating effects of molecular viscosity. Small eddies feed on the large eddies. Turbulence is more effective at transporting quantities than molecular diffusivity, and it allows for boundary layer response to changes in surface forcings.

The ABL is divided into surface layer, mixed layer, residual layer, and stable boundary layer (Figure 2). The **Surface layer** (SL) is the region at the bottom of the boundary layer. In this region, turbulent fluxes and stress vary by less than 10% of their magnitude (vertical flux invariability). Therefore, the flux measured at an arbitrary height inside the SL equals that at the surface. This concept is the basis of micrometeorological techniques such as EC. Within this layer, there is a thin layer called the *interfacial layer*, which is found in the air within a few centimeters of the surface, in which molecular transport dominates over turbulent transport. In the **mixed layer** (ML), turbulence is created by convection process and by wind shear. Convective sources include heat transfer

from a warm ground surface, which creates thermals of warm air rising from the ground, and radiative cooling from the top of the cloud layer, which creates thermals of cool air sinking from cloud top.

Residual layer (RL) is the portion of the ML that remains when thermals stop to form (in the absence of cold air advection). It happens about a half hour before sunset, allowing turbulence to decay. It is called residual because its variables are the same as those of the recently-decayed mixed layer. The RL does not have direct contact with the ground. The bottom portion of RL at a direct contact with the ground is called **stable boundary layer** (SBL), and it occurs during the night. In this layer, the air is stable with weak or sporadic turbulence. Wind speed just above the surface often becomes light or even calm, while at the top of the SBL a nocturnal low-level jet evolves. SBL can also form during the day when the underlying surface is colder than the air.

Since SL is the layer where fluxes are relatively constant, it is in this zone that fluxes measurements can take place. In fact, in this layer fluxes are independent from surface distance, and the profiles show a logarithmic function with height. Therefore, the top of the SL is the maximum distance from the top of vegetation where it is possible to take measurements of mass and energy fluxes. Usually, it is assumed that measurements can be made at height above canopy equal to 0.01 *fetch* (i.e., from smooth surface to rough surface) or to 0.05 *fetch* for the opposite situation. Fetch is defined as an upwind distance with uniform surface characteristics, and it represents the large area of surface where it is possible to measure fluxes. A measurement is representative of a particular surface type or process when the whole fetch has the same surface type. Therefore, it is important to have a wide and homogeneous surface around sensors, and the area amplitude depends on sensor's height. The ratio fetch/height of the boundary layer is equal to 100:1 that means that if fetch is 100 m, the height of sensor above the zero plane displacement must be 1 m (Baldocchi et al., 1988).

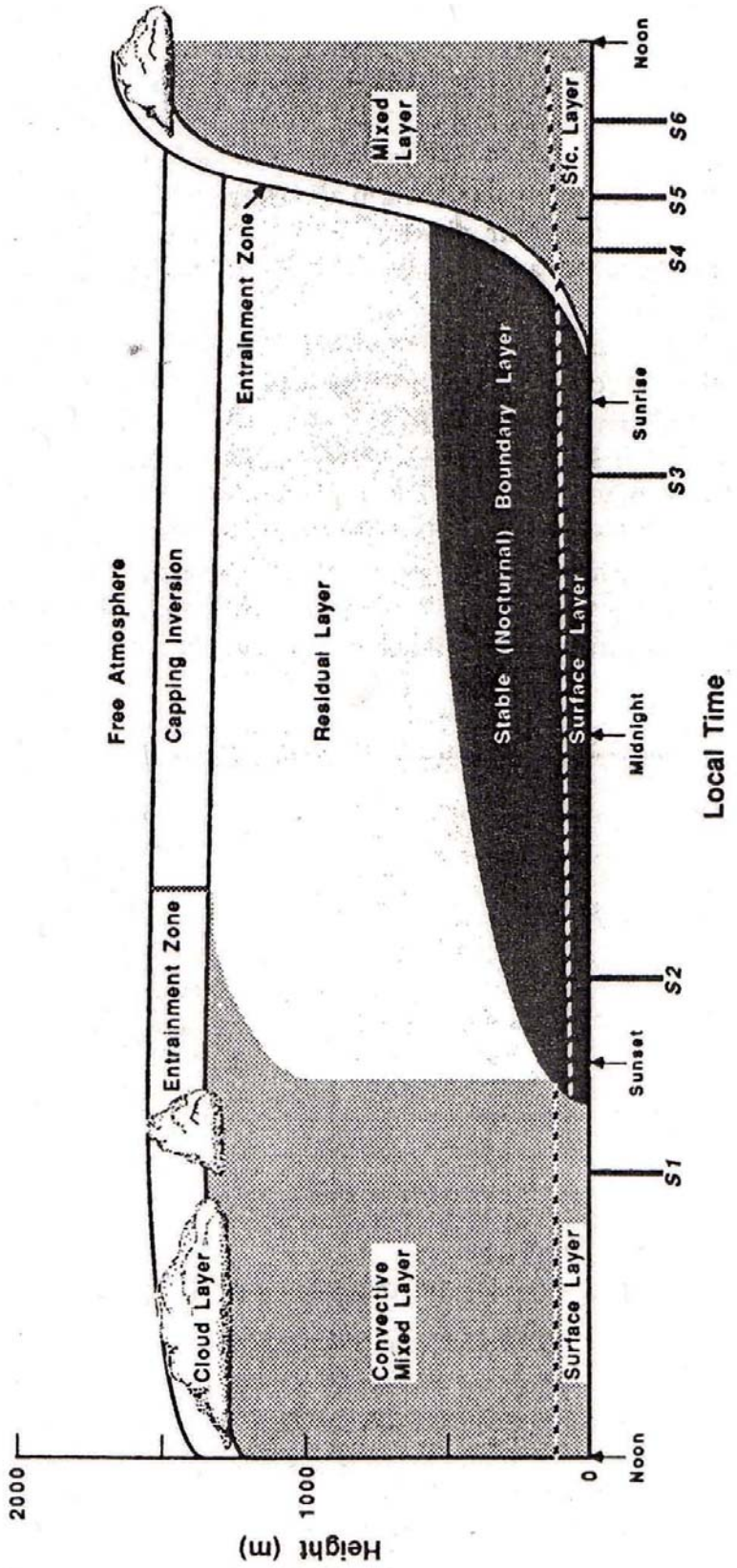

Figure 2. Schematic representation of atmospheric boundary layer subdivision (from Stull, 1988).

2.2 Turbulence characteristics

Flow over a smooth surface is laminar. Over a rough surface, the flow motion changes and it becomes turbulent. The passage from laminar to turbulent flow is quantified by the *Reynolds' number* (Re) which is a measure of the ability of molecular-viscous forces to absorb the energy of the turbulent movement. It is used to indicate if the flow is getting turbulent. The Reynolds' number is a function of the wind velocity (U) in m s^{-1}, boundary layer height (h) in meters, and kinematic viscosity (v) in m^2 s^{-1} as shown in equation 2.1

$$\mathrm{Re} = Uh / v \tag{2.1}$$

If Re is higher than 10^4 or 10^5, the flow becomes turbulent.

Some important characteristics of turbulent flow are

- **Irregularity**: the main variables are irregular, not constant, and random. These characteristics are typical of stochastic phenomena. For this reason, a method for investigating flow should be statistical.
- **Diffusivity**: mass transport increases within a turbulent flow.
- It is a **three-dimensional phenomenon:** within turbulent flow there are three-dimensional structures.
- **Dissipation**: turbulent flow always disperses energy. Turbulence requires energy to compensate the energy lost by viscous forcings. This energy derives from kinetic energy lost by flow itself.
- **Continuity**: turbulence is not a microscopic phenomenon, but it is a macroscopic phenomenon.

Each variable within the flow can be separated in an average part and a turbulent part, following Reynolds' rule (Stull, 1988)

$$x = \bar{x} + x' \tag{2.2}$$

where x is the actual instantaneous value, $\bar{x}$ is the average value, and x' is the fluctuation of the value around the mean (turbulent part).

Describing turbulence requires the knowledge of eddies spatial and temporal distribution. This analysis is possible thanks to the Taylor's hypothesis (Stull, 1988) called *turbulence frozen*. In 1938, Taylor suggested that turbulence might be considered to be frozen as it advects past a sensor. In this way, the mean wind speed can be used to translate turbulence measurements as a time function of their corresponding measurements in space. Obviously, this hypothesis is not true in the reality, but it becomes true in those cases where turbulent eddies evolve with a timescale longer than the time that eddy takes to be advected past a sensor. Taylor's hypothesis leads to

$$\frac{\partial T}{\partial t} = -u\frac{\partial T}{\partial x} \tag{2.3}$$

where $\frac{\partial T}{\partial t}$ is the air temperature gradient with time, u is the horizontal wind speed, and $\frac{\partial T}{\partial x}$ is the air temperature gradient with space along x axis direction. Air temperature variation with time is related to the variation in space by the wind speed. This hypothesis is valid only if eddy does not change significantly during its transit along the sensor. This condition happens when $\sigma_u < 0.5u$, where σ_u is the standard deviation of wind speed, and it is an indicator of turbulence intensity. Thus, Taylor's hypothesis should be satisfactory when the turbulence intensity is small relative to the mean wind speed.

2.3 Wind profile and parameters to define turbulence

Turbulence concepts require the description of the wind profile within the boundary layer. A parameter used to define turbulence is the *friction velocity* (u*). Friction velocity is a characteristic velocity of the flow, and it relates to the effectiveness of turbulent exchange over the surface (Rosenberg et al., 1983). It is given by

$$u_* = \sqrt{\overline{u'w'}} = \sqrt{\tau / \rho_a} \tag{2.4}$$

where $\overline{u'w'}$ is the Reynolds' stress, τ is the shearing stress, and ρ_a is the air density. Reynolds' stress is the stress that turbulence motion exerts over a surface, and it exists only if turbulence is present. Reynolds' stress is represented by the turbulent momentum flux.

Wind speed variation with height over a regular surface shows a logarithmic profile within the surface layer (Figure 3). It is given by

$$u_z = \frac{u_*}{k} \ln \frac{z - d}{z_0} \tag{2.5}$$

where u_z is the mean wind speed at height z, k is the von Karman constant equals to 0.41, z_0 is the roughness length, and d is the zero plane displacement. *Roughness length* represents a measure of the aerodynamic roughness of the surface over which the wind speed profile is measured. The *zero plane displacement* indicates the mean level at which momentum is absorbed by plant elements, and is, therefore, equal to zero. Under d there is no turbulence. The term (z_0 + d) is defined as the height where wind speed becomes zero.

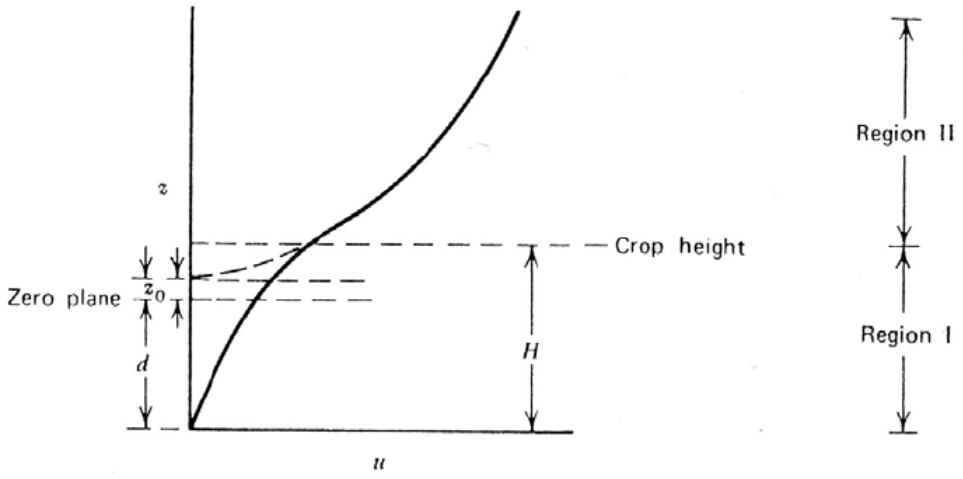

Figure 3. Vertical wind profile within and above canopy with a particular scheme of roughness parameter (z_0) and of zero plane displacement parameter (d) (from Monteith and Unsworth, 1990).

Turbulence description is also possible using the *Monin-Obukhov stability* parameter (*z/L*) given by

$$z/L = \frac{kzgH}{\rho_a C_p T u_*^3} \tag{2.6}$$

where *L* is the Obukhov length, *k* is the von Karman constant equals to 0.41, *z* is the measurements height, and *g* is the acceleration due to gravity. Monin-Obukhov stability is derived as the ratio between buoyancy production to mechanical turbulence production. In practice, *z/L* is considered a parameter indicating atmospheric stability conditions. If *z/L* value is positive than the atmosphere is under *stability* condition (i.e., no convection, so air parcel that are moved up or down come back to initial position); if it is negative there is *instability* (i.e., convection occurs, so the air parcels are mixed and go up and down as thermals). *Neutral* condition occurs when turbulence is main produced by mechanical forces rather than buoyancy terms. This occurs on cloudy days, with strong wind speeds, and with little difference in temperature between the air and surface (Stull, 1988).

2.4 Reynolds' equations

To describe quantitatively the boundary layer (BL) state, fluid mechanic equations are used to illustrate the dynamics and thermodynamics of atmospheric gases. The complete set of equations applied to boundary layer are so complex that no analytical solution is known, so approximate solutions are used to solve them. Either exact analytical solutions or approximate numerical solutions can be used to simplify these equations (Stull, 1988).

Newton's second law gives the Navier-Stokes' equations. Using the gases' law, conservation equations, and applying Reynolds' average and rules, the equations for studying fluxes in the boundary layer are presented as in the following section.

Conservation of momentum equation is given by

$$\frac{\partial \overline{U}_i}{\partial t} + \overline{U}_j \frac{\partial \overline{U}_i}{\partial x_j} = -\delta_{i3} g + f_c \varepsilon_{ij3} \overline{U}_j - \frac{1}{\overline{\rho}} \frac{\partial \overline{P}}{\partial x_i} + \nu \frac{\partial^2 \overline{U}_i}{\partial x_j^{\,2}} - \frac{\partial \left(\overline{u_i' u_j'} \right)}{\partial x_j} \qquad (2.7)$$

I II III IV V VI X

where the term *I* represents the mean momentum storage (inertia), term *II* describes the mean momentum advection due to the mean wind, term *III* allows gravity to act only in the vertical direction, term *IV* describes the influence of Earth's rotation (Coriolis effects), term *V* describes the mean pressure-gradient forces, term *VI* represents the influence of viscous stress on the mean motions, and term *X* represents the influence of Reynolds' stress on the mean motions. It can also be described as the divergence of turbulent momentum flux. The last term implies that turbulence has to be always considered, even if only mean quantities are described. The term *VI* can be neglected because it is small.

Introducing the components of geostrophic wind, $\overline{u}_g$ and $\overline{v}_g$ defined as

$$f_c \overline{u}_g = -\frac{1}{\overline{\rho}} \frac{\partial \overline{P}}{\partial y} \qquad f_c \overline{v}_g = -\frac{1}{\overline{\rho}} \frac{\partial \overline{P}}{\partial x} \qquad (2.8)$$

the conservation of momentum equation becomes

$$\frac{\partial \overline{u}}{\partial t} + \overline{u}_j \frac{\partial \overline{u}}{\partial x_j} = -f_c\left(\overline{v}_g - \overline{v}\right) - \frac{\partial \overline{u'_j u'}}{\partial x_j} \tag{2.9a}$$

$$\frac{\partial \overline{v}}{\partial t} + \overline{u}_j \frac{\partial \overline{v}}{\partial x_j} = -f_c\left(\overline{u}_g - \overline{u}\right) - \frac{\partial \overline{u'_j v'}}{\partial x_j} \tag{2.9b}$$

Conservation equations can also be written for other variables, such as heat, scalar, and humidity.

Conservation of humidity equation is equal to

$$\frac{\partial \overline{q}_T}{\partial t} + \overline{u}_j \frac{\partial \overline{q}_T}{\partial x_j} = +S_{qT} / \overline{\rho}_{air} - \frac{\partial \overline{u'_j q'_T}}{\partial x_j} \tag{2.10}$$

Conservation of heat equation is given by

$$\frac{\partial \overline{\theta}}{\partial t} + \overline{u}_j \frac{\partial \overline{\theta}}{\partial x_j} = -\frac{1}{\overline{\rho} C_p}\left[LE + \frac{\partial \overline{Q}_j^{\,*}}{\partial x_j}\right] - \frac{\partial \overline{u'_j \theta'}}{\partial x_j} \tag{2.11}$$

where $\overline{Q}_j^{\,*}$ is the component of net radiation in the jth direction.

The last equation is the conservation of a scalar given by

$$\frac{\partial \overline{c}}{\partial t} + \overline{u}_j \frac{\partial \overline{c}}{\partial x_j} = +S_c - \frac{\partial \overline{u'_j c'}}{\partial x_j} \tag{2.12}$$

In each equation, the term *I* is the storage, the term *II* represents advection, the term *III* represents sundry body forcings, and the last term represents the turbulent flux divergence.

Some simplifications can be made regarding characteristics of BL, but these equations represent the basis for studying fluxes exchange within the BL.

They constitute the starting point for micrometeorological techniques application, and for model application.

3. ENERGY BUDGET

Micrometeorological techniques are based on the energy budget concept. At the Earth's surface, energy arrives from the sun and energy is also reflected or absorbed by the surface and atmosphere. It is important, therefore, to understand which part of the atmosphere and surface are involved in the energy budget.

Microclimate is defined as the climate in the portion of atmosphere near to the ground (i.e., the climate in which plants and animals live). Macroclimate is, instead, the climate at a height of few meters over the ground, and it differs from microclimate in the rate at which changes occur with elevation and with time (Rosenberg et al., 1983). For example, temperature changes drastically in the first few ten millimeters from the surface into the soil or into the air, and humidity changes a lot with elevation near the surface. In addition, exchanges of water and heat occur near the surface. Therefore, climate in the portion of atmosphere near to the surface is different from the climate just at few meters above it. Climate above surface, in fact, is more stable, and mixing processes in the atmosphere are more active.

Energy fluxes occurring within an ecosystem respect different laws depending on their nature. If a system is constituted by two elements (e.g., soil and atmosphere), the energy exchanges occur in *electromagnetic way* (i.e., short and long waves) and *thermal way* (i.e., heat). Canopy is neglected because it is too thin regarding the system extension. Thermal energy in the soil is moved by conduction (i.e., direct interaction between molecules), while in the atmosphere it is moved by conduction and convection (i.e., by fluid motion that in meteorology moves with vertical motion). In the atmosphere, energy can also move by advection (i.e., with motion along a horizontal plane), and by mass transport when phenomena of changes of state (i.e., evaporation or condensation) occur.

The budget equation for surface energy flux is formulated by the first law of thermodynamic (i.e., conservation of energy)

$$Rn + H + LE + G + \Delta S + M = 0 \qquad (3.1)$$

where *Rn* is the net radiation available at the surface to carry out job, *H* is the sensible heat flux density between the surface and air, *LE* is the latent heat flux density to and from the surface (i.e., evaporation and condensation processes), *G* is the soil heat flux density, and *ΔS* is the storage term. This term is due to sensible and latent heat flux divergence within the air column and to the energy stored in the biomass. The last term (*M)* is the metabolic term that accounts for metabolic processes occurring in the ecosystem (e.g., photosynthesis and respiration). Generally, the metabolic term is small, so it is neglected in the energy balance equation.

Fluxes between the vegetation and atmosphere are, in truth, flux densities, so they are measured in W m^{-2}. The analysis of a surface, therefore, is not specific to a particular surface area considered.

Rn and *G* direction is considered positive (i.e., heating process) when it is directed downward and negative (i.e., cooling process) when it is upward. The other terms, instead, have a positive direction when they are upward and negative when they are downward (Figure 4).

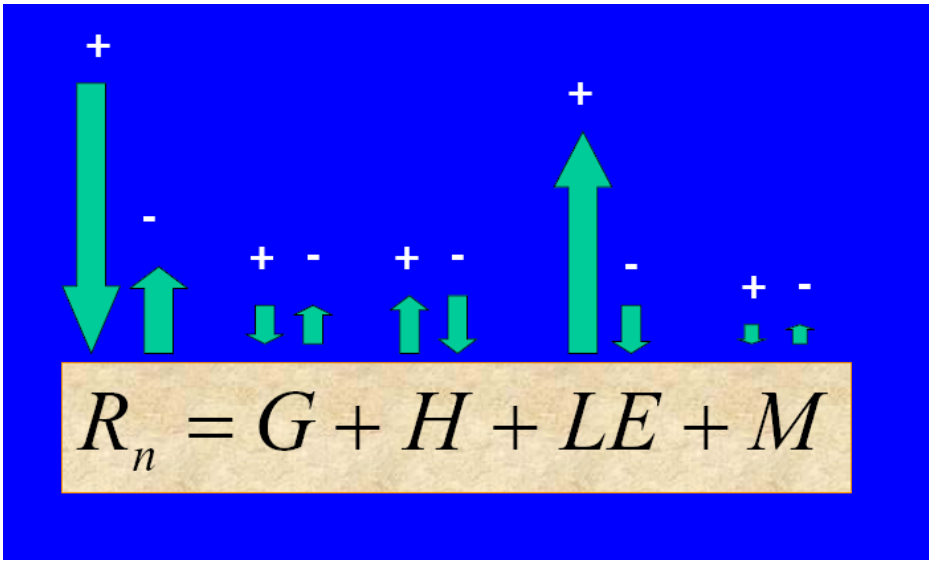

Figure 4. Surface energy balance equation and sign of terms.

The energy balance equation is applicable on the scale of a single plant or an entire crop field or forest, and to a global scale. It explains how energy is used to warm soil and to evaporate water (e.g., ecosystem scale), or how the energy is used by continents and oceans (e.g., global scale).

The energy balance equation is important for ecosystem life, so a brief description of the individual terms of this equation is presented. It is important to understand how each term of the energy budget equation is related and what is their meaning.

3.1 Net Radiation

Net radiation is the energy available for all processes that occur on the Earth, which are important for plant, animal and human life. Ignoring the small amount of energy used for metabolism, net radiation can be expressed as

$$Rn = H + LE + G + \Delta S \tag{3.2}$$

showing the importance of *Rn* in the energy balance. Energy from *Rn* is used to warm or cool the air (*H*) and the soil (*G*), to evaporate or condensate water (*LE*), and it is stored in the biomass (*ΔS*). *Rn* is constituted by short (*Rsw*) and long (*Rlw*) wave radiation, and the streams radiation can be downward (↓) and upward (↑). The *Rn* equation can be written in the following manner

$$Rn = Rsw\downarrow - Rsw\uparrow + Rlw\downarrow - Rlw\uparrow \tag{3.3}$$

The absorbed portion (or net) of total direct and diffuse solar radiation (*Rsn*) is equal to the difference between upward and downward short wave radiation fluxes, and it depends on the albedo or reflectivity (*r*) of the underlying surface as follow

$$Rsn = Rsw\downarrow - Rsw\uparrow = (1 - r)Rsw\downarrow \tag{3.4}$$

The long net wave radiation (*Rln)* balance is given by

$$R\ln = Rlw\downarrow - Rlw\uparrow \tag{3.5}$$

Net radiation equation, therefore, becomes

$$Rn = Rsn + R\ln = (1-r)Rsw\downarrow + Rlw\downarrow - Rlw\uparrow \tag{3.6}$$

Equation 3.6 shows that *Rn* is the difference between total upward and downward radiation fluxes, and it represents a measure of net radiation energy at the ground surface. It drives all surface processes. *Rn* is positive during the day and negative during the night.

The net radiometer is an instrument to measure *Rn* that absorbs radiation of solar wavelengths directed downward toward the surface and upward away from it. The net radiometer should be mounted on a tower with the arm extending out in a south direction with no objects shading the sensor. It should be mounted so that the surface of the net radiometer is parallel to the vegetation surface. Normally, the surface is flat, so the bubble level in the net radiometer is commonly used to level the sensor. Most net radiometers record a voltage in millivolts, which is multiplied by a calibration factor to estimate *Rn*. The *Rn* sensor should be mounted sufficiently high above the surface, so the albedo of short waveband radiation and upward long waveband radiation is representative of the underlying surface.

3.2 Sensible Heat Flux

Convection is the process that allows transfers of large quantities of available energy between surface and the air. It is defined as “mass motion of fluid (e.g., air) resulting in transport and mixing of the properties of that fluid” (Huschke, 1959). By convection, surfaces absorb or release energy, resulting in a cooling or heating of air and the surrounding objects. Flux deriving from this

transfer is defined as sensible heat flux (*H*). The word "sensible" refers at the transport that determines air temperature, an air property that we can sense.

Normally, during the daytime, heat is transferred from the warm ground or crop surface to the cooler air above. At night, when the air is warmer and the surface is cool, the converse situation prevails, and heat is transferred to the surface. Therefore, on a daily time scale, *H* is positive in the morning (i.e., vertical velocities transfer heat upward from the warm canopy surface and cool air transfers downward). *H* is negative at night, when there is net downward transfer of warmer air into a cooler canopy (i.e., the air near the surface cools due to radiation losses).

In the boundary layer, the transfer of *H* is largely controlled by turbulence. Vertical flux of *H* can be estimated by

$$H = \rho C_p K_h \frac{\partial \theta}{\partial z} \tag{3.7}$$

where ρ is the air density, *Cp* is the specific heat of the air at constant pressure and K_h is the turbulent exchange coefficient (thermal diffusivity). $\frac{\partial \theta}{\partial z}$ is the vertical gradient of potential temperature. In the first 2-3 meters above the ground, $\frac{\partial \theta}{\partial z}$ can be approximated by $\frac{\partial T}{\partial z}$, the vertical gradient of actual temperature (*T*). A typical value for thermal diffusivity is 2.2 (10^{-5}) m^2 s^{-1}. The sign of *H* is positive when the flux is upward and negative when the flux is downward (Figure 4).

Equation 3.7 is obtained by the aerodynamic theory, but *H* can also be estimated using micrometeorological techniques.

3.3 Latent Heat Flux

Latent energy is the energy associated with phase changes of water, which may be recovered when the phase change is reversed. In agriculture, we refer to the change from water to water vapour and vice versa. The process depends on temperature, which drives both the rate and the energy associated with the phase change.

The phase change from liquid water to vapour requires energy to break hydrogen bonds between the molecules. When the water vapour condenses, the hydrogen bonds form again and energy is released to the environment as sensible heat. Therefore, the flux of water vapour is not only a mass flux, but also an energy flux. It is called "latent" heat flux because the energy is latent until condensation occurs. An increase in water temperatures causes an increase of energy stored in the surface water, and more energy is available to break the bonds. *Rn*, *H,* and *G* are all sources of energy for vaporization of surface water. The wind speed, vapour deficit, and advection of air with different temperature and humidity, affect transfer and, hence, evapotranspiration (Allen et al., 1994).

LE flux is obtained by multiplying latent heat of vaporization (*L*) by the mass flux density of water vapour (*E*). *L* is 2.50 (10^6) J Kg^{-1} at 0° C and decreases to 2.406 (10^6) J Kg^{-1} at 40 °C. Mass flux density of water vapour (*E*) (Kg m^{-2} s^{-1}) is obtained from aerodynamic theory

$$E = -K_w \frac{\partial \rho_v}{\partial z} \tag{3.8}$$

where K_w is the turbulent vapour transport coefficient (m^2 s^{-1}). In this research *LE* flux density was estimated using EC technique. Latent heat flux is positive when flux is upward and negative when flux is downward (Figure 4).

3.4 Soil Heat Flux and Storage term

Soil is a major heat storage volume, and it generally acts as a *sink* of energy during the day and a *source* at night. On the annual cycle, the soil stores energy during the warm season, and it releases energy during the cold portions of the year. Soil heat flux is due to conduction (i.e., molecular motions from faster molecules to adjacent, slower molecules); therefore, soil heat flux density (G) is a measure of how fast energy is conducted upward or downward per unit area at the soil surface.

G is expressed by a gradient and a coefficient (Rosenberg et al., 1983) as

$$G = K\frac{\partial T}{\partial z} = -\rho_s C_p c\frac{\partial T}{\partial z} \tag{3.9}$$

where K is the soil thermal conductivity, which varies with soil characterisitcs, and $\frac{\partial T}{\partial z}$ is the temperature gradient within the soil, ρ_s is the soil density, Cp is the mass specific heat capacity, and c is the thermal diffusivity. Specific heat for a typical soil and water are 0.837 and 4.19 J g^{-1} K^{-1}, respectively. The thermal conductivity is a function of soil composition, soil moisture content, and soil structure. The soil heat flux can be estimated as 10% of Rn during the daytime and up to 50% during the night (Oke, 1987).

The measure of G is difficult because of accuracy. Soil heat flux can be measured at some depths (e.g., 0.05 m) in the soil using heat flux plates. Then, the change in heat storage in the soil layer above plate is used to estimate G at the surface. The change in heat storage (ΔS) within the soil layer depends on the difference in heat flux at the surface (G) and the heat flux measured by the plate (G'). Factors affecting ΔS are also the soil volumetric heat capacity (C_v) and the change in soil temperature (ΔT) in the layer above plates (over the sampling period).

C_v is estimated from minerals volume fractions (V_m), organic matter (V_o), and volumetric water content (θ) using

$$C_v = \left(1.93V_m + 2.51V_o + 4.19\theta\right)10^6 \tag{3.10}$$

Since V_o is typically small and soil bulk density (ρ_b) is related to V_m, one can also estimate C_v using the equation

$$C_v = \left(0.837\rho_b + 4.19\theta\right)10^6 \tag{3.11}$$

where ρ_b is expressed in Mg m^{-3}. The factor 10^6 converts soil and water densities from Mg m^{-3} to g m^{-3}. Multiplying the densities by specific heat (Cp) gives C_v in J m^{-3} K^{-1}. Typical ρ_b values are 1.6, 1.4, 1.3, and 0.3 Mg m^{-3} for sand, loam, clay, and peat soils, respectively, and the θ values vary from about 0.2 to 0.4 for sand, loam, and clay soils.

ΔS in the soil layer above heat flux plates per unit surface area is expressed as

$$\Delta S = C_v\left(\frac{T_f - T_i}{t_f - t_i}\right)d_g \tag{3.12}$$

where T_f is the final temperature (°C) at time t_f and T_i is the initial temperature (°C) at time t_i, d_g is the depth (m) of the heat flux plate, and C_v is expressed in J m^{-3} K^{-1}. The length of sampling interval is $t_f - t_i$ (s). In addition, ΔS can be determined as the difference in soil heat flux at the plate (G') and at the surface (G) as

$$\Delta S = -\left(G' - G\right) \tag{3.13}$$

where the negative sign before the bracket forces ΔS to be positive when more heat is added to the layer than it is lost from the layer. Combining the equations 3.12 and 3.13 and solving for G we obtain

$$G = G' + C_v \left(\frac{T_f - T_i}{t_f - t_i} \right) d_g \tag{3.14}$$

G at the surface is hence estimated by measuring G' at some depth (e.g., d_g = 0.05 m) and the change in temperature with time of the soil layer above heat flux plates to determine ΔS.

Soil layer temperature is measured by inserting soil temperature sensors horizontally near the top and the bottom of the layer. Metallic sensors can also be inserted at an angle from near the bottom to near the soil layer top. It is important that temperature sensors are not inserted too close to the surface. If the soil cracks, radiation and/or sensible heat flux to or from the sensors can cause false data. Generally, it is best to not place the temperature sensors any closer than 0.01 m from soil surface, and deeper placement is needed in soils that have large cracks due to soil drying.

G sign is positive if the flux comes from the air to the surface and negative if the flux comes away from the surface (Figure 4).

4. MODELLING

A biological system is a complex system that involves the interrelationships of many different "species" (e.g., molecules, cells, tissues or organisms), and a model represents a description of the system. Building a good ecosystem model means to capture the essential details of biology. A model is a simplification of biology, but it has the advantage to express an idea that might have been expressed purely verbally and make it more explicit.

In a model, we can fix some variables and vary characteristics. The aim is to understand the role of individual characteristics under investigation and to make predictions. In ecology, it is hard to make good models because of the large number of variables involved in an ecosystem. Model predictions will always differ from measurements because models are idealisations, and repeated measurements are not identical. To be realistic, a model should accurately predict measured values. The measurements support the model, and give no reason to change or replace assumptions.

A simple classification subdivides models in two main categories: deterministic models and stochastic models.

Deterministic models are simple. They use mathematical representations of the underlying regularities that are produced by the entities being modelled and generate theoretically perfect data. Parameters and variables are not subject to random fluctuations. They are fixed, so the system is at any time entirely defined by the initial conditions, in contrast with a stochastic model. Deterministic models can be solved by numerical analysis or computer simulation. They are often described by sets of differential equations. Deterministic models are appropriate when large numbers of individuals of species are involved, and it can safely be supposed that the importance of statistical variations in the average behaviour of the system are relatively unimportant. For many biological systems, however, this assumption may not be valid.

Stochastic models are more complex. They use computational elements that represent the entities and processes by which they interact and create a

procedural algorithm to generate realistic data. They take into consideration the presence of some randomness in one or more of its parameters or variables. Model predictions, therefore, do not give a single point estimate, but a probability distribution of possible estimates. Stochastic models should be used where either the number of individuals is small or there is a reason to expect random events to have an important influence on the system behaviour. Often, a stochastic model will be more appropriate when we need to take account of species as discrete units rather than as continuous variables. It may also be necessary to take account of events occurring at random times.

The essential difference between a stochastic and deterministic model is that, in a stochastic model, different outcomes can result from the same initial conditions. Stochastic model are more reliable because they account for the randomness and, so they give output closer to reality.

4.1 Modelling of canopy microenvironment

Several models have been used to simulate crop microenvironment, physical and physiological processes involved in the production and transport of heat and water vapour in the canopy. It is important to make accurate simulations of these processes, as like as for wind velocity, temperature, humidity, heat, and moisture flux profiles in the vegetative surface layer to identify the important factors or limitations, and to provide more reliable forecasts.

The main types of models used in crop microenvironment are: Lagrangian (stochastic) models (L-theory), models based on gradient diffusion theory (K-theory), and higher-order closure models (ACASA).

A **Lagrangian (stochastic) model** describes the paths of particles in a turbulent flow, given knowledge (i.e., statistical description) of the random velocity field. With this kind of model, it is possible to describe many interesting atmospheric processes (e.g., the trajectories of pollutants in the air). It is a simple model and it provides an excellent description of dispersion of particles in the atmosphere (Wilson and Sawford, 1996). In particular, L-Theory represents an analytical turbulent transfer model for predicting scalar concentration profiles

produced by a specified canopy *source* (or *sink*) distribution. Turbulence characteristics are defined by empirical equations of standard deviation of vertical wind velocity and Lagrangian time scale (i.e., the time scale over which the vertical velocity remains correlated to itself due to persistence of turbulent motions). It was first developed by Raupach (1989a, b). Lagrangian models, therefore, can be used to predict concentration profiles of scalars, as heat, water vapour and CO_2 (Wilson et al., 2003). The problem with the L-theory is that no test for nighttime conditions (when wind speed is near zero) have been done (Wilson et al., 2003), and it requires information about turbulent velocity field and time scales (Meyers and Paw U, 1987).

K-theory, on the other hand, is simpler to apply for simulating transport in plant canopies and it is valid with small errors (Wilson et al., 2003). K-theory defines turbulent flux (*Fc*) of any scalar as a product of the scalar concentration gradient, *dC/dz*, and eddy diffusivity *K*

$$Fc = -K\frac{dC}{dz} \tag{4.1}$$

where *z* is the height above ground.

The application of these concepts to canopy flow have several limitations. First, K-Theory does not predict the counter-gradient fluxes, which occasionally occur in vegetative canopies (Denmead and Bradley, 1985, 1987). Second, within the canopy there are numerous length scales including the leaf width, plant spacing, and height above ground, and K-theory is seen to work properly in situations where the flow is characterized by a single length scale. In addition, gradients often change within the canopy, so fluxes can not be uniquely determined by the product of eddy diffusivity and the gradient. Third, K-theory accounts for only a local transport, but, within the canopy, there is also a non-local transport. This characteristic can not be described with local gradient diffusion concepts (Meyers, 1985).

A solution of these problems seems to be the use of **higher-order closure models.** These models require the formulation of flux equations to obtain a number

of unknowns exceeding the number of equations (Stull, 1988), so for a finite set of those equations the description of turbulence is not closed. This is called the *closure problem*. One approach to solve the closure problem is to use only a finite number of equations, and then approximate the remaining unknowns in term of known quantities (parameterization). Such a closure approximation takes the name from the highest order equations that are retained. Hence, the additional unknowns are parameterized or neglected to close the system of equations. There are several works supporting the use of higher-order closure models for simulating turbulent fluxes in vegetative canopies (Wilson and Shaw, 1977; Andre et al., 1978; Sun and Ogura, 1980). Limitations of these models include the use of gradient diffusion concepts to parameterize the higher order moments (Meyers, 1985; Meyers and Paw U, 1986). In any case, simulation of turbulent flows in the canopy environment with higher-order closure models has overcome some of the difficulties found with gradient diffusion models.

Several models are used to study ecosystem functioning and its response to environmental characteristics. We will briefly describe some of these models and, then, we will describe the main characteristics of ACASA model. The most well-known models are: Century model, LPJ model, and 3PG model.

Century model is developed by the Natural Resource Ecology Laboratory (NREL) of Colorado State University. It is a general model of plant-soil nutrient cycling which has been used to simulate carbon and nutrient dynamics for different types of ecosystems including grasslands, agricultural lands, forests, and savannas. The primary purposes of the model are to provide a tool for ecosystem analysis, to test the consistency of data and to evaluate the effects of changes in management and climate on ecosystems. Century is a model especially developed to deal with a wide range of cropping system rotations and tillage practices for system analysis of the effects of management and global change on productivity and sustainability of agroecosystems. The Century model simulates the long-term dynamics of Carbon (C), Nitrogen (N), Phosphorus (P), and Sulfur (S) for different Plant-Soil Systems.

The time step is monthly and the model requires the following driving variables as input:

- Monthly average max and min air temperature
- Monthly precipitation
- Soil texture
- Plant nitrogen, phosphorus, and sulfur content
- Lignin content of plant material
- Atmospheric and soil nitrogen inputs
- Initial soil carbon, nitrogen (phosphorus and sulfur optional)

These variables are available for most natural and agricultural ecosystems. Several sub models are included in Century: a soil organic matter decomposition sub model, a water budget model, a grassland/crop sub model, a forest production sub model, and management and events scheduling functions. The Soil-Organic-Matter (SOM) sub model is based on multiple compartments for SOM and is similar to other models of SOM dynamics. It includes three soil organic matter pools (active, slow and passive) with different potential decomposition rates, above and below ground litter pools and a surface microbial pool, which is associated with decomposing surface litter. The SOM side of Century accounts for Carbon, Nitrogen, Phosphorus and Sulphur cycles. The Century model also includes a simplified water budget model that calculates evaporation and transpiration water loss and water content of soil layers. Dynamics of grasslands, agricultural crops, forests and savanna systems are simulated, and these plant production sub models assume that the monthly maximum plant production is controlled by moisture, temperature, photosintetically active radiation and that maximum plant production rates decreased in nutrient limitation conditions (the most limiting nutrient constrains production). Century allows to model fertilizer use, irrigation, cultivation method, grazing, fire impact, CO_2 increases, and also precipitation and temperature statistics. The model output includes soil organic matter content, NPP, and GPP for different ecosystems.

LPJ (Lund Potsdam Jena Dynamic Global Vegetation) model is developed at the Max Planck Institute for Biogeochemistry, Jena, Germany. It is mainly used to understand vegetation dynamics and the terrestrial carbon cycle (Prentice et al., 2000; Sitch et al., 2003). The model has several features such as feedback through canopy conductance between photosynthesis and transpiration. These "fast" processes are coupled with other ecosystem processes including tissue turnover, population dynamics, soil organic matter and litter dynamics, and fire disturbance. The model approach is a mechanistic approach, modular, and the vegetation is grouped into a set of plant functional types. Photosynthesis, evapotranspiration, and soil-water dynamics are modelled on a daily time step. The model can run with temporal scale of hundred years and spatial scale of 0.5 degrees of latitude and longitude. The inputs are climate data from fields of monthly averaged temperature, total monthly precipitation and monthly averaged daily percentage of sunshine hours at appropriate spatial resolution. The model simulates processes at daily to decadal time scales.

The LPJ model is one of a family of models derived from the BIOME terrestrial biosphere model (Prentice et al., 1992). The model simulates the distribution of 10 plant functional types (PFTs) with different physiological (C3 or C4 photosynthesis), phenological (deciduous, evergreen), and physiognomic (tree, grass) attributes, based on bioclimatic limits for plant growth and regeneration and plant specific parameters that govern plant competition for light and water. Photosynthesis is calculated as a function of absorbed photosynthetically active radiation, temperature, atmospheric CO_2 concentration, day length, and canopy conductance using a form of the Farquhar scheme (Farquhar and Von Caemmerer, 1982; Collatz et al., 1991) with canopy-level optimised nitrogen allocation (Haxeltine and Prentice, 1996a, b) and an empirical convective boundary layer to couple the C and H_2O cycles (Monteith 1995). Soil hydrology is simulated using two soil layers (Haxeltine et al., 1996).

Annual NPP is allocated to the four carbon pools (representing leaves, sapwood, heartwood, and fine-roots) of each PFT population on the basis of allometric relationships linking height, diameter and the leaf-area to sapwood area ratio to these pools. Litterfall from vegetation enters separate above- and below

ground litter pools, which themselves provide input to a fast and a slow decomposing soil carbon pool. Decomposition rates of soil and below ground litter organic carbon depend on soil temperature and soil moisture (Lloyd and Taylor, 1994; Foley et al., 1996). Vegetation dynamics are modeled based on light competition, fire disturbance, re-establishment rates, and a set of temperature-related limits to survival or establishment (Sitch et al., 2003).

One of the limitations of the LPJ-DGVM is a pseudo-daily time step (linear interpolation of mid-month values). Indeed, dynamic of carbon fluxes and pools, biomass burnt and soil water content should be described by a set of non-linear equations at a daily time step. Due to non-linearity of these equations, an application of interpolated linearly daily temperature and precipitation from their mid-month values does not allow reliable estimates of daily carbon and water fluxes needed for contemporary studies in atmospheric chemistry and climatology.

3PG (Physiological Principles in Predicting Growth) model is a stand growth model based on physiological processes (Landsberg and Waring, 1997). It is a process-based model that provides a tool that can be used to simulate growth and yield of forest stands and the effects of environmental factors on growth. It can also be used as an analytical tool to evaluate the probable effects of altering, by breeding or selection, the physiological processes that govern tree growth. 3PG can be used to evaluate site potential and analyze the probable effects of varying growing conditions or management actions such as thinning or fertilization. It has considerable potential as a tool for estimating carbon sequestration by forests and plantations and has been shown to be a very valuable teaching tool. The model requires, as inputs, standard weather data, and information about soil depth and water- holding characteristics. It works on monthly time steps and requires as input data:

- Values of total short wave (375-2500 nm) incoming radiation
- Monthly mean day-time vapour pressure deficit
- Total monthly precipitation

- Number of day per month with frost
- Values of initial biomass
- Soil characteristics and maximum available soil water
- Canopy characteristics and stand properties

Each of these model is a useful tool to estimate physiological processes and energy and carbon fluxes, but it works using monthly input data. In this research we choose to use the ACASA model, which has the advantage of a higher order-closure model. It is a complex model, but it gives more information about fluxes and turbulent profiles within and above canopy that are needed for this research.

4.2 ACASA higher-order closure model

The Advanced-Canopy-Atmosphere-Surface Algorithm (ACASA) is a higher-order closure model (Pyles et al., 2000a; b; Pyles et al., 2003). Specifically, it uses third-order equations to estimate fluxes of heat, water vapour, and momentum within and above canopy. It also estimates turbulent profiles of velocity, temperature, and humidity within and above canopy. ACASA uses twenty atmospheric layers (ten within the canopy and ten above the canopy) and 15 layers into the soil. Surface energy fluxes are estimated either for wet or dry canopies elements, and they are estimated for nine sunlit angle classes and one shaded class within each canopy layer. ACASA can be used alone or it can be coupled with other models. Pyles et al. (2003) showed the results of ACASA model coupled with a mesoscale climate model (MM5). Coupling of ACASA with a mesoscale model gives an advanced representation of complex relationships among soil, canopy turbulent microenvironment, and plant physiological state in an atmospheric model.

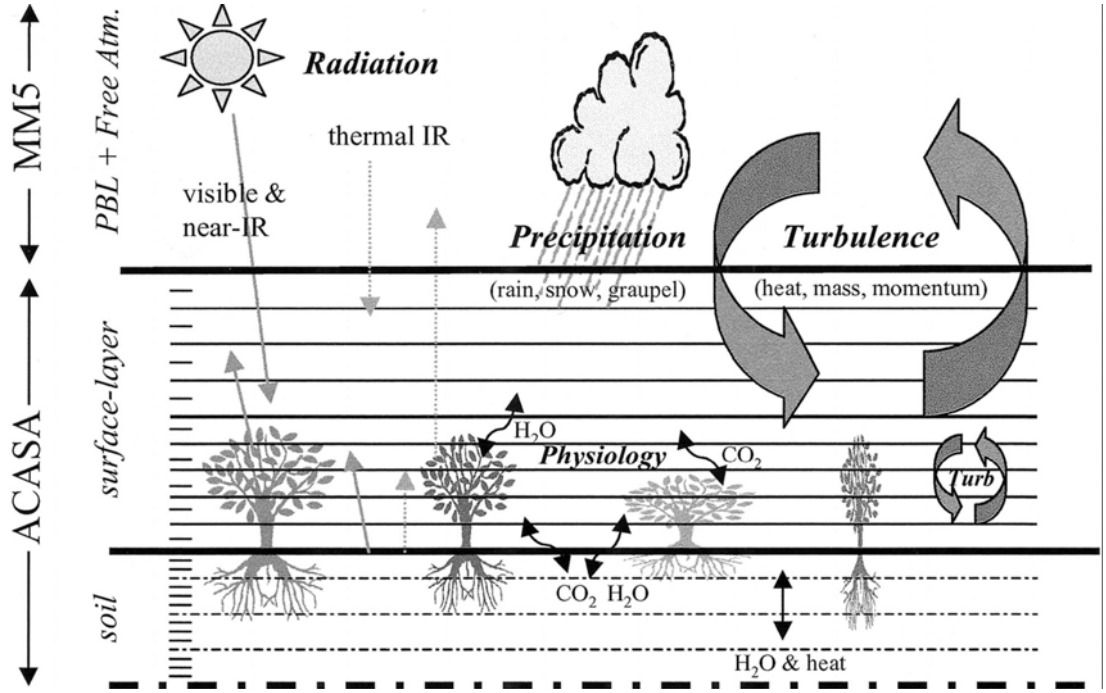

Figure 5. Visual representation of MM5-ACASA.

Figure 5 shows the scheme of MM5-ACASA coupling. ACASA is used to estimate energy and mass fluxes, and plant physiological characteristics in the soil (15 layers) and in the canopy (10 layers within canopy and 10 layers above it). MM5 is used to simulate regional scale atmospheric circulation.

ACASA has been used over forest ecosystem (Pyles et al., 2000a; b; Pyles et al., 2003), but it can also be used in different ecosystem. In this research, ACASA model is tested over maquis and grapevine ecosystems. ACASA simulates energy and mass fluxes indifferently over land and water. Urban ecosystem can be also investigated using the ACASA model. This is an important use of the model because gives the possibility to know how cities respond to atmospheric global change. As for vegetation, urban ecosystems can be a carbon *sink* or *source*. The knowledge of their behaviour regarding to the atmospheric carbon allows a better manage of the city and to take political decisions following the Kyoto Protocol suggestions.

5. MICROMETEOROLOGICAL MEASUREMENTS

Micrometeorological techniques are useful tools to obtain short and long-term measurements of energy and mass exchanges between the vegetation and atmosphere. They represent the standard methodology used in all international and regional networks of ecosystems monitoring. Actually, models are also used to estimate energy and mass exchange in an ecosystem, but they require measured data to evaluate their performance and accuracy. So, micrometeorological techniques are important either to obtain direct measurements or to contribute to model development.

Continuous flux measurements give direct information on the net CO_2 exchange (NEE) between the atmosphere and vegetation (Baldocchi, 2003). At the beginning of ecosystem study, the energy and mass fluxes were investigated at level of single leaf using simple instruments (e.g., cuvettes) (Field et al., 1982; Collatz et al., 1991) or at whole plant level (Denmead et al., 1993). Soil was investigated using chambers (Livingston and Hutchinson, 1995; Goulden and Crill, 1997). Although cuvette and chamber systems are able to measure diurnal variations of carbon fluxes and to define environmental response functions (Schulze and Koch, 1969; Collatz et al., 1991), they may produce biases and artefacts.

Micrometeorological techniques are the first means to study such processes on canopy and ecosystem scale, thus avoiding difficult up-scaling problems. They are the only direct means of measuring canopy-atmosphere mass and energy exchanges. The main advantages of micrometeorological methods are

- They are *in situ,* so they are non-intrusive methods, and they do not alter surface under investigation.
- They can be applied on a quasi-continuous time basis making possible to study both short-term variations (e.g., diurnal cycle) and long-term balances.

- Measurements made at one point represent a really-averaged ensemble of mass and energy exchange, with a length scale of 100 m to 2 km.

Main micrometeorological methods to assess mass and energy exchange across the landscape-atmosphere interface are:

1) Eddy covariance
2) Flux gradient
3) Eddy accumulation
4) Mass balance method
5) Surface Renewal

This research presents results based on the EC method because it is commonly applied in all international and regional flux networks. While the other methods are older than EC or they are newer (i.e, Surface Renewal), they still need EC measurements to confirm their performance.

5.1 Eddy Covariance technique

5.1.1 Theory

Theoretical bases for the EC method was established by Sir Osborne Reynolds (Reynolds, 1895), but a lack of adequate instrumentation delayed the application of the method until 1926 (Scrase, 1930). First EC studies were conducted over short vegetation with extremely level terrain and windy, sunny climates. The studies focused on the structure of turbulence in the atmospheric boundary layer, and on the transfer of heat and momentum (Kaimal and Wyngaard, 1990). They did not concentrate the attention on the CO_2 exchange.

In 1950s-1960s studies were conducted over short and ideal agricultural crops (Lemon, 1960; Monteith and Szeicz, 1960) and they investigated on the CO_2 fluxes. Measurements were made using the flux-gradient method because of the lack of fast responding anemometers and CO_2 sensors. The flux gradient method was also used over forest in 1960s and 1970s (Denmead, 1969; Jarvis et al., 1976), but it was difficult because of the different behaviour between forest and short canopies.

The first EC measurements of carbon dioxide exchange occurred in the early 1970s (Desjardins and Lemon, 1974; Desjardins, 1974). The development and commercial availability of sonic anemometers, fast response hygrometry, and infrared spectrometry in the early 1980s led to an increase in these studies. EC method was used over native vegetation, such as temperate deciduous forests (Wesely et al., 1983; Verma et al., 1986), a prairie grassland (Verma et al., 1989; Kim and Verma, 1990), a tropical forest (Fan et al., 1990) and Mediterranean maquis (Valentini et al., 1991). After 1990, the duration of EC measurements increased and Wofsy et al (1993) were the first to conduct the study of CO_2 exchange with EC technique over the year.

Since 1993, additional EC studies measuring CO_2 and water vapour exchange were conducted over forests in North America (Baldocchi, 1997b; Goulden et al., 1996; Greco and Baldocchi, 1996), Japan (Yamamoto et al., 1999), and Europe (Valentini et al., 1996; Valentini, 1998; Dore and Valentini, 2002). Studies were also conducted over agricultural crops (Spano et al, 2000), in

different environmental conditions, and in flat or complex terrains (Magliulo et al., 1998; Sirca et al., 2001; Drexler et al., 2004; Paw U et al., 2004).

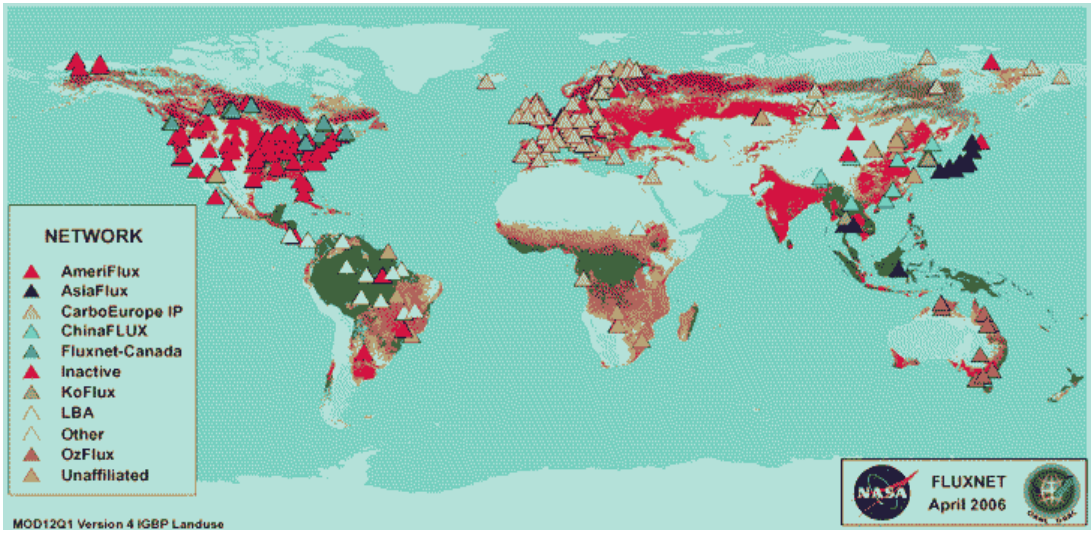

Figure 6. International networks of energy and mass fluxes monitoring, combined into the global network FLUXNET.

A global network of research teams (FLUXNET) was formed to continuously monitor energy and mass fluxes over a spectrum of ecosystems. Measurements are inserted into the regional CarboEuroflux (Aubinet et al., 2000; Valentini et al., 2000), AmeriFlux (Running et al., 1999), Fluxnet-Canada, China-Flux, AsiaNet, Ozflux and LBA (Brazil) networks, and they are combined into the global network, FLUXNET (Figure 6) (Valentini et al., 1999).

The application of the eddy covariance method requires some assumptions, which are

- Steady-state conditions
- Horizontal homogeneity in source-sink
- Flat topography

If these assumptions are satisfied, the vertical EC measured flux (i.e., the covariance between the vertical wind velocity and scalar concentration fluctuations) is equal to the scalar flux

$$F = \overline{w'c'} \tag{5.1}$$

where w is the vertical wind speed, and c is the quantity of interest (e.g., temperature, humidity or gas concentration). The overbar denotes the time average, and a prime denotes the fluctuation of an instantaneous value (w) from the average ($\overline{w}$) as showed in the following equation

$$w' = w - \overline{w} \tag{5.2}$$

The flux is directed downward when F<0 and it is directed upward when F>0 (Baldocchi et al., 1988).

EC measurements are carried out using fast response instruments sampling typically at 10–20 Hz to cover the entire frequency range of turbulent variations. Direct measurements of energy and mass fluxes are, hence, made through high frequency measurements of vertical wind velocity and scalar (Baldocchi et al., 1988; Wofsy et al., 1993). For CO_2 flux, such measurements are feasible using a sonic anemometer and a fast-response infrared gas analyzer.

EC methodology is derived from the law of mass conservation (Stull, 1988)

$$\frac{\partial \rho_s}{\partial t} + \frac{\partial u\rho_s}{\partial x} + \frac{\partial v\rho_s}{\partial y} + \frac{\partial w\rho_s}{\partial z} = S \tag{5.3}$$

where ρ_s is the scalar density, S is the *sink*/*source* term, and u, v and w are the wind velocity components in the x, y and z directions of a rectangular coordinate frame, respectively. Molecular diffusion is significant only in the molecular sublayer (i.e., within the first centimeters of the surface), and the molecular sublayer is considered part of the surface being included in the *sink*/*source* term (Stull, 1988). Using the Reynolds' decomposition (Garratt, 1992), the instantaneous values of u, v, w and ρ_s are divided into an average and a

fluctuation (Eq. 5.2). Averaging over time and assuming that air is incompressible, the following equation is obtained

$$\frac{\partial \overline{\rho}_s}{\partial t} + \underbrace{\overline{u}\frac{\partial \overline{\rho}_s}{\partial x} + \overline{v}\frac{\partial \overline{\rho}_s}{\partial y}}_{\text{II}} + \underbrace{\overline{w}\frac{\partial \overline{\rho}_s}{\partial z}}_{\text{III}} + \underbrace{\frac{\partial \overline{u'\rho_s'}}{\partial x} + \frac{\partial \overline{v'\rho_s'}}{\partial y}}_{\text{IV}} + \underbrace{\frac{\partial \overline{w'\rho_s'}}{\partial z}}_{\text{V}} = \underbrace{S}_{\text{VI}} \qquad (5.4)$$

I

where *I* represent the local time rate of change in scalar mixing ratio (storage), *II* and *III* are the horizontal and vertical advective fluxes of the ρ_s, respectively, *IV* and *V* are the horizontal and vertical flux divergences, respectively, and *VI* represents the *sources* and *sinks* of the constituent. Horizontal flux divergence (*IV*) is significantly smaller than the vertical flux divergence (*V*) and may be neglected (Finnigan, 1999). Integrating from the surface (z=0) to the measurement height (z=h) and setting $\overline{w'\rho_s'} = 0$ at the surface, the equation becomes

$$\overline{w'\rho_s'}_{z=h} = \underbrace{\int_0^h S dz}_{\text{V}} - \underbrace{\int_0^h \frac{\partial \overline{\rho}_s}{\partial t}}_{\text{VI}} - \underbrace{\int_0^h \overline{u}\frac{\partial \overline{\rho}_s}{\partial x}dz - \int_0^h \overline{v}\frac{\partial \overline{\rho}_s}{\partial y}dz}_{\text{II}} - \underbrace{\int_0^h \overline{w}\frac{\partial \overline{\rho}_s}{\partial z}dz}_{\text{III}} \qquad (5.5)$$

I

Assumptions made earlier (i.e., steady-state conditions, horizontal homogeneity in *source-sink*, and flat topography) are usually valid. Generally, they do not cause significant error using the EC method (Aubinet et al., 2000; Finnigan, 1999). The stationarity and the horizontal homogeneity are assumptions that are usually stated as prerequisites for EC measurements. Under such ideal conditions, the storage term (*I*) and the horizontal advection term (*II*) are negligible. The mean vertical wind speed is typically small, especially above short vegetation, and it may be assumed that the vertical advection term (*III*) also vanishes. Under ideal conditions, the EC turbulent flux at a height h would equal the integrated *sources* and *sinks* below the measurement height.

CO_2 flux is defined as (Aubinet et al., 2000)

$$\overline{w'\rho'_s}_{z=h} = \int_0^h Sdz = NEE \qquad (5.6)$$

where the *source* term includes the soil respiration.

If the assumptions are not satisfied, errors occur in the flux estimates. Paw U et al. (2000) calculated new equation to account for situation when both advection and air density variation are present. They found that under low turbulent conditions (especially during the night) the mean horizontal and vertical advection (*II*, *III*, equation 5.4) and the storage terms (*I*, equation 5.4) should be estimated.

EC technique allows for estimation of turbulent transport of the following scalars (Rosenberg et al., 1983; Verma, 1990)

- Sensible heat flux $H = \rho Cp\overline{w'T'}$ (W m^{-2}) (5.7)
- Latent heat flux $LE = L\overline{w'q'}$ (W m^{-2}) (5.8)
- Carbon dioxide flux $F_c = \overline{w'c'}$ (μmol m^{-2} s^{-1}) (5.9)
- Momentum flux $\tau = -\rho\overline{u'w'}$ (kg $m^{-1}s^{-2}$) (5.10)
- Friction velocity $u^* = \sqrt{\overline{u'w'}}$ (m s^{-1}) (5.11)

where u and w are the horizontal and vertical velocities, ρ is the air density, q is the absolute humidity, c is the carbon dioxide concentration, T is the air temperature, Cp is the specific heat of the air, and L is the latent heat of vaporization.

5.1.2 Instrumentation

An Eddy Covariance system consists of a sonic anemometer, an Infrared Gas Analyzer (IRGA), and a temperature, humidity probe (Figure 7). This system can measure carbon dioxide flux, latent heat flux, sensible heat flux, momentum flux, temperature, humidity, horizontal and vertical wind speed and wind direction.

Figure 7. The EC system constituted by a 3-D sonic anemometer an infrared gas analyser, and a temperature and humidity probe.

The EC system also needs a data logger to collect data, a laptop, and a power system. The laptop, using an adequate software, allows the data acquisition and the archival of raw data files (Figure 8). The data are processed, in the office to obtain fluxes.

In the following section, a description of the sonic anemometer and infrared gas analyser features is provided.

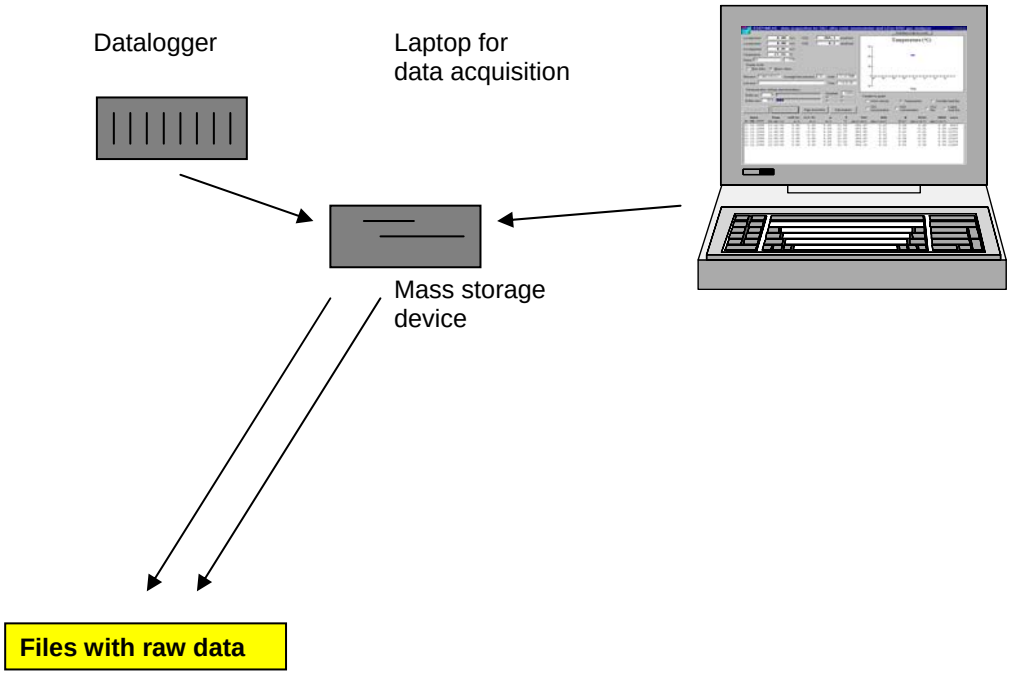

Figure 8. Schematic representation of data acquisition system.

Sonic anemometer

Turbulence measurements are made using a sonic anemometer, which uses the propagation speed of sound between points of known separation to determine the speed and direction of the moving air mass. The still air speed of sound is not a constant, but it is mainly a function of temperature and atmospheric pressure.

The 3-D sonic anemometer uses three pairs of non-orthogonally oriented transducers (Figure 9) that can serve alternately as transmitter and receiver. The transducers take two measurements, in opposite directions, of the sound propagation velocity. The anemometer determines the propagation velocity by measuring the time of flight (TOF) of a sonic impulse from transmitter to receiver. Transmit and receive functions are then swapped, and a second TOF measurement is taken by the transducers. The result is the wind velocity parallel to the line between the two transducers. The signal is measured at high frequency (10-20 Hz). Velocity measured in one direction is equal to the sound's speed emitted plus the air velocity. In the opposite direction, it is equal to the sound's speed emitted minus the air velocity. Therefore, the air velocity between the transducers, w, is

$$w = \frac{d}{2}\left(\frac{1}{t_1} - \frac{1}{t_2}\right) \qquad (\text{m s}^{-1}) \tag{5.12}$$

where d is the distance between the transducers (m), and t_1 and t_2 are the time that signal takes to go from each transducers (s). The sonic anemometer calculates in the same manner the other wind components, u, and z.

The sound's speed (c) is also calculated as

$$c = \frac{d}{2\cos\alpha}\left(\frac{1}{t_1} + \frac{1}{t_2}\right) \qquad (\text{m s}^{-1}) \tag{5.13}$$

where α is the angle between the sound's speed direction and the horizontal line between the transducers, and it is calculated as

$$\alpha = \sin^{-1}\left(\frac{v}{c}\right) \tag{5.14}$$

The sound's speed is directly related to the air density (e.g., temperature and humidity).

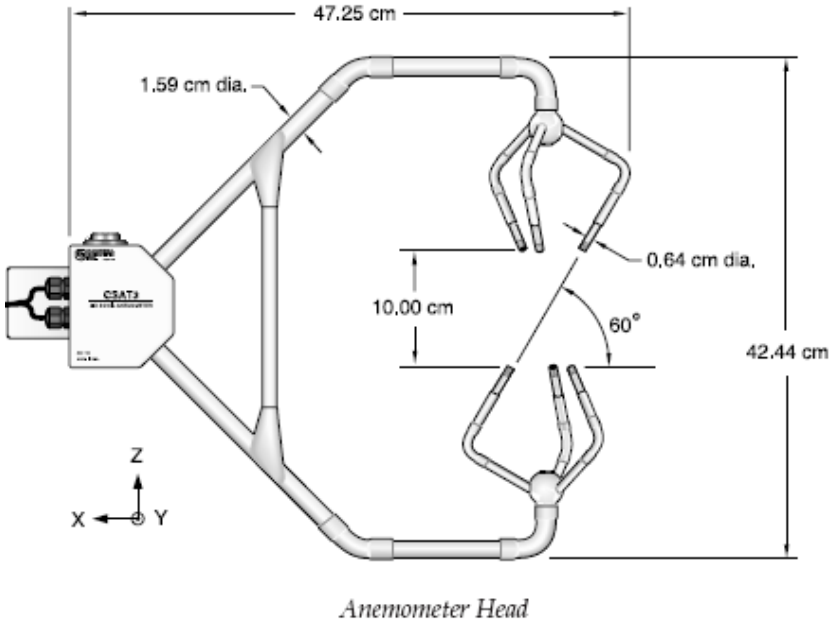

Figure 9. The head of the CSAT3 sonic anemometer (from Campbell Scientific).

From *c* it is possible to calculate the air temperature (Moncrieff et al., 1997a)

$$c = 403T_a\left(1 + 0.32\,e/P\right) \tag{5.15}$$

where *e* is the air water vapour pressure, *P* is the atmospheric pressure, and *Ta* is the air temperature.

Air temperature can also be calculated by the sonic temperature (*Ts*) obtained by the anemometer as follow

$$T_s = \frac{c^2}{403} = T_a\left(1 + 0.32\,e/P\right) \tag{5.16}$$

Sonic temperature is close to the virtual temperature or potential temperature (θ), according to Stull (1988)

$$\theta = T_a\left(1 + 0.38\, e/P\right) \qquad (5.17)$$

Sonic temperature can not be used for calculation of *H* when wind speed is more than 8-10 m s^{-1} because of mechanical deformation of the probe head (Grelle and Lindroth, 1996). Under this limit, one can use the sonic or virtual temperature to calculate *H*, but it is necessary to apply the Schotanus correction for the humidity. Using the sonic temperature without applying the correction leads to overestimate *H* (Schotanus et al., 1983). Some sonic anemometers can set a fine wire thermocouple to directly obtain fast air temperature measurements.

Sonic anemometers work in a temperature range between -30°C to +50°C, with wind speed < 30 m s^{-1} and wind angles between ± 170°. Accuracy is determined primarily by the distance between the transducers. Most sonic anemometer designs include microprocessor or microcontroller that can determine the quality of the collected data. If the microprocessor determines that a measurement can not be made, the sensor reports that a data is missing instead of providing an incorrect value. The small size and fixed orientation of the transducers allow them to be heated at minimum power expense to prevent icing.

Infrared Gas Analyser

Concentration of CO_2 and H_2O are measured using an Infrared Gas Analyser (IRGA). Every compound (e.g., CO_2 and H_2O) absorbs infrared radiation (FIR) at a certain wavelength, and the absorption is proportional to its concentration. The IRGA measures the FIR attenuation in the air between FIR *source* and FIR detectors. The detectors absorb at a wavelength of 4.26 μm for CO_2 and 2.59 μm for H_2O, and they calculate CO_2 and H_2O concentration in the analyzed air. These features minimize sensitivity to drift and dust, which can accumulate during normal operation.

Two types of gas analyser exist: closed path and open path. The **closed path** system has two chambers, (1) an analysis chamber where air pass through, and (2) a chamber of reference where air is without CO_2 and H_2O. Air is carried into the first chamber by a tube. CO_2 and H_2O concentration is given by the

difference of the two chambers values. The transport from the sampling point to the IRGA is made using a pump action. It induces a time lag between *u*, *v* and *w* data, and CO_2 and H_2O data. For the closed path, an appropriate time lag value is needed (Moncrieff et al., 1997a). The **open path** system has no chambers or transportation system, so there is not time lag. The most used open path system is the LICOR 7500 (Campbell Scientific, USA), and it allows fast, precise measurements of in situ CO_2 and H_2O densities, which are present in turbulent air structures. In EC studies, CO_2 and H_2O densities are used in conjunction with sonic anemometer turbulence data to determine CO_2 and H_2O fluxes.

The IRGA works at high speed and it has an accuracy of 1% over a range between 0 and 3,000 ppm. It operates over a temperature range of -25°C to +50°C. The open path system LI-7500 needs a factory calibration and a user calibration. The *factory calibration* consists of determining the values of the calibration coefficients. *User calibration* (performed weekly or monthly) consists of setting analyzer zero and span. The accuracy of the LI-7500 depends on both calibrations. The calibration coefficients determined at the factory should be valid for several years. The zero and span settings make the analyzer's response agree with the previously determined factory response at a minimum of two points. Gases calibration of 1% accuracy can often be obtained without much difficulty.

5.1.3 Response time

Instrumentation used for EC measurements must be fast enough to capture the variation of the phenomena under investigation. This is necessary to avoid an aliasing problem, which occurs when the trend obtained does not correspond to the real trend. Near the surface, vegetation roughness creates eddies with the rotation frequency (*n*)

$$n = \overline{u} / l \tag{5.18}$$

where $\overline{u}$ is the mean wind velocity and *l* is the eddy diameter.

Eddy frequency is a useful parameter in the spectral analysis of turbulence. Because $\overline{u}$ values change with height, to compare spectra obtained at different height it is necessary to use a normalized frequency (*f*)

$$f = n(z-d)/u \tag{5.19}$$

where *z* is the measurement height, *d* is the zero plane displacement and *(z-d)* corresponds to the height above *d*. Usually, *(z-d)* = 0.7 to 0.8 *h*, where *h* is the vegetation height. In most cases, fluxes are transported by eddies with a frequency range between 0.001 to 10. For example, if the normalized frequency is *f* = 10, the mean wind speed u =3 m s^{-1}, the measurements height is *z*=3 m, then the maximum frequency of response for the sensors must be

$$n = 10u/(z-d) = 10 \qquad \text{(Hz)} \tag{5.20}$$

It seems that a response frequency of 5-10 Hz is adequate to obtain fluxes above crop and forest. Measurement height is, usually, equal to 1.3-1.5 times the vegetation height.

The calculation of the covariance between the wind speed *w* fluctuations and the scalar fluctuations for estimating fluxes is made on a period of 15-30 minutes to avoid changes of the mean and to include turbulent part fluctuations.

5.1.4 Corrections and data quality check

To apply the EC method it is necessary to meet the assumptions of steady state conditions, horizontal homogeneity in *source* and *sink*, and flat topography. The assumptions are only satisfied in ideal sites. Natural environment, rarely, satisfies the ideal conditions. The main problems in real sites are, usually, due to three kinds of errors (Baldocchi et al., 1996; Goulden et al., 1996):

1. **Systematic uniform errors,** are constant and independent by environmental conditions, due to several factors depending on

instrumentation (e.g., not corrected calibration, low speed of response, inadequate distance between sensors).

2. **Systematic selective errors**, due to environmental conditions (e.g., flux underestimates during calm wind period).
3. **Uncertainty of sampling**, when uncompleted or approximate datasets are used for estimating long term exchanges between the vegetation and atmosphere (e.g., due to malfunctioning of instrumentation or unsuitable measurement conditions).

Problems can also occur when surfaces have different characteristics, or with extreme weather conditions (high wind speed or wind too much weak), or when the terrain is not flat and topography is complex.

When assumptions are not satisfied and some problems listed above are met, then errors can occur in flux estimates. Therefore, it is necessary to make corrections to obtain reliable flux estimates (Foken and Wichura, 1996; Moncrieff et al., 1997b; Aubinet et al., 2000). Screening and corrections are made during the raw data "processing." In addition, quality controls need to be made to make sure that data are reliable.

In this research, data corrections and quality check controls were made, so a brief description of main corrections and quality controls needed to correctly apply the EC method is presented in the Appendix.

5.1.5 Footprint analysis

EC data (*H* and *LE*) are affected by fluxes over large surfaces. Knowledge of the soil and vegetation area that influences flux and concentration measurements is important both in planning the site configuration and in understanding if the collected data are valid. Commonly, measurements used to infer such surface flux estimates are conducted at an appropriate height, with instruments mounted on a mast or tower. A factor of 100 times the effective sensor height in the horizontal is given as a first approximation for the horizontal fetch (or upwind distance of similare surface) requirement (Baldocchi et al.,

1988). It is important to consider whether the fluxes measured at a height *z* are representative of the ecosystem under investigation.

Due to the combination of horizontal advection and vertical turbulent diffusion, such instruments are exposed to the surface influence of a potentially large area: the surface *source area*. The *source area* is the area representing the source of surface information that reaches the instrument; the "field of view" (Schmid, 1994). Thus, every micrometeorological point measurement represents a spatial average of surface conditions. The scale of this spatial average, and thus of the observation, depends on the type of quantities involved in the measurements (e.g., radiation, scalar flux, scalar concentration profile), on the measurement height, the stability, and the intensity of cross-wind turbulence. This scale can be determined by footprint models or *source area* models designed for the relevant method of measurement.

Over the last decade, numerous investigators have applied Lagrangian (Leclerc and Thurtell, 1990; Horst and Weil, 1992; Flesch, 1996) and Eulerian (Gash, 1986; Schuepp et al., 1990; Horst and Weil, 1992; Schmid, 1994; Leclerc et al., 1997) diffusion theory to assess "flux footprints" in the surface boundary layer *above* vegetation and across horizontal inhomogeneities (Luhar and Rao, 1994). Baldocchi (1997a) has conducted the first study to assess "flux footprint" *within* the canopy. Schimd (2002) has proposed a review of the different footprint models available to use.

The objective of the measurements is to capture the signal that reflects the influence of the underlying surface on the turbulent exchange. This is not a problem over a homogeneous surface, but it is difficult in surfaces with inhomogeneous characteristics. Over inhomogeneous surface, in fact, the measured signal depends on which part of the surface has the strongest influence on the sensor, and thus on the location and size of its footprint. Canopy structure and topography have a big influence on the *source area*. A tall canopy versus a short canopy or flat terrain, with varying atmospheric stability throughout the day and night, will create various size turbulent eddies that bring energy and scalars fluxes into and out of an ecosystem. Footprint functions depend on the measurement level and differ for fluxes and concentrations (Schmid, 1994). So,

different terms of the mass-balance equation have different spatial contexts (Schmid, 2002). Thus, footprints are expected to be useful in defining the spatial context influencing tower flux measurements, but not to estimate ecosystem exchange in complex terrain.

The footprint of a measurement is the transfer function between the measured value and the set of forcings on the surface–atmosphere interface. Formally, this notion is expressed in an integral equation, following Pasquill and Smith (1983)

$$\eta(r) = \int_{\Re} Q_{\eta}(r + r') f(r, r') dr' \tag{5.21}$$

where η is the measured value at location r, $Q_{\eta}(r + r')$ is the distribution of *source* or *sink* strength in the surface-vegetation volume, and $f(r, r')$ is the footprint or transfer function, depending on r and on the separation between measurement and forcing, r'. The integration is performed over a domain $\Re$.

Figure 10 shows a schematic representation of the footprint function and of the sensor relation at height above the surface. The value of the footprint function or *source* weight (*f*) rises to a maximum at some distances upstream and falls off smoothly to all sides. The integral beneath the footprint function expresses the total surface influence on the signal measured by the sensor. The *source area* can be determined using various atmospheric stability parameters and information about the canopy structure.

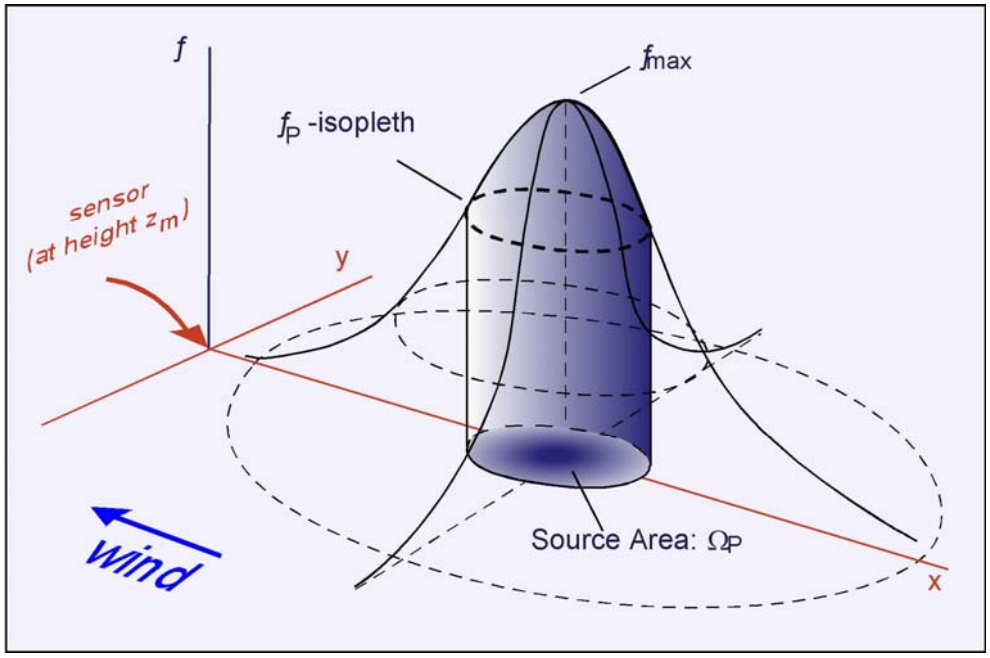

Figure 10. The source area based on a Gaussian distribution from a maximum source.

The average values for the footprint model are: an instrument reference height (z_m), the surface roughness length (z_o), which is based on the height where wind speed goes to zero (Monteith, 1973), the frictional velocity u^*, the Obukhov length L, and the standard deviation of lateral wind speed fluctuations σ_v (i.e., magnitude of the cross wind turbulence) (Schmid, 1994).

6. MEDITERRANEAN ECOSYSTEMS

A maquis and a grape ecosystem were studied in this research to improve our knowledge on the behaviour of these ecosystems as a *source* or *sink* of carbon. They were also investigated on the energy and water vapour fluxes. The results provide information on the potential influence of the ecosystems on climate and on the response of the ecosystems to climate change.

6.1 Maquis

Mediterranean maquis is a sclerophyllous species of shrubs that are always green, with leathery leaves, small height, and with a moderately sparse canopy. It is adapted to live in a semi-arid climate. The name Mediterranean maquis is used because this vegetation is the most representative in the Mediterranean area. We can, however, find maquis in four regions with similar climate that are outside of the Mediterranean area. These areas are between 30° and 45° degrees north and south latitude. The regions are characterised by a climate having most of precipitation during the winter, a long period of summer dryness, high variability in annual precipitation, and a hot summer and cool winter with short periods with snow and frost. The regions with Mediterranean maquis are located in the Mediterranean basin, California, Chile, South-Africa, and southern Australia (Figure 11) (Specht, 1969; Valiente-Bonuet et al., 1998; Spano et al., 2003).

Figure 11. Global distribution of areas with Mediterranean maquis (from Spano et al., 2003).

The name of the maquis-type vegetation varies with location. It is called "maquis" in the Mediterranean basin countries, "chaparral" in California, "matorral" in Spain and Chile, "mallee scrub" in southern Australia, and "finbos" in South Africa (Specht, 1969; Di Castri et al., 1981). In Italy, maquis covers an area of about 900,000 ha.

Most representative species in Mediterranean maquis are arbutus (Arbutus unedo L.), lentisk (Pistacia lentiscus L.), oleaster (Olea europaea L. var. sylvestris), phyllirea (Phyllirea latifolia L. and Phyllirea angustifolia L.), true myrtle (Myrtus communis L.), juniper (Juniperus spp.), heather (Erica spp.), rockrose (Cistus spp.) and other shrubs and trees such as live oak (Quercus ilex L.). In addition, there are other annual or perennial species that are considered maquis (Mooney and Dunn, 1970; Specht, 1969).

Recall that Mediterranean maquis is widespread in semi-arid climates, so it is adapted to live in severe water stress conditions (i.e., hot summers and winter

precipitation). The plants can adapt to stress conditions through the following mechanisms:

- **drought avoidance,** allows the plants to postpone tissue dehydration when available by allowing an osmotic adjustment to maintain cell turgor and delay leaf wilt (Aber and Melillo, 1991; Jones, 1992).
- **drought tolerance,** is the ability of the plant to survive and produce under periods of limited moisture. Plants can exhibit various reactions to drought stress depending on their genetic makeup.

One can quantify a plants ability to adapt to stress using **water use efficiency**, which is the ratio of the CO_2 assimilation to the transpiration (μmol CO_2 per mmol H_2O). Maquis species have morphological characteristics that avoid drought by reducing losses of water. Maquis leaves are always green, small and leathery, and with a thick cuticle. The cuticle is often covered by hair or wax. The leaves have a well developed palisade mesophyll, and they are mostly hypostomatous (i.e., with stomata on the underside the leaf). The stomata guard cells are located deep within the lower epidermis, which allows CO_2 absorption with minimal transpiration loss. These water-stress adaptive morphological characteristics are called "sclerophyll."

To optimize the water use efficiency (WUE), sclerophyll species increase photosynthesis relative to transpiration, so the water loss per unit of dry matter produced is reduced. The WUE term is important because is an useful mean to monitor adaptation of species to drought (Lauteri et al., 1997). In the Mediterranean maquis ecosystem, the vegetative activity is concentrated during the spring and fall when drought and high temperature are not limiting factors and water and nutrient are widely available.

Grime (1977) suggests a classification of maquis based on the strategies adopted by plants to survive in different environments. Stress due to low availability of water, and nutrients and disturbance due to fire, frost, animals, and diseases are the environmental factors that most affect biomass production. Plants follow a *stress-tolerator strategy (S)* in environments with high stress factors and

low disturbance, and they follow *ruderal strategy (R)* in environments with high disturbance and low stress factors. In both cases, the species have a short life cycle and fast growth. If there are low disturbance and low stress factors, plants are *competitive (C)* in regards to other species.

Typical maquis species are present in environments with high disturbance and stress, so the Mediterranean maquis ecosystem exists in a difficult environment where climate change or other changes make them particularly vulnerable. Maquis is considered a *secondary* formation because it grows in regions where disturbing factors eliminated the primary live oak forests. The *secondary* maquis dominated over the live oak forest because of livestock grazing, wildfire, and logging. On the other hand, *primary* maquis grows in areas without live oak where environmental factors limit arboreal vegetation (Pignatti, 1978; Barbero et al., 1989). Maquis is mostly present along coastal areas where it is threatened by human presence (tourism, streets, railroads, and cities). These disturbance factors reduce the number of species and, hence, biodiversity (Davis and Richardson, 1995).

Maquis is important to avoid rainfall and wind erosion processes and to maintain soil properties. Consequently, a decrease in maquis biodiversity will negatively affect the benefits that maquis provide to soils (Piccini and Piotto, 2001). In addition, reduced biodiversity is detrimental to genetic diversity, and it affects the ability of the maquis ecosystem to adapt to climate change (Mueller-Starck, 1989). In fact, global climate change resulting from temperature and carbon dioxide increases could alter equilibrium within the ecosystem and put in danger the maquis survival (Rossi et al., 1999).

6.2 Grape vineyard

Grapes are the largest fruit crop on Earth and grow around the globe in the temperate bands between 20° and 50° north or south latitude. They grow at elevations from sea level to about 1,000 meters. They are successfully grown in the Balkans area, Asia, Mediterranean basin, South Africa, South Australia, New Zealand, North America, and a good portion of South America. More than half of the global production, however, comes from Europe with the main production in Spain, Italy and France (Figure 12).

Vitis vinifera is commonly known as the European grapevine; however, really should be defined as euro-asiatic. The area origin is not well-known, but it likely that the grapevine originated in the Caucasus. In fact, there are Sumerian writings of the first half of III millennium that mention using grapes to produce wine.

Grapevines are fairly adaptable plants, growing in a wide variety of soil types, from light sand to packed clay, and they have good adaptation to climate. The distribution of viticulture is related to natural and social conditions of the regions, and climatic adaptation varies by species. The extreme latitude and/or elevation limitations are mainly due to frost.

The grapevine prefers the temperate climate where it evolved (i.e., with warm, dry summers and mild wet winters). They are not adapted to the cooler parts of the temperate zone, where growing seasons may be too short to allow the fruit to reach maturity or where low winter temperatures (less than -15°C) may kill the vine. Late spring frosts can cause considerable damage to the fruit, so wine grapes are not a good crop in regions with a high probability of temperatures at or below about -2°C during or after bud break in the spring. High humidity can also have negative effects on grape production because of vine diseases.

Grapevines need adequate precipitation during winter and spring and/or irrigation during the summer in dry regions for good production and quality. Severe summer drought affects vine production because severe water stress can reduce both yield and fruit quality. Moderate water stress is generally considered beneficial for wine grape production as long as the stress allows the plants to

maintain leaf functions. Severe vine stress, however, negatively affects physiological parameters (e.g., a decrease in net photosynthesis and transpiration rate) (Smart and Robinson, 1991; Sivilotti et al., 2005). Some researchers report that a moderate level of stress might be attained by maintaining the root-zone at soil water content varying between -0.4 to -0.6 MPa of predawn leaf water potential ψ_{PD} (Smart and Coombe, 1983; Ojeda et al., 2002). On the other hand, a decrease in fruit quality occurs when summer and fall rainfall causes a low level of sugar and high acid content. Rainfall can also lead to problems with mildew and other diseases.

Vitis vinifera shows wide adaptation to soils and it is commonly graphed to American rootstocks, which are more resistant to Phylloxera. Soil composition is an important factor because it affects quality and quantity of grape production. Soil directly affects chemical and physical fruit composition and colour. Therefore, when soil composition is altered the effects can be seen overall in an alteration of quality production.

Grapevine trellising methods vary around the world. The main growing systems used in Italy are: Geneva Double Curtain (GDC), overhead, single curtain, vertical shoot-positioned (VSP), high bush, and short bush. Each training system has unique effects on the canopy and microclimate. Smart and Robinson (1991) classified the canopy as *continuous*, when the foliage from adjacent vines down the row inter-mingles. It is classified as *discontinuous* when individual vines have separate canopies. Canopies are *divided* when they are separated into discrete curtains or walls of foliage. Canopies are *dense* when they have excess leaf area within the canopy. They are *open* when the canopy is less dense and the lower leaves are less shaded.

Figure 12. Global distribution of grape cultivation.

Differences in exposed canopy surface area, spatial distribution of leaves, ratio of adult to young leaves, and canopy management cause unique interactions between the leaf canopy and the surrounding environment. These interactions imply a specific physiological response by leaves to environmental conditions.

Dense canopies have more shaded lower leaves and reduced wine quality, so pruning and trellising are important to obtain good production. Dense canopies do not permit light penetration to lower leaves and fruit clusters. This reduces photosynthesis and transpiration, and the lower leaves become importers rather than exporters of photosynthesis products. Changing the canopy so that clusters and leaves are better exposed to the sun has been shown to improve wine quality and yield (Smart, 1985; Smart and Robinson, 1991). Therefore, the best yield and quality response is achieved by training the vines to have the greatest exposed leaf surface area during optimal environmental conditions for photosynthetic activity. For example, Baeza et al. (2005), in a study on different training systems, found greater photosynthesis activity in high bush vine due to higher levels of sunlight incident on the leaves. They also found higher stomatal conductance in short bush

and lower stomatal conductance in VSP as a defence against water loss through their larger surface area.

The grapevine is a perennial plant that lives for a long time. The grapevine season is divided in several phenological stages. The main stages are:

- **Winter dormancy**.
- **Budburst**, This stage occurs when mean daily temperatures are about 10°C. The plants begin vegetative activity. At first, shoots grow slowly, but as temperature increases, they elongate rapidly. The budburst date varies between years because of temperature differences during winter dormancy.
- **Bloom**, The flowers begin to open. Usually this period begins in March-April. Grapevines need mild temperature (between 16 and 20°C) during bloom without freezing temperatures.
- **Berry set**, Small fruit begins to form.
- **Veraison**, This is an important stage in the annual cycle of grapevines. It divides the vegetative stage from the fruit-forming stage. Grapes begin to develop and the berries change colour. In this stage sugar storage begins in the berries and the acid level decreases.
- **Technological development**, The grapes are mature when sugar and acid levels are optimal.
- **Harvest**.

The time between these phenological stages varies greatly with variety, climate, and geographic location. In regions with cool climates and short growing seasons, early-ripening varieties are necessary, whereas in hot climates, later-ripening varieties have sufficient time to achieve full maturation. The developmental stages are synchronized to the ability of the grapevine to yield fruit. Early and fully expressed phenological events usually result in larger yields (Jones, 1997; Mullis et al., 1992).

Climate directly affects the length of phenological stages. Jones and Davis (2000) found that in Bordeaux, France, the dates of harvest were nearly 13 days earlier than in 1950s, due to higher temperatures in recent years. One possible

effect of global warming on grapevines is to decrease the time between phenological stages and, hence, to shorten the season.

Climate affects water availability during the growing season. For unirrigated vineyards, a lack of winter and spring precipitation can cause soil-water deficits during the summer when plants need water. The summer deficits can be detrimental for physiological activity of the vines. A direct consequence of limited soil water is the progressive midday stomatal closure as the deficit increases. This is followed by parallel decreases of net photosynthesis. Stomatal conductance is controlled by a complex interaction of factors that are internal and external to the leaf. There is a drought-induced root-to-leaf signal, which is promoted by soil drying that reaches the leaves through the transpiration stream. The root-to-leaf signal induces stomatal closure. This biochemical signal comes from abscisic acid (ABA), which is synthesized in the roots in response to soil drying (Davies and Zhang, 1991).

Temperature, rainfall, soil type, cultivar characteristics, and management all have important effects on grapevine growth. A scheme showing how these parameters relate to grapevine growth and production is shown in Figure 13. In this scheme, soil, climate and cultural practices have direct effects on canopy microclimate, and the canopy microclimate has indirect effects by altering vine physiology.

It is important to determine what factors have the greatest effect on growth and development of the vegetative and reproductive organs of the vine and subsequent effects on the wine. van Leeuwen et al. (2004) conducted a study in Bordeaux, France, in which the effects of climate, soil, and cultivar on wine quality and quantity were studied simultaneously for the first time. In fact, previous studies have only examined one or two of the parameters at the same time. Winkler et al. (1974) and Huglin (1978) studied climate, whereas Huglin and Schneider (1998) reported on cultivar effects. Few studies were made on the impact of soil type differences.

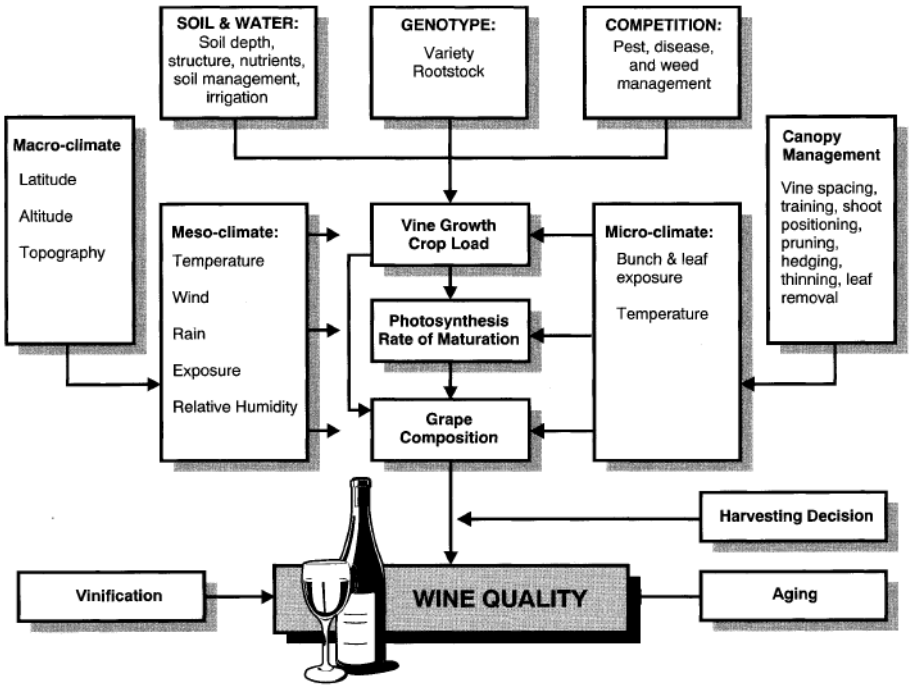

Figure 13. Conceptual model to show how soil, climate, and cultural practices can affect wine quality via affect on canopy microclimate.

In their study, van Leeuwen et al. (2004) found that soil type can influence vine development and fruit ripening through mineral supply, but mineral uptake does not affect fruit quality. This agrees with the conclusions of Seguin (1986). Most research, however, has shown that climate has the biggest effect on yield and quality; mainly because of its influence on vine water status. In fact, grapevines need moderate water stress for optimal quality (Matthiews and Anderson, 1988; van Leeuwen and Seguin, 1994; Ojeda et al., 2002), whereas the quality and yield decrease with severe water stress.

Italy is one of the larger producers of wine in the world and viticulture is largely widespread. Grapevines are cultivated in almost all Italian regions, and there are more than 300 wine grape varieties. Some varieties are widely distributed while others are found only in small regions (Figure 14). Varieties are classified depending on the final product:

- white wine varieties
- black wine varieties
- table grapes.

Figure 14. Areas of grapevine cultivation in Italy.

Grapevines are an important crop because of the different uses. It can be consumed fresh as table grapes, raisins, or to make wine. In addition, grapes are used to obtain juice, syrups for fruit salad, and alcoholic products. The leaves have some astringent property when cooked.

Grapevines are an important crop around the world. They are widely studied, but more studies are necessary to understand the behaviour and responses to climate and soil changes. This helps us to prevent severe modifications of the grapevine ecosystem and to protect it from alteration.

OBJECTIVES

In recent years, the discussion on climate change and global warming has become important. Fossil fuel emissions and deforestation are major causes of anthropogenic climate change. Carbon exchange between vegetation and the atmosphere is a key process for predicting global climate change and there is a need to better understand mechanisms that control these exchanges.

Micrometeorological techniques are useful to monitor fluxes of carbon, heat, momentum and water vapour between vegetation and the atmosphere, and models are used to understand the mechanisms involved in these exchanges.

Most carbon budget flux measurements were collected over forest, and to my knowledge there are few papers showing energy and mass exchanges between the atmosphere and Mediterranean maquis. Also, there is limited information available on exchanges between the atmosphere and orchard crops and grape vines. The contribution of these two ecosystems to carbon exchange with the atmosphere needs further investigation.

Models are sometimes used to quantify energy and mass fluxes on micro and regional scales. One of the more elaborate models for flux modelling is the Advanced Canopy-Atmosphere-Soil Algorithm (ACASA) model (Pyles et al., 2000b), which provides micro-scale as well as regional-scale fluxes. ACASA is a model that allows for characterization of energy and carbon fluxes. It is unique because it uses a third-order closure model for estimating fluxes. ACASA model also elaborates plant physiology models to determine photosynthesis and respiration processes over an ecosystem. ACASA model is also unique because subdivides the canopy, the atmosphere above it, and the soil in different layers. ACASA model estimates energy and carbon fluxes for each layer, and the profiles of water, carbon and energy fluxes can be obtained by this model.

The main objectives of this thesis are to:

- Investigate CO_2 and water vapour flux variation in maquis and grape vineyard ecosystem, due to environmental conditions, using *Eddy Covariance* micrometeorological technique.
- Parameterize and simulate fluxes using the ACASA (Advanced Canopy-Atmosphere-Soil Algorithm) model to estimates energy and mass fluxes between vegetation and the atmosphere in the two ecosystems.

- Evaluate the ACASA performance by comparing modelled and measured results.

Data from the Mediterranean maquis were collected within the CARBOEUROPE project (www.carboeurope.org), and the CarboItaly project (www.ecplanet.com). Data from the grape vineyard have been collected within a national project "*Ecophysiological, healthful and molecular studies for the qualitative valorization and the environmental protection, in viticultural system*s" funded by the Ministry of Education, University and Research in collaboration with other Italian Universities.

MODEL DESCRIPTION

1. ACASA MODEL FEATURES

ACASA is a complex model for estimating energy and mass fluxes between vegetation and the atmosphere, and it treats the canopy microenvironment and associated fluxes as an interconnected system. The model has four main features that make it an interesting and useful tool (Pyles, 2000a)

1. The canopy system is represented as a multi-layer system regime through which exchanges of energy, mass, and momentum occur.
2. ACASA uses a near-exact quartic energy balance formulation. This allows the calculation of surface temperature with accuracy even if temperatures of leaf, stem, or soil surface differ from air temperature.
3. ACASA incorporates a diabatic, third-order closure treatment of turbulent transfer within and above the canopy.
4. ACASA contains a formulation representing plant physiological responses to changing micro environmental conditions, including changes to carbon dioxide concentrations.

Additional features include:

- a soil model with thermal and hydrological exchanges,
- calculations of canopy heat storage,
- inclusion of canopy interception of precipitation.

The following sections will describe some of the main features model, and the equations that govern ACASA (Meyers and Paw U, 1987; Paw U and Gao, 1988; and Su et al., 1996).

1.1 Vertical resolution

The ACASA model employs several above ground layers and the vertical resolution is adjustable. Tests show that a minimum of ten within canopy and ten above-canopy layers extending to a minimum of twice the canopy height enables accurate vertical finite-difference calculations (Pyles 2000a, b). The entire domain extends to either twice the canopy height or to the level at which measurements were taken, whichever is greater. Into the soil, there are 15 layers of variable thickness.

Using the adjustable vertical resolution for each site insures that all fluxes and physiological responses occur within the multi-layer domain, and the turbulent statistics apply. The vertical resolution can not exceed 100 meters above the top of the canopy, because turbulence assumptions become invalid.

1.2 Surface temperature calculations

Calculating of leaf, stem, and soil surface temperature is based on the fourth-order technique of Paw U and Gao (1988). To calculate the surface temperatures, ACASA considers ten leaf angle classes (nine sunlit and one shaded), which are used to estimate the energy fluxes at each layer. First, a 4^{th} order, best-fit polynomial is expanded around $20^{o}C$ for the saturation vapour pressure as a function of leaf, stem, and soil surface temperature. Then this polynomial is combined with the appropriate energy budget, yielding a quartic expression for surface temperature for each case. Average leaf, stem, and surface temperatures within each layer are obtained by weighting individual shaded and sunlit values within a layer. When surface temperatures differ from air temperature by more than a few degrees Celsius, mathematical errors can occur (Paw U and Gao, 1988).

1.3 Turbulence closure

The biggest difficulty in turbulence modelling is the *closure problem*. Equations describing the turbulent flow contain a large number of unknowns exceeding the number of equations (Stull, 1988), so that, for a finite set of those equations, the description of turbulence is not closed. To solve the closure problem, the unknowns are approximated in terms of known quantities (parameterization). The closure approximation takes the name from the highest order equations that are retained.

ACASA uses third order equations to calculate fluxes and their transport. In ACASA, ten second-order equations and seventeen third-order equations are calculated independently. The aim of these calculations is to predict effects that higher-order turbulent kinetic and thermodynamic processes have on the canopy-surface microenvironment and associated fluxes of heat, moisture, and momentum. These processes include turbulent production and dissipation to turbulence kinetic energy, turbulent vertical transport of heat, mass, and momentum fluxes.

Using a set of governing equations, ACASA creates vertical profiles of temperature, humidity, mean wind, and CO_2 concentration. These higher order turbulence statistics account for the heat, moisture and momentum transport that occurs in the presence of large eddies (Meyers, 1985). Theoretical basis for turbulence calculations in the ACASA model are presented by Meyers (1985), Meyers and Paw U (1986), and Meyers and Paw U (1987). A full set of equations, is reported in Meyers and Paw U (1986).

1.4 Physiological response

ACASA accounts for the effects of all known factors on transpiration. In particular, it accounts for the effects of short wave radiation, CO_2 concentration, temperature, vapour pressure deficit, and soil moisture content.

Estimates of plant physiological responses are made using a combination of the Ball-Berry stomatal conductance (Leuning 1990; Collatz et al., 1991) and

the Farquhar and von Caemmerer (1982) photosynthesis equations described by Su et al. (1996) for unstressed stomata. Leaf temperature and radiative transfer estimates for ten leaf angle classes (nine sunlit and one shaded), in combination with air temperature, aerodynamic resistance, CO_2 concentration, and humidity, are used to estimate stomatal resistance by canopy layer.

In the model, it is possible to change the stomatal resistance to adjust for characteristics of individual species by modifying the slope of Ball-Berry relationship. Stomatal resistance values responde to soil moisture stress (Ek and Mahrt, 1991; Dickinson et al., 1993) and reflect the above and below ground influences.

1.5 Soil moisture and heat transport

A 1D Planetary Boundary Layer soil module from the Oregon State University is used to estimate soil surface evaporation, soil moisture, and soil temperature (Ek and Mahrt, 1991). The soil surface albedo (α_s) is estimated following Dickinson et al. (1993). A quartic energy budget equation is used to calculate the soil surface temperature and potential surface evaporation. Values of mean wind, temperature, and humidity estimated at 10% of canopy height above the ground are used. Then, the surface temperature and potential surface evaporation are used as boundary conditions for the soil calculations. The soil moisture and temperature for each soil layer are iterated until convergence for a given time step is achieved.

1.6 Additional features

ACASA has several additional features including (1) radiative transfer within the canopy, (2) canopy heat storage processes, and (3) precipitation and interception effect on soil water uptake.

The radiative transfer is calculated separately for three wavelength bands: visible, near infrared, and thermal. Equations to calculate both visible and near

infrared radiation (beam and diffuse shortwave radiation) are taken from Meyers (1985). ACASA uses a similar method for thermal radiation calculations and adjusts it to reflect the changes in leaf and soil temperatures occurring within each layer. Modifications to the earlier code of Meyers (1985) are found in Pyles (2000a).

The canopy heat storage S (W m^{-2}) is calculated as the sum of biomass, sensible, and latent heat storage:

$$S = S_c + S_H + S_{LE} = c_{bm} M_c \frac{\Delta T_c}{\Delta t} + c_p M_a \frac{\Delta T_a}{\Delta t} + \lambda_e \frac{\Delta q_a}{\Delta t}, \qquad \text{(C.1)}$$

where M_c and M_a (kg m^{-2}) are the column masses of biomass and air within a canopy layer, respectively; $\frac{\Delta T_c}{\Delta t}$ is the rate of change in leaf and stem canopy temperature (K s^{-1}), $\frac{\Delta T_a}{\Delta t}$ is the rate of change in air temperature (K s^{-1}), and $\frac{\Delta q_a}{\Delta t}$ is the rate of change in specific humidity (kg kg^{-1} s^{-1}); c_p (J kg^{-1} K^{-1}) and λ_e (J kg^{-1}) represent the specific heat of air and the latent heat of vaporization; c_{bm} (J kg^{-1} K^{-1}), appearing in the biomass thermal storage term (S_c), is the effective canopy heat capacity. It is set to 0.18 J kg^{-1} K^{-1}, which is a normalized value suggested by Moore and Fisch (1986) for a tropical forest with M_c=70 kg m^{-2}.

ACASA estimates precipitation and dew interception by canopy layer. Dew that accumulates on the surfaces of the leaves is treated as precipitation. Water remains on the leaves until removed by evaporation. When the canopy water content of a layer is nonzero, separate calculations for flux partitioning under free-evaporation conditions are performed. The resulting flux divergence estimates are then weighted by the fraction of the intercepted water to the maximum capacity within each layer. Water uptake from roots is correspondingly attenuated when the canopy moisture content is nonzero. Maximum canopy interception capacity is set to 0.1 mm per unit of total Leaf Area Index (LAI) as suggested by Dickinson et al. (1993) and Ubarana (1996).

2. GOVERNING EQUATIONS OF ACASA

This section presents the list of variables and the governing equations used in ACASA. The governing equations are described in sections associated with the variable or characteristic being calculated

- Radiative transfer equations (Meyers, 1985; Paw U, 1992).
- Surface energy budget and temperature equations (Meyers, 1985; Paw U and Gao, 1988).
- Steady-state turbulence equations closed to the 3rd order and all parameterizations (Meyers, 1985).

2.1 Variable list

The following list contains the variables used in the governing equations of ACASA. Additional variables and parameters are defined as they appear.

Symbol	Definition	Units
$\overline{u}$	streamwise wind speed	m
$\overline{\theta}$	potential temperature	K
$\overline{\theta_v}$	virtual potential temperature	K
$\overline{q}$	specific humidity	g kg^{-1}
$\overline{u'^2}$	streamwise horizontal velocity variance	m^2 s^{-2}
$\overline{v'^2}$	crosswise horizontal velocity fluctuation variance	m^2 s^{-2}
$\overline{w'^2}$	vertical velocity fluctuation variance	m^2 s^{-2}
$\overline{u'w'}$	streamwise component of Reynolds stress	m^2 s^{-2}

Symbol	Definition	Units
$\overline{w'\theta_v'}$	covariance of vertical wind speed and potential virtual temperature fluctuation	K m s^{-1}
$\overline{w'q'}$	covariance of vertical wind speed and humidity fluctuation	g m s^{-1}
$\overline{u'\theta_v'}$	covariance of streamwise velocity and potential virtual temperature fluctuation	K m s^{-1}
$\overline{\theta_v'^2}$	potential temperature fluctuation variance	K^2
$\overline{\theta_v'q'}$	potential temperature-humidity fluctuation covariance	K g
$\overline{w'u'^2}$	vertical transport of horizontal streamwise velocity fluctuation variance	m^3 s^{-3}
$\overline{w'v'^2}$	vertical transport of horizontal crosswise velocity fluctuation variance	m^3 s^{-3}
$\overline{w'^3}$	skewness of vertical velocity fluctuation	m^3 s^{-3}
$\overline{w'^2 u'}$	vertical transport of streamwise component of Reynolds' stress	m^3 s^{-3}
$\overline{u'^2 \theta_v'}$	streamwise horizontal transport of streamwise horizontal sensible heat flux density	K m^2 s^{-2}
$\overline{v'^2 \theta_v'}$	crosswise transport of crosswise horizontal heat flux density	K m^2 s^{-2}
$\overline{w'u'\theta_v'}$	vertical transport of streamwise horizontal heat flux density	K m^2 s^{-2}
$\overline{w'^2 \theta_v'}$	vertical transport of vertical heat flux density	K m^2 s^{-2}
$\overline{v'^2 q'}$	crosswise horizontal transport of crosswise horizontal water vapour flux density	m^2 s^{-2}
$\overline{w'\theta_v'^2}$	vertical transport of potential temperature variance	K^2 m s^{-1}
$\overline{w'\theta_v'q'}$	covariance of vertical wind speed, potential virtual temperature, and absolute humidity fluctuation	g K ms^{-1}
$\overline{u'\theta_v'^2}$	streamwise horizontal transport of horizontal sensible heat flux density	K^2 m s^{-1}
$\overline{\theta_v'^2 q'}$	covariance of potential virtual temperature fluctuation variance and humidity fluctuation	K^2 g
$\overline{\theta_v'^3}$	skewness of potential virtual temperature	K^3

2.2 Radiative transfer

Calculations of radiative transfer are made following Meyers (1985). ACASA calculates radiative transfer for 100 layers to minimize numerical errors. Leaves in the canopy are assumed to be horizontally homogeneous and distributed in nine leaf angle classes, each of which falls between 0 and 90 degrees. Stems and leaves share the same angle distribution and optical properties. All radiative fluxes are in $W\ m^{-2}$ units.

Energy budgets for the ground surface and canopy levels are calculated by combining radiative divergence/convergence estimates for each canopy layer. Absorbed available energy is partitioned into sensible and latent heat flux densities by the Bowen ratio to ensure conservation of energy. Energy budgets are calculated for wet and dry leaves and for stems. Total available energy is estimated as the sum of net values of short and long wave radiation minus heat storage in the soil and canopy. This estimate is made for by layer and each leaf angle class for wet leaf, dry leaf, and stems.

The fraction of radiation that is near-infrared is assumed constant at 0.54 (it changes with the sun). Thus, ACASA treats the shortwave fluxes separately. Short wave radiation is subdivided in visible (0.4–0.7 μm), near-infrared (0.7–2.0 μm), and thermal-infrared (>2.0 μm) radiation. Shortwave radiation (R_s) arriving at the Earth's surface is separated into direct beam (SB) and diffuse (SD) components

$$R_s = SB + SD \tag{C.2}$$

Diffuse radiation is assumed to be 25% of the total downward shortwave flux entering the top of the domain ($SD = 0.25R_s$), but this percentage varies depending on clouds cover and atmospheric aerosols. When ACASA is coupled to a climate model, knowledge of cloud cover is used to determine the fraction of diffuse shortwave radiation.

The incident direct beam radiation at the bottom of layer j, that will not be intercepted by the leaf area (ΔLAI), is given by

$$SB_j = SB_{j+1}\left(IB_j\right) = SB_{j+1}\left(\exp[-k(\xi)\Delta LAI_j]\right) \quad \text{(C.3)}$$

$k(\xi)$ is an extinction coefficient, which depends on solar zenith angle (ξ) and the angle of the leaves, IB_j is the fraction of beam radiation at the top (SB_{j+1}) that penetrates to the bottom of level j, and ΔLAI_j is the leaf area index of layer j.

The extinction coefficient $k(\xi)$ depends on leaf orientation at a single orientation angle, but there are nine leaf angle classes, so the extinction coefficient is given by

$$k(\xi) = \sum_{i=1}^{9} f_i k_i(\xi) \quad \text{(C.4)}$$

where f_i is the fraction of leaves that are inclined at angles varying from 0 to $\pi/2$. The extinction coefficient is also used to compute the penetration of diffuse radiation through the canopy. Assuming diffuse radiation is isotropic, the amount of diffuse radiation that penetrates to the bottom of layer j, without being intercepted by the leaves, integrated over the sky hemisphere, is:

$$SD_j = SD_{j+1}\left(ID_j\right) = SD_{j+1}\left(2\int_0^{\pi/2}\exp[-k(\theta)\Delta LAI_j]\sin\theta\cos\theta\, d\theta\right) \quad \text{(C.5)}$$

where ID_j is the fraction of diffuse radiation at the top of the layer (SD_{j+1}) that reaches the bottom of layer j.

The total downward fluxes of diffuse radiation at the top of a given layer j, including both sky and canopy contributions, is

$$SD_{\downarrow j} = SD_{\downarrow j+1}(ID_{j+1} + (1-ID_{j+1})\tau_r) + SD_{\uparrow j}(\rho_r(1-ID_{j+1})) + SB_{j+1}(1-IB_{j+1})\tau_r \quad \text{(C.6a)}$$

where $SD_{\uparrow j}$ is the upward diffuse radiation at the bottom of layer j, SB_{j+1} is the direct beam component at the top of layer j+1, τ_r is the portion of incident radiation that is transmitted and ρ_r is the portion reflected by layer j.

The upward diffuse radiation at the bottom of layer j+1 (the top of layer j) is

$$SD_{\uparrow j+1} = SD_{\uparrow j}(\tau_r(1-ID_{j+1}) + ID_{j+1}) + SD_{\downarrow j+1}(\rho_r(1-ID_{j+1})) + SB_{j+1}(1-IB_j)\rho_r \tag{C.6b}$$

It is important to note that SB_{j+1} is downward beam radiation at the top of layer j and $(1\text{-}IB_j)\rho_r$ is the fraction intercepted by foliage in layer j that is reflected upwards. All shortwave radiation back-reflected within the canopy is assumed to be diffuse. Norman (1979) suggests that for this formulation to be accurate, the amount of total canopy element area needs to be less than 0.15 in each layer. For most vegetated surfaces, total LAI is in the order of 0 to 10, and the above condition is easily met given the 100 layer resolution of the radiation code. This is the primary reason why ACASA uses 100 layers for radiative transfer.

To solve these equations, the initial beam component is ignored, and the ratios of down welling to up welling diffuse radiation are estimated using the Eqs. C.6a and C.6b. *ID* for each layer is estimated by integrating the expression for *SD* (Eq. C.5) from the soil surface to the canopy top. At the soil surface, the soil albedo (*A*) varies with the volumetric soil moisture fraction (q_{soil}) between 0.35 q_{soil} and 0.40 q_{soil}. Ignoring the direct beam component at the surface, the upward diffuse radiation for the soil is given by

$$SD_{\uparrow j} = SD_{\uparrow j-1}\left(\frac{(\tau_r(1-ID_j) + ID_j)A_j}{A_j + \rho_r(1-ID_j)}\right) \tag{C.7a}$$

$$SD_{\downarrow j} = SD_{\downarrow j+1}\left(\frac{(\tau_r(1-ID_{j+1}) + ID_j)}{1-\rho_r(1-ID_{j+1})A_j}\right) \tag{C.7b}$$

Estimates of SD_j can then be made in terms of an effective albedo A_j:

$$A_{\uparrow j+1} = \frac{SD_{\uparrow j+1}}{SD_{\downarrow j+1}} = \frac{(\tau_r(1-ID_{j+1}) + ID_{j+1})^2 - (\rho_r(1-ID_{j+1}))^2 A_j + \rho_r(1-ID_{j+1})}{1-\rho_r(1-ID_{j+1})A_j} \tag{C.8}$$

Equations (C.7a), (C.7b), and (C.8) provides initial estimates for diffuse fluxes at level *j*, and they are substituted into the expressions for the diffuse fluxes at the top of layer *j*. These equations are iterated until there is negligible change from one iteration to the next, which usually requires fewer than 10 cycles.

The same equations can be applied to the long wave radiation (>2 μ m) because of scattering in the long wave bandwidths within the canopy can be neglected. Assuming long wave radiation is isotropic and that leaves are perfect blackbodies, with an emissivity of 1.0, the downward and upward fluxes of long wave radiation at level j are

$$L_{\downarrow j} = L_{\downarrow j+1} ID_{j+1} + \varepsilon_m \sigma T_{\ell j+1}^4 (1 - ID_{j+1}) \qquad \text{(C.9a)}$$

$$L_{\uparrow j} = L_{\uparrow j-1} ID_j + \varepsilon_m \sigma T_{\ell j}^4 (1 - ID_j) \qquad \text{(C.9b)}$$

where σ = 5.67 10^{-8} W m^{-2} K^{-4} is the Stefan-Boltzmann constant, ε_m is the thermal emissivity (1.0 for leaves, 0.93 for ground surface). The value of downward long wave at the top of the canopy is simply the input value *LW* mentioned in the meteorological driven data file (Table 4 in Material and Methods section).

2.3 Surface temperature and energy balance

Surface energy budget is calculated by using the equation 3.1, and it is used to compute the surface temperature. In the *LE* and *H* equations, the resistance formulations, F_q and F_T are included within each canopy layer for each leaf angle class, respectively

$$LE = \rho \lambda F_q = \rho \lambda_e \frac{\kappa_q}{V} \iint_S \frac{\partial \bar{q}}{\partial \vec{n}} ds = f_f \left(f_d \frac{2LAD(q_{sfd} - q_a)}{(r_s + r_b)} + (1 - f_d) \frac{2LAD(q_{sfw} - q_a)}{r_b} \right) + (1 - f_f) \frac{2LAD(q_{ssd} - q_a)}{(5000 + r_b)}$$

(C.10)

$$H = \rho c_p F_T = \rho c_p \frac{\kappa_h}{V} \iint_S \frac{\partial \bar{\theta}}{\partial \hat{n}} ds = f_f \left(f_d \frac{2LAD(T_{sfd} - T_a)}{r_b} + (1 - f_d) \frac{2LAD(T_{sfw} - T_a)}{r_b} \right) + (1 - f_f) \frac{2LAD(T_{ssd} - T_a)}{r_b}$$

(C.11)

where $\hat{n}$ is a unit vector normal to the surface (s), κ_q, κ_h are exchange coefficients for water vapour and sensible heat, V is the volume in which exchanges take place (for 1D column calculations, V has units of m^{-1}). LAD is the total canopy area density including stems, leaves and buildings, f_d and f_f represent the fractions of dry leaves and the fraction of the total LAD that is leaves, r_s and r_b are the stomatal and aerodynamic resistances (s m^{-1}). Subscripts *sfd*, *sfw*, and *ssd* for temperatures (T) and specific humidity (q) represent dry leaf surface, wet leaf surface, and dry stem surface values, respectively. T_a (^oC) and q_a (g kg^{-1}) represent the air temperature and specific humidity within a given layer, respectively. ρ, λ_e, and c_p symbols are air density (kg m^{-3}), latent heat of vaporization (J g^{-1}), and specific heat capacity of air at constant pressure (J kg^{-1}), respectively. Values of specific humidity are taken as the saturation value at a given surface temperature.

Each surface temperature used in the above equations is calculated for each leaf angle class and each layer (301 separate calculations for 10 canopy layers). Only dry stem values are considered in the stem stomatal resistance and they are assumed constant at 5000 s m^{-1}. ACASA also assumes same optical properties and drag coefficients for leaves and stems for radiative and turbulence calculations.

T_a and q_a values, as also $\bar{u}$, derive from the higher order turbulence equations described in the next sections.

The surface energy budget equation using the equations C.10 and C.11 can be written as

$$R_{inc} - S = L_{\uparrow} + H + LE = \left(2\varepsilon\sigma T^4\right)_s + 2H + 2LE \qquad \text{(C.12)}$$

where R_{inc} is the combined radiative flux absorbed on both sides of the leaves. The subscript *s* on the radiative emission term (first on the RHS) represents the weighted sum of thermal emissions over each leaf angle class for dry leaves, wet leaves, and stems (for layer 1 this is just the ground surface temperature).

Calculations for aerodynamic resistances (s m^{-1}) to both sensible and latent heat transfers from leaf surfaces are similar to Gates' formulation (1980)

$$r_b = \left(C\left(\frac{D}{\bar{u}}\right)^{0.5} \qquad T_s \le T_a \ or \ j > 1 \right) \tag{C.13}$$

Values of the constants *D* and *C* are 0.05 and 200, respectively. Here, surface temperatures (*Ts*) are used to calculate fluxes that are then weight averaged over wet leaf, dry leaf, and stem temperature scenario within the canopy layers estimated from Eq. C.15.

Surface temperature (*Ts*) is estimated using the fourth-order approximation of Paw U and Gao (1988) for the saturation vapour pressure e_s (Pa), evaluated at the surface temperature

$$e_s(T_\ell) \approx \xi + \alpha T_\ell + \beta T_\ell^2 + \psi T_\ell^3 + \mu T_\ell^4 \tag{C.14}$$

where T_l (°C) represents the ground or stem surface temperature, or shaded or sunlit wet or dry leaf temperatures for each leaf angle class of leaf at a particular level, ξ = 6.174 (10^2) Pa, α = 4.222 (10^1) Pa C^{-1}, β = 1.675 (10) Pa C^{-2}, ψ = 1.408 (10^{-2}) Pa C^{-3}, and μ = 5.818 (10^{-4}) Pa C^{-4}.

T_l values are then obtained combining the equations C.13 and C.14 as follow

$$\begin{aligned} 0 = & \left(\varepsilon_m \sigma + \mu \frac{\rho c_P}{r_b} \right) T_\ell^{\,4} + \left(4\varepsilon_m \sigma k_1 + \psi \frac{\rho c_P}{r_b} \right) T_\ell^{\,3} + \left(6\varepsilon_m \sigma k_1^2 + \beta \frac{\rho c_P}{r_b} \right) T_\ell^{\,2} \\ & + \left(4\varepsilon_m \sigma k_1^3 + \alpha \frac{\rho c_P}{r_b} + \frac{\rho c_P}{\gamma (r_b + r_s)} \right) T_\ell - \left(RSW_{inc} + RLW_{inc} - S \right) + \varepsilon_m \sigma k_1^4 + \left(\xi - e_a \right) \frac{\rho c_P}{r_b} \\ & + T_a \frac{\rho c_P}{\gamma (r_b + r_s)} \end{aligned} \tag{C.15}$$

where k_1 = 273.15 that is the conversion factor between Celsius and Kelvin scales, e_a is the ambient vapour pressure (calculated from q_a), $\gamma = (pc_p / \varepsilon)/(de_s(T_\ell)/dT_\ell)$, r_s is the stomatal resistance which equals 0 for wet leaves and 5000 for stem surfaces. The ground surface resistance to evaporation is r_s for the first node. Using this quartic solution provides accurate energy budget calculations, even when leaf and air temperatures significantly differ (Paw U and Gao, 1988).

2.4 Plant physiological controls

Transpiration and the stomatal closure are affected by several factors including shortwave radiative flux density, CO_2 concentrations, temperature, vapour pressure deficit, and soil moisture content. The model accounts for these factors to predict plants physiological response to environmental conditions. ACASA uses a combination of the Ball-Berry stomatal conductance (Leuning, 1990; Collatz et al., 1991) and the Farquhar and von Caemmerer (1982) photosynthesis equations based on the paper of Su et al. (1996).

ACASA estimates the stomatal conductance for unstressed leaves as a function of two empirical parameters [the coefficient m and base conductance g_o (m/s)] and of other parameters including relative humidity at the leaf surface (rh_s), the net CO_2 assimilation rate A_n (μmol/m^2 s), and the CO_2 concentration at the leaf's surface C_s (μmol/m^3).

$$g_s = \frac{m\, A_n rh_s}{C_s} \qquad \text{(C.16)}$$

This equation is important because stomatal conductance depends on ecophysiological and biogeochemical factors, such as leaf photosynthetic capacity and nutrition (Schulze et al., 1994; Kelliher et al., 1994; Korner, 1994; Leuning et al., 1995), and ambient CO_2 concentration. In addition, research has shown that the coefficient m assumes mostly values between 8 and 12 (Collatz et al., 1991; Leuning, 1990; Harley and Tenhunen, 1991; de Pury, 1995), even if in case of soil

moisture deficit (Sala and Tenhunen, 1994; Baldocchi, 1997b) or with old trees showing a decreased hydraulic conductivity (Falge et al., 1996), its value can lie significantly outside of that range.

Carbon exchange processes are estimated using the equations given by Farquhar and von Caemmerer (1982) and Harley et al. (1992), and the net CO_2 assimilation rate per unit of leaf area (A_n) is given by

$$A_n = V_c - 0.5 V_o - R_d \tag{C.17}$$

where V_c, V_o, and R_d are the carboxylation, oxygenation (photorespiration), and dark respiration rates of CO_2 exchange between the leaf and the atmosphere ($\mu mol/m^2s$). The term V_c - 0.5 V_o is expressed as:

$$V_c - 0.5 V_o = \min[W_c, W_j](1 - \frac{\Gamma}{C_i}) \tag{C.18}$$

where W_c ($\mu mol/m^2s$) is the rate of carboxylation when ribulose bisphosphate (RuBP) is saturated, Wj ($\mu mol/m^2s$) is the carboxylation rate when RuBP regeneration is limited by electron transport, Γ is the CO_2 compensation point in the absence of dark respiration, and C_i is the intercellular CO_2 concentration ($\mu mol/m^3$).

All these equations are combined to estimate the total stomatal resistance for unstressed plants as a function of leaf temperature and biochemical parameters (Su et al., 1996). Ek and Mahrt (1991) and Dickinson et al. (1993) suggest using a soil water retention curve to adjust for soil moisture stress. The parameter A_n is weighted by LAI in order to link its value to the turbulent CO_2 of the microenvironment.

2.5 Soil physic and physiology

ACASA uses the PBL1 soil model from the Oregon University (Ek and Mahrt, 1991) and it estimates thermal and hydraulic transports in five layers of variable thickness. Thermal conduction is estimated as a function of the soil temperature gradient and the thermal conductivity, while for the hydraulic transport estimates are considered the effects of gravitational drainage. In addition, the effects of soil type on both thermal and hydraulic transports are included.

The equation to compute soil temperature, assuming no horizontal heat transfer, is

$$\frac{\partial T}{\partial t} = \frac{\partial T}{\partial z}\left(\kappa_s \frac{\partial T}{\partial z}\right) \tag{C.19}$$

where κ_s is thermal diffusivity of the soil ($m^2\ K^{-1}s^{-1}$), which depends on the soil type, organic content, and soil moisture. In the model, the lower boundary condition for soil temperature is set to a constant value, and the upper boundary condition is determined from energy budget calculations (see Section 2.3)

At the top of soil layer of depth z_1, the soil heat flux is estimated by

$$\rho_s c_s z_1 \frac{\partial T_o}{\partial t} = G_o - G_1 \tag{C. 20}$$

where subscripts 0 and 1 represent the surface and adjacent level beneath, G_o is the heat flux at a given level (W m^{-2}), ρ_s is the soil density (kg m^{-3}), and c_s is the soil specific heat capacity (J kg^{-1}), which includes a moisture component.

ACASA computes the soil heat flux transport from one layer to the next

$$G_n = \frac{2\kappa_s \rho_s c_s \left(T_{n-1} - T_n\right)}{\left(z_n + z_{n-1}\right)} \tag{C.21}$$

where subscript n represents a particular soil layer and k_s is the soil thermal diffusivity ($m^2 s^{-1}$).

The water balance is determined by

$$\frac{\partial W}{\partial t} = \frac{\partial}{\partial z}\left(D(W)\frac{\partial W}{\partial z} \right) + \frac{\partial k(W)}{\partial z} \qquad \text{(C.22)}$$

where W is the volumetric soil moisture content, $D(W)$ is the soil water diffusivity ($m^2 s^{-1}$), $k(W)$ is the hydraulic conductivity ($m s^{-1}$). $D(W)$ and $k(W)$ are related to soil type.

Soil model was modified to accounts for soil physics (Pyles, 2000a). Some modifications are reported as

- Soil model uses the potential surface evaporation, which is the maximum value that can occur at the potential evaporative temperature (PET) and the actual soil surface temperature.
- Precipitation that is not intercepted by the canopy is treated as the input moisture.
- Litter deriving from leaf or stem is considered as an insulator mean.
- Soil organic content has been added in ACASA in the upper two layers by modifying the soil thermal conductivity (Jury et al., 1991).

Soil conductivity, modified by soil organic content, is given by:

$$k_s = k_{sm}(1 - f_{ll})(1 - f_h) \text{ in the top layer} \qquad \text{(C.23)}$$
$$k_s = k_{sm}(1 - f_h) \text{ within layer 2}$$

where k_s is the soil thermal conductivity, f_{ll} is the fraction of leaf litter, f_h is the fraction of soil humus. A constriction is present such that when the humus content is 100%, the values of the expressions ($1 - f_h$) are 0.1.

The model accounts for the influence of roots on the soil moisture. Roots, in fact, decrease soil moisture because of their losses for transpiration that occurs in the upper seven layers.

The weighted sum of fractional soil moisture content (W_s) for each root zone layer is

$$W_s = \sum_{i=1}^{7} a_i w_{si} \tag{C.24}$$

where subscript i represents values in each layer, a_i is a weighting value representing the fraction of roots in a particular layer (assumed exponentially decaying away from layer 1), and w_{si} is the fractional soil moisture content in a particular layer.

Eventual soil moisture stress is accounted for by the relationship

$$r_{st} = \begin{cases} MAX\left(\dfrac{0.2}{W_s - w_c}, \quad 1.0\right), & w_c + 0.008 < W_s < w_c + 0.05 \\ 25.0, & W_s \le w_c + 0.008 \end{cases} \tag{C.25}$$

where r_{st} is the soil moisture stress factor. This factor modifies the slope of the Ball-Berry stomatal conductance response relation (*SBB*) when averaged to the species specific stomatal resistance

$$SBB = 9.29\left\{MAX\left(\frac{2}{r_{st} + r_{sp}}, \quad 0.04\right)\right\} \tag{C.26}$$

where r_{sp} is the species-specific stomatal conductance response factor (which should be 1.0 for grasses, crops and drought-intolerant deciduous trees).

If the soil temperature is less than 273 K or greater than 318 K in the root zone, stomatal resistance is set to 5000.

Respiration of microbes in the soil is estimated using the following equation

$$\overline{w'C'}_s = \gamma_1 \left(f_{ll} f_h \right) e^{\left(\frac{T_g}{\gamma_2} \right)} \tag{C.27}$$

where $\overline{w'C'}_s$ is the CO_2 flux from the soil (μmol m^{-2} s^{-1} m^{-2} of tissue), f_{ll} and f_h are as defined in Eq. 23, T_g is the soil temperature of the uppermost layer (K), γ_1 = 1.02949 μmol m^{-2} s^{-1} m^{-2} of tissue, and γ_2= 13.58857 K^{-1}.

Under dry conditions, microbes can die or fall into dormancy, so the CO_2 exchange decrease in the following manner. When the soil moisture of the top layer falls below 0.2, then the CO_2 emission drops off such that it is 50% of the unstressed value when the soil moisture is 0.1.

The soil model gives the values of soil surface evaporation to ACASA. It, then, iterates soil heat flux density at the surface to reach a solution, but the soil moisture and temperature fields are not updated until after ACASA reaches convergence. This feature avoids incorrected changes in the soil moisture and temperature values that can happen when they are far away from a solution for the soil surface temperature.

2.6 Turbulence closure

This section reports the set of steady-state turbulent governing equations (Meyers, 1985), where numerical methods are used to solve for each unknown. The following equations calculate the mean values of air temperature (potential), humidity, scalar concentration, and wind speed.

$$\frac{\partial \overline{\theta}}{\partial t} = 0 = -\frac{\partial}{\partial z} \overline{w'\theta_v'} + \frac{\kappa_h}{V} \int\int_S \frac{\partial \overline{\theta_v}}{\partial \hat{n}} ds = -\frac{\partial}{\partial z} \overline{w'\theta_v'} + H \tag{C.28}$$

$$\frac{\partial \overline{q}}{\partial t} = 0 = -\frac{\partial}{\partial z} \overline{w'q'} + \frac{\kappa_q}{V} \int\int_S \frac{\partial \overline{q}}{\partial \hat{n}} ds = -\frac{\partial}{\partial z} \overline{w'q'} + LE \tag{C.29}$$

$$\frac{\partial \overline{C}}{\partial t} = 0 = -\frac{\partial}{\partial z} \overline{w'C'} + \frac{\kappa_c}{V} \int\int_S \frac{\partial \overline{C}}{\partial \hat{n}} ds = -\frac{\partial}{\partial z} \overline{w'C'} + 2LAD\left(A_n \right) \tag{C.30}$$

$$\frac{\partial \overline{u_i}}{\partial t} = 0 = -\frac{\partial}{\partial z}\overline{u_i' w'} - \frac{1}{\overline{\rho}}\frac{\overline{\partial p'}}{\partial x_i} - \frac{1}{\rho}\frac{\partial \overline{p}}{\partial x_i} - f_c \varepsilon_{ij3}\frac{\partial \overline{u_j}}{\partial z} + \nu\overline{\nabla^2 u_i'} \qquad \text{(C.31)}$$

where C represents either CO_2 or O_3 concentrations, H and LE are the heat and moisture fluxes, respectively, f_c is the Coriolis parameter, ε_{ijk} is the alternating unit tensor, K_h, K_q, and K_c are the exchange coefficients for heat, moisture and scalar concentration, respectively, and the subscripts i and j represent either the x or y directions. In the equation C.30, for CO_2 concentration calculation, the source term A_n is the CO_2 assimilation rate per unit of leaf area discussed earlier.

From these equations it ts possible to compute the vertical gradient $\overline{w'\theta_v'}$, $\overline{w'q'}$, $\overline{u'w'}$, and $\overline{w'C'}$. To estimate the heat and moisture vertical gradient, ACASA insures conservation of energy using the Bowen ratio to partition the available energy into H and LE flux densities (W m^{-2}). These vertical gradients are then integrated to estimate total values.

For steady-state horizontally homogeneous conditions, the spatially averaged rate equations (2nd order eqs.) for $\overline{w'\theta_v'}$, $\overline{w'q'}$ and $\overline{u'w'}$, and for the set of variances are

$$\frac{\partial}{\partial t}\overline{u_i'^2} = 0 = -\delta_{i1} 2\overline{u_i' w'}\frac{\partial \overline{u_i}}{\partial z} - \frac{\partial}{\partial z}\overline{w' u_i'^2} + 2\delta_{i3}\beta\overline{u_i'\theta_v'} - \frac{2}{\overline{\rho}}\frac{\overline{u_i'\partial p'}}{\partial x_i} - \frac{2\overline{\varepsilon}}{3} \qquad \text{(C.32)}$$

$$\frac{\partial}{\partial t}\overline{u_i' w'} = 0 = -\frac{\partial \overline{w'^2 u_i'}}{\partial z} - \overline{w'^2}\frac{\partial \overline{u_i}}{\partial z} - \frac{1}{\overline{\rho}}\frac{\overline{u_i'\partial p'}}{\partial z} - \frac{1}{\overline{\rho}}\frac{\overline{w'\partial p'}}{\partial z} + g\beta\overline{u_i'\theta_v'} \qquad \text{(C.33)}$$

$$\frac{\partial}{\partial t}\overline{u_i'\theta_v'} = 0 = -\overline{u_i' w'}\frac{\partial \overline{\theta_v}}{\partial z} - \overline{w'\theta_v'}\frac{\partial \overline{u_i}}{\partial z} - \frac{\partial}{\partial z}\overline{w' u_i'\theta_v'} - \frac{1}{\overline{\rho}}\frac{\overline{\theta_v'\partial p'}}{\partial z} \qquad \text{(C.34)}$$

$$\frac{\partial}{\partial t}\overline{\theta_v'^2} = 0 = -2\overline{w'\theta_v'}\frac{\partial \overline{\theta_v}}{\partial z} - \frac{\partial}{\partial z}\overline{w'\theta_v'^2} - 2\overline{\varepsilon}_{\theta\theta} \qquad \text{(C.35)}$$

$$\frac{\partial}{\partial t}\overline{\theta_v' b'} = 0 = -\frac{\partial}{\partial z}\overline{w'\theta' b'} - \frac{1}{\overline{\rho}}\overline{b'\frac{\partial p'}{\partial z}} \tag{C.36}$$

$$\frac{\partial}{\partial t}\overline{w' a'} = 0 = -\overline{w'^2}\frac{\partial \overline{a}}{\partial z} - \frac{\partial}{\partial z}\overline{w'^2 a'} - \frac{1}{\overline{\rho}}\overline{a'\frac{\partial p'}{\partial z}} + g\beta\overline{\theta_v' a'} \tag{C.37}$$

where the symbol b represents either q, CO_2, or O_3 concentrations, a can be either θ_v, q, CO_2, or O_3 concentrations, β represents the thermal expansion coefficient, subscript i (Eq. C.32) can represent either x, y, or z directions, while in the Eqs. C.33 and C.34 it represents either x or y directions, g is the gravitational acceleration, ν is the kinematic viscosity, and β is the inverse of the virtual potential temperature. Terms represented with the symbol ε (except in the radiation formulations) denote viscous dissipation (molecular), and δ_{ij} is the Kronecker delta function (δ_{ij}=1 when i=j; δ_{ij}=0 otherwise). $\overline{w'u'^2}, \overline{w'v'^2}, \overline{w'^3}, \overline{w'^2u'}, \overline{w'^2v'}$ are triple correlations and they represent turbulent transports that give a non-local contribute to the turbulence (a feature not present in the first order closure). They can be written in the general form

$$\begin{aligned}\frac{\partial}{\partial t}\overline{u_i' u_j' w'} = 0 = &-\overline{u_i' w'^2}\frac{\partial \overline{u}_j}{\partial z} - \overline{u_j' w'^2}\frac{\partial \overline{u}_i}{\partial z} - \overline{w'^2}\frac{\partial}{\partial z}\overline{u_i' u_j'} - \overline{u_i' w'}\frac{\partial}{\partial z}\overline{u_j' w'} - \overline{u_j' w'}\frac{\partial}{\partial z}\overline{u_i' w'} \\ &- \frac{1}{\overline{\rho}}\left(\overline{u_i' u_j'\frac{\partial p'}{\partial z}} + \overline{u_i' w'\frac{\partial p'}{\partial x_j}} + \overline{u_j' w'\frac{\partial p'}{\partial x_i}}\right) + \frac{1}{\overline{\rho}}\left(\overline{u_i' w'}\frac{\overline{\partial p'}}{\partial x_j} + \overline{u_j' w'}\frac{\overline{\partial p'}}{\partial x_i}\right) \\ &+ \beta g\left(\overline{u_i' u_j' \theta_v'} + \overline{u_i' w' \theta_v'}\delta_{3j} + \overline{u_j' w' \theta_v'}\delta_{3i}\right) - 2\varepsilon_{ij3}\end{aligned} \tag{C.38}$$

where subscripts i and j represent the x and y directions, and δ_{3n} =1 when n=3 and is 0 otherwise. The two terms in the third parenthetical group from the end of the above equation arise as a result of spatial averaging, and they represent form drag on the mean flow by canopy elements.

ACASA has a difference regarding other third-order models because the average of the pressure gradient variations about the mean does not automatically equal zero. This occurs when high pressure zones accumulate on the windward

sides of the canopy elements and low pressure zones occur on the leeward sides of canopy, so there is no horizontal pressure gradient.

As for triple correlations related to the velocity terms, we can write similar equations for the unknowns related to the buoyancy contributions $\left(\overline{u'^2\theta_v'},\ \overline{v'^2\theta_v'},\ \overline{w'u'\theta_v'},\ \overline{w'v'\theta_v'},\ \overline{w'^2\theta_v'}\right)$

$$\frac{\partial}{\partial t}\overline{u_i'u_j'\theta_v'} = 0 = -\overline{u_i'u_j'w'}\frac{\partial\overline{\theta_v}}{\partial z} - \overline{u_i'w'\theta_v'}\frac{\partial\overline{u}_j}{\partial z} - \overline{u_j'w'\theta_v'}\frac{\partial\overline{u}_i}{\partial z} - \overline{w'\theta_v'}\frac{\partial\overline{u_i'u_j'}}{\partial z}$$
$$-\overline{u_i'w'}\frac{\partial}{\partial z}\frac{\partial\overline{u_j'\theta_v'}}{\partial z} - \overline{u_j'w'}\frac{\partial\overline{u_i'\theta_v'}}{\partial z} + \beta g\left(\overline{u_i'\theta_v'^2}\delta_{3j} + \overline{u_j'\theta_v'^2}\delta_{3i}\right) - \frac{1}{\overline{\rho}}\left(\overline{u_i'\theta_v'\frac{\partial p'}{\partial x_j}} + \overline{u_j'a'\frac{\partial p'}{\partial x_i}}\right)$$
$$-\varepsilon_{ij\theta}$$

(C.39)

where subscripts *i* and *j* represent either the *x* or *y* directions.

When the triple correlations are in the general form $\overline{w'a'b'}$ as in the case of additional unknown buoyancy terms $\left(\overline{w'\theta_v'^2},\ \overline{w'\theta_v'q'},\ \overline{v'\theta_v'^2},\ \overline{u'\theta_v'^2}\right)$ the general form of the equation is

$$\frac{\partial}{\partial t}\overline{u_i'a'b'} = 0 = -\overline{w'a'b'}\frac{\partial\overline{u}_i}{\partial z} - \overline{u_i'w'a'}\frac{\partial\overline{b}}{\partial z} - \overline{u_i'w'b'}\frac{\partial\overline{a}}{\partial z} - \overline{u_i'w'}\frac{\partial\overline{a'b'}}{\partial z} - \overline{w'a'}\frac{\partial\overline{u_i'b'}}{\partial z} - \overline{w'b'}\frac{\partial\overline{u_i'a'}}{\partial z}$$
$$+\beta g\left(\overline{\theta_v'a'b'}\delta_{3i}\right) - \frac{1}{\overline{\rho}}\left(\overline{a'b'\frac{\partial p'}{\partial z}}\right) - \varepsilon_{uab}$$

(C.40)

where subscript *i* represents either the *x* or *y* directions.

Finally, there are the set of buoyancy contributions in the form of pure scalar triple correlations $\left(\overline{\theta_v'^3},\ \overline{\theta_v'^2q'}\right)$ which are expressed generally as

$$\frac{\partial}{\partial t}\overline{a'^2b'} = 0 = -\overline{w'a'^2}\frac{\partial\overline{b}}{\partial z} - 2\overline{w'a'b'}\frac{\partial\overline{a}}{\partial z} - \overline{w'b'}\frac{\partial\overline{a'^2}}{\partial z} - \overline{w'a'}\frac{\partial\overline{a'b'}}{\partial z} - \overline{w'b'}\frac{\partial\overline{u_i'a'}}{\partial z} - \varepsilon_{aab}$$

(C.41)

where θ_v is represented by either *a* or *b* and *q* is represented by *b*.

In the same manner, third-order equations with 4rd order correlations appearing in each equation can be generated.

To solve these higher order equations and close the system of equations, it is necessary to make parameterizations of several terms in the above equations. In particular, canopy drag, pressure correlations, and viscous dissipation need parameterization.

First, ACASA treats the 4th moment contributions by invoking a quasi-Gaussian approximation

$$\overline{a'b'c'd'} = \overline{a'b'}\,\overline{c'd'} + \overline{b'c'}\,\overline{a'd'} + \overline{a'c'}\,\overline{b'd'} \tag{C.42}$$

Thus, ACASA estimates the vertical gradients of 4th moment quantities that appear in the above governing set of equations in the general form

$$\frac{\partial}{\partial z}\overline{a'b'c'd'} = \overline{c'd'}\frac{\partial \overline{a'b'}}{\partial z} + \overline{a'b'}\frac{\partial \overline{c'd'}}{\partial z} + \overline{a'd'}\frac{\partial \overline{b'c'}}{\partial z} + \overline{b'c'}\frac{\partial \overline{a'd'}}{\partial z} + \overline{b'd'}\frac{\partial \overline{a'c'}}{\partial z} + \overline{a'c'}\frac{\partial \overline{b'd'}}{\partial z} \tag{C.43}$$

where *a, b, c*, and *d* can represent turbulent scalar or turbulent vector quantities. This approximation has already been incorporated into the governing set of equations listed above.

Combining form drag and skin friction for the horizontal momentum (C.33) into one term with an effective drag coefficient C_d, we have

$$\frac{\overline{\partial p'}}{\partial x} + \nu\overline{\nabla^2 u'} = c_d LAD\overline{u}^2 \tag{C.44}$$

for each layer in the canopy.

Pressure covariance terms (C.32), were parameterized following the suggestions of Zeman and Tennekes (1975), Launder (1975), and Zeman and Lumley (1976). The general form of these parameterizations is

$$\frac{2}{\bar{\rho}}\overline{\frac{u_i'\partial p'}{\partial x_k}}=\frac{C_1}{\tau}(\overline{u_i'u_k'}-\frac{1}{3}\delta_{ik}\bar{e})-\alpha_0\bar{e}S_{ik}-\bar{e}\alpha_1\left\{\left(\frac{\partial\bar{u}_i}{\partial x_j}+\frac{\partial\bar{u}_j}{\partial x_i}\right)b_{jk}-\left(\frac{\partial\bar{u}_j}{\partial x_k}+\frac{\partial\bar{u}_k}{\partial x_j}\right)b_{ij}-\frac{2}{3}\left(\frac{\partial\bar{u}_j}{\partial x_l}+\frac{\partial\bar{u}_l}{\partial x_j}\right)b_{lj}\delta_{ik}\right\}$$
$$-\bar{e}\alpha_2(\left(\frac{\partial\bar{u}_i}{\partial x_j}-\frac{\partial\bar{u}_j}{\partial x_i}\right)b_{jk}-\left(\frac{\partial\bar{u}_j}{\partial x_k}-\frac{\partial\bar{u}_k}{\partial x_j}\right)b_{ij})+\frac{3}{10}\beta(\overline{\theta_v'u_i'}g_k+\overline{\theta_v'u_k'}g_i-\frac{1}{3}\delta_{ik}\overline{\theta_v'u_3'}-0.2\overline{u_k'e}$$

(C.45)

where, $b_{ik}=\left(\overline{u_i'u_k'}-\bar{e}/3\right)/\bar{e}$, $\bar{e}=\overline{u'^2}+\overline{v'^2}+\overline{w'^2}$, C_1 = 3.62, α_0 = 0.15, α_1 = 0.43, and α_2 = 0.2302.

In the case of the second-order steady-state flux equations (Eqs. C.32-37), the parameterization of the scalar-pressure covariance terms changes

$$\overline{\frac{a'\partial p'}{\partial x_i}}=\frac{C_2}{\tau}\overline{u_i'a'}-\frac{8}{10}\frac{\partial\bar{u}_k}{\partial x_j}(\overline{u_j'a'}\delta_{ik}-\frac{1}{4}\overline{u_i'a'}\delta_{kj}+\overline{u_k'a'}\delta_{ij})-\frac{1}{3}g\beta\overline{\theta_v'a'}\delta_{i3}$$

(C.46)

where a can be either θ_v, q, CO_2 or O_3 concentrations, and C_2 = 8.00.

For the third-order pressure covariances appearing in equations C.38-40, the parameterization follows Andre (1981)

$$\frac{1}{\rho}\left(\overline{u_i'u_j'\frac{\partial p'}{\partial x_3}}+\overline{u_i'u_3'\frac{\partial p'}{\partial x_j}}+\overline{u_j'u_3'\frac{\partial p'}{\partial x_i}}\right)+M_{ijw}=C_8\frac{\overline{u_i'u_j'u_3'}}{\tau}+C_{11}\beta g(\overline{u_i'u_j'\theta_v'}$$
$$+\overline{u_i'u_3'\theta_v'}\delta_{3j}+\overline{u_j'u_3'\theta_v'}\delta_{3i})$$

(C.47)

$$\frac{1}{\rho}\left(\overline{a'u_i'\frac{\partial p'}{\partial x_j}}+\overline{a'u_j'\frac{\partial p'}{\partial x_i}}\right)=C_8\frac{\overline{u_i'u_j'a'}}{\tau}+C_{11}\beta g(\overline{u_i'a'\theta_v'}\delta_{3j}+\overline{u_i'a'\theta_v'}\delta_{3i}+\frac{2}{3}\overline{u_3'a'\theta_v'}\delta_{ij})$$

(C.48)

$$\frac{1}{\rho}\left(\overline{a'b'\frac{\partial p'}{\partial xi}}\right)=C_8\frac{\overline{u_i'a'b'}}{\tau}+C_{11}\beta g\overline{a'b'\theta_v'}\delta_{3i}$$

(C.49)

where a or b can represent θ_v, q, CO_2 or O_3 concentrations, C_8 = 9.25, and C_{11} = 0.20.

For the viscous dissipation terms parameterizations are made. In the second and third-order equations they are:

$$\bar{\varepsilon} = \frac{\bar{e}}{\tau} \qquad \bar{\varepsilon}_{ab} = \frac{\overline{a'b'}}{\tau} \qquad \bar{\varepsilon}_{abc} = C_{10}\frac{\overline{a'b'c'}}{\tau} \tag{C.50}$$

where $\tau = \Lambda/\sqrt{\bar{e}}$, $C_{10} = 6.0(2/\tau)$, and $\Lambda = 23.053\alpha_c k(2h_c - d_0)/(2c_d LADh_c)$ for $z < h_c$, or $\Lambda = 23.053zk(2h_c - d_0)/2h_c$ for $z > h_c$, $c_d = 0.12$, $\alpha_c = 0.05$, and zero-plane displacement (d_0) is calculated using

$$d_0 = \left(\frac{\left(\overline{u'w'}\right)_{h_c} - \left(\overline{u'w'}\right)_0}{\left(\overline{u'w'}\right)_{h_c}}\right)\frac{\int_0^{h_c} z\frac{\partial\overline{u'w'}}{\partial z}dz}{\int_0^{h_c}\frac{\partial\overline{u'w'}}{\partial z}dz} + \left(\frac{\left(\overline{v'w'}\right)_{h_c} - \left(\overline{v'w'}\right)_0}{\left(\overline{v'w'}\right)_{h_c}}\right)\frac{\int_0^{h_c} z\frac{\partial\overline{v'w'}}{\partial z}dz}{\int_0^{h_c}\frac{\partial\overline{v'w'}}{\partial z}dz} \tag{C.51}$$

where subscripts 0 and h_c represent values at the ground surface and canopy height, respectively.

MATERIALS AND METHODS

1. SITES DESCRIPTION

1.1 Mediterranean maquis

The study site is located inside a natural reserve called “Prigionette”, but it is also known as “Arca di Noè” (40° 36’ 18’’N, 8° 9’ 7’’ E; 74 m elevation above sea level). The area is in the Capo Caccia peninsula, Northwest Sardinia, near Alghero (SS), Italy. The site has a surface area of 1,200 ha and it is delimited by a dropping to the sea cliff on the Northwest and West boundaries (Figures 15-16).

Climate is Mediterranean, semiarid with a warm summer, mild winter, and a high water deficit from May through September. Mean annual temperature is 15.9°C, mean minimum temperature is 7°C, and mean maximum temperature is 28°C. Annual mean thermal excursion is of 14°C (10°C in January and 24°C in August). Precipitation is mainly concentrated during the spring and the mean value is 588 mm. During fall, there are often intense rainstorms with high runoff and low water storage.

The study area is bordered by three hills: [Mt. Timidone (361 m), Pt. Cristallo (326 m), Mt. Pegna (271 m)] and by the sea.

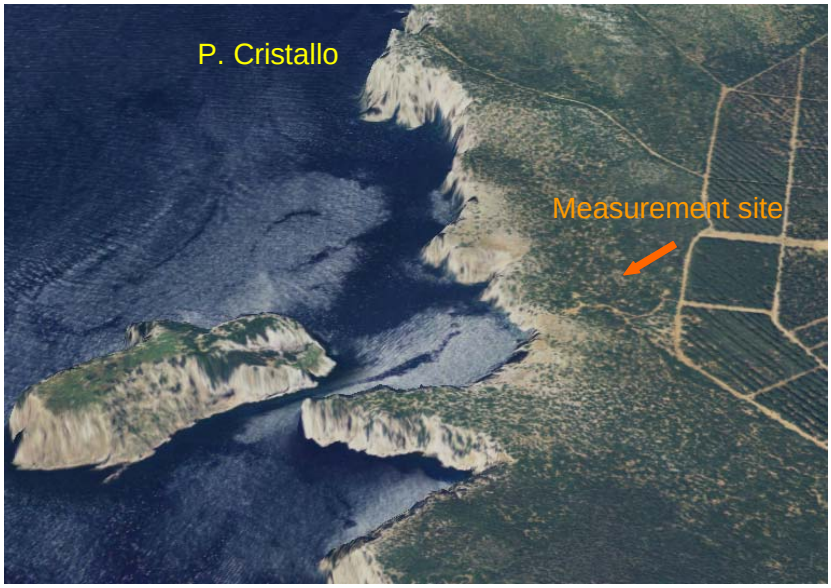

Figure 15. View of Capo Caccia peninsula.

Figure16. Capo Caccia peninsula and the experiment site (indicated by the red arrow).

The soil is Lithic Xerorthent, 0.3–0.4 m deep, mainly composed of clay, and erosion is common. Table 1 shows soil chemical analysis of the experimental area.

The ecosystem is a typical coastal Mediterranean maquis (schlerophyll species) consisting of juniper (*Juniperus Phoanicea* L.), lentisk (*Pistacia lentiscus* L.), tree phyllirea (*Phyllirea angustifolia* L.), and dwarf fan palm (*Chamaerops humilis* L.). The species form a sparsely vegetated shrub land, in which juniper and lentisk cover 53% and 22% of vegetated surface, respectively, and they are aggregated into variable sized patches. *Phillyrea* and palm are found only as isolated elements inside the main patches. Other species present in the experimental site are rosemary (*Rosmarinus officinalis* L.), *Genista corsica* (Loisel) DC., *Daphne gnidium* L., *Smilax aspera* L., *Euphorbia characias* L., *Helichrysum microphyllum* DC., *Asphodelus microcarpus* Salzm., and *Ferula communis* L. The vegetation is a secondary succession following a fire event in 1963 and agricultural abandonment in 1970. Currently, this area has limited human activity.

Table 1. Chemical–Physical characteristics of experimental area for the two horizons A and Bt.

LAYER	**A**	**Bt**
deep (cm)	0-10	10-25/35
Rocks (>2mm)	44	69
Coarse sand (‰)	108	31
Thin sand (‰)	392	167
Total sand (‰)	500	198
Silt (‰)	338	154.5
Clay (‰)	162	648
pH H_2O	6.26	6.5
pH KCl	5.3	5.17
Carbon (‰)	40	24
Organic matter (‰)	69	41
Total N (‰)	2.24	1.89
C/A ratio	17.60	13
P_2O_5 as assimilated (ppm)	28	81
K_2O as assimilated (ppm)	308	618
Calcium (meq 100 g^{-1})	11.37	11.12
Magnesium (meq 100 g^{-1})	3.78	4.93
Sodium (meq 100 g^{-1})	0.91	1.29
Potassium (meq 100 g^{-1})	0.95	1.33

Mean maquis height ranges between 0.93 to 1.43 m. Ground cover varies between 42% and 91%. Leaf Area Index (LAI) values were 2.8 in 2004 and 2006, and 3.0 for 2005 (Pisanu, 2005).

1.2 Grapevine

An experiment was conducted at Col d'Orcia vineyard near Montalcino, Tuscany, Italy (43° 05′ N, 11° 48′ E, 220 m elevation above sea level). The town of Montalcino is located 40 kilometers to the south of Siena. The Montalcino area is located at about 40 km from the sea. Montalcino landscape is delimited by the valleys of Orcia, Ombrone, and Asso and it is dominated by the Amiata mountain with a height of 1740 m. The area has a nearly circular shape with a diameter of 16 km and a surface area of 24,000 hectares. The surface area constits of 29% flat terrain, 70% hills, and only 1% mountain. The area is subdivided in specialized crops, 50% woods and uncultivated land, 10% olive trees, 8% vineyards, and the rest is planted to grain, pasture, and other crops. Although, wine grapes are not the main crop, the area is known for its oenological activity that has taken an overriding role in the last decades producing a famous wine called Brunello (obtained from Sangiovese grapes variety). On 28 March 1966, Brunello became a wine with a denomination of controlled origin (DOC), and on 1 July 1980, it became the first Italian wine DOCG. The air flows coming from the sea arrive in that area affecting the air temperature. Air temperature is, therefore, not too high during the summer, and it is not too low during the winter.

The climate is Mediterranean with precipitation concentrated in the months of May, October and November (700 millimeters annually on the average). In winter, snow is common above an elevation of 400 meters. The mountain Monte Amiata represents a natural barrier that protects Montalcino from most severe weather events (e.g., sudden downpours and hail-storms). The hill strip of moderate elevation, where must part of the winemaking estates are located, is not affected by fog, ice or late frost as are the surrounding valleys, while the normal, persistent winds insure the best conditions for the health of the plants. The fundamentally mild climate and the large number of days of serene weather during the entire vegetative cycle assure the gradual and complete ripening of the grape clusters. The existence of slopes with different orientation, the pronounced modulations of the hills and the elevation disparity between the

low lying areas and the higher districts, produce climatic microenvironments that are diverse despite the small size of the area (Figure 17).

Regional soil characteristics are difficult to describe because the soils originated in different geological eras. The lowe areas consist of terrain created by the deposit of alluvial material with an active stratum that is deep and loose, dating from the Quaternary Period. Further uphill, the terrain, enriched by fossil material, has a reduced active stratum of soil formed by the decomposition of origin rocks, especially marl and limestone. The terrains are moderately sandy, rich in lime, mingled with wide areas of volcanic soil, but tending to be thin.

Figure 17. Map of Montalcino's territory (from the website: www.consorziobrunello.it)

During the 2005, 2006 experiments, the Col d'Orcia vineyard consisted of about 30 year old Sangiovese grapevines trained in a curtain system. The rows were oriented in North-South direction with 1.0 m between plants and 3.0 m between rows. The vines were about 2.0 m tall and there was approximately 400 m of fetch in the upwind direction. The canopy was estimated to have about 50% ground cover (Figure 18).

LAI values ranged between 1.55 and 1.39 in June-July and August 2005, respectively, and between 1.26 and 1.48 in June-July and August 2006. Measurements were made in the rows located in the portion of soil with grass. The vineyard was not irrigated.

Soil chemical characteristic and analysis of the clay soil are listed in Table 2. Figure 19 shows the soil classification diagram.

Figure 18. A view of Col d'Orcia grape vineyard and the landscape around it.

Table 2. Soil analysis for the Col d'Orcia vineyard in 2005 for bare soil and rows with and without grass.

	Bare Soil	**Soil without grass**	**Soil with grass**
	0-0.20 m	0-0.20 m	0-0.20 m
sand (%)	20	47	28
silt (%)	43	30	32
clay (%)	37	23	40
USDA texture	Clay loam/ silt clay loam	loam	Clay/ clay loam
pH (in H_2O)	8.13	8.02	8.04
total lime (%)	32.2	27.9	4.3
active lime (%)	16.6	7.2	2.4
organic matter (%)	2.3	4.93	2.68
total N (%)	1.3	2.6	1.3
C/N	10.2	11.0	12.0
salt (mS/cm)	0.12	0.14	0.10
P (ppm)	8.7	20.4	10.2
P_2O_5 (ppm)	19.9	55.8	23.4
K (ppm)	277	389	477
K_2O (ppm)	334	469	574
C.S.C. (meq/100g)	21.0	16.3	28.5

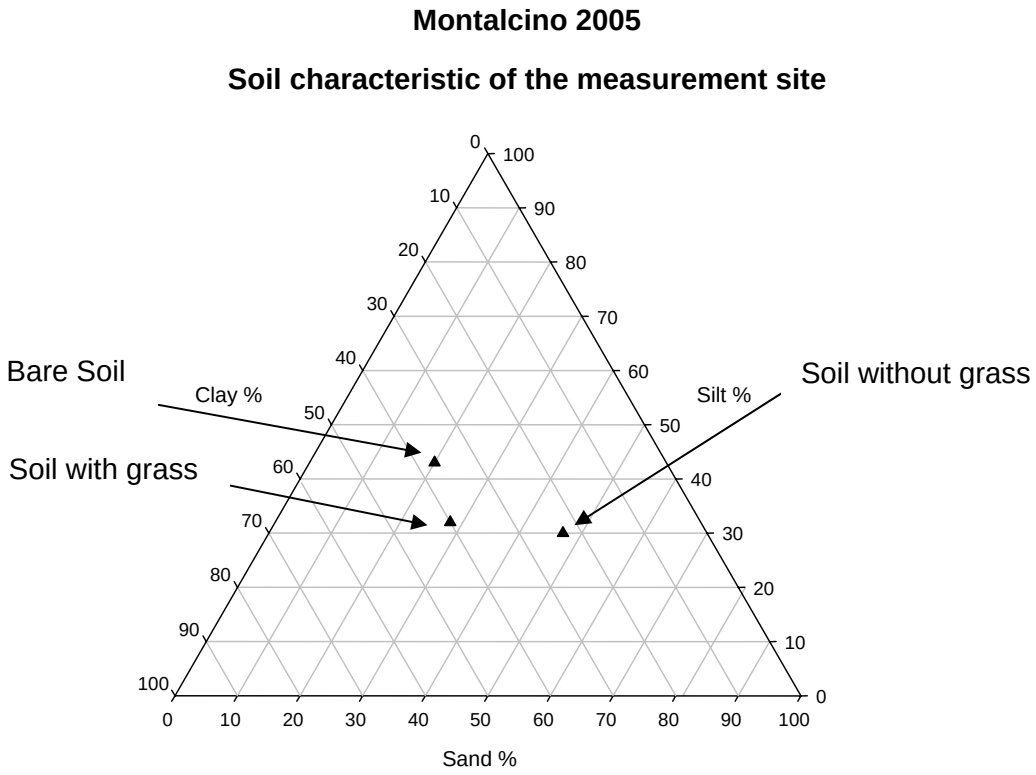

Figure 19. Diagram of USDA soil classification. The rows used for the measurements were located on typically clay soil with grass.

2. FLUX MEASUREMENTS

Eddy Covariance (EC) technique was used to measure energy balance components and CO_2 fluxes in maquis ecosystem and grape vineyards. Field observations for maquis were taken from April 2004 to December 2006. Measurements for grapes were taken during the fruit set (June-July) and veraison (August) phenological stages in 2005 and 2006. During 2006, measurements covered the entire period from the end of June to August. The instrumentation was identical in all experiments.

Vertical wind speed fluctuations and scalars were collected at a 10 Hz frequency using an EC system, including a CSAT3 sonic anemometer (Campbell Scientific, Logan, UT, USA) and a Li-7500, an open path gas analyzer from Li-cor, (Lincoln, NE, USA) for measuring CO_2 and water vapour concentrations.

Net radiation was measured using a four-component net radiometer (MR40, Eko Instruments, Tokyo, Japan). Air temperature and humidity were measured using a HMP45C temperature and humidity probe (Campbell Scientific, Logan, UT, USA).

Maximum maquis vegetation height was about 2 m, so the instruments were mounted at 3.5 m above the ground. The fetch was about 800 m. In grapes vineyard, vegetation height was 2.2 m and instrumentation was mounted at 0.60 m above the canopy top, and the fetch was about 400 m. Thirty minute averaging periods were used for all computations, and *LE* and *Fc* were corrected for density fluctuations (Webb et al., 1980). Figure 20 shows the EC system used in grapevine ecosystem.

Soil heat flux density (*G*) measurements were made in four different locations (completely and partially sunlit, and shaded), in shrub land ecosystem, to obtain a good weighted soil heat flux. In the grape vineyard, *G* measurements were made along a transect between rows to account for soil portions under and between the vines. Mean *G* at the surface during a 30-minute sampling interval was estimated using heat flux plates and thermocouples to account for stored energy above plates. Four heat flux plates (HFP01SC, Hukseflux, Delft, NL) were

installed at the 0.08 m depth and four thermocouples for each plate were buried to measure the change in temperature between plate and the soil surface to determine *G*.

Two Time-Domain Reflectometry probes (Model CS616-L, Campbell Scientific, Logan, UT, USA) were buried at 0.20 and 0.30 m, respectively, in maquis ecosystem to measure soil water content. In the grape vineyard, five ECH2O probes for measuring soil moisture were buried at 0.20 m depth in a transect between two rows with probes 1 and 5 in the rows and 2-4 distributed equally spaced between rows. Two sets of five thermistors each were located in a parallel transect to the ECH2O probes with the same spacing. One set was at 0.05 m depth and the other was at 0.10 m depth.

In the grape vineyard, measurements of soil respiration data were also collected by a closed path gas analyser (ADC 2250), Li-cor, Lincoln, NE, USA. Two sets of five collars were located in two transect lines, that were parallel to the other transect rows with the same spacing as for the ECH2O probes. Soil respiration data were collected every four hours for five consecutive days in 2005 and 2006. Carbon dioxide efflux from soil was measured by placing the portable gas exchange system over collars. A scheme of measurement locations is shown in Figures 21 and 22.

Precipitation data were collected every half hour using an aerodynamic rain gauge (ARG100, Environmental Measurements Limited, UK).

Data were collected using CR5000 and CR1000 data loggers, from Campbell Scientific (Logan, UT, USA). EC raw (10 Hz) data included three wind velocity components, virtual air temperature, and CO_2 and H_2O air concentration. Half hourly mean or sample data from 1-second recordings of net radiometer, soil heat plates, thermistors, humidity, and temperature probes were collected by the data logger. Instrumentation was powered by batteries that were charged by solar panels located near the towers.

LAI measurements were collected using AccuPAR LP-80 sensor (Decagon, Pullman, WA, USA) for the grape vineyard, and they were made using LAI2000 from Li-cor (Lincoln, NE, USA) for the maquis.

Figure 20. The EC system instrumentation used over grapevine canopy consists of a sonic anemometer, gas analyzer, and net radiometer (Campbell Scientific, Logan, UT, USA)

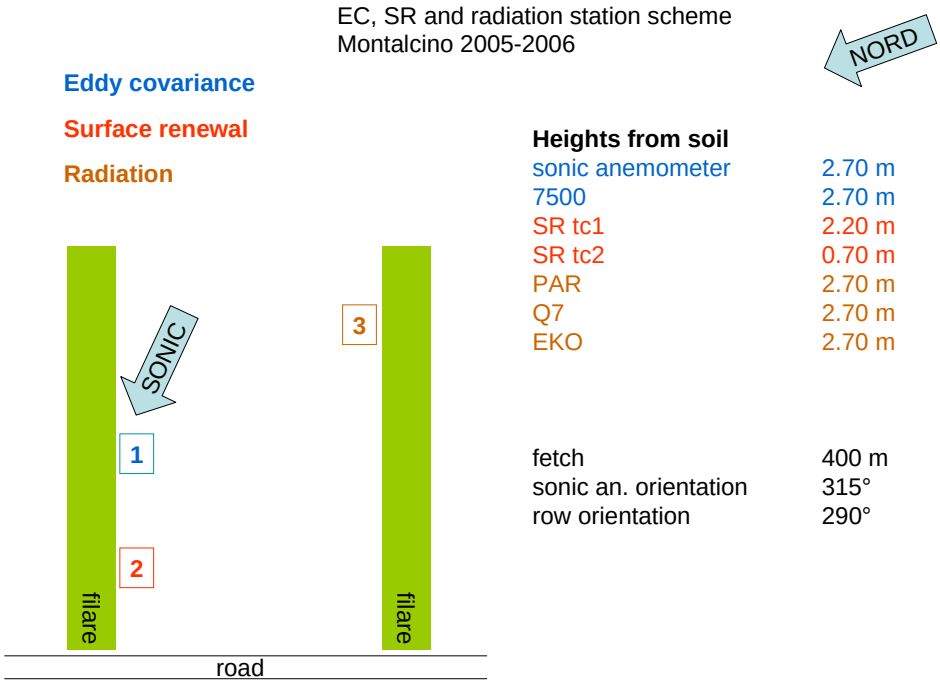

Figure 21. Scheme of measurement station in the grape vineyard.

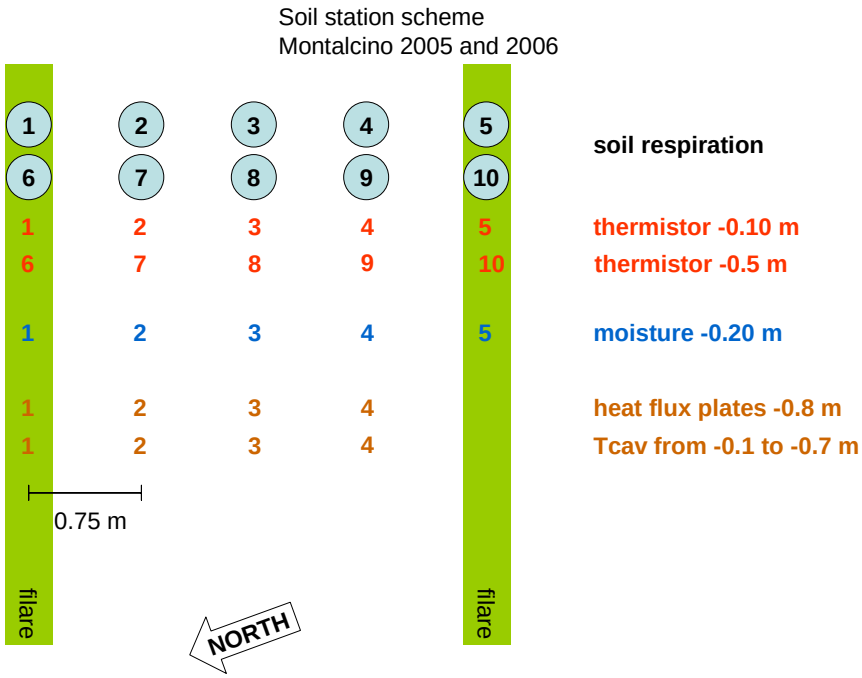

Figure 22. Scheme of soil instrumentation locations in the grape vineyard.

2.1 Data analysis

Collected data were processed using a software (EOLO) developed at University of Sassari (Sirca, 2006). This software corrects raw data and calculates CO_2, sensible heat, latent heat, soil heat, and momentum fluxes.

Data quality checks were made following procedures presented by Baldocchi et al. (1997a), Aubinet et al. (2000), Schmid et al. (2000)., and Papale et al. (2006). Raw data spikes, anomalous data, and data collected sub optimal conditions (e.g., during rain) were rejected. Half-hour flux data were eliminated if (1) data were incomplete, (2) precipitation occurred during that half-hour, or (3) spurious variance values were observed for either of the three wind velocities or scalars.

A three-dimensional coordinate rotation for the mean vertical wind velocity to the mean wind direction (Kaimal and Finnigan, 1994) was applied assuming a zero mean vertical wind speed fluctuation about the mean.

A WPL correction (Webb et al., 1980) for the effect of air density fluctuations was applied to the open-path IRGA system data to correct *LE* and CO_2 flux.

It is a general practice, for long-term ecosystem NEE studies to exclude nighttime respiration data during conditions with low mixing, which is characterized by low friction velocity conditions (Goulden et al., 1996; Paw U et al., 2000; Aubinet et al., 2000). Under these conditions measured *Fc* is not exactly equal to the real exchange between the vegetation and atmosphere. When the friction velocity (u*) is below a threshold, the CO_2 flux is underestimated. Therefore, data collected when u* values were under a threshold were rejected (Aubinet et al., 2000; Katul et al., 2004; Papale et al., 2006). The method by Reichstein et al. (2005) was used for the u* correction. The minimum u* threshold was set to 0.1 m s^{-1}, and a value of 0.4 m s^{-1} was used when u* < 0.1 m $^{-1}$.

Baldocchi (2003) estimated that 65-70% of data are lost during a year of measurements. Data rejection by the screening criteria listed above ranged from about 25 % for *H* and *LE* to about 46 % for NEE in the maquis ecosystem. Grape vineyard showed lower percentage of rejected data with a range from 4 % for *H* and *LE* to 36% for NEE. However, data were collected over a shorter time period. The percentage of good net radiation and *G* data collected during measurement periods was high (about 95-100%) in both ecosystem. An algorithm from Falge et al. (2001 a, b) and Reichstein et al. (2005) was used to fill data gaps. In this algorithm, three different conditions for gap filling missing flux data are identified: (1) all meteorological data are available; (2) air temperature and vapour pressure deficit (VPD) are missing, but radiation data are available; (3) radiation data are also missing. In case (1), the missing value is replaced by the mean value within a time-window of ± 7 days. During this period, *Rg*, *Tair* and VPD values do not deviate by more than 50 W m^{-2}, 25°C, and 5 hPa, respectively. If these conditions are not met in this time window, the averaging window is increased to ± 14 days. In case (2), only the *Rg* values do not have to deviate by more than 50 W m^{-2}, and the window size can not vary. In case (3), the missing value is replaced by the average value at the same time of the day (± 1 h) that is the mean

diurnal course. The window size starts with ± 0.5 days. The procedure is repeated, with increased window, until all values are filled. The filled data are classified into three categories (A, B, C) based on the method (1, 2, or 3) used and the window size. Categories A gives the best results because the data are filled knowing all meteorological conditions.

To estimate GPP and Reco, NEE data was separated into nighttime data and daily time data. Night-time data was selected according to a global radiation threshold of 20 Wm^{-2}, cross-checked against sunrise and sunset data derived from the local time and standard sun-geometrical routines. Reichstein et al. (2005) introduced an algorithm that defines a short-term temperature sensitivity of ecosystem respiration, and thus, largely avoids the bias introduced by confounding factors in seasonal data. In this method, Reco was calculated accounting for its sensitivity to air temperature by Lloyd and Taylor (1994). After the temperature sensitivities were estimated, the reference respiration (Rref) (i.e. the temperature independent level of respiration), was estimated using the Lloyd and Taylor (1994) model. The Rref estimates were assigned to a point in time, which represents the "centre of gravity" of the data. After the Rref parameters were estimated for each period, they were linearly interpolated between the estimates. Then, for each point in time, an estimate of Reco was provided.

To estimate NEE, GPP, and Reco the seasons were so distributed:

- Winter, December - February
- Spring, March - May
- Summer, June - August
- Fall, September - November

Data quality was evaluated using the energy balance closure. From equation 3.1 the sum of turbulent heat and latent flux were compared with the available energy flux, to obtain $(H+LE)/(Rn-G)$. The $(H+LE)/(Rn-G)$ ratio was 0.94 for maquis during the 2004-2006 period with $R^2 = 0.95$, and it was 0.76 for the vineyard with a $R^2 = 0.92$ for the 2005 and 2006 periods.

The reference evapotranspiration (ET_0) was estimated using the modified Penman-Monteith equation (Allen et al., 1998)

$$ET_0 = \frac{\Delta(Rn - G)}{\Delta + \gamma\left(1 + \frac{r_c}{c}\right)} + \frac{\rho Cp[e_s(T) - e]/r_a}{\Delta + \gamma\left(1 + \frac{r_c}{r_a}\right)} \quad \text{(D.1)}$$

where Δ is the slope of saturation water vapour pressure curve at the air temperature (kPa K^{-1}), γ is the psychrometric constant (kPa K^{-1}), r_a is the aerodynamic resistance (s m^{-1}), r_c is the canopy resistance (s m^{-1}), e_s is the vapour pressure at saturation level (kPa) , and e is the actual vapour pressure (kPa).

2.2 Decoupling coefficient

The estimation of physiological processes and biomass factors affecting water exchange was made by calculating the decoupling coefficient using the Penman-Monteith equation. The half-hourly canopy surface conductance (g_c, m s^{-1}) was calculated as

$$g_c = \frac{\gamma LE g_a}{\Delta(Rn - G) + \rho CpVPD - LE(\Delta + \gamma)} \quad \text{(D.2)}$$

where Δ is the slope of saturation water vapour pressure curve at the air temperature (kPa K^{-1}), γ is the psychrometric constant (kPa K^{-1}), LE is the latent heat flux (W m^{-2}), Rn is the net radiation (W m^{-2}), G is the soil heat flux (W m^{-2}), ρ is the air density (kg m^{-3}), Cp is the specific heat of air (J kg^{-1} K^{-1}), VPD is the air vapour pressure deficit (kPa), g_a is the aerodynamic conductance (m s^{-1}) calculated using the Monteith-Unsworth equation

$$g_a = \left(\frac{\overline{u}}{u*^2} + 6.2u* - 0.67\right)^{-1} \quad \text{(D.3)}$$

where $\overline{u}$ is the mean wind speed (m s^{-1}), and $u*$ is the friction velocity (m s^{-1}). The dimensionless decoupling coefficient (Ω) (McNaughton and Jarvis, 1983) was determined by

$$\Omega = \frac{\Delta/\gamma + 1}{\Delta/\gamma + 1 + g_a/g_c} \quad \text{(D.4)}$$

Only daily half-hour values (from 8.00am to 6.00pm) were considered for Ω calculation.

2.3 Footprint analysis

A major difficulty, when measuring above heterogeneous terrain, is to know what sources are responsible for the measured flux. Footprint models help to answer this question. The flux footprint may be defined (Horst and Weil, 1992) as the contribution per unit emission of each element of a surface area source to the vertical scalar flux measured at a given height.

Footprint analysis was made using the Schuepp et al. (1990) method. The *source area* (area of surface information that reaches the instrument) was estimated for both ecosystems. This analysis is important to consider if fluxes measured at a height *z* are representative of the ecosystem under investigation. Homogeneity of the footprint area is a classical assumption for the eddy covariance measurements. The source area corresponding to any given time period is the function of wind direction, stratification, intensity of turbulence and surface roughness. Because the vegetation did not change during years it was fullfilled in these experiments.

Figure 23 shows the footprint analysis for maquis during 2005. The area had an extent of about 800 m, and it represented the source area for 90% of fluxes measured by the instruments. Most of fluxes came from North and Northwest directions. Similar results were found for 2006 (Figure 24). Ninty percent of the fluxes came from an area of about 800 m in every direction, but most of fluxes arrived from North and Northwest directions.

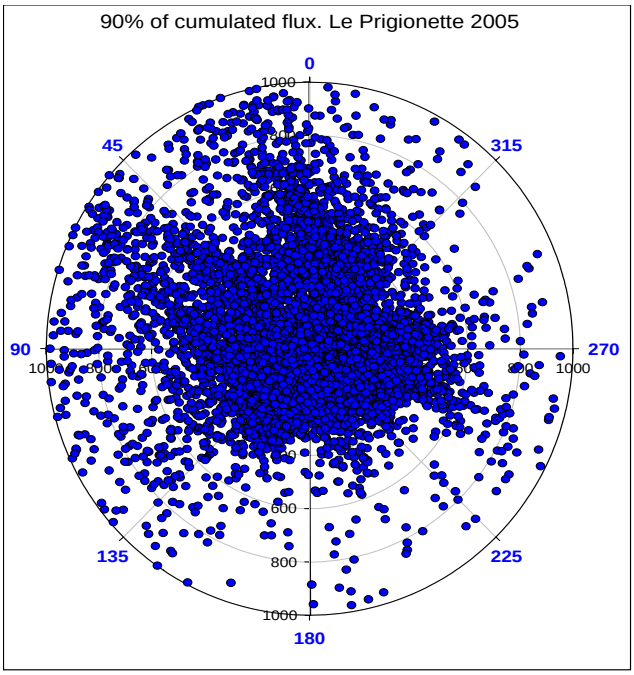

Figure 23. Footprint analysis for measurements taken over maquis in 2005. It represents the area from which the 90% of fluxes comes and are measured from the instruments.

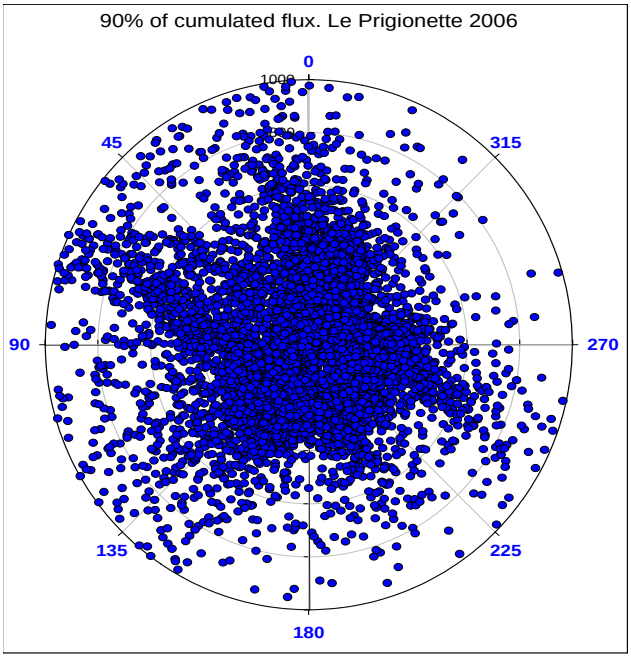

Figure 24. Footprint analysis for measurements taken over maquis in 2006.

For the grapevines, the footprint analysis was made for each measurement period. In June-July 2005, the area was of about 300 m indicating that 90% of the measured fluxes originated from this area (Figure 25).

The instruments saw fluxes coming from a footprint area of about 400 m during August 2005. Main wind direction was clearly Northwest (Figure 26).

Figure 27 shows footprint analysis for grape vineyard during 2006 measurement period. Fluxes came mainly from Northwest direction and the footprint area was about 400 m.

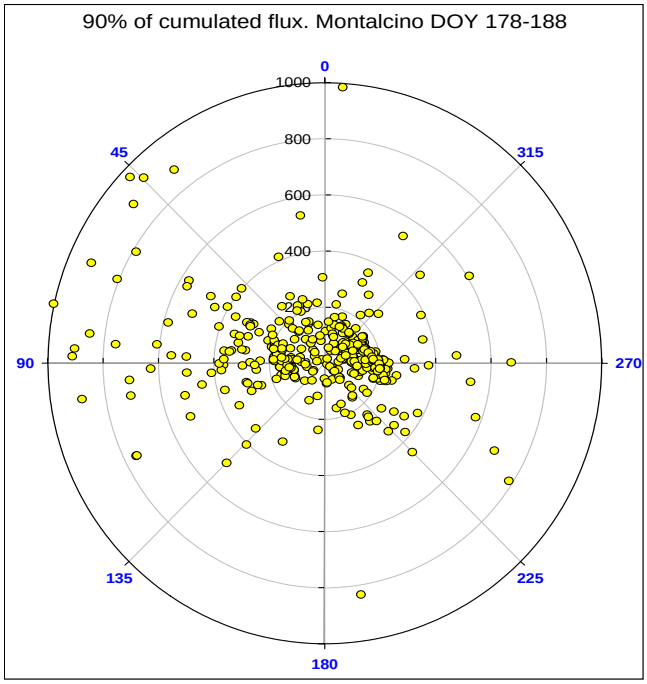

Figure 25. Footprint analysis for measurements taken over grapevines in June-July 2005.

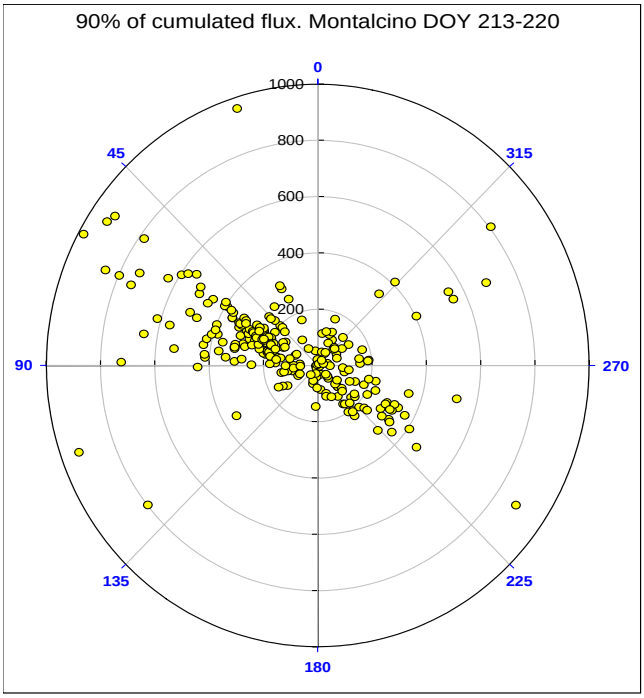

Figure 26. Footprint analysis for measurements taken over grapevines in August 2005.

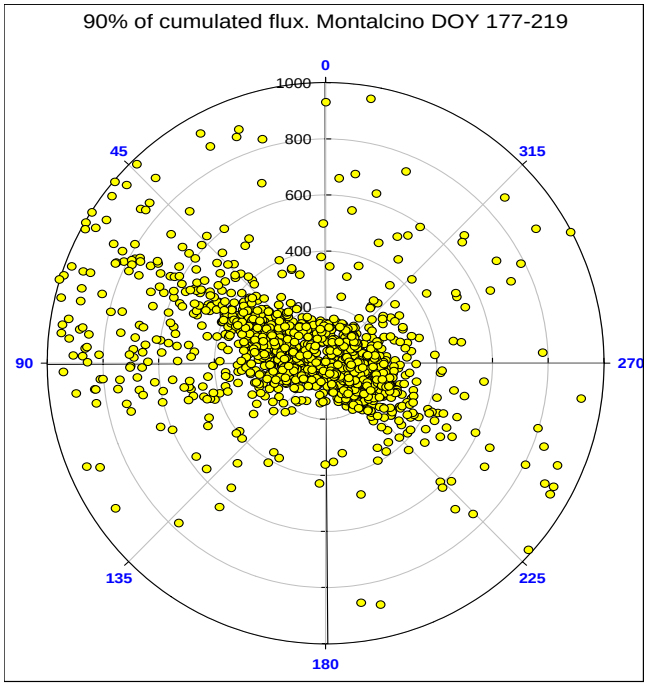

Figure 27. Footprint analysis for measurements taken over grapevines in 2006.

3. ACASA MODEL FOR ESTIMATING ENERGY AND MASS FLUXES

3.1 Input files

ACASA estimates fluxes using twenty atmospheric layers. In this research, the model vertical resolution was set to ten layers within the canopy and ten above-canopy, even if variations in the height or density of vegetation existed. The number of soil layers was set to 15 with adjustable thickness per layer. The first layers from the surface had a thickness of about 0.01 m, then the thickness increased until to reach a maximum value of about 0.20 m in the layers nine-fifteen.

Three types of input files are requires including:

- Plant and soil data (Table 3)
- Meteorological (30 minute) data (Table 4)
- Initial soil data (Table 5)

Tables 3-5 specify the variables and the data sources. Whenever possible, *in situ* measurements of the above quantities were used to drive ACASA. Values that were not directly measured were chosen from the literature. These include leaf optical properties, canopy drag coefficients, basal respiration rate for leaf, stem, roots and microbes, and Q_{10} values. The choices of site specific parameters were made in a manner that was physically consistent. For this investigation, canopy drag coefficients, mean leaf diameter, and leaf optical properties were assumed vertically constant throughout the canopy.

In Table 3, LAI values vary over a range due to seasonal differences. ACASA model can estimate fluxes over land and water, so a value of zero was set in the correspondence “land” parameter.

Soil type is specified using the USDA classification. There are 16 classes of soil type in the model code, from sandy to clay soil, accounting for organic matter content, presence of rocks, ice or water. The wilting point soil moisture

content must be input. Both maquis and grapevine were grown over clay soil, and the wilting point suggested by FAO guide on crop water requirement (2007) were used.

ACASA requires the input of a stress factor, "0" for plants that are water stress sensitive and "1" for plants that are stress tolerant. In this study, "0" was input for grapevines and "1" was input for maquis. The difference between using "1" or "0" is reflected on stomatal closure sensitivity and, therefore, on leaf exchanges. Plants water stress tolerant reduced water losses closing the stomata, and reducing energy and CO_2 fluxes when in water stress conditions.

Basal respiration rate is the minimum level of energy required to sustain vital functions of an organism. ACASA needs to indicate this term for single plant organs (leaves, stems, and roots) and for microbes. It is hard to estimate these terms separately, but the same range of values for basal repiration was found for these single components. Hamilton et al. (2001) and Mullins et al. (1992) suggested a range between 0.07 and 0.10 for forest and between 0.50 and 1.0 for crops.

By definition, Q_{10} is the factor by which the respiration rate changes for a temperature interval of 10 ºC:

$$Q_{10} = \frac{R_{T+10}}{R_T} \tag{D.5}$$

where R_T and R_{T+10} are respiration rates at temperature of T and T+10°C. Many authors report a Q_{10} value of about 2 for leaves and stems (Vose and Bolstad, 1999; Hu et al., 2006; Kim et al., 2007; Zhang et al., 2007). Measured soil respiration data at each site showed a Q_{10} range between 1.50 and 4.0 for roots and soil microbe respiration rates (Sirca, unpublished data).

ACASA needs values of leaf transmissivity and reflectivity of near infrared and visible radiation. Rossi et al. (2001) measured leaf reflectivity and transmissivity for maquis in the same site of our measurements, and Renzullo et al. (2006) reported values for grapevine. These values were used in the ACASA model (Table 3). Optimal photosynthesis temperature were input for maquis and

grapevines (Table 3). Maquis plants photosynthetize at lower temperatures than grapes (Mullins et al., 1992).

A common way to express the aerodynamic effect of a canopy is in terms of its resistance to the air flow using a drag coefficient (Jacobs, 1985). Villagarcia et al. (2007) found a leaf drag coefficient of 0.07 for vegetation stands in a semiarid environment, while Molina et al. (2006) found values ranging from 0.22 to 0.26 for several horticultural crops. These values were selected for leaf drag coefficient values for maquis and grapevine.

The maximum carboxilation rate (V_{cmax}) due to Rubisco activity represents the maximum activity of Rubisco in optimal temperature conditions (25°C). A wide variation (25-60 μmol CO_2 m^{-2} s^{-1}) was found depending on the species and the influence of vapour pressure deficit (VPD) and irradiance (Frak et al., 2002). Iacono et al. (1998) and Bigot et al. (2007) found similar values for grapevine (Table 3).

Stomata density factor accounts for the number of stomata and their activity. The value is typically lower in plants with more stomata (e.g., amphistomata grapes) and it is higher when there are fewer stomata (e.g., for maquis).

The normalized leaf area index profile is also needed to drive ACASA. A LAI profile was developed for maquis and grapevine based on LAI measurements and canopy shape. Figure 28 shows the shape of LAI profile for maquis during 2005, and Figure 29 shows the LAI profile for grapevines during 2005.

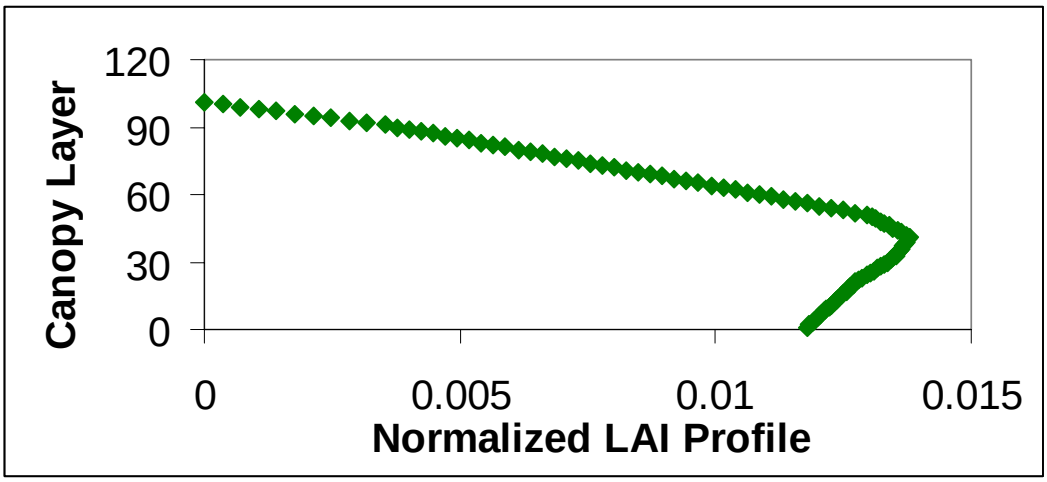

Figure 28. Shape of normalized LAI profile over maquis during 2005.

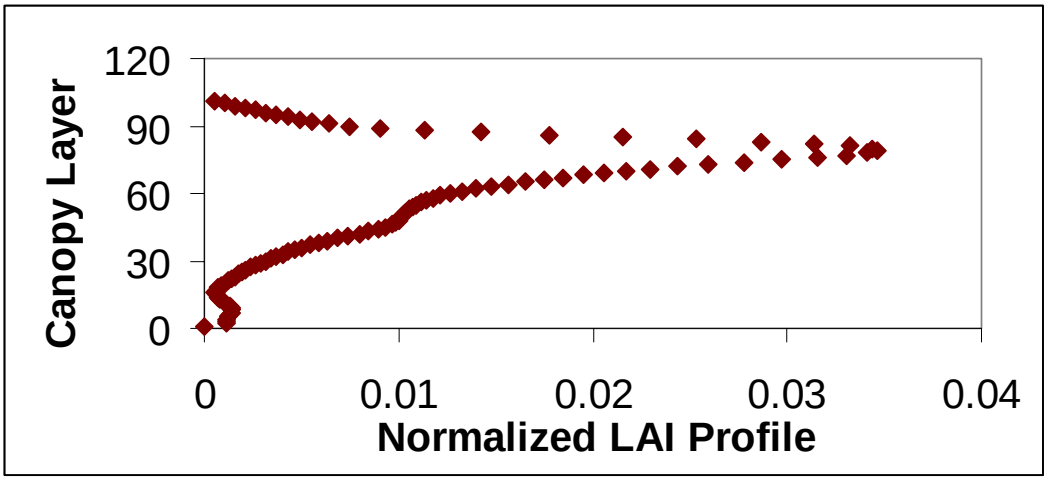

Figure 29. Shape of normalized LAI profile over grapevines during 2006.

Table 3. Plant and soil input for maquis and grape vineyard ecosystem.

Description	Units	Maquis	Grapevine	Reference
LAI		2.7-3.0	1.37-1.55	This study
Canopy height	m	1.20	2.2	This study
Ocean **Land**		0-1	0-1	
Wetland (1) **No standing water (0)**		0-1	0-1	
Soil type		1-16	1-16	This study
Wilting point soil moisture		0.17-.24	0.17-0.24	FAO 2007
Latitude	deg	40°36' N	43° 05' N	
Human population density	#people/m^2	0	0	
Time step length	s	1800	1800	
Stress index		0-1	0-1	
Leaf basal resp. rate	µmol m^{-2} (leaves) s^{-1}	0.07-0.1	0.5-1.0	Hamilton et al., 2001; Mullins et al., 1992
Stem basal resp. rate	µmol m^{-2} (stems) s^{-1}	0.07-0.1	0.5-1.0	Hamilton et al., 2001; Mullins et al., 1992
Root basal resp. rate	µmol m^{-2} (roots) s^{-1}	0.07-0.1	0.5-1.0	Hamilton et al., 2001; Mullins et al., 1992
Microbe basal resp. rate	µmol m^{-2} (microbes) s^{-1}	0.07-0.1	0.5-1.0	Hamilton et al., 2001; Mullins et al., 1992
Q_{10} leaf resp		2.0	2.0	Vose and Bolstad, 1999; Hu et al., 2006
Q_{10} root resp		1.5-4.0	1.5-4.0	This study

Description	Units	Maquis	Grapevine	Reference
Q_{10} microbes		1.5-4.0	1.5-4.0	This study
Q_{10} stem resp		2.0	2.0	Vose and Bolstad, 1999; Hu et al., 2006; Kim et al., 2007; Zhang et al., 2007
Near-IR leaf reflectivity		0.3	0.4	Rossi et al., 2001; Renzullo et al., 2006
Near-IR leaf transmittivity		0.35	0.35	Jones, 1992
Visible leaf reflectivity		0.05	0.05	Rossi et al., 2001; Jones, 1992; Renzullo et al., 2006
Visible leaf transmissivity		0.08	0.08	Rossi et al., 2001; Jones, 1992;
Optimal photosynth. temperature	°C	20	25-35	Mullins et al., 1992
Leaf drag coefficient		0.07	0.22-0.26	Villagarcia et al., 2007; Molina et al., 2006
Mean leaf diameter	m	0.03	0.15	This study
Max carboxylization rate (V_{cmax})	µmol m^{-2} (tissue) s^{-1}	30-40	25-60	Bigot et al., 2007; Frak et al., 2002; Iacono et al., 1998
Stomata density factor		1.8	1.0	This study
Normalized leaf area index profile				This study

Table 4 describes meterological input needed to drive ACASA. The data were measured at both research sites.

Initial soil conditions (Table 5) were used to make the soil moisture and temperature profiles for each of 15 soil layers. The soil moisture profile was created with values of soil moisture measured at 0.20 and 0.30 m depth and integrating to about 2 meters depth. Figures 30 and 31 show the soil moisture profile over maquis and grapevines during 2005 and 2006, respectively. Temperature profiles were made using the average temperature measured at 0.05 and 0.10 m and calculating the damping depth for each of 15 soil layer. Figures 32 and 33 show the shape of soil temperature profile over maquis and grapevine during 2005 and 2006, respectively.

Time step length was set to 1800 s indicating a 30 min average period used to estimate fluxes.

Table 4. Meteorological input for maquis and grape vineyard. Measured half-hourly data were inserted in the input file for the experimental period.

Description	Units	Maquis	Grapevine
Fractional day			
Rain	mm	This study	This study
Specific humidity	g Kg^{-1}	This study	This study
Wind speed	m s^{-1}	This study, EC measurements	This study, EC measurements
Solar radiation (Rg)	W m^{-2}	This study, EC measurements	This study, EC measurements
Long wave incoming radiation (LWin)	W m^{-2}	This study, EC measurements	This study, EC measurements
Air temperature	K	This study, EC measurements	This study, EC measurements
Air pressure	hPa	This study, EC measurements	This study, EC measurements
CO_2 concentration	ppm	This study, EC measurements	This study, EC measurements

Table 5. Initial soil input for maquis and grape vineyard. Profiles account for 15 soil layers.

Description	Units	Maquis	Grapevine
Soil temperature	K	This study	This study
Soil moisture	Volumetric fraction	This study	This study

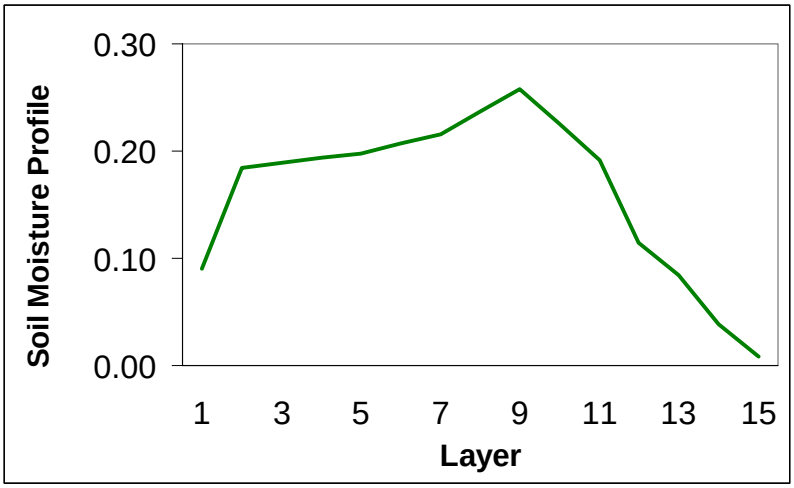

Figure 30. Shape of soil moisture profile over maquis during 2005.

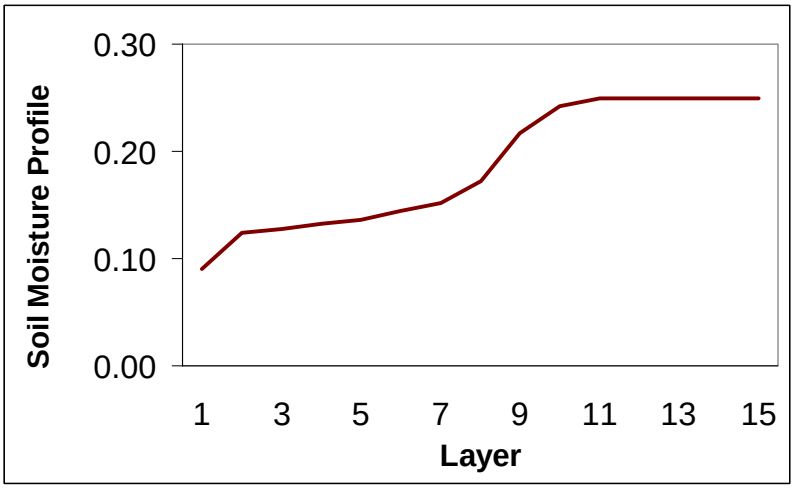

Figure 31. Shape of soil moisture profile over grapevines during 2006.

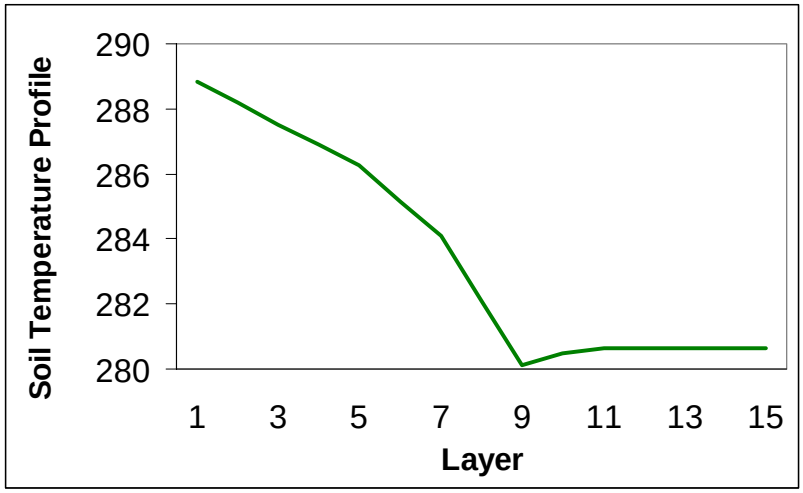

Figure 32. Shape of soil temperature profile over maquis during 2005.

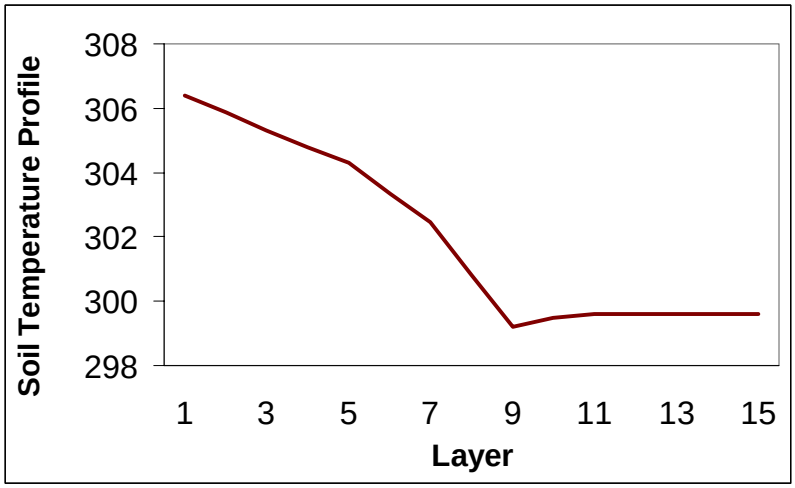

Figure 33. Shape of soil temperature profile over grapevine during 2006.

3.2 Numerical procedures

As in many higher turbulence closure models, ACASA requires iterating to arrive at steady-state solutions for the governing set of equations (Figure 34). Initially, ACASA calculates the: initial stomatal resistances, canopy water storage, short wave radiative fluxes throughout the canopy, and preliminary surface energy balance. When these computations are finished, the iteration cycles begin. Each iteration cycle repeats itself until convergence (i.e., when there is less than $2.5\ W\ m^{-2}$ in the latent heat flux and 2.5% change in vertical wind shear estimated at the top of the canopy over 4 iterations). Thus, both kinematic and diabatic processes are converging, thereby reducing the probability of errors. After convergence, ACASA updates the soil conditions and returns any needed outputs.

Several constraining methods are used by ACASA to enhance numerical stability as the model iterates toward a solution. In fact, velocity and temperature variances can not assume negative values. Mean wind shears are not allowed to become negative above canopy layers. This restriction is needed because such patterns, in steady state vertical wind shears immediately above the canopy top, are physically unreasonable and do not appear in observations (Kaimal and Finnigan, 1994). Some lower limits are established by the model. For example, the upper-boundary mean wind inputs that are less than $0.5\ m\ s^{-1}$ are set to $0.3\ m\ s^{-1}$. ACASA uses concepts similar to the reliability principles of André et al. (1976a, b), which restrict values of the third moments to constrain velocity variances and 2^{nd} moment turbulent quantities.

Spin-up time is necessary to avoid spurious flux estimates resulting from initialization of soil moisture and temperature profiles. When time series were insufficiently long to establish true soil thermal and hydrological equilibrium conditions, using the observed mean air temperatures averaged over the entire record, and a 10-hour spin-up time prior to the sample period eliminated spurious ground heat flux values. The first two days of a run are needed to initialize fluxes before comparisons are made with measured data. Figure 34 shows a schematic diagram of the ACASA program steps.

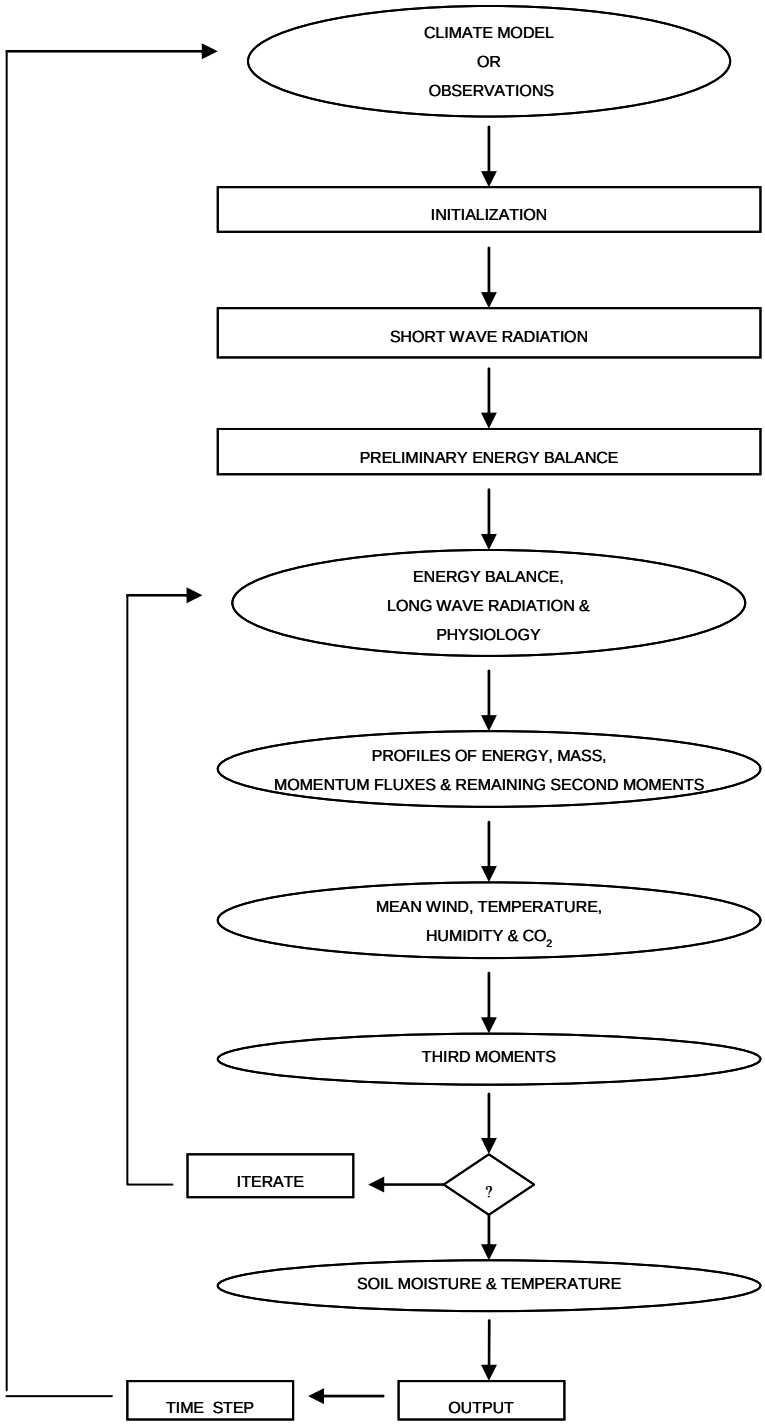

Figure 34. Components and numerical implementation of ACASA with a scheme of the iterative cycles.

3.3 Statistical analysis

ACASA model accuracy was evaluated with three different statistical parameters. All these indeces have as optimal value zero. The first parameter used was the root mean squared error (RMSE) between predicted and observed data

$$RMSE = \sqrt{\frac{\sum_{i=1}^{N}\left(d_p - d_o\right)^2}{N}} \qquad \text{(D.6)}$$

where d_p is the predicted data and d_o is the observed data, and N is the number of data. Small values of RMSE indicate better model predictions.

A second parameter used to test the accuracy of modelled flux data was the the mean absolute error (RA)

$$RA = \frac{\sum_{i=1}^{N}\left|d_p - d_o\right|}{N} \qquad \text{(D.7)}$$

A small value for RA is indicative of a better match along the 1:1 line comparison of predicted and observed values.

Model results were also evaluated by the mean bias error (MBE). It indicates the percentage of error of modelled data and it was calculated as

$$MBE = \sum_{i=1}^{n}\frac{d_p - d_0}{N} \qquad \text{(D.8)}$$

Positive values of MBE indicate a model overestimate with respect to measured data, while negative values indicate a model underestimate.

Regression significance between simulated and measured net radiation, sensible heat, latent heat, soil heat, and CO_2 fluxes were evaluated by the F test. Significance was tested at 0.95 and 0.99 levels.

RESULTS AND DISCUSSION

1 FIELD OBSERVATIONS

A) Maquis ecosystem

1.1 Environmental conditions

Understanding water and energy exchanges between maquis ecosystems and the atmosphere requires an analysis of observed environmental variables. Table 6 shows the annual solar radiation (*Rg*), mean annual air temperature (*Tair*), and the annual total precipitation (*Pcp*) measured at the flux tower during the years 2004, 2005, and 2006. The mean climate data were computed from 1960 to 1991 data. There were minimal differences in temperature during the experiments, except for 2004 when the mean *Tair* was considerably higher than climate means. Solar radiation did not show large variation between years, except for 2004 when measurements were collected from April.

Table 6. Climate data from a nearby weather station and mean annual air temperature (*Tair*), rainfall (*Pcp*), and solar radiation (*Rg*) amount.

	Climate	**2004**	**2005**	**2006**
Air Temperature (°C)	15.9	18.3	16.3	16.7
Precipitation (mm)	588	478	596	442
Rg (MJ)		4729	5743	6000

Figures 35-37 show the daily variation in *Rg*, *Tair*, *Pcp*, and soil water content. The pattern of *Rg* and air temperature were clearly related (Figures 35 and 36). Trends in air temperature occurred in correspondence, but slightly delayed from *Rg* values. Maximum values in air temperature occurred in July each year.

The main differences in environmental conditions were due to the amount of precipitation during the three years, especially for 2004 and 2006, which had considerably lower *Pcp* than the mean. The pattern of seasonal *Pcp* was similar in the three years, with rainfall mostly from November through March. The summer clearly showed long drought periods.

In 2004 and 2005, rainfall was concentrated in the fall, and in 2005 there were more days that recorded more than 20 mm of daily precipitation. During 2006, daily rainfall was less frequent, but the precipitation per day was often higher (Figure 37). During 2004, the rain distribution was fall (118 mm), spring (96 mm), and summer 70 mm. A similar trend was found in 2005; when there were 160 mm, 73 mm, and 28 mm during the fall, spring, and summer. In 2006, 163 mm of precipitation occurred in the fall, but during the spring the precipitation was less (41 mm). The summer had a long drought period with 24 mm of precipitation.

Measured variations in soil water content were related to precipitation patterns. Values of volumetric soil water content were the mean of data measured at 0.20 m and 0.30 m. These values ranged from 13.6% to 37.5% in the three years (Figure 37). In 2004, it was higher than other years due to higher precipitation during the winter. In any case, the range was similar for the three years. Data clearly showed a deficit in soil water content recorded during the summer periods.

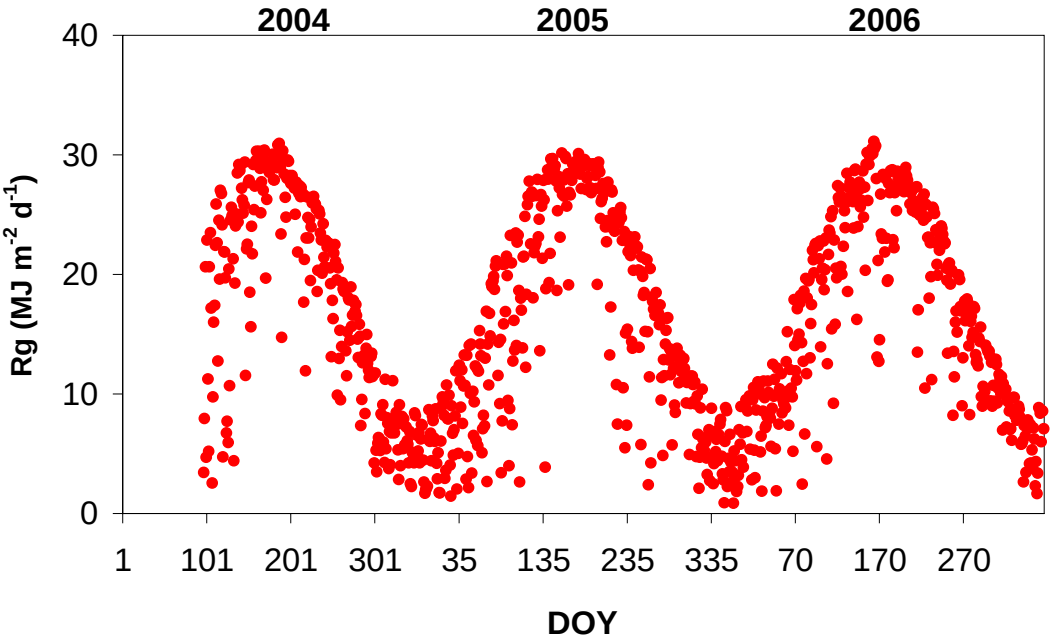

Figure 35. Interannual variation in daily total solar radiation (Rg).

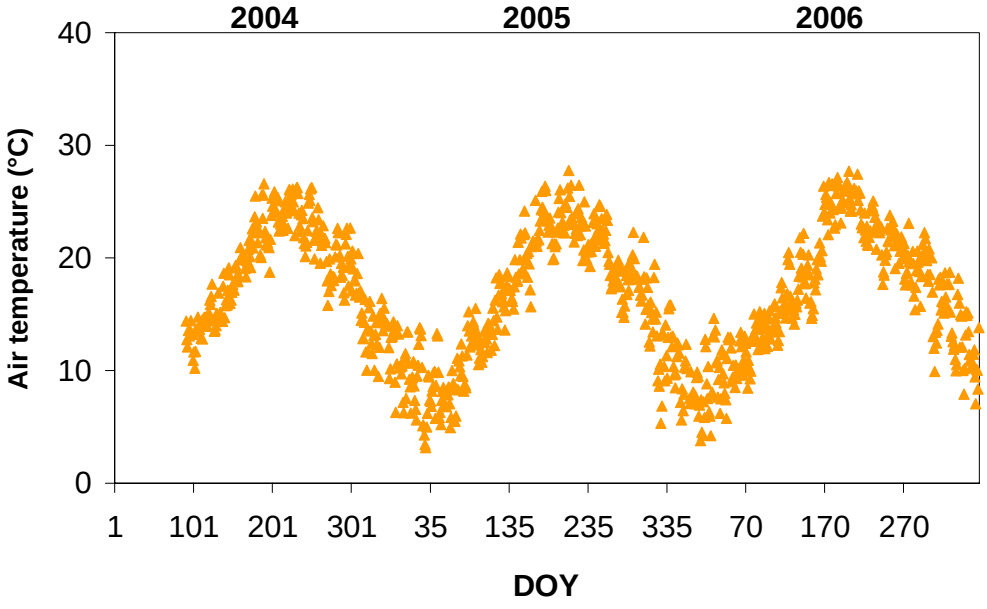

Figure 36. Interannual variation in daily mean air temperature (Tair).

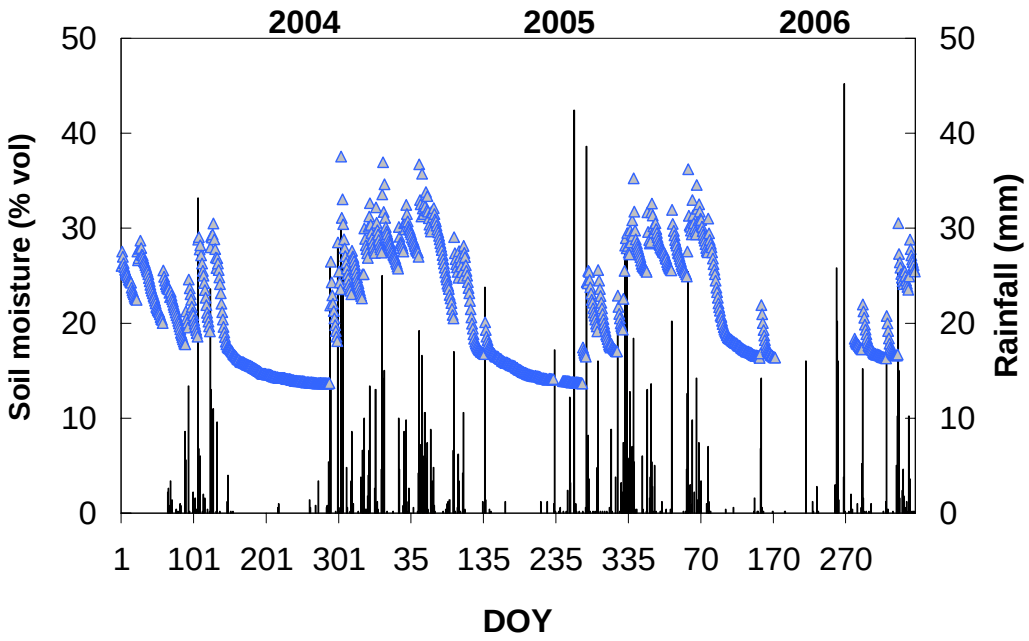

Figure 37. Interannual variation in daily total precipitation and daily mean volumetric soil water content at 0.25 m soil depth.

1.2 Radiation budget and albedo

Figure 38 shows the daily variation of short and long wave radiation components. *Rg* corresponds to the short wave radiation incoming from the sky into the surface. Maximum values were around 30 MJ m^{-2} day^{-1} in summer. There were no differences between years.

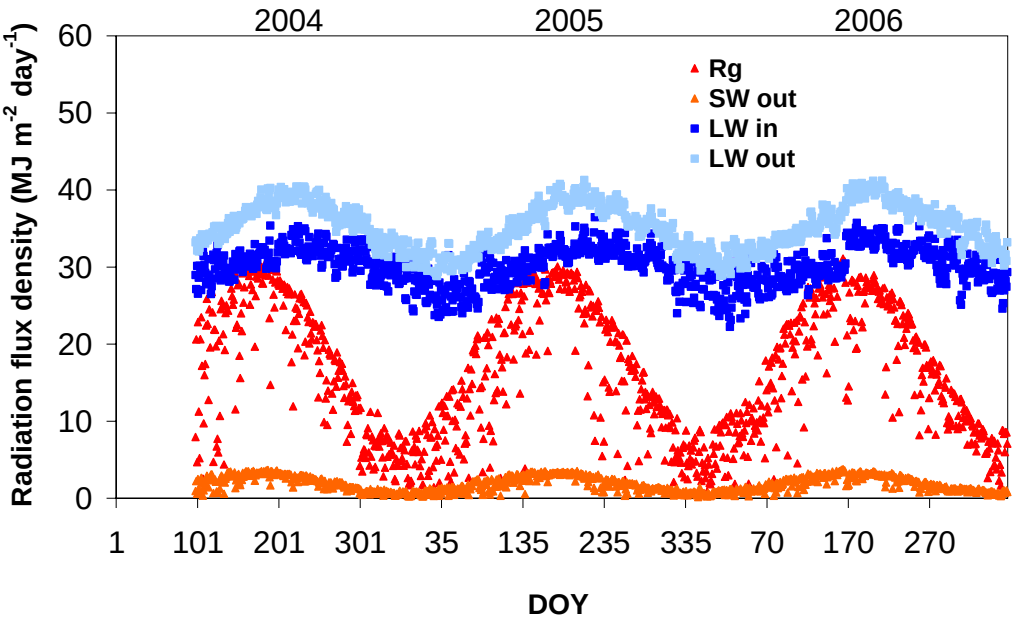

Figure 38. Daily variation in shortwave radiation incoming into the surface (Rg), shortwave radiation outgoing from the surface (SWout), long wave radiation incoming (LWin), and long wave radiation outgoing from the surface (LWout).

Short wave radiation reflected from the surface (*SWout*) showed low values, similar for the three years. These values ranged between 0.2 to 3.8 MJ m^{-2} day^{-1}. Long wave radiation values ranged from 22.2 to 36.5 MJ m^{-2} day^{-1}, and from 28.8 to 41.3 MJ m^{-2} day^{-1} for incoming (*LWin*) and outgoing (*LWout*) components, respectively.

The ratio of reflected to incoming shortwave radiation is defined as albedo. Figure 39 shows the average albedo values during the day. In maquis ecosystem, the average albedo was around to 10%. There were no differences between years.

Daily variation of albedo (Figure 40) shows values varying between 10 and 15%. The higher values were recorded during the summer.

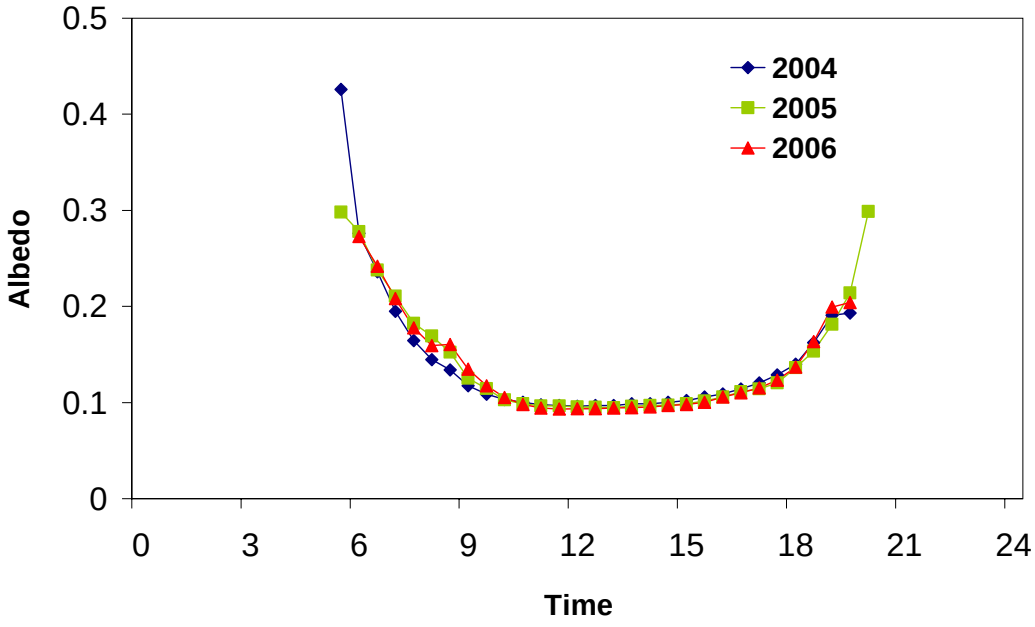

Figure 39. Daily variation of albedo of the mean day of the year.

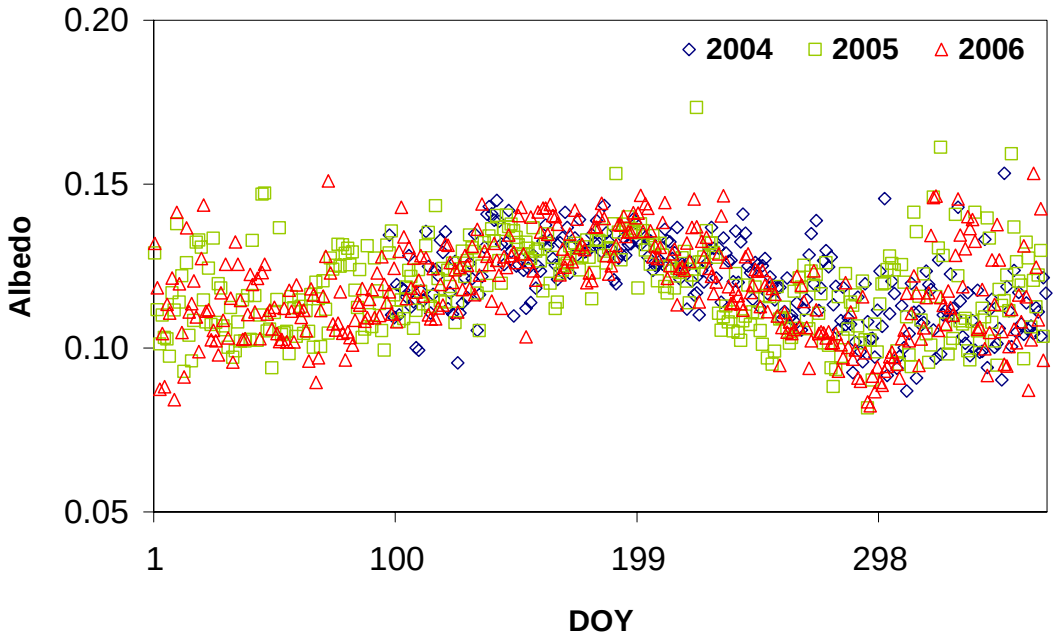

Figure 40. Seasonal and interannual variation in daily average albedo.

1.3 Energy closure and exchange

The energy budget closure indicator was used to evaluate reliability of the measured data (Baldocchi et al., 1988; Goulden et al., 1996; Aubinet et al., 2000). If the sum of turbulent fluxes (*H*+*LE*) is equal to the available energy (*Rn*-*G*), then the data quality is considered good. A lack in energy closure does not necessary mean errors in turbulent flux measurements, but it can indicate presence of advection conditions or absence of turbulence. The energy balance closure, however, is a useful mean to qualitatively evaluate the reliability of measurements.

To determine the closure level, we calculated the slope of linear regression forced through the origin of (*H*+*LE*) versus (*Rn*-*G*). The storage term can be neglected because it is usually small. It generally accounts for only a small fraction of *Rn* compared with the contribution of the other components. In ideal conditions, this parameter should be equal to 1. The energy budget closure from half-hour EC data was acceptable with a slope of 0.93 for the 2004-2006 period (Figures 41-43).

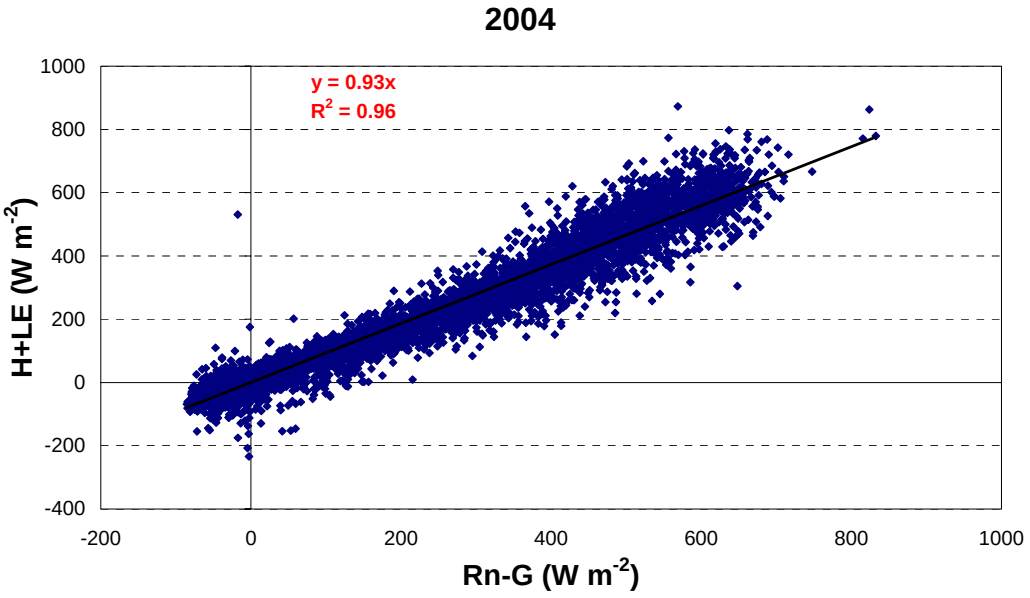

Figure 41. Energy budget closure and linear regression for measurements collected in 2004.

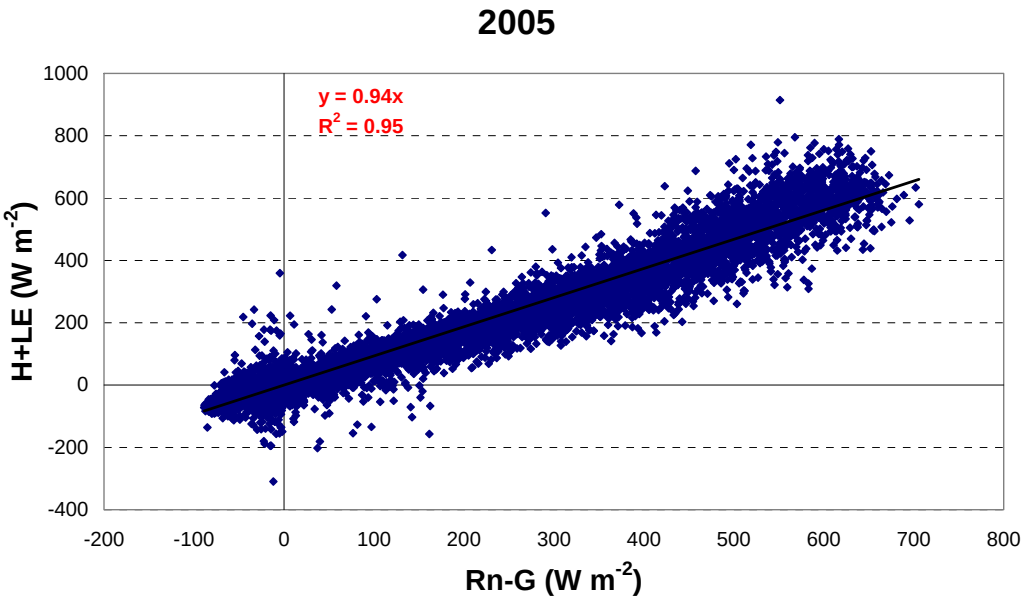

Figure 42. Energy budget closure and linear regression for measurements collected in 2005.

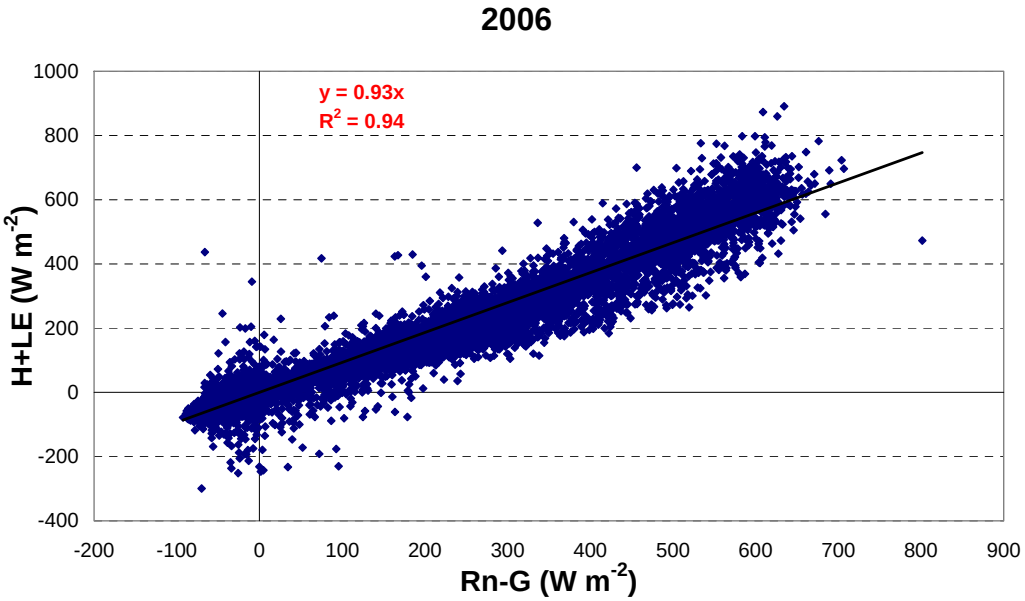

Figure 43. Energy budget closure and linear regression for measurements collected in 2006.

Quantification of energy and mass fluxes between vegetation and the atmosphere allows the evaluation of ecosystems functioning, and the understanding of complex relationships between the ecosystem live components. There is a narrow link between ecophysiological processes and the trends (daily, seasonal, and annual) of radiative and turbulent fluxes, so there is a need to study the single components of the energy budget. The analysis of the single energy budget components allows the interpretation of ecosystem functioning in relation to the environmental characteristics. Figure 44 shows the annual trends of net radiation (*Rn*), sensible heat flux (*H*), latent heat flux (*LE*), and soil heat flux (*G*).

The energy partitioning exhibited distinct seasonal pattern (Figure 44). The *Rn* trend showed lower values during winter and higher values during summer. The *H* trend was similar to *Rn*, but lower and delayed. Most available energy was used to heat the air. In general, *H* values were big compared to other ecosystems (e.g., crops and forest). *LE* values were clearly higher in spring and fall. During the summer, the ecosystem experienced a severe water deficit, and there was not enough water into the soil to allow forfull evaporation. Maquis species have mechanisms to function in drought conditions. *LE* values, therefore, were lower than most crop and forest ecosystems showing a decreasing *LE* in the summer. This behaviour was common to all years; showing a typically response to Mediterranean climate.

Two peaks, in spring and fall, clearly appeared during measurement years for *LE*. In 2004, the maximum value occurred in May, and the trend showed a decrease during the summer, due to the drought stress, until to reach a minimum value in September. *LE* values increased in October, due to rainfall and higher soil water content. Data showed the same trend in 2006 with a minimum value in July and two peaks, one in April and the other one in October. In 2005, the trend was a little different, with *LE* showing a minimum value in January and a clear decrease from May to July. Higher values occurred from August to November.

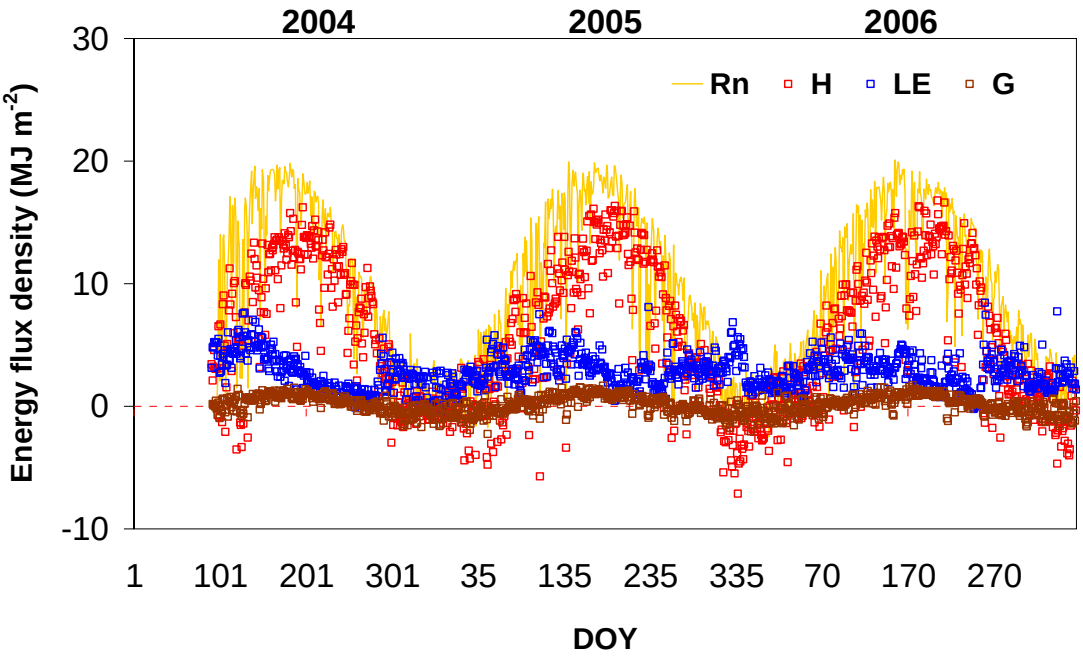

Figure 44. Partitioning of net radiation (Rn) into sensible heat flux (H), latent heat flux (LE), and soil heat flux (G) for the period 2004-2006.

Soil heat flux showed similar values in the three years. Minimum values were recorded in November (2004 and 2005) and in December (2006). The summer period showed higher values of *G*.

A useful parameter to indicate the relative importance and the partitioning between *LE* and *H* is the Bowen ratio (β), which is the ratio *H*/*LE*. The Bowen ratio values were clearly lower during the wet season (Figure 45) and higher during the dry season.

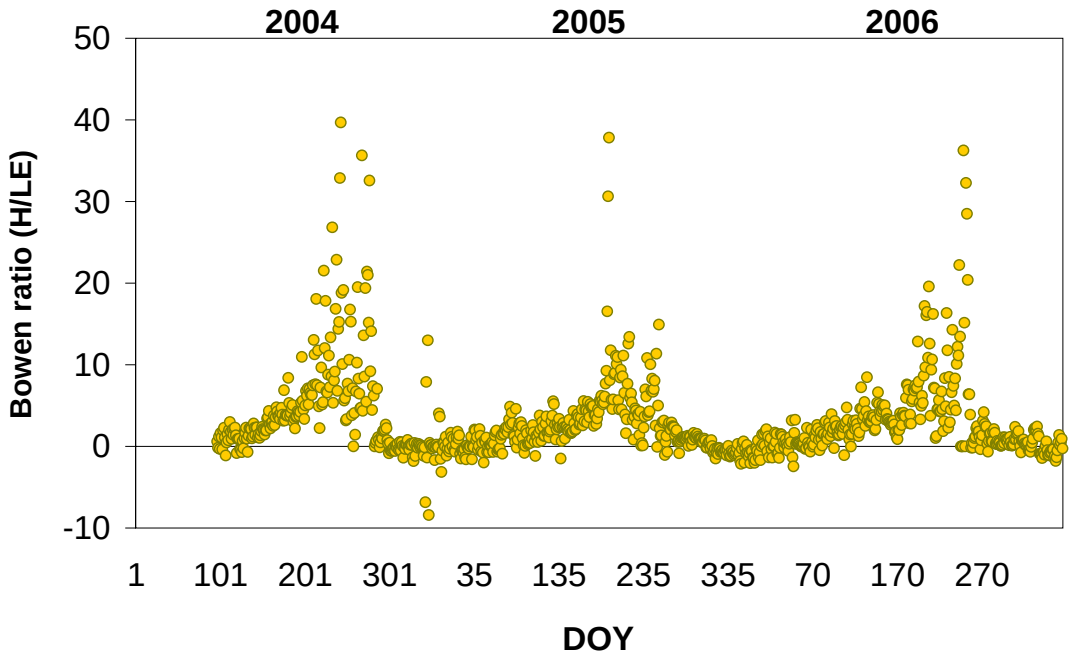

Figure 45. Trend of daily mean values of Bowen ratio (H/LE) measured in 2004, 2005, and 2006.

1.4 Variation in evapotranspiration

Figure 46 shows the daily variation in evapotranspiration for maquis ecosystem. The seasonal course of evapotranspiration showed peaks in spring and fall when the soil water content was higher (Figure 37). During the summer, *ET* values decreased due to drought. The months with the maximum total *ET* were May in 2004 and 2005, and April in 2006 (74.6, 59.5, and 50.3 mm, respectively). During these months, daily maximum *ET* was about 3 mm. The lowest values for *ET* occurred in 2006 when the precipitation was less (Table 6). The *ET* decreased from June to September in 2004 and 2005, and from May to August in 2006.

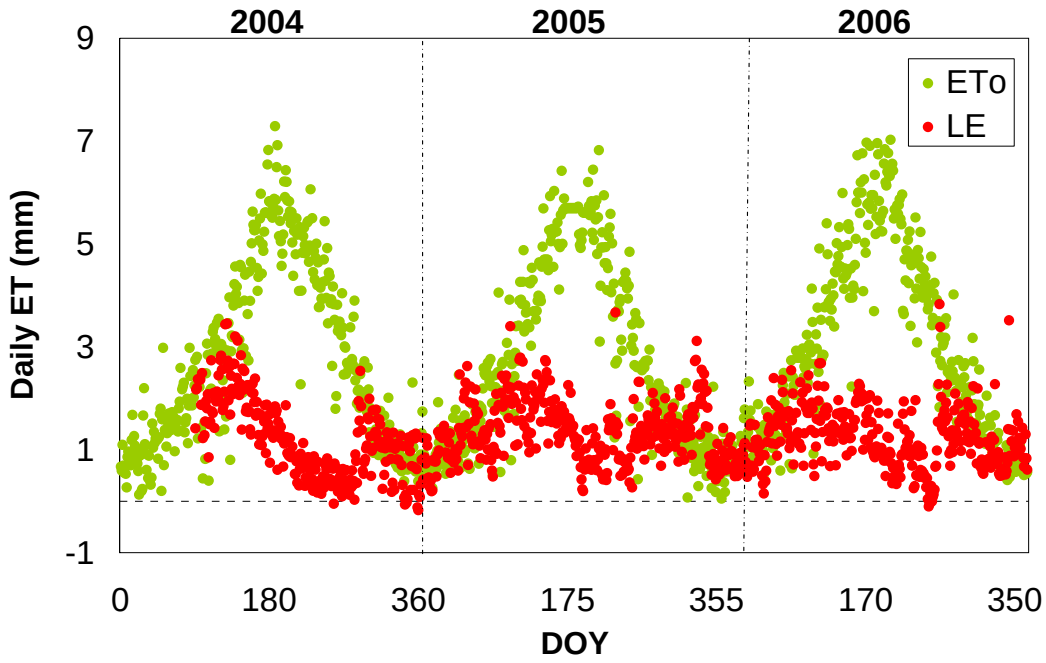

Figure 46. Daily variation in potential evapotranspiration (ETo) and actual evapotranspiration (LE) measured with EC technique.

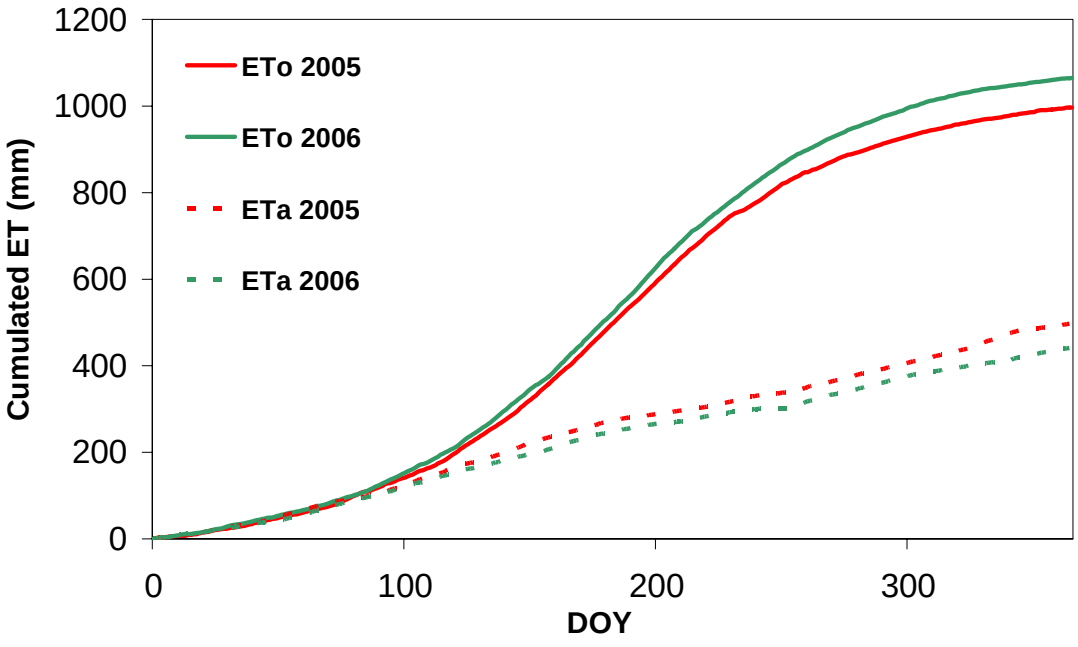

Figure 47. Comparison of cumulative ETo and ETa in maquis ecosystem for the experimental period.

Figure 47 shows the trends of cumulated reference evaoptranspiration (*ETo*) and *ETa* (i.e., *LE*) for 2005 and 2006. Data of 2004 were not included because they were not complete. There were minimal differences between years in the amount of evapotranspiration. In 2006, the cumulative *ETa* was slightly lower than in 2005.

1.5 Coupling analysis

McNaughton and Javis (1983) developed the concept of a coupled atmosphere-vegetation system. The decoupling coefficient (Ω) is used to assess the coupling of water exchange between the surface and the atmosphere. Values of Ω range from 0 for perfect coupling to 1 for complete isolation. Ω value approaching 1 indicates that the canopy water vapour flux is decoupled from the atmosphere and that evapotranspiration is mostly controlled by net radiation. Values approaching zero indicate that water vapour flux is largely controlled by vegetation. Stomatal control of transpiration grows progressively weaker as Ω approaches 1.

In 2005, the Ω values varied from 0.11 (July) to 0.78 (March), while in 2006 Ω varied from 0.08 (January) to 0.71 (January). Similar trends were found in the two years (Figure 48). Higher values were recorded during winter and spring, and lower values were recorded during summer (average value of 0.2 in the two years). The month showing the lowest average value (0.15) was July in both years. This trend confirmed that the available energy was mainly used to heat the air (*H* flux) rather to evaporate water (*LE* flux) during summer (Figure 44). On a daily basis, high values of Ω were observed during the morning indicating that evapotranspiration was influenced more by solar radiation than the vegetation. The low values of Ω recorded at the midday indicate the strong influence of vegetation on evapotranspiration. After 4 PM, values increased indicating a stronger *Rn* influence on evapotranspiration. The standard error was low for the two years. It ranged between 0.01 and 0.06 in 2005, and from 0.01 to 0.10 in 2006.

Vegetation with short and dense canopy (resulting in high g_c and low g_a) such as agronomic crops tend to have higher values of Ω (Meinzer, 1993; Baldocchi, 1994). Vegetation with open canopies and small leaf area (resulting in high g_a) such as coniferous forest, tend to have Ω values between 0 and 0.2 (they are well coupled). Broadleaved forests usually fall somewhere between the two extreme cases, with Ω values ranging between 0.4 and 0.6 (Meinzer, 1993; Hinckley et al., 1994).

The values of Ω obtained in the present research were similar to those of Hao et al. (2007). In a study over steppe in Mongolia they found Ω values varying from 0.2 to 0.6, in the period from May to July. They also observed the lowest value in July. For wet mixed grassland the values lie between 0.1 and 0.3, while for serpentine grassland Ω values varied from 0.1 to 0.8 (Wever et al., 2002). No clear diurnal cycle was found by Kumagai et al. (2004). In a study over a tropical rainforest (Malaysia), they found the values ranging from 0.1 to 0.4 during July, with an average value of 0.2. In a study conducted over grassland in Davis (CA) (Mediterranean climate), the Ω values varied from 0.69 to 0.93, with average of 0.83 (Pereira, 2004), a value close to 0.8 reported by McNaughton and Jarvis (1983). An Eucalypt forest in Portugal was investigated for three years (2003-2005) and the Ω values were under a 0.2 threshold during the three summers indicating that in these months the lowering of evapotranspiration was related to increased stomatal resistance and high water vapour deficit values, during a dry period (Mateus et al., 2006).

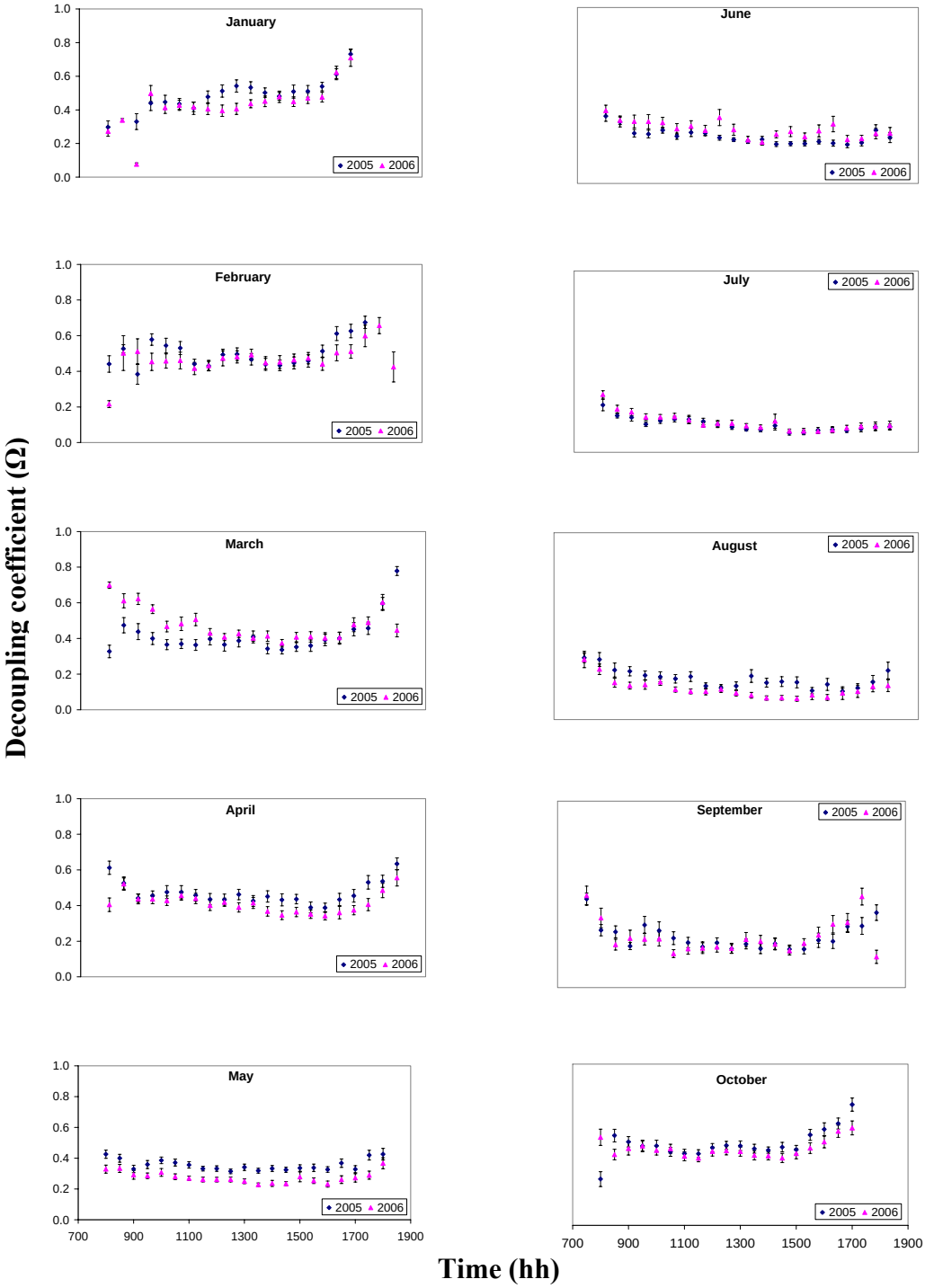

Figure 48. Seasonal and interannual variation in the mean diurnal course of the decoupling coefficient (Ω) and its standard error for data from 2005 and 2006.

1.6 Variation in NEE, GPP, and Reco.

Carbon flux measurements provided an accurate quantification of carbon absorbed or released from the ecosystem. The net carbon flux determines if an ecosystem is a *source* or a *sink* of atmospheric carbon, and helps to understand the role of that ecosystem in the global carbon balance. The net balance of carbon absorbed or released from vegetation was estimated by continuous measurements of instantaneous flux data. These data were expressed in μmol m^{-2} s^{-1} and they were converted to g C m^{-2} for each 30 minute period. Sums of the half-hour carbon flux data provided the net carbon exchange for periods of interest (day, season, or year). Negative values of NEE imply that the ecosystem is a *sink* for carbon (uptake by photosynthesis is greater than losses by respiration). Positive values mean that the ecosystem is a *source* of carbon.

Figure 49 shows the temporal variation of daily net carbon exchange (NEE) between the ecosystem and atmosphere. The average value of NEE was –0.48 g C m^{-2} day^{-1} in 2004. It was a partial average because the data were not collected during the entire year. In 2005 and 2006, the average values were -0.62 and -0.33 g C m^{-2} day^{-1}, respectively.

In general, the highest monthly values of carbon uptake in 2004 (Figure 50) occurred in spring (March, April, and May). The maximum uptake was -80.4 g C m^{-2} in May and the maximum loss was 35.1 g C m^{-2} in October 2004. In 2005, the maximum uptake occurred in April (-65.5 g C m^{-2}) and the maximum loss was 27.6 g C m^{-2} in October. The same trend occurred in 2006, with a value of -67.2 g C m^{-2} in April and 46.4 g C m^{-2} in September (Figure 50).

In general, the sign of NEE remained negative (*sink*) from January to July in each year, with the exception for 2004 in which the measurements began in April. The ecosystem acted as a carbon *source* during the summer and fall (respiration greater than photosynthesis) and it returned to a *sink* in November and December. This behaviour can be easily seen in Table 7, where a synthesis of seasonal trend in NEE, gross primary production (GPP), ecosystem respiration (Reco), and precipitation is presented.

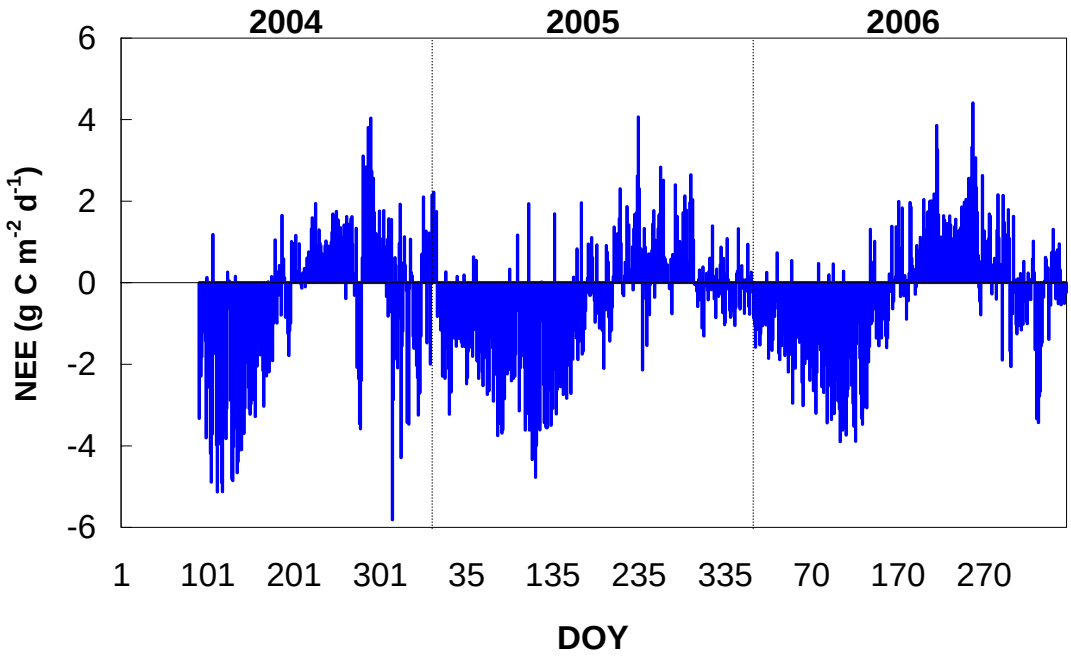

Figure 49. Daily variation in mean CO_2 flux (NEE) (g C m^{-2} day^{-1}).

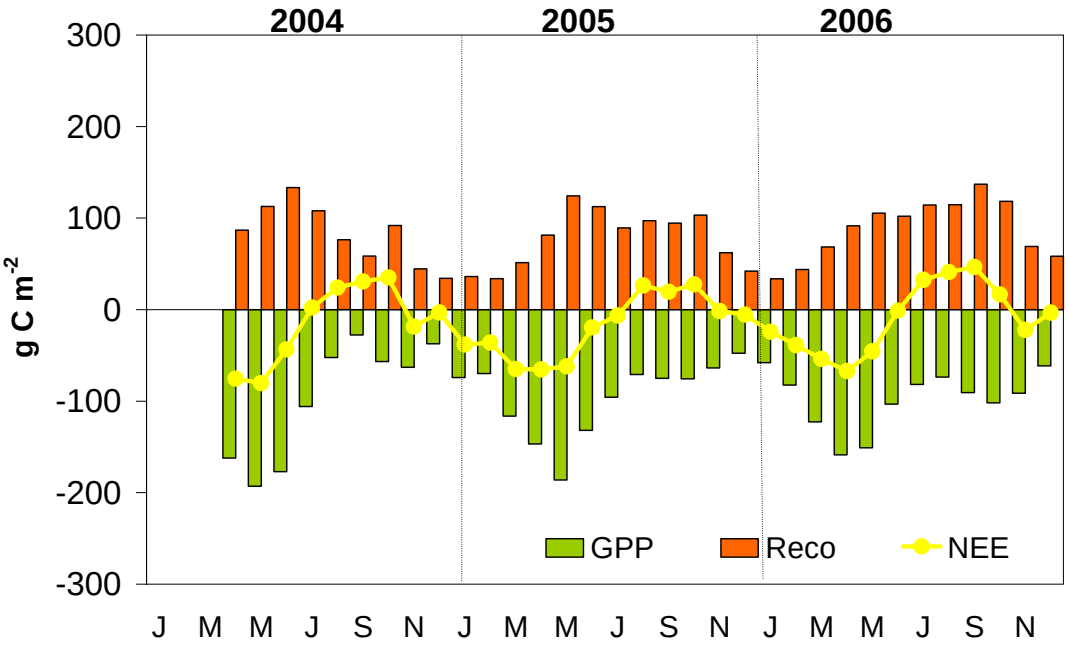

Figure 50. Monthly variation in CO_2 flux (g C m^{-2} $month^{-1}$).

Table 7. Seasonal values of NEE, GPP, Reco, and Rain for the measurement years. Win = winter, Sp = spring, Sum = summer. The ratio GPP/Reco is also shown.

SEASONAL TABLE

	NEE	GPP	Reco	Rain	GPP/Reco
	g C m^{-2} $season^{-1}$	g C m^{-2} $season^{-1}$	g C m^{-2} $season^{-1}$	mm	
2004 Win.					
2004 Sp.	-155.85	-355.41	199.57	166.80	-1.78
2004 Sum.	-17.46	-335.24	317.77	1.80	-1.05
2004 Fall	47.25	-147.58	194.82	191.60	-0.76
2005 Win.	-77.35	-181.58	104.23	244.80	-1.74
2005 Sp.	-192.53	-449.51	256.97	100.60	-1.75
2005 Sum.	0.40	-298.54	298.94	22.80	-1.00
2005 Fall	45.48	-214.56	260.03	263.80	-0.83
2006 Win.	-68.56	-188.16	119.60	189.20	-1.57
2006 Sp	-167.05	-432.57	265.51	43.60	-1.63
2006 Sum.	72.47	-258.60	331.06	42.60	-0.78
2006 Fall	40.65	-283.71	324.34	164.20	-0.87

The ecosystem was generally a *source* of carbon in summer and fall, whereas the C uptake (*sink*) occurred mainly in the spring. Uptake occurred in winter, but less than in spring. During the spring, the vegetative activity of the ecosystem increased due to the availability of energy and water, which led to higher CO_2 transfer to the vegetation. During the summer, instead, the drought controlled the ecosystem functioning. The soil was not deep, so there was limited water storage. Maquis plants adapt to drought stress and still photosynthetize under extreme drought conditions. The photosynthesis, however, is reduced to a smaller magnitude than respiration resulting in positive NEE.

Daily values of NEE found in this research were lower than reported by Granier et al. (2007) for forest. They analyzed carbon exchange in deciduous and coniferous forest, and in Mediterranean vegetation. Generally, the highest CO_2 uptake was observed in the deciduous forests (-10 g C m^{-2} day^{-1}), while the coniferous forests showed medium values (-6 or -7 g C m^{-2} day^{-1}). The lowest rates were measured in the Mediterranean vegetation (-4 g C m^{-2} day^{-1}), which also exhibited the lowest seasonal variation in NEE. In a study by Papale and Valentini (2003), European forests were subdivided by latitude. In South Europe (<44°N), the maximum observed uptake was -3 g C m^{-2} day^{-1}.

GPP and Reco were determined using the methodology proposed by Reichstein et al. (2005). Daily average values of GPP were similar in the three years (about -3.20 g C m^{-2} day^{-1}). In 2005, GPP was lowest (-3.16 g C m^{-2} day^{-1}). Figure 48 shows the monthly values of GPP and Reco for the measurement years. The differences among years are important features of the variables, which can be partially explained by meteorological conditions. The monthly fluctuations showed a wider range in GPP and Reco during the 2004-2005-2006 experimental periods. The monthly trend showed higher value of GPP in spring when plants found better conditions for growing (-193 g C m^{-2} $month^{-1}$ in May 2004, -186 g C m^{-2} $month^{-1}$ in May 2005, and -159 g C m^{-2} $month^{-1}$ in April 2006), and a reduced GPP from summer to fall. During the fall, the ecosystem increased carbon uptake but less than in spring. In 2004, the magnitude of GPP decreased from May to September when it reached the value -28 g C m^{-2} $month^{-1}$, and it increased during the fall. In 2005, the magnitude of GPP decreased from July to

December (value of -48 g C m^{-2} $month^{-1}$), but the values were similar during the fall months (about -75 g C m^{-2} $month^{-1}$). In 2006, absolute GPP decreased from April to August and increased during the fall (about -90 g C m^{-2} $month^{-1}$). The minimum value occurred in December (-62 g C m^{-2} $month^{-1}$).

The seasonal values of carbon exchange are shown in Table 7. Spring was the season with the greatest GPP. The largest production of carbon occurred in 2005 (-450 g C m^{-2} $season^{-1}$), while the smallest 2005 GPP was recorded during the winter (-182 g C m^{-2} $season^{-1}$). Comparable values were found for 2006, and the difference between spring and summer was similar to 2005 (about 150 g C m^{-2} in 2005 and 173 g C m^{-2} in 2006). This difference was much less in 2004 (only 20 g C m^{-2}). The precipitation was only 1.80 mm during the summer of 2004, but apparently this water deficit had little effect on the GPP.

Daily average ecosystem respiration (Reco) was about 2.72 g C m^{-2} day^{-1} in 2004, 2.54 g C m^{-2} day^{-1} in 2005, and 2.89 g C m^{-2} day^{-1} in 2006. The year 2005 had the lowest daily average values of Reco, while the same year showed higher values of daily average NEE. In 2004, the Reco increased during the spring until a maximum value of 133 g C m^{-2} $month^{-1}$ in June, and it decreased during the summer until September (58 g C m^{-2} $month^{-1}$). After the drought stress, a peak occurred in October (92 g C m^{-2} $month^{-1}$); following the first rainfall events that stimulated microbes and plants activity. In 2005, after the maximum value in May (124 g C m^{-2} $month^{-1}$), Reco remained stable at about 100 g C m^{-2} $month^{-1}$ until October. A severe decrease occurred in November and December (42 g C m^{-2} $month^{-1}$). This trend can be seen in Table 7 showing Reco values of 257, 299, and 260 g C m^{-2} $season^{-1}$ in spring, summer, and fall, respectively. In 2006, Reco gradually increased during the spring until reaching a stable value of about 110 g C m^{-2} $month^{-1}$ from May to August. The Reco peaked in September (137 g C m^{-2} $month^{-1}$) with a severe drop in November and December (58 g C m^{-2} $month^{-1}$). Similar values were found in the summer and fall (Table 7).

Figure 51 shows the cumulated values of NEE for 2005 and 2006. The years 2004 is not included because the measurement periods started in April. Similar trends in CO_2 absorbed occurred in the first part of both years. Major differences occurred during summer; due to different regimes of available water

during the year. There was considerably more rainfall during the winter and spring 2005 and somewhat less rainfall during the summer (Table 7). This would likely lead to more soil water storage in the spring that could extend the spring photosynthesis period. Rainfall during the summer will have little effect on photosynthesis, but it could increase soil respiration. The combination of these factors possibly explains the bigger magnitude of NEE during the summer 2005.

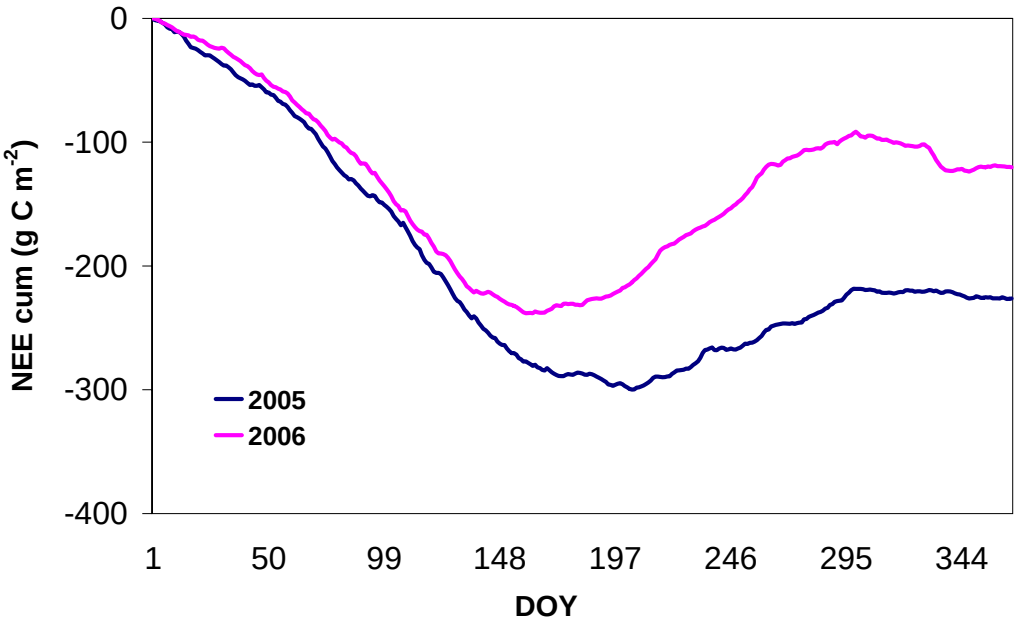

Figure 51. Cumulated values (g C m^{-2}) of NEE in the years 2005 and 2006.

Table 8. Annual sums of NEE, GPP, Reco, rain, and sir temperature (*Tair*) for 2005 and 2006. It is also shown the annual ratio GPP/Reco.

YEAR	NEE	GPP	Reco	Rain	Tair	GPP/Reco
	g C m^{-2} $year^{-1}$	g C m^{-2} $year^{-1}$	g C m^{-2} $year^{-1}$	mm	°C	
2005	-226	-1454	928	596	15.7	-1.57
2006	-120	-1122	1057	442	16.6	-1.06

On an annual scale, the ecosystem acted as a carbon *sink* showing variability between years (Table 8). In 2005, the ecosystem accumulated 226 g C m^{-2} $year^{-1}$, while in 2006 the NEE exchanged was 120 g C m^{-2} $year^{-1}$. These values were higher than those recorded by Hastings et al. (2005) in a shrub land (-39 and -52 g C m^{-2} $year^{-1}$ in 2002 and 2003, respectively). These values were low because the site was located in a desert in Mexico, with a low annual precipitation rate. A pine plantation in the Yatir forest in Israeli, with annual precipitation of 275 mm per year, was found to be a *sink* of between -130 and -240 g C m^{-2} $year^{-1}$ (Grunzweig et al., 2003). Powell et al. (2006) measured NEE in scrub oak ecosystem in Florida for six consecutive years. They found annual NEE values varying between 107 to 407 g C m^{-2} $year^{-1}$. The annual NEE increased from 2000 to 2006, and carbon accumulation was higher in spring and less in summer. Another study was conducted over mixed vegetation (crops and forest patches) by Haspzra et al. (2005). During the seven measurement years, the site acted as a carbon *sink* except for the year 2003. In the last measurement year (2004), the NEE exchanged between vegetation and the atmosphere was -107 g C m^{-2}.

One of the few study over shrubland ecosystem was conducted by Luo et al. (2007). They studied energy and mass fluxes over a mature semiarid Mediterranean type chaparral ecosystem in southern California for seven consecutive years from 1996 to 2003. A carbon *sink*, from -96 to -155 g C m^{-2} $year^{-1}$ was determined under normal weather conditions, while a weak *sink* of -18 g C m^{-2} $year^{-1}$ and a strong *source* of 207 g C m^{-2} $year^{-1}$ were observed as a consequence of a severe drought.

In Europe, several studies were conducted to investigate forest behaviour regarding carbon cycle. Marcolla et al. (2005) studied carbon exchange over a mixed forest at Renon (Italy). They found annual NEE values of -669 g C m^{-2} $year^{-1}$ (2002) and -782 g C m^{-2} $year^{-1}$ (2003). GPP values varied from 1277 to 1126 g C m^{-2} $year^{-1}$ in 2002 and 2003, respectively. Another study conducted in Italy (San Rossore) over Mediterranean pine, showed NEE values rangin from -430 (2002) to -359 (2003) g C m^{-2} $year^{-1}$, and GPP values of 1878 and 1517 g C m^{-2} $year^{-1}$ in the two years (Tirone et al., 2003).

Granier et al. (2000) observed carbon fluxes over a beech stand in France for two consecutive years. NEE values were -218 and -257 g C m^{-2} $year^{-1}$ in 1996 and 1997, respectively. GPP ranged from 1000 to 1300 g C m^{-2} $year^{-1}$, and the ecosystem respiration had the major role in the annual C balance of this forest. Reco varied from 800 to 1000 g C m^{-2} $year^{-1}$. This forest was also studied in 1998 and 1999, and NEE showed lower values in 1998 (-68 g C m^{-2} $year^{-1}$) due to higher respiration and lower photosynthesis. In 1999, the NEE value was higher than in the two previous years (-296 g C m^{-2} $year^{-1}$) (Granier et al., 2002). They reported a similar trend in Denmark over beech forest for the same years. NEE was low in 1998 (-71 g C m^{-2} $year^{-1}$) and it was high in 1999 (-227 g C m^{-2} $year^{-1}$).

In a study conducted by Valentini et al. (2000) the authors analyzed European forest at different latitudes. In Italy (41° 52'N), NEE was -660 g C m^{-2} $year^{-1}$. In another Italian site (46° 18'N), the value of NEE was -450 g C m^{-2} $year^{-1}$. Valentini et al. (1996, 2000) studied a deciduous forest in Italy. NEE ranged from -470 to -660 g C m^{-2} $year^{-1}$. GPP showed a value of 1302 g C m^{-2} $year^{-1}$ in 1999, and photosynthesis process prevailed over respiration (Reco value was 636 g C m^{-2} $year^{-1}$) during the two years.

In Germany, Grunwald et al. (2007) found NEE values ranging from -698 g C m^{-2} $year^{-1}$ (1999) to -395 g C m^{-2} $year^{-1}$(2003). The values in 2003 were lower due to a severe drought during that summer. Owen et al. (2007) examined 15 forest sites to estimate NEE over Europe from western oceanic to eastern continental, and from boreal to Mediterranean climates. In the case of deciduous forest sites, they found a general decrease in annual GPP from south to north in response to growing season length with the exception of Collelongo (1560 m a.s.l.), which is influenced by elevation. NEE values for coniferous forest in Germany was -534 g C m^{-2} $year^{-1}$ in 2001 and -685 g C m^{-2} $year^{-1}$ in 2002. GPP ranged from 1681 to 1930 g C m^{-2} $year^{-1}$, and Reco varied from 1147 to 1245 g C m^{-2} $year^{-1}$ (Bernhofer et al., 2003). Over mixed forest in Belgium, the NEE value was -600 g C m^{-2} $year^{-1}$ in 1996-1997 (Aubinet et al., 2001). In a successive study, NEE was -355 g C m^{-2} $year^{-1}$ in 2002, and the GPP value was 1528 g C m^{-2} $year^{-1}$. The ecosystem respiration was the determining factor for the carbon balance with 1173 g C m^{-2} $year^{-1}$ (Aubinet et al., 2002).

Although the ecosystems studied by these authors are different from maquis ecosystem, they provide some useful information on the general behaviour of different ecosystems in response to environmental conditions. To know how maquis ecosystem responde to environmental factors, we investigated the relationships between NEE, GPP, and Reco and the driving ecosystem forcings. In particular, we analyzed the importance of air temperature, precipitation, and water availability on carbon exchange.

1.7 Ecosystems functioning and driving forcings

As seen before, maquis ecosystem has intense activity in the spring and fall. During the spring, the ecosystem was a carbon *sink*, while it was a carbon *source* in summer and fall (Table 7). During the winter, carbon uptake was low because of limited radiation and low air temperatures. To know the forcing factors on ecosystem processes, we analyzed the GPP and Reco trends at seasonal and daily scales. The forcing factors are the available water for evaporation (*LE*) and the air temperature. No relationships were found between gross photosynthesis (GPP) and ecosystem respiration (Reco) with rainfall. Clear relationships were instead found with *LE* and air temperature.

Figure 52 shows the relationship between GPP and *LE*. During the spring there was a clear relationship between these terms indicating that the availability of water was the driving factor for photosynthesis process. Also air temperature had a role in carbon production during the spring (Figure 53). During the fall, instead, GPP did not show a relationship with *LE* and air temperature showing that ecosystem photosynthetic activity was low and not controlled by these factor. In fact, during the fall, the respiration was the prevalent process and it was related to the available water (Figure 54). During the summer, characterized by the drought period, microbes and plants slowed down their activity. With the first precipitations, the microbe activity increased, whereas there was little effect on the vegetation. As a result, the respiration increased more than photosynthesis in the late summer and fall.

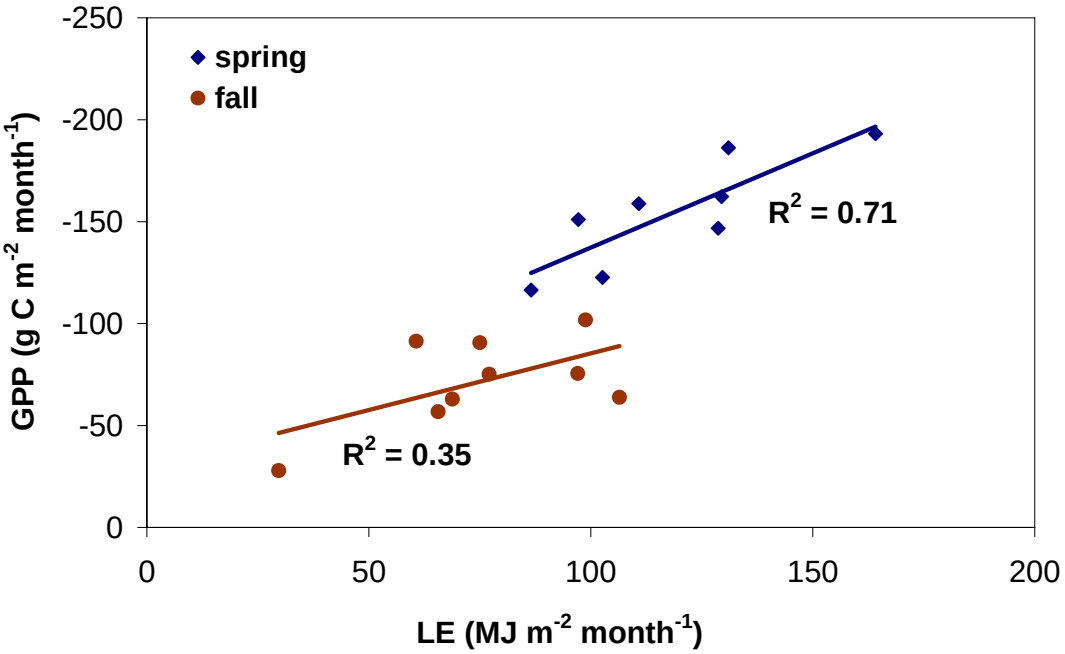

Figure 52. Relationship between gross primary production (GPP) and latent heat flux (LE) during spring and fall.

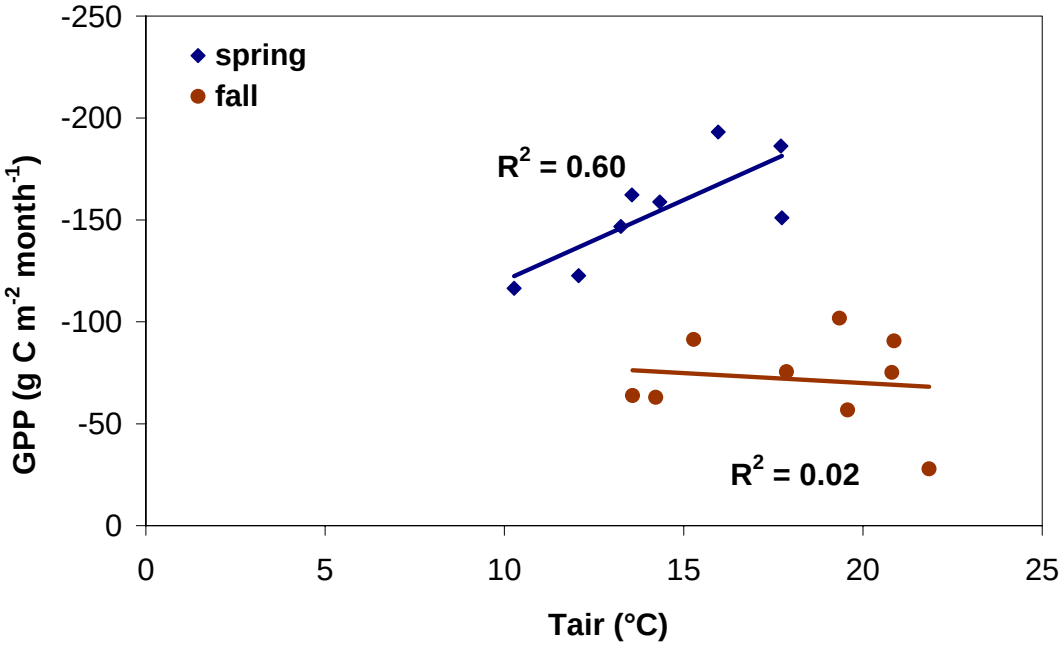

Figure 53. Relationship between GPP and air temperature in spring and fall.

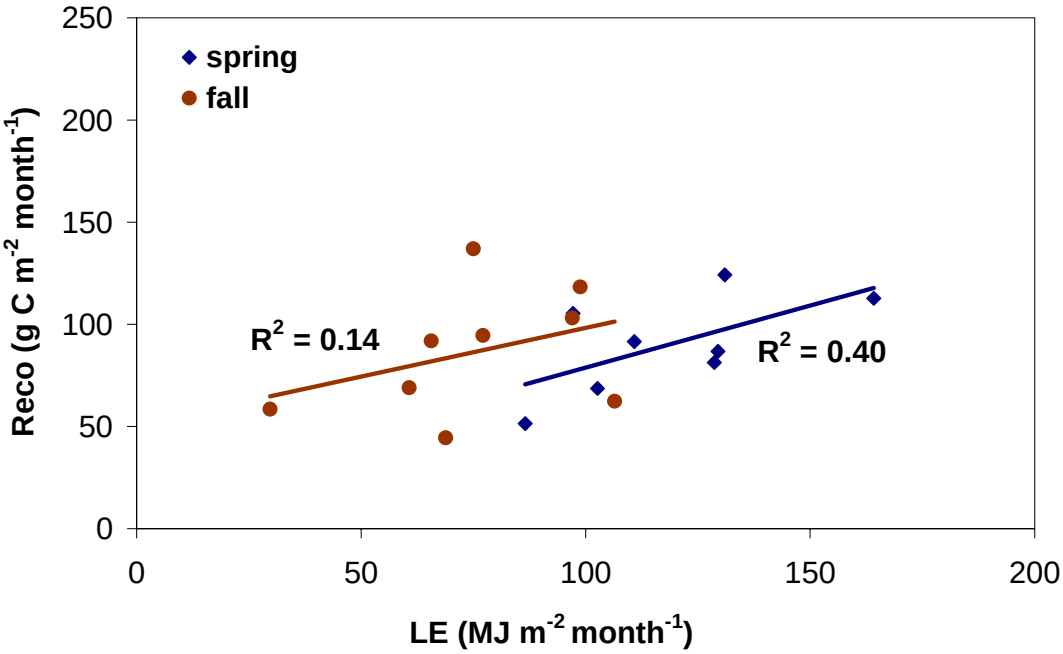

Figure 54. Ecosystem respiration (Reco) and LE relationship during spring and fall.

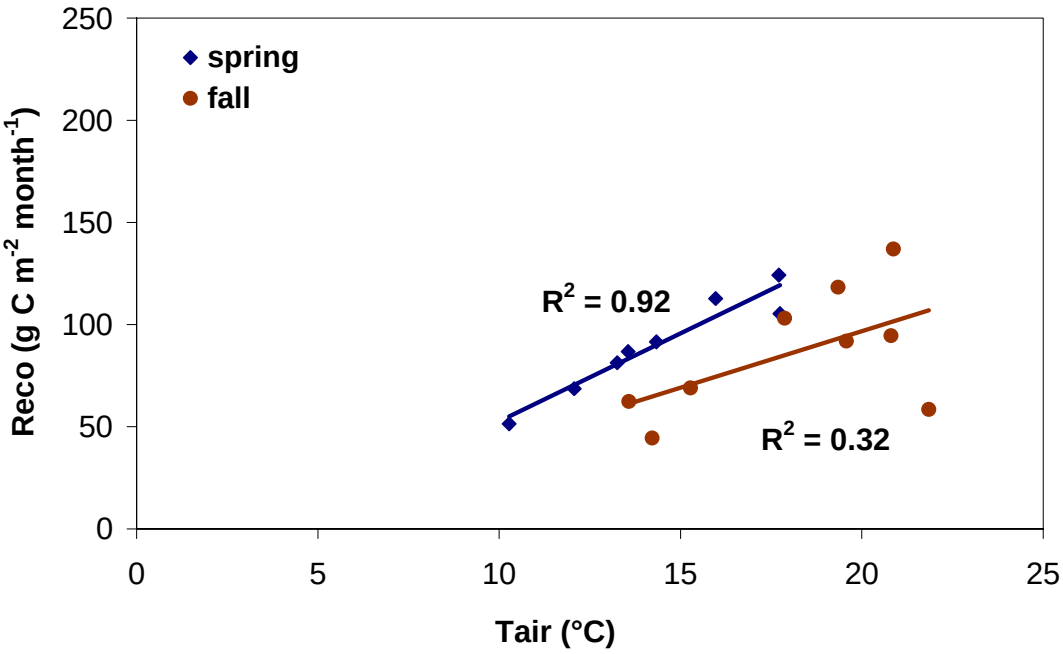

Figure 55. Relationship between ecosystem respiration (Reco) and air temperature (Tair) in spring and fall.

Ecosystem respiration was clearly correlated to air temperature (Figure 55). This relation was higher during the spring, when air temperature values were optimal for ecosystem activity. Microbes tend to be more active when the conditions are warm and moist. Since the spring was wetter than fall, the observed response (Figure 55) was most likely due to the interacting effects of temperature and water.

Relationships between GPP and Reco to *LE* and air temperatures were also analyzed using bins of these variables. *LE* was subdivided in bins of 1 MJ m^{-2} day^{-1} each, while air temperature was subdivided in bins of 3°C each. Daily data of the three years of GPP and Reco were used.

Gross primary production showed a good linear regression with bins of *LE* (Figure 56). GPP increase was about 1 g C m^{-2} day^{-1} per each MJ m^{-2} day^{-1} of *LE*. Therefore, more water (and energy) available led to more carbon absorbed by the ecosystem. These conditions occurred mainly during the spring. Even if water was available in the fall, the other driving factor (*Tair*) limited GPP. A non linear relationship was found between GPP and *Tair*. GPP increased up about 15-18°C and then decreased because as the temperature increased above the optimal for photosynthesis (Figure 57).

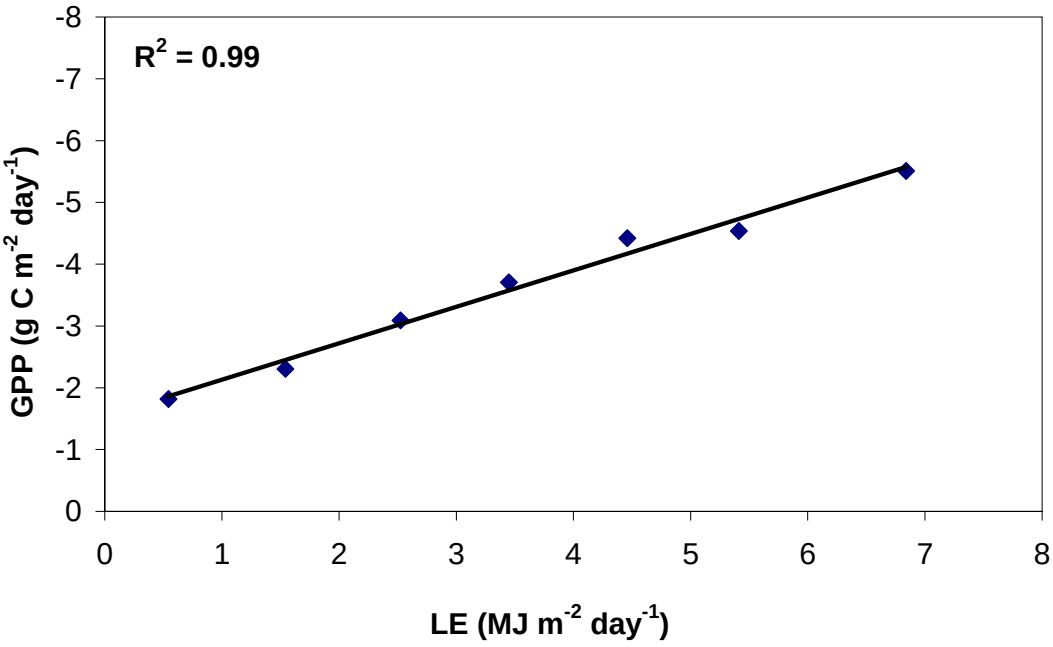

Figure 56. Daily relationship between gross primary production (GPP) and bins of latent heat flux (LE).

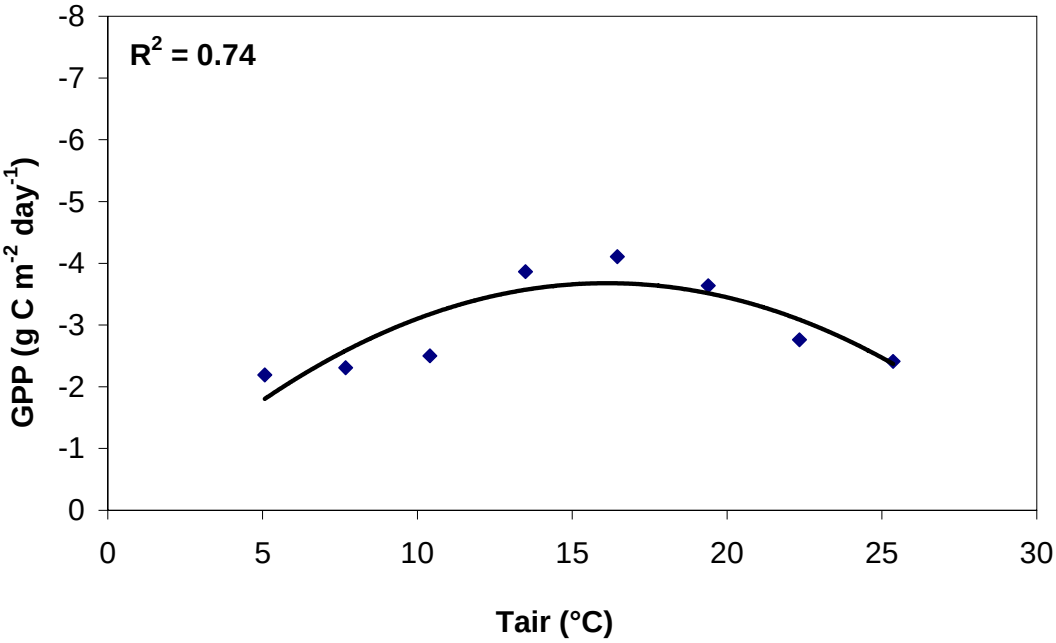

Figure 57. Daily relationship between gross primary production (GPP) and bins of air temperature (Tair).

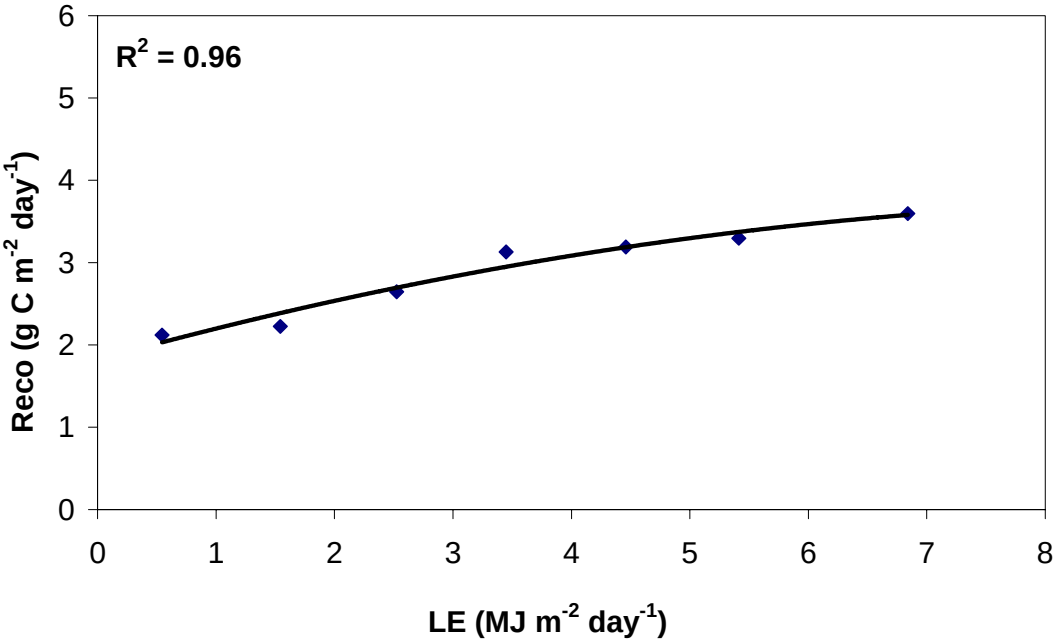

Figure 58. Daily relationship between ecosystem respiration (Reco) and bins of latent heat flux (LE).

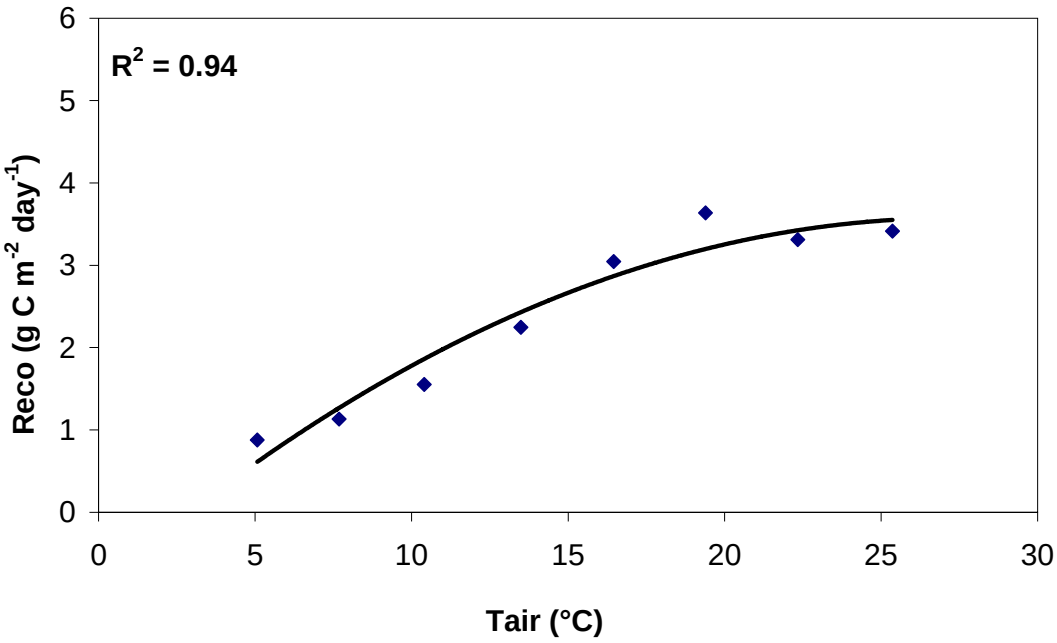

Figure 59. Daily relationship between ecosystem respiration (Reco) and bins of air temperature (Tair).

A similar *LE* trend was found for ecosystem respiration. Reco increased less than 1 g C m^{-2} day^{-1} per each MJ m^{-2} day^{-1} of *LE* (Figure 58). Ecosystem respiration also increased with air temperature. The Reco increased at a rate of about 1 g C m^{-2} day^{-1} for every 5°C, but it seemed levelling off at temperatures above 20°C. This levelling off might due to deficits of soil water which occurred mainly in the summer when temperatures were high. Because the photosynthesis decreased more than respiration during the hot, dry summer, the ecosystem became a *source* of carbon.

These results were confirmed by the GPP/Reco ratio values. It ranged between -0.76 (fall 2004) and -1.78 (spring 2004) (Table 7). Lower values were found in summer and fall (Reco prevailed over GPP), while higher values were found in spring.

B) Grape vineyard

1.8 Environmental conditions

Environmental data were collected over grapevines during three periods. The first measurement period was 28 June-8 July 2005 (Figure 60). The second period was 1-9 August 2005 (Figure 61). The last period was in 2006 from 26 June to 5 August (Figure 62).

Daily average air temperature was 24.6°C during the first measurement period with a maximum of 34.6°C on 29 June and a minimum of 14.5°C on 6 July. Maximum air temperature was typically over 30°C (Figure 61). In August 2005, the average temperature was 22.5°C, the maximum temperature was 31.7°C, and the minimum was 14.3°C. An important rainfall event occurred on 7 August (Figure 61). Air temperature exceeded 30°C only for few days during August 2005.

Figure 62 shows the daily trend of these variables during 2006. The air temperature peaked at 37.1°C in July and reached a minimum in August (13.3°C).

Rainfall mainly occurred in August 2005. In July 2005, it rained only once while in August 2005 the amount of precipitation was 15 mm (Figures 60 and 61). In 2006, the rainiest month was July (18.8 mm). There were only a few events with 9.2 mm falling on one day. In August, 3.4 mm fell, but it was distributed over several days (Figure 62).

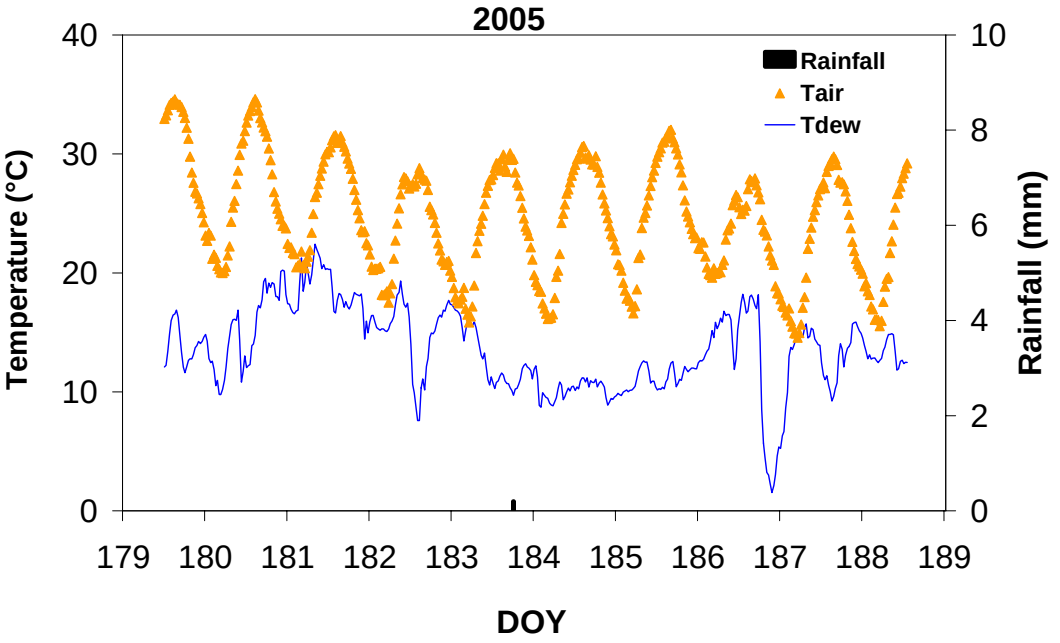

Figure 60. Daily mean air (Tair) and dew point (Tdew) temperature and precipitation during June-July 2005.

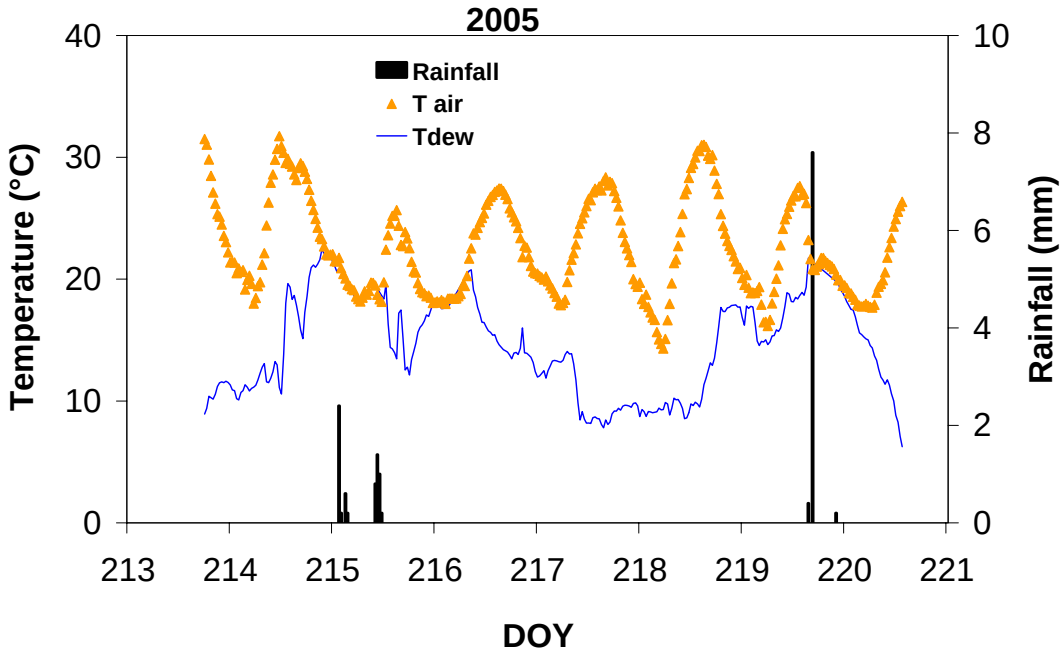

Figure 61. Daily mean air (Tair) and dew point (Tdew) temperature and precipitation during August 2005.

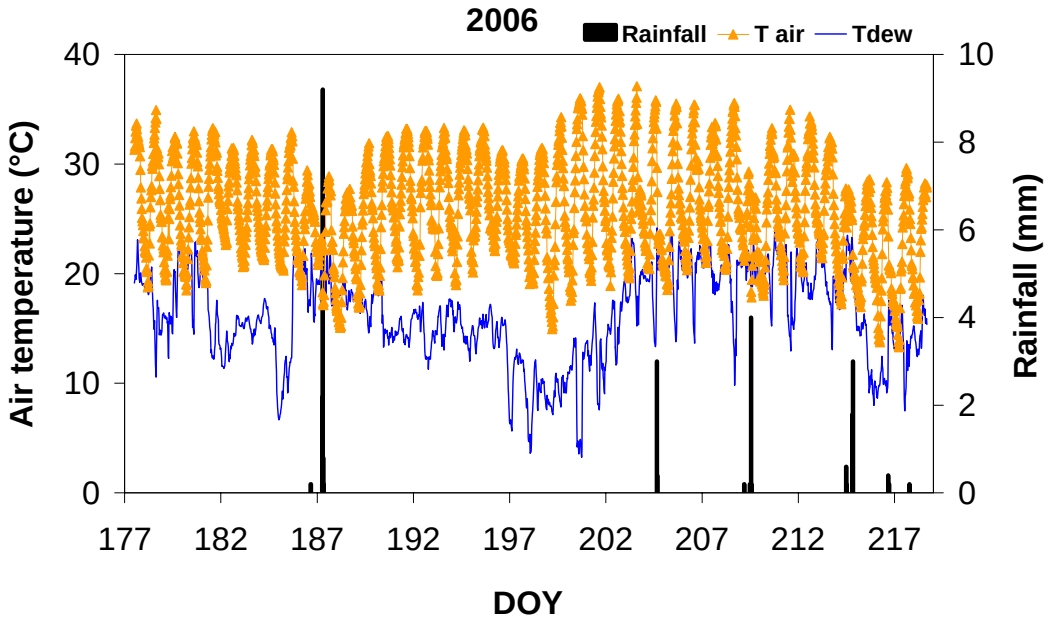

Figure 62. Daily mean air (Tair) and dew point (Tdew) temperature and precipitation during June-August 2006.

1.9 Radiation budget

Half hourly radiation data are shown in Figures 61-63. A maximum value of *Rg* occurred on 6 July 2005 (978.6 W m^{-2}), while the maximum value was 1000 W m^{-2} on 3 August.

The albedo or short wave reflected radiation (*SWout*) showed a range between 0.73 and 158.8 W m^{-2} in July 2005, 0.67 and 132.2 W m^{-2} in August 2005, -0.0 and 179.5 W m^{-2} in 2006. The values were similar in the three measurement periods.

Similar trends for long wave incoming radiation *LWin* and long wave outgoing radiation *LWout* were observed in all experiments. *LWin* radiation ranged between 331 to 409 W m^{-2} in July 2005, with a difference of 78 W m^{-2}. The difference in August 2005 was bigger (121 W m^{-2}) and the values ranged between 297 to 418 W m^{-2}. In 2006, *LWin* ranged between 277 to 442 W m^{-2}. Maximum values were 558, 541, and 550 W m^{-2} in June-July 2005, August 2005, and 2006, respectively. Minimum value was 374 W m^{-2} in the first measurement period of 2005, and it was about 369 W m^{-2} in August 2005 and 2006 period.

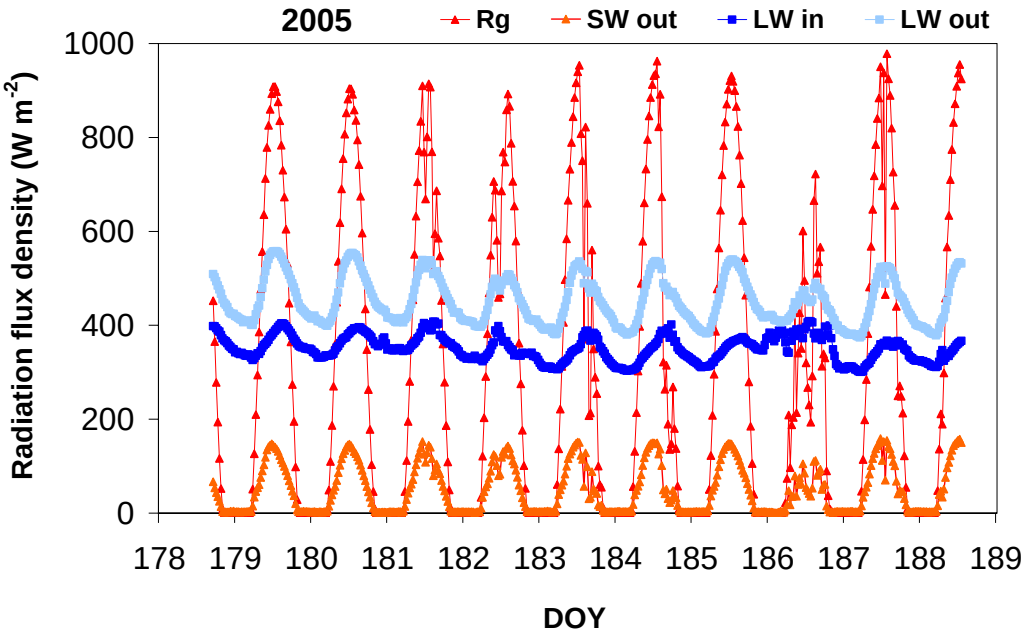

Figure 63. Half-hourly radiation budget for the period June-July 2005. Rg is the downward solar radiation, SWout is the short wave radiation reflected from the surface, LWin is the long wave radiation incoming into the surface, and LWout is the long wave radiation outgoing from the surface.

Figure 66 shows the daily variation of albedo during the three measurement periods. In grapevine ecosystem, the average albedo was about 16% with small differences between experiments. The period June-July 2006 showed higher values (19%) than the other periods. The lowest values were found in August 2005 (14%), while in June-July 2005 the values were initially similar to 2006 (19%).

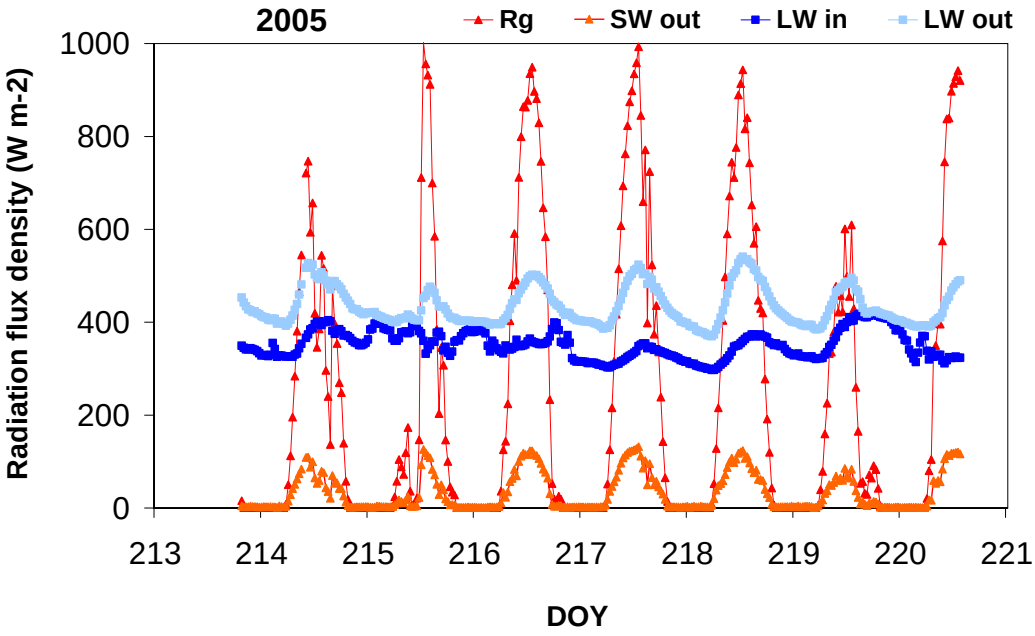

Figure 64. Daily mean radiation budget for August 2005.

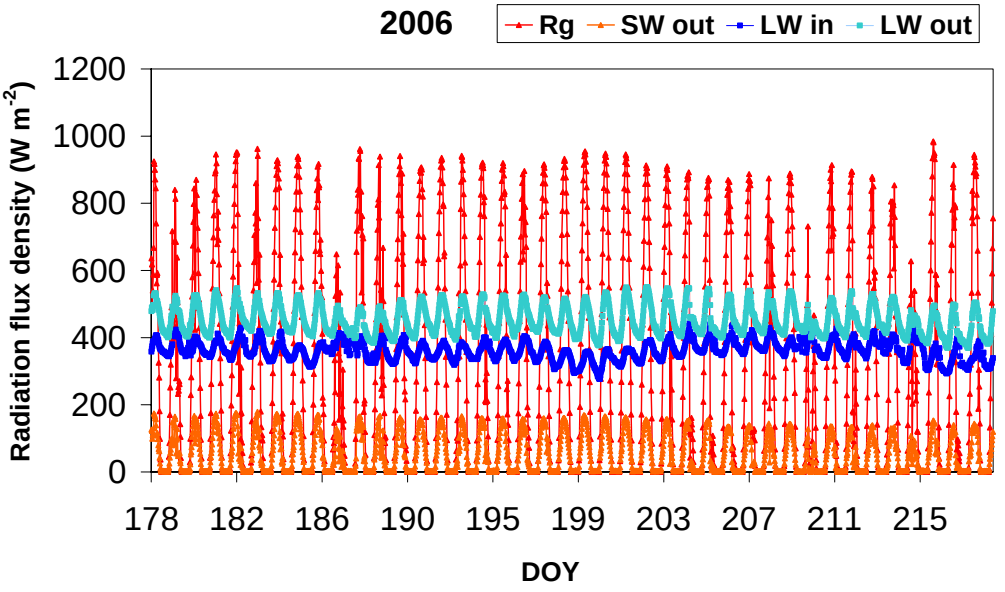

Figure 65. Daily mean radiation budget for the 2006 period.

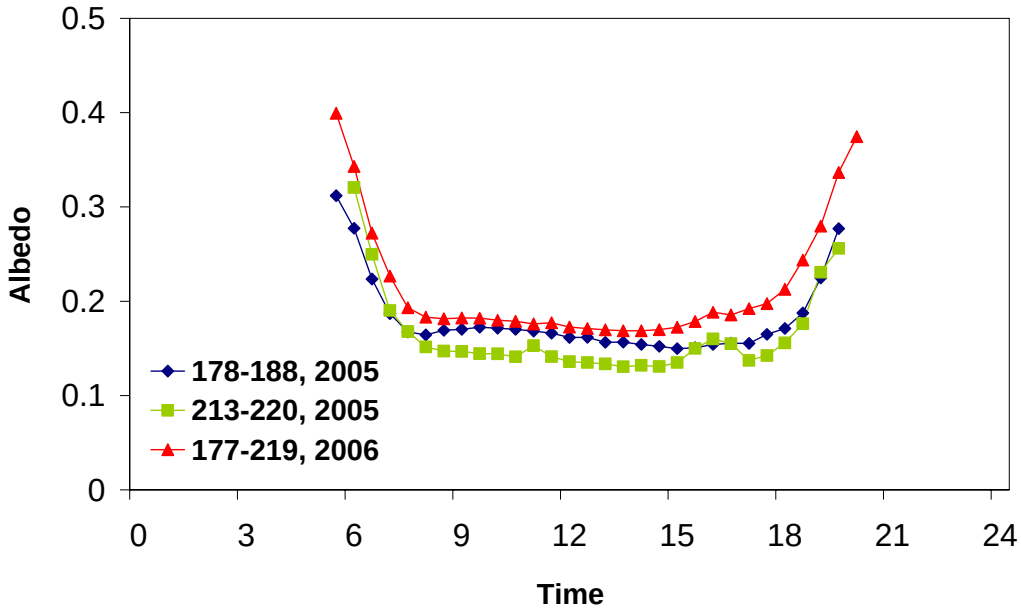

Figure 66. Daily variation of albedo of the mean day of the period.

1.10 Energy budget closure and exchange

Total energy fluxes (*H*+*LE*) were plotted against available energy (*Rn*-*G*) and the slope of linear regression through the origin was calculated. Under ideal condition, the slope is equal to 1, but this condition rarely occurs. In general, the closure is considered acceptable if the differences between ideal and real conditions are less of about 20-30% (Baldocchi et al., 1988).

Energy budget closures for grapevine ecosystem are shown in Figures 67 and 68. The energy budget closure from half-hour EC data was acceptable with an average (*H*+*LE*)/(*Rn*–*G*) ratio approximately equal to 0.77 for the two periods in 2005 and it was 0.75 in 2006. The R^2 was good for both periods (92%) indicating that the regression line matches the data well.

To evaluate the relationship between the environmental conditions and the ecosystem behaviour we analyzed the trend of individual energy budget components. Figure 69 shows the energy budget for June-July 2005. In general, the August 2005 *Rn* values were higher than June-July, except when it rained. The

same trend occurred in 2006, with a maximum value of 701 W m^{-2} in August and lower values in June and July (Figure 71).

Variations of the energy budget components during daylight hours showed that most of available energy was contributing to *LE* rather than *H*. This is especially evident in June-July 2005 and 2006. During August 2005, the available energy was used both for heating air and evaporating water.

The prevalence of latent heat flux over sensible heat flux can be seen by Bowen ratio ($\beta=H/LE$). Average β was about 0.40 during the June-July 2005 experiment, and it increased to 0.56 on day 187 due to reduced available energy. During August 2005, the average β was 0.55. In 2006, the average β was 0.27 showing a prevalence of *LE* over *H*.

Soil heat flux showed similar values in the three experimental periods. In 2005, the maximum values were higher in June-July (about 80 W m^{-2}) than in August (about 70 W m^{-2}). In 2006, *G* values were lower (about 60 W m^{-2}). As with the other fluxes, *G* showed a clear response to environmental conditions (clouds and rainfall); decreasing its value when these phenomena occurred.

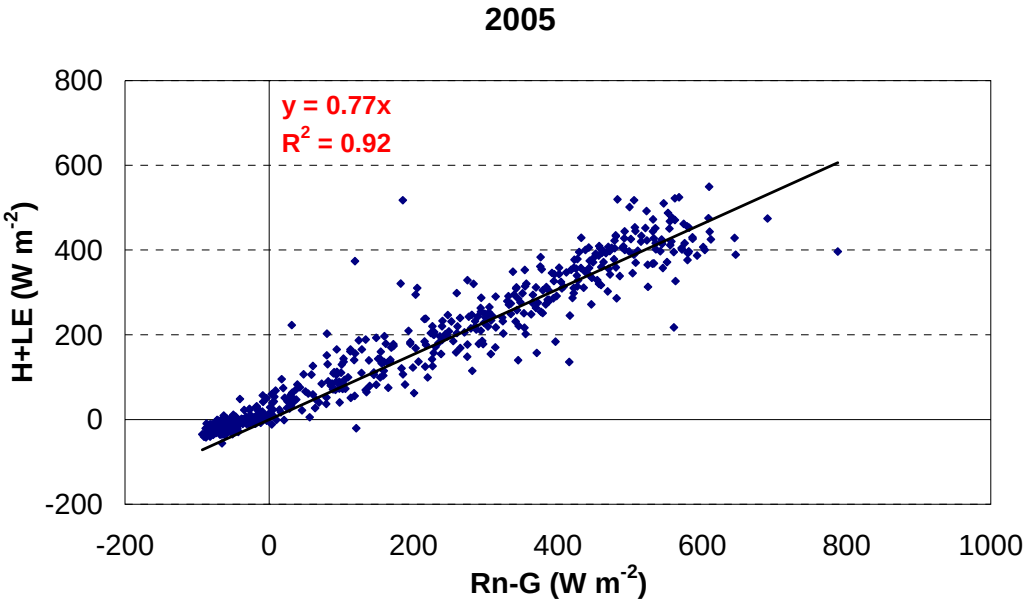

Figure 67. Energy budget closure for 2005 measurements.

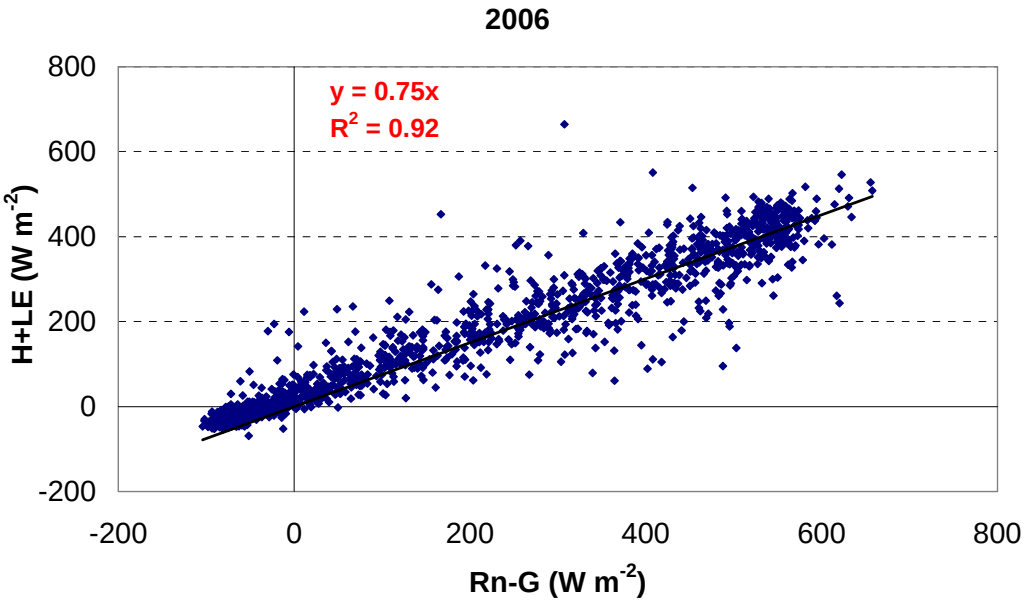

Figure 68. Energy budget closure for June-August 2006.

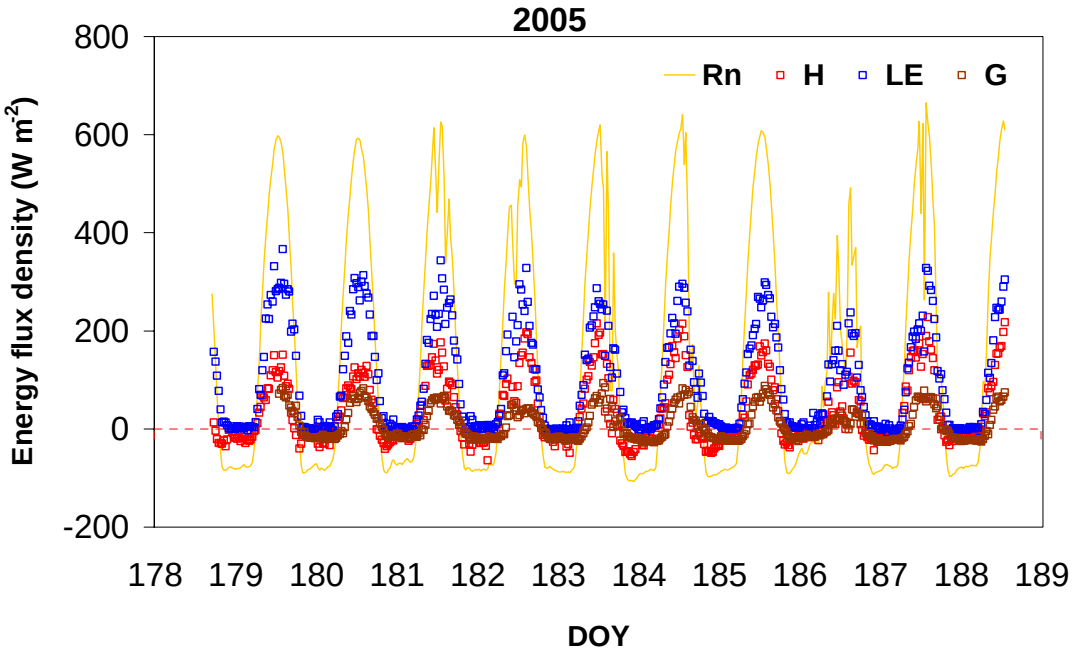

Figure 69. Half hourly net radiation (Rn), sensible heat flux (H), latent heat flux (LE), and soil heat flux (G) for the measurement period of June-July 2005.

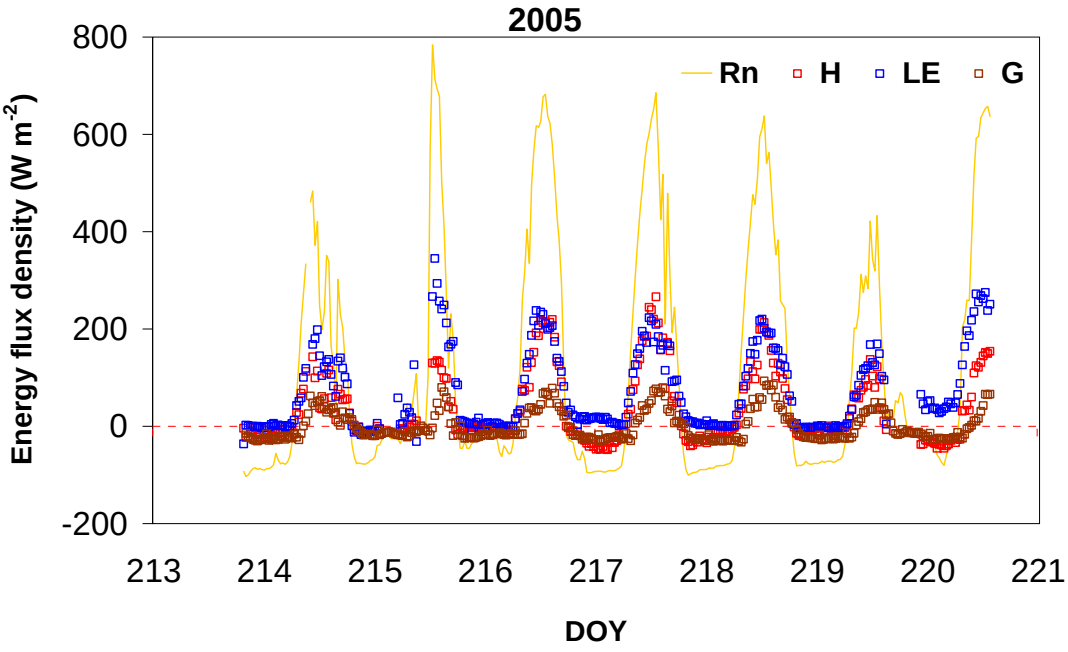

Figure 70. Half-hourly net radiation (Rn), sensible (H) and latent (LE) heat fluxes, and soil heat flux (G) in August 2005.

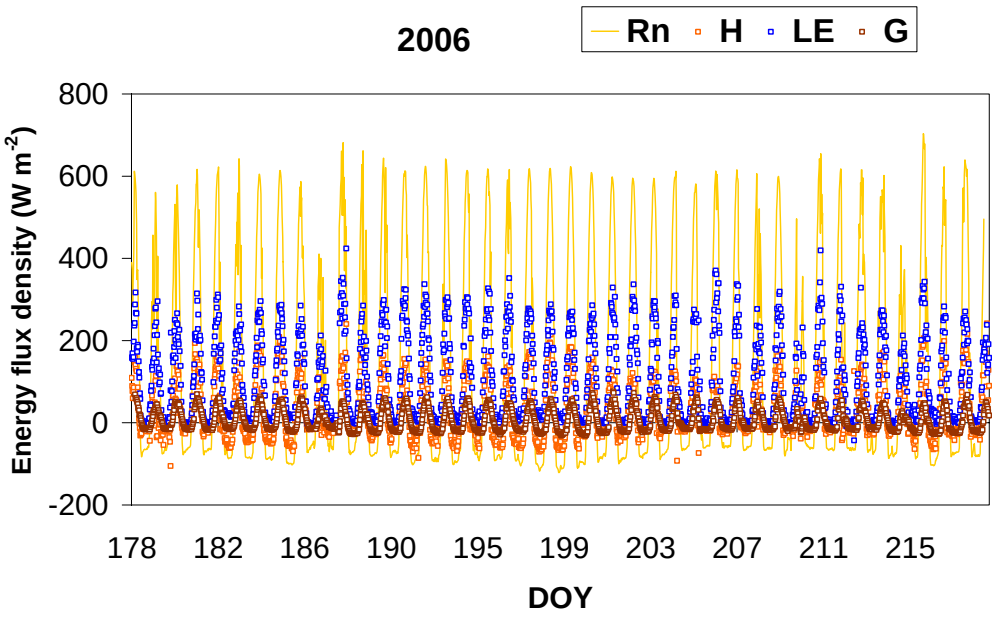

Figure 71. Half-hourly net radiation (Rn), sensible (H) and latent (LE) heat fluxes, and soil heat flux (G) for 2006 period.

1.11 Variation in NEE and GPP

Thet CO_2 balance values are reported in Figures 72 and 73, where negative fluxes indicate CO_2 uptake by the plants. Generally, there was more net CO_2 uptake in mid summer, but the net CO_2 uptake decreased during cloudy and rainy days. This was most likely caused by an increase in soil respiration rate and a decrease in photosynthesis under reduced radiations conditions. GPP values gradually decreased from the maximum value of 6.72 g C m^{-2} day^{-1}during the first measurement period. During June-July, the grapevine ecosystem was a carbon *sink*, while it was mainly a *source* of carbon during August. The average uptake was about -2 g C m^{-2} day^{-1} and the maximum uptake of carbon occurred the day 187 (-2.97 g C m^{-2} day^{-1}). During August, the grapevine released 1.40 and 1.28 g C m^{-2} day^{-1} (day 215 and 216). On those days, the ecosystem respiration (Reco) prevailed over GPP by releasing more than 2 g C m^{-2} day^{-1}. Reco increased after a rainfall event (day 215), which stimulated microbe activity. The GPP also increased following the rainfall.

During the experimental period in 2006, the grapevines were a *sink* for carbon (Figure 69). The ecosystem exchanged an average NEE of 1.6 g C m^{-2} day^{-1} and the exchange ranged between -3.06 to 0.28 g C m^{-2} day^{-1}. GPP showed a high variability depending on the rainfall events. During rainfall events, GPP values decreased, and then increased again. Reco also increased after rainfall events. This was clear during the first part of August when rainfall events led to increasing Reco.

Table 9 is a summary of NEE, GPP, Reco, energy and mass fluxes, and environmental variables. It reports the daily values of all variables analyzed and the average for each measurement period. The largest carbon uptake occurred in June-July 2005 (-1.84 g C m^{-2} day^{-1}), while in August 2005 the ecosystem was a *source* of carbon (0.25 g C m^{-2} day^{-1}). In 2006, the ecosystem was a carbon *sink* again with an average uptake of carbon of -1.62 g C m^{-2} day^{-1}.

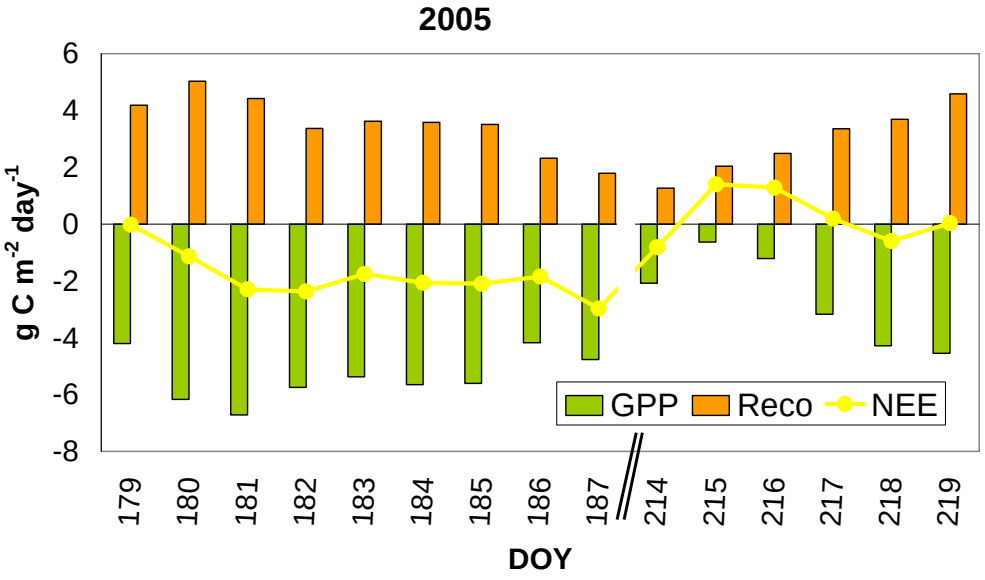

Figure 72. Daily mean CO_2 balance in 2005. NEE is the net ecosystem exchange, GPP is the gross primary production, and Reco is the ecosystem respiration. The period 28 June-6 July and 2-7 August are shown.

June-July 2005 showed higher values of GPP and Reco (-5.38 and -3.54 g C m^{-2} day^{-1}). The average air temperature was similar during the three periods, so the differences in carbon exchanges were mainly due to the different water regimes. The amount of precipitation was only 0.2 mm in June-July 2005, while it was 15.0 mm in August 2005, and 27.4 mm in 2006 which showed more variability and less total amount of carbon exchanged.

Few studies have been conducted over grapevineyard ecosystems to investigate the role of this ecosystem in the carbon balance. A previous study, in the same vineyard, was conducted during August 2002. Results showed that the vineyard acted as a carbon *sink* with an average daily value of -2.14 g C m^{-2} day^{-1}. In that study, rainfall events also caused an increase in soil respiration (Spano et al. 2004). A comparison with another grapevineyards located in Sardinia (Italy) was made by the same authors in 2003. NEE values in Sardinia were higher than Tuscany, with an average value of -4.32 g C m^{-2} day^{-1}. That vineyard also acted as a carbon *sink*, with a net prevalence of photosynthesis over respiration (Spano et al., 2004). Rossi et al. (2004) investigated carbon exchanges in a vineyard for

table grapes in Puglia (Italy) in two consecutive years (2001 and 2002). The total ecosystem exchange was higher in 2001, with a NEE of -2.07 g C m^{-2} day^{-1}, while in the warmer year 2002 the net ecosystem exchange was lower (-1.68 g C m^{-2} day^{-1}).

Generally, agricultural ecosystems act as a carbon *sink*. In Germany, studies were conducted over winter wheat and potato fields in 2004, and the crops acted as carbon *sinks*; absorbing an average value of -4 g C m^{-2} day^{-1} and -2 g C m^{-2} day^{-1} for winter wheat and potato, respectively (Anthoni et al., 2004).

In Table 9 are also shown the daily energy and mass fluxes. *LE* flux was higher than *H* in each measurement period, with only a small difference in August 2005 (average $\beta = 0.5$).

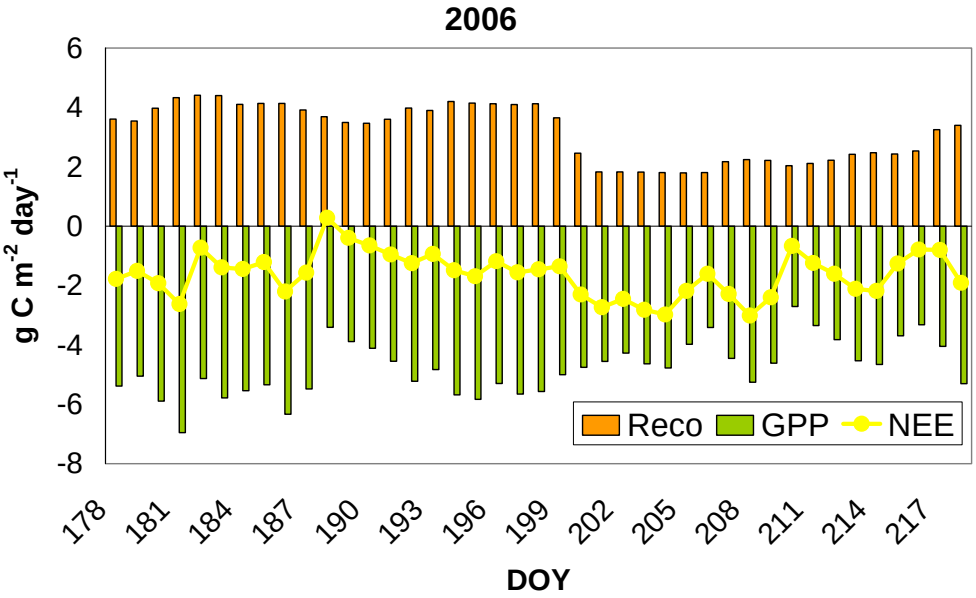

Figure 73. Daily mean variation in NEE, GPP and Reco fluxes during 27 June through 6 August 2006.

Table 9. Daily values of carbon fluxes (NEE, GPP, Reco), energy fluxes (*Rn*, *H*, *LE*, and *G*) and air temperature, relative humidity, and Bowen ratio (*H*/*LE*). The sums over sampling period are also shown.

YEAR	DOY	NEE	GPP	Reco	Rain	GPP/Reco	Tair	RH	Bowen	Rn	H	LE	G
		g C m^{-2}	g C m^{-2}	g C m^{-2}	mm		°C	%	H/LE	MJ m^{-2} d^{-1}	MJ m^{-2} d^{-1}	MJ m^{-2} d^{-1}	MJ m^{-2} d^{-1}
2005	179	-0.02	-4.20	4.18	0	1.0	30.7	32.8	0.27	14.6	2.7	10.2	1.0
2005	180	-1.14	-6.17	5.03	0	1.2	27.0	44.1	0.26	14.5	2.5	9.6	1.2
2005	181	-2.30	-6.72	4.42	0	1.5	26.0	55.6	0.39	14.3	3.5	9.0	1.0
2005	182	-2.37	-5.74	3.37	0	1.7	23.5	54.3	0.48	13.1	3.9	8.2	0.4
2005	183	-1.76	-5.38	3.62	0.2	1.5	24.0	47.9	0.37	12.0	3.0	8.1	0.8
2005	184	-2.07	-5.65	3.58	0	1.6	24.4	38.5	0.35	11.9	2.9	8.3	0.7
2005	185	-2.10	-5.61	3.51	0	1.6	25.1	39.2	0.41	14.9	3.7	8.9	1.0
2005	186	-1.85	-4.17	2.32	0	1.8	23.1	47.8	0.26	8.0	1.6	6.1	0.0
2005	187	-2.97	-4.76	1.79	0	2.7	22.7	51.8	0.56	14.0	4.6	8.2	0.8
2005	179-187	-1.84	-5.38	3.54	0.2	1.6	25.2	45.8	0.40	13.0	3.2	8.5	0.8
2005	214	-0.81	-2.08	1.27	0	1.6	24.8	51.2	0.55	7.0	2.6	4.8	0.3
2005	215	1.40	-0.63	2.03	6.8	0.3	20.5	73.5	0.27	8.8	1.6	5.8	-0.4
2005	216	1.28	-1.21	2.49	0	0.5	22.6	61.2	0.70	14.4	4.	6.5	0.6
2005	217	0.19	-3.17	3.36	0	0.9	23.1	42.9	0.66	12.5	4.3	6.5	0.4
2005	218	-0.59	-4.28	3.69	0	1.2	23.2	46.9	0.71	12.2	4.3	6.0	0.6
2005	219	0.04	-4.55	4.59	8.2	1.0	21.5	73.0	0.39	6.1	1.5	3.8	-0.3
2005	214-219	0.25	-2.65	2.90	15.0	0.9	22.6	58.1	0.5	10.2	3.1	5.6	0.2
2006	178-218	-1.62	-4.78	3.17	27.40	1.5	25.82	51.52	0.27	12.3	2.3	8.3	0.5

1.12 Ecosystems functioning and driving forcings

The grapevine ecosystem was mainly driven by the same variables as the maquis ecosystem. Latent heat flux and air temperature were the main factors related to ecosystem production. The grapevines were a carbon *sink* in June-July 2005 and in 2006, while they were a *source* of carbon in August 2005. This behaviour was mainly due to the different water regime. Rainfall events occurred mainly in August (Table 9). Net ecosystem exchange (NEE) represents the difference between gross primary production and ecosystem respiration, so it depends on the behaviour of these variables under different environmental conditions.

GPP and Reco showed good relationships with evaporation (*LE*) and *Tair*. Because of limited data, we analyzed the relationships with daily data subdivided into bins. *LE* bins of 1 MJ m^{-2} day^{-1} and *Tair* bins of 3 °C were created to evaluate relationships with carbon exchange.

Figure 74 shows the relationship between GPP and *LE*. Since photosynthesis reaches a maximum value and *LE* varies depending on available energy, one would expect a range of *LE* for the peak photosynthesis when soil water is not limiting. As water becomes limiting, stomata begin to close and reduce both *LE* and photosynthesis. Thus, one would expect GPP to increase with *LE* under water deficits and it should plateau for a range of *LE* when there is no water deficit. This relationship is clear in Figure 74.

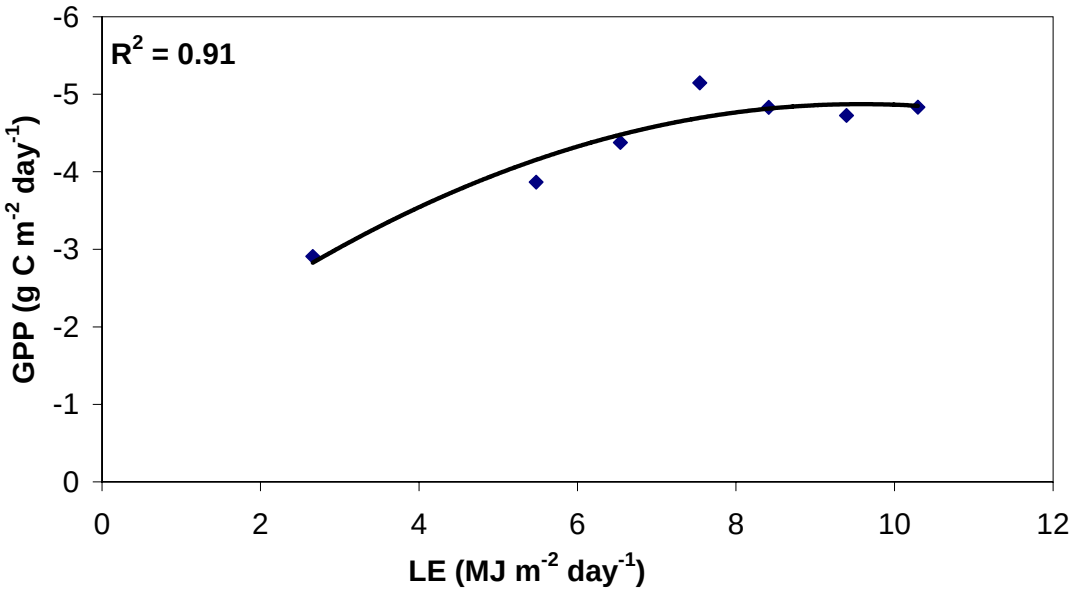

Figure 74. Relationship between gross primary production (GPP) and latent heat flux (LE) during the measurement periods.

On the other hand, Reco continued to increase linearly as a function of *LE* (Figure 75). Since NEE is the sum of GPP and Reco, these data showed an increase in NEE as *LE* increased from about 3 to 8 MJ m^{-2} day^{-1} with a leveling off at higher *LE*.

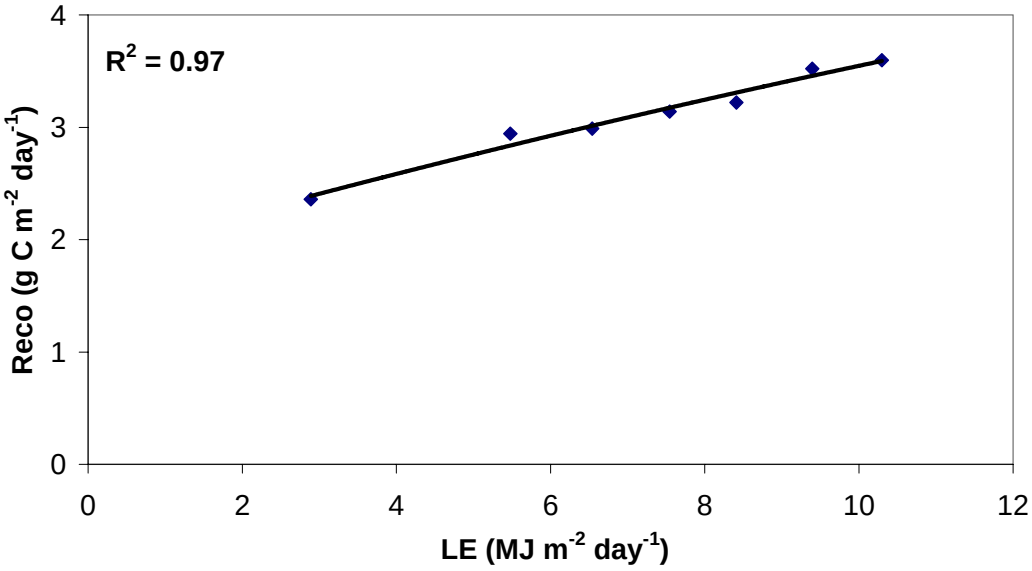

Figure 75. Relationship between ecosystem respiration (Reco) and latent heat flux (LE) during the measurement periods.

Air temperature was also related to carbon ecosystem production and release. Optimal temperature for the photosynthesis process was about 27°C. Temperature higher than 30°C were related to a decrease in GPP (Figure 76). In fact, the maximum value of GPP was recorded during June-July, when optimal temperature values occurred (Table 9). Ecosystem respiration was positively related to air temperature (Figure 77). Reco values were high in June-July when the temperatures were optimal, but they were also high in August due to rainfall events, and the vineyard released more carbon than it absorbed.

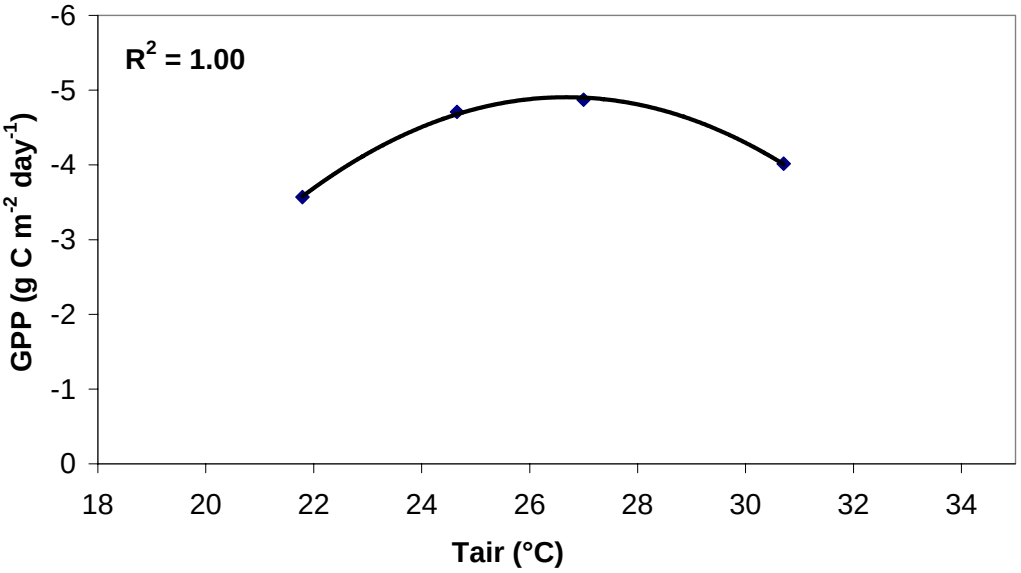

Figure 76. Relationship between gross primary production (GPP) and air temperature (Tair) during the measurement periods.

The GPP/Reco ratio (Table 9) was 1.6 in June-July 2005, showing the prevalence of photosynthesis processes, while it was 0.9 in August 2005, showing respiration higher than photosynthesis process. In 2006, GPP/Reco ration was 1.5, and the vineyard was a *sink* in this period (Figure 73). The large amount of precipitation during 2006 stimulated more photosynthesis process than respiration, which led to the higher GPP/Reco. Soil respiration was negatively affected by the large precipitation.

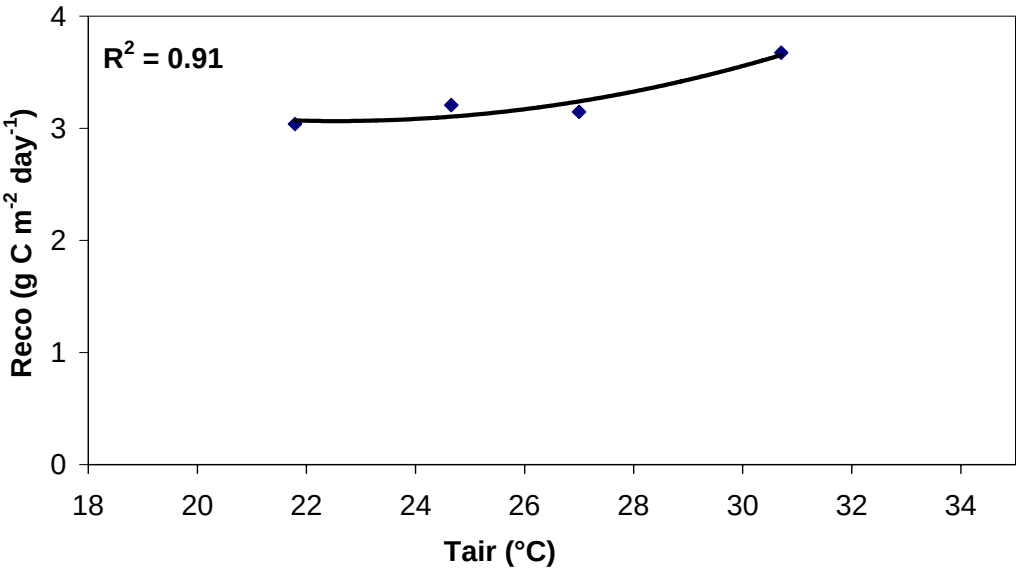

Figure 77. Relationship between ecosystem respiration (Reco) and air temperature (Tair) during the measurement periods.

2. MODELLING

2.1 Model parameterization

ACASA model was run initially to select morphological input leading to the better results. A measurement period from each site was used for model parameterization. For the year 2004, DOY 97-112 were used for the maquis ecosystem parameterization. For grapevines, the measurement period June-July 2005 was choosen for the model parameterization. The other measurement periods were used to validate the model.

The exact values used to drive ACASA for both ecosystems are listed in Table 10. The input values were selected by running the model several times varying the one parameter per time. The value of basal respiration rate for grapevine was slighlty lower than proposed in the literature (see Table 3). The value 0.25 led to the better result than values between 0.5 to 1.0 (Mullins et al., 1992). A second step in the parameterization process was the simultaneously variation of some parameters. For example, good combinations of input values for both V_{cmax} and stomata density factor were selected and the model was run to find the best results.

Figure 78 and 79 show the trend of modelled and measured sensible and latent heat fluxes in the maquis ecosystem. ACASA's estimates of *H* flux were good (Figure 78) with only small differences between modelled and measured data. The modelled *H* flux was too negative on DOY 105, but it was due to rainfall (0.20 mm). Therefore, ACASA was sensitive to even low rainfall events. Figure 79 shows the comparison between modelled and measured *LE* flux. The match was quite good on most days except DOY 105 when the rainfall occurred. Since EC estimates are not valid during rainfall, the real accuracy of ACASA can not be tested during rainfall events.

Table 10. Plant and soil input file for maquis and grapevine with values used to run the ACASA model.

Description	Units	Maquis	Grapevine	Reference
LAI		2.7-3.0	1.37-1.55	This study
Canopy height	m	1.20	2.2	This study
Ocean **Land**		 1	 1	
Wetland (1) **No standing water (0)**		 0	 0	
Soil type		12	9	This study
Wilting point soil moisture		0.17	0.20	FAO 2007
Latitude	deg	40°36' N	43° 05' N	
Human population density	#people/m^2	0	0	
Time step length	s	1800	1800	
Stress index		1	0	
Leaf basal resp. rate	µmol m^{-2} (leaves) s^{-1}	0.1	0.25	Hamilton et al., 2001; Mullins et al., 1992
Stem basal resp. rate	µmol m^{-2} (stems) s^{-1}	0.1	0.25	Hamilton et al., 2001; Mullins et al., 1992
Root basal resp. rate	µmol m^{-2} (roots) s^{-1}	0.1	0.25	Hamilton et al., 2001; Mullins et al., 1992
Microbe basal resp. rate	µmol m^{-2} (microbes) s^{-1}	0.1	0.25	Hamilton et al., 2001; Mullins et al., 1992
Q_{10} leaf resp		2.0	2.0	Vose and Bolstad, 1999; Hu et al., 2006
Q_{10} root resp		2.0	2.0	This study

Description	Units	Maquis	Grapevine	Reference
Q_{10} microbes		2.0	2.0	This study
Q_{10} stem resp		2.0	2.0	Vose and Bolstad, 1999; Hu et al., 2006; Kim et al., 2007; Zhang et al., 2007
Near-IR leaf reflectivity		0.3	0.4	Rossi et al., 2001; Renzullo et al., 2006
Near-IR leaf transmissivity		0.35	0.35	Jones, 1992
Visible leaf reflectivity		0.05	0.05	Rossi et al., 2001; Jones, 1992; Renzullo et al., 2006
Visible leaf transmissivity		0.08	0.08	Rossi et al., 2001; Jones, 1992
Optimal photosynth. temperature	°C	20	30	Mullins et al., 1992
Leaf drag coefficient		0.07	0.23	Villagarcia et al., 2007; Molina et al., 2006
Mean leaf diameter	m	0.03	0.15	This study
Max carboxylization rate (V_{cmax})	µmol m^{-2} (tissue) s^{-1}	35	50	Bigot et al., 2007; Frak et al., 2002; Iacono et al., 1998
Stomata density factor		1.8	1.0	This study
Normalized leaf area index profile				This study

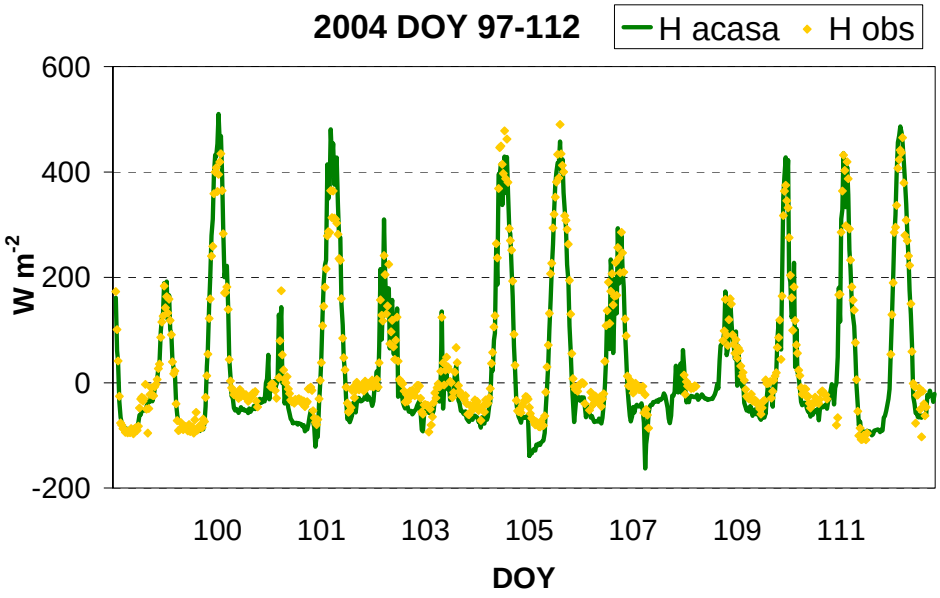

Figure 78. Comparison between sensible heat flux (H) of modelled data (line) and observed data (dot) from April to June 2004 in maquis ecosystem.

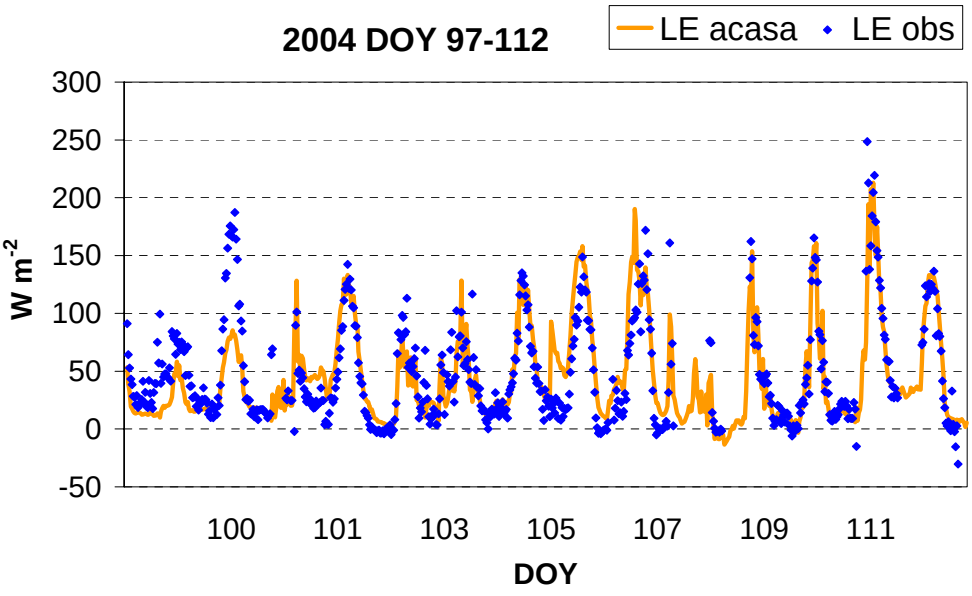

Figure 79. Comparison between simulated daily value of LE (line) and LE observed values (dot) from April to June 2004 in maquis ecosystem.

For grapevine ecosystem, the results are shown in Figures 80-82. ACASA generally predicted higher *H* (Figure 80) and lower *LE* (Figure 81).

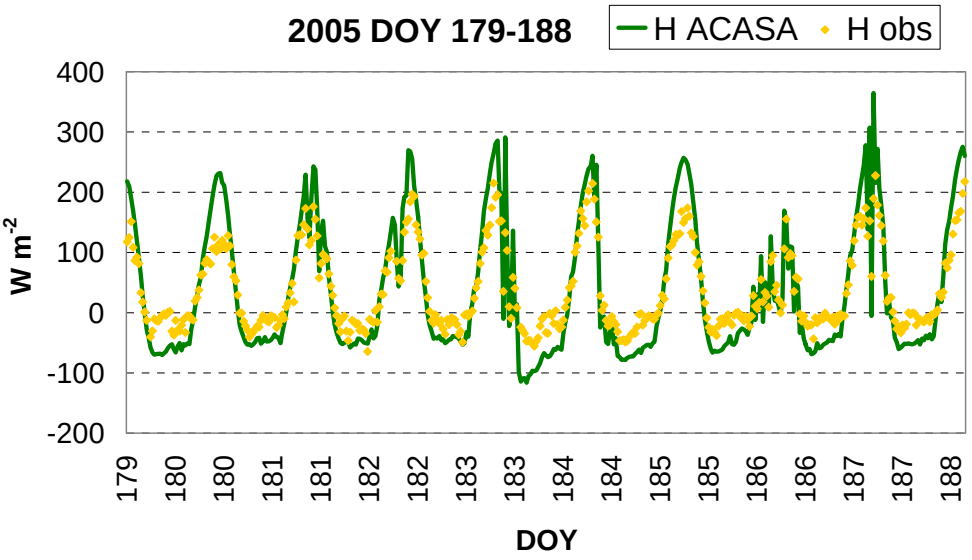

Figure 80. Comparison between simulated daily value of H (line) and H observed values (dot) in June-July 2005 for grapevines.

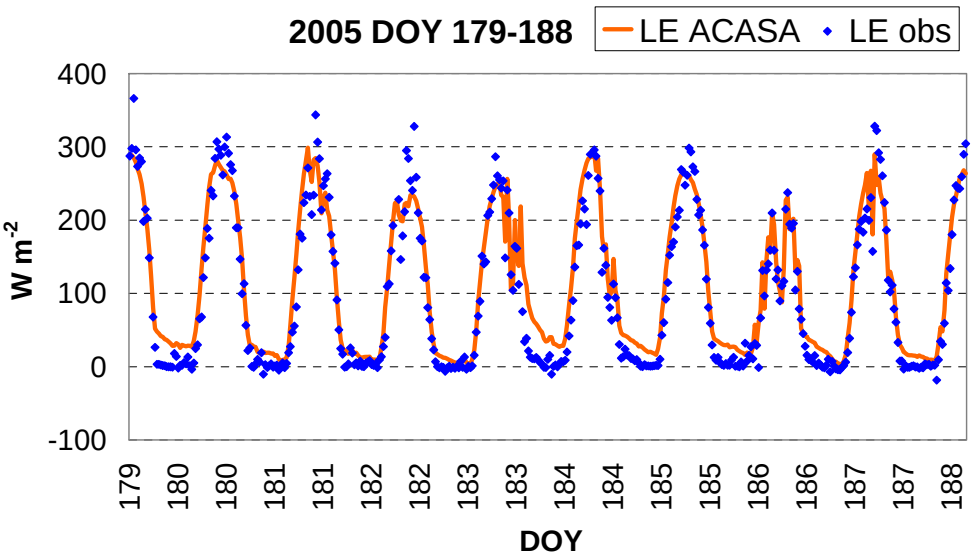

Figure 81. Comparison between simulated daily value of LE (line) and LE observed values (dot) in June-July 2005 for grapevines.

Regarding CO_2 flux, the model predictions were good (Figure 82) with both positive and negative fluxes well predicted by the model.

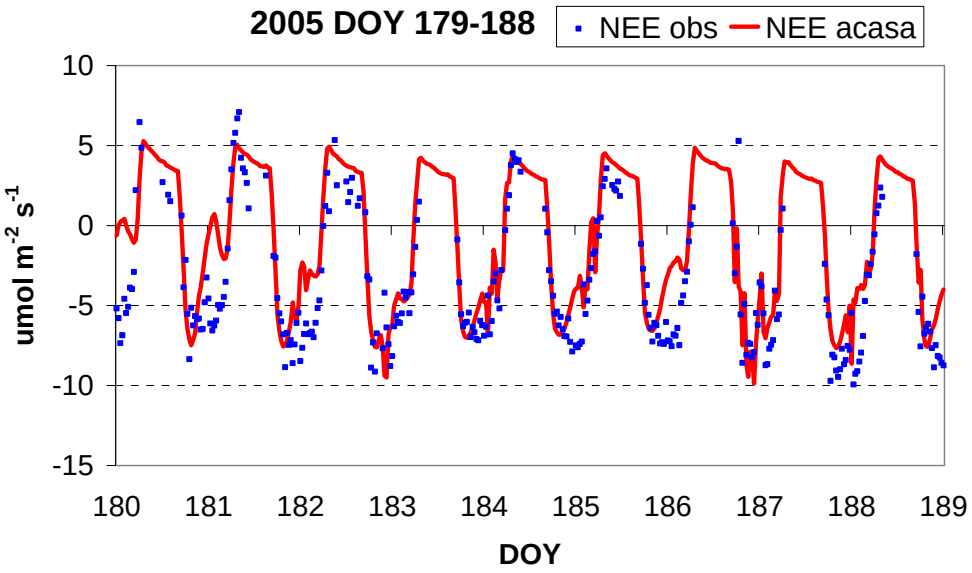

Figure 82. Comparison between simulated daily value of CO_2 (line) and CO_2 observed values (dot) in June-July 2005 for grapevine.

2.2 Model performance

A) Maquis ecosystem

2.2.1 Energy Budget Closure

ACASA model estimated the net radiation (*Rn*), sensible heat flux (*H*), latent heat flux (*LE*), and soil heat flux (*G*). Energy budget closure was calculated using the simulated fluxes. Figure 83 shows the 2004 closure. To run the model, the year was subdivided into three periods: the first from DOY 97 to 112 (used for model parameterization); the second from DOY 126 to 168; and the third from DOY 175 to 307. The energy budget closure in Figure 83 includes data from all three periods.

ACASA energy budget closure were good in comparison with the closure from measured fluxes (Figure 41). Simulated energy budget closure showed higher R^2 indicating less data dispersion. This trend was common to the three measurement periods.

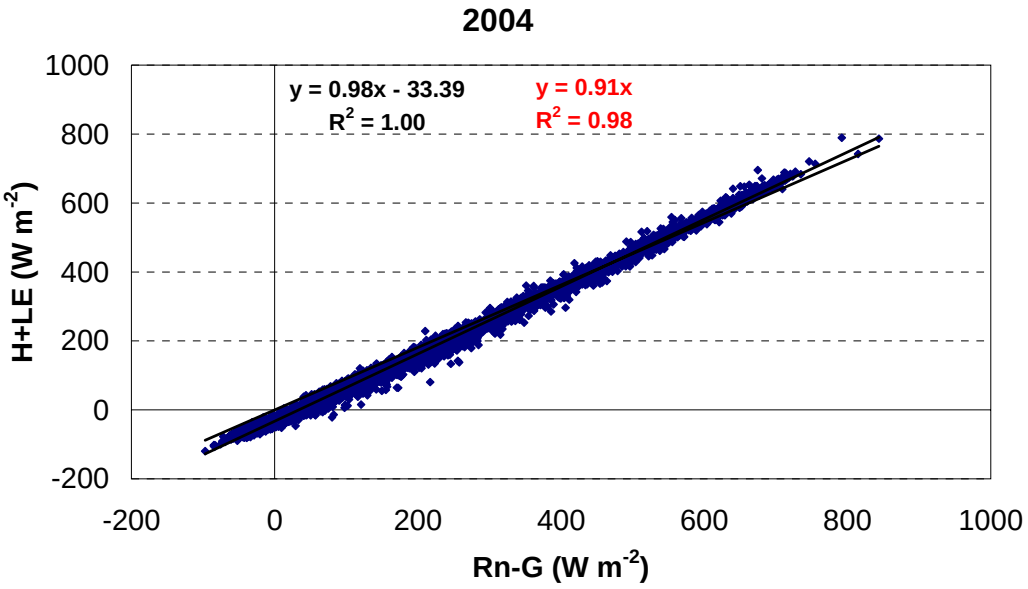

Figure 83. ACASA energy budget closure for the 2004 period.

The year 2005 was not subdivided in separate periods. Simulated fluxes are referred to the period from DOY 1 to 350. Figure 84 shows that *H+LE* was 90% of *Rn-G*. In the measured data (Figure 42), the closure was 94%, but the scatter was greater.

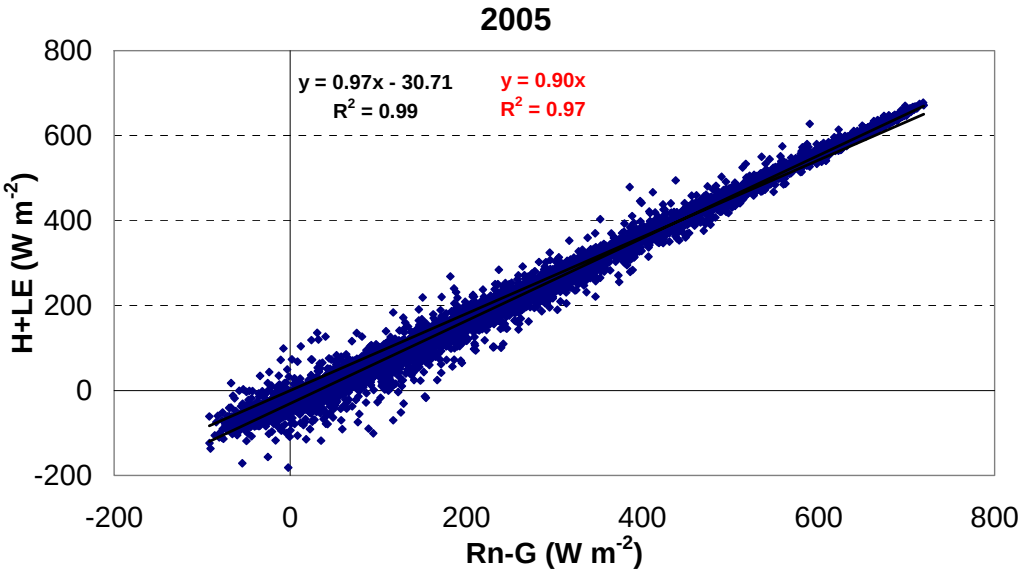

Figure 84. ACASA energy budget closure for the year 2005.

The year 2006 was subdivided into two periods: the first from DOY 1 to 151, and the second from DOY 164 to 365, but they were considered together for estimating simulated energy budget closure. Figure 85 shows the linear regression for 2006. The angular coefficient was slightly lower than the observed energy budget closure (Figure 43), but the R^2 was higher.

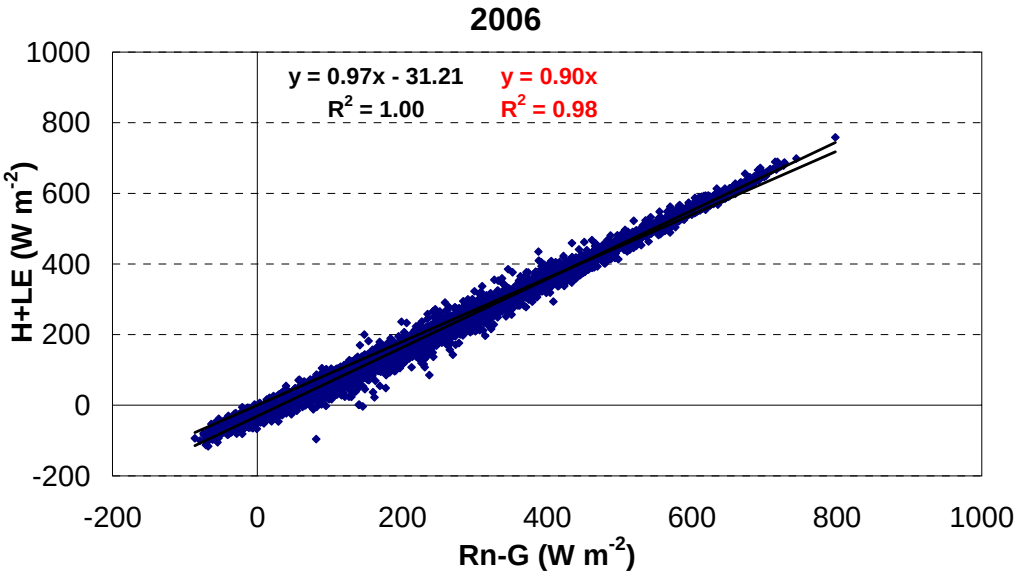

Figure 85. ACASA energy budget closure for the year 2006.

2.2.2 Flux simulations

Simulated energy and mass fluxes during 2004-2006 were compared with observations using half-hourly time steps. This section reports some simulations of *H*, *LE*, and CO_2 fluxes. The regression statistics for each measurement period are summarized in Table 11. During June-July 2004, *H* simulations were good (Figure 86). The slope and interception values in Table 11 showed that ACASA generally had similar *H* values. The model predicted lower *LE* for the same period (Figure 87) and in 2005 and 2006 (Table 11). The underestimation of *LE* during midday may be due to the lower stomatal conductance, which was estimated using the Ball-Berry sub model (Eq. C.16). Similar results were found by Ju et al. (2006) using the Boreal Ecosystem Productivity Simulator (BEPS) that calculates stomatal conductance using Ball-Berry model. In addition, ACASA *LE* values were less negative at night, and the reason needs further investigation.

Table 11. Statistics from the regression (Y=aX+b) of simulated (as Y) on observed (as X) half-hourly energy fluxes (W m^{-2}) and net ecosystem CO_2 flux (μmol m^{-2} s^{-1}) on maquis ecosystem. (RMSE=root mean squared error; RA=mean absolute error; MBE=mean bias error).

Flux	**Year**	**a**	**b**	**R^2**	**RMSE**	**RA**	**MBE**
					W m^{-2}	**W m^{-2}**	**W m^{-2}**
Rn	2004	0.94	23.56	1.00**	22.6	20.9	14.9
	2005	0.94	21.17	1.00**	21.6	19.8	14.6
	2006	0.94	21.24	1.00**	21.6	19.9	14.7
H	2004	1.03	-23.66	0.95**	45.5	34.2	-18.5
	2005	1.00	-20.62	0.95**	39.1	27.1	-16.3
	2006	0.97	-14.93	0.95**	36.9	24.6	-13.4
LE	2004	0.65	25.64	0.56**	34.0	22.2	12.3
	2005	0.67	20.63	0.57**	28.9	17.3	5.9
	2006	0.63	20.47	0.47**	30.3	17.9	5.9
G	2004	0.51	-3.26	0.69**	31.4	20.1	-5.6
	2005	0.56	1.48	0.60**	27.9	18.4	1.0
	2006	0.58	-1.18	0.58**	27.0	17.1	-1.6
NEE	2004	0.73	0.11	0.72**	2.0	1.2	0.2
	2005	0.85	-0.08	0.72**	2.0	1.1	0.1
	2006	0.82	0.08	0.72**	1.9	1.1	0.2

** significant values at 99% probability level.

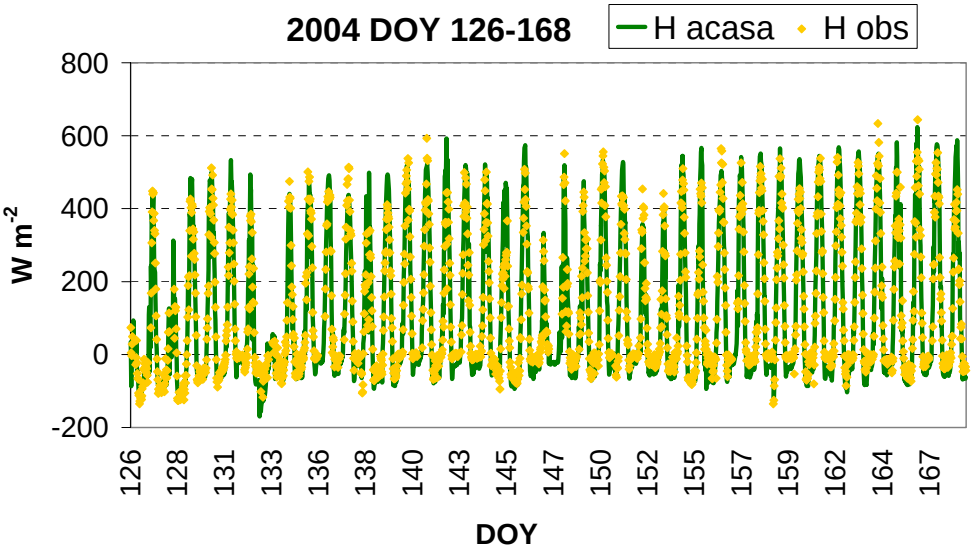

Figure 86. Comparison between modelled and observed H from June and July 2004.

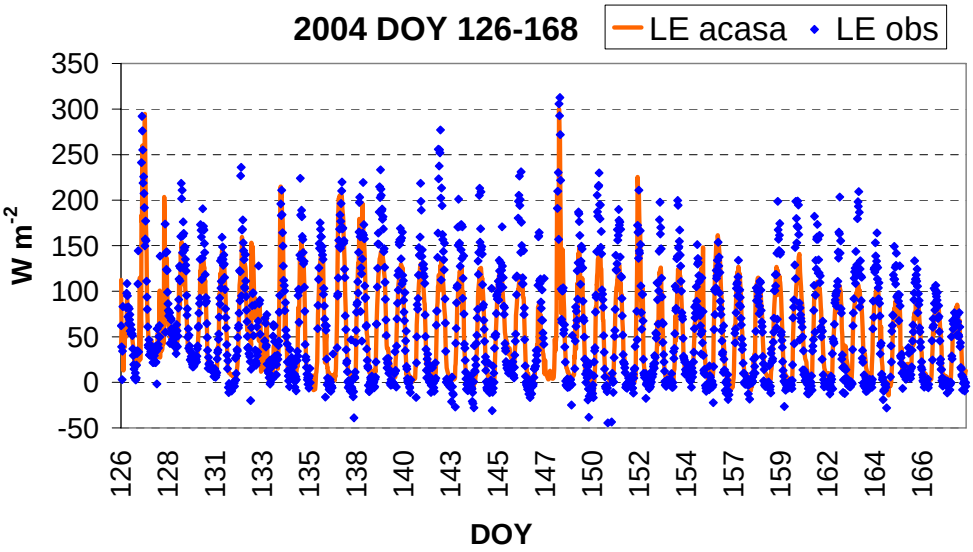

Figure 87. Comparison between modelled and observed LE flux from June and July 2004.

Simulated and measured CO_2 flux are shown in Figures 88 and 89. Figure 88 shows flux comparison in year 2005, while Figure 89 shows simulated and measured CO_2 flux in 2006. The ACASA model was able to capture the seasonal variation in CO_2 flux. In 2005, a reduction in NEE values during the summer, due to drought, was clear. ACASA's decrease was somewhat more pronounced. The difference was due to a strong response to water stress in ACASA calculation of CO_2 exchanges. Maximum carboxilation rate (V_{cmax}), in the plant and soil input file, is an important parameter involved in the CO_2 exchange control, so the value was selected to give better predictions. Maquis species are typical sclerophillous plants, which are able to function in water stress conditions. They do not stop energy and mass fluxes with the atmosphere, but the exchanges are reduced. The difference in simulated and measured CO_2 flux during the drought period may be due to higher sensitivity to water stress in not sclerophyllous plants. During winter and spring 2005, when maquis plants found better weather conditions, ACASA simulations matched well.

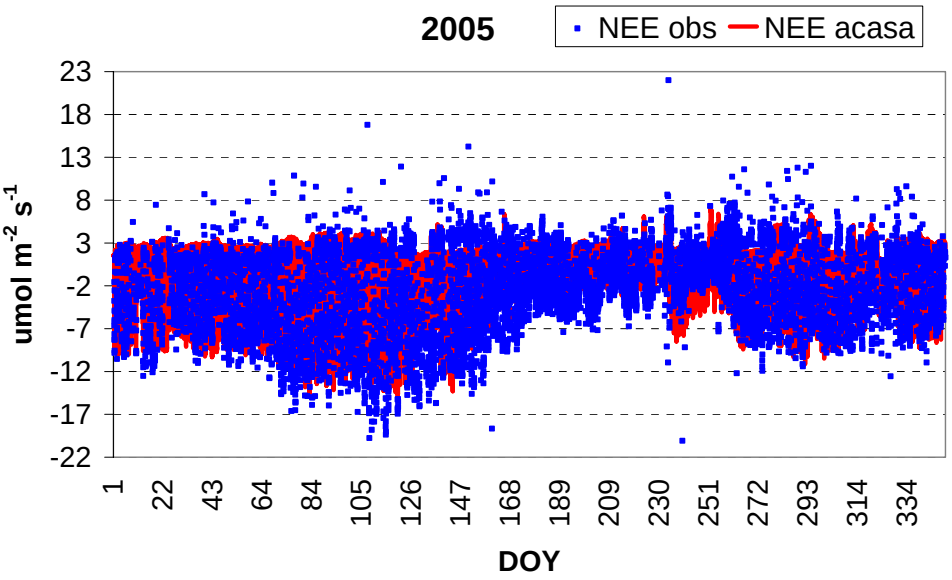

Figure 88. Comparison between modelled data and observed data of CO_2 flux ($\mu mol\ m^{-2}\ s^{-1}$) during 2005.

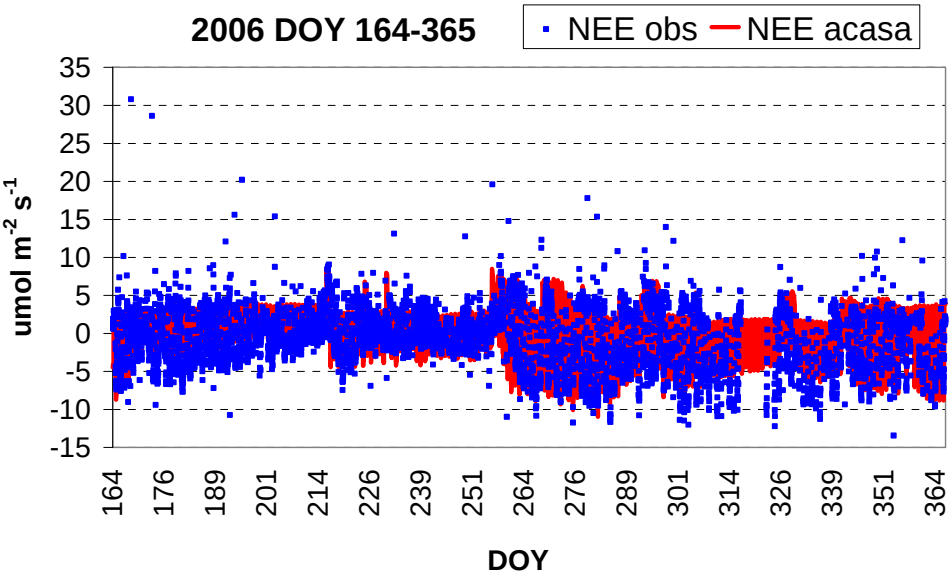

Figure 89. Comparison of modelled and observed data of CO_2 flux (µmol m^{-2} s^{-1}) from July to December 2006.

Figure 89 shows the comparison between modelled and observed CO_2 flux during the second part of 2006 (from July to December). NEE showed the typical decrease in summer, and simulations predicted lower CO_2 flux. The reason for the response pattern is the different behaviour between maquis sclerophyllous plants and not sclerophyllous plants considered by the model.

The model was able to capture the increase in respiration (positive NEE values), which occurred after rainfall events during the two years. Rain occurred on days 215, 257, 268, and 326, and the model showed peaks in respiration on those days. Respiration peaks also occurred in 2005 due to precipitation. Model response was fast either during the summer (when few rainfall events occurred) or during fall and winter (when rainfall was frequent).

2.2.3 Statistical analysis

Statistical analysis was made to compare model results with observations. Figures 90-94 show the linear regression equations for net radiation (*Rn*), sensible heat flux (*H*), latent heat flux (*LE*), soil heat flux (*G*), and CO_2 flux (NEE) for 2005. Linear regression equations were calculated both passing through and not through the origin. Table 11 only reports values of slope, intercept, and R^2 for linear regression not passing through the origin for the three years. Table 11 also reports the root mean squared error (RMSE), mean absolute error (RA), and mean bias error (MBE). Differences between simulated and observed fluxes were significant at 0.001 probability. ACASA simulations, therefore, are considered good. Some changes can be made in the future to improve the results.

The regression explained 100% of half-hourly variance of *Rn*. The RMSE of simulated versus observed net radiation and the RA had about 2% of error. MBE was about 15 W m^{-2}.

The regression explained 95% and from 47% to 56% of half-hourly variance of *H* and *LE*, respectively. The RMSE of simulated sensible heat (*H*) and latent heat (*LE*) showed good agreement. The mean absolute error was about 3% for *H* and *LE*. ACASA predicted lower *H* (negative values of MBE) and higher *LE* (positive values of MBE) in the three years.

ACASA soil heat flux (*G*) was lower than observed in 2004 and 2006, and higher in 2005. The regression explained about 62% of *G* half-hourly variance. The RMSE was 7-13% of the range. The mean absolute error ranged from 4.7 to 8%. ACASA assumes a closed canopy and this may be the reason for some discrepancy in the diurnal cycle. Maquis ecosystem presents a sparse canopy and the model was not able to perfectly capture exposed soil surface. Incorrected input of soil conductivity and soil diffusivity can affect soil heat flux estimation. In addition, model *G* simulations varies with soil layers depth. Using soil layer depth of 0.15 m, the amplitude of *G* values was low. It increased using a depth of few cm for each soil layer.

Net ecosystem exchange (NEE) was generally overestimated (positive value of MBE), even if the difference between simulated and measured values were low (0.5% of MBE). The regression explained 72% of half-hourly variance of NEE, and the RMSE was about 2 µmol m^{-2} s^{-1} (3% of the range). The mean absolute error was in the range from 2 to 3%. Possibly the ACASA stress factor was set to cause a CO_2 flux underestimation during the summer drought in that period. The comparison was good, and future adjustment of the stress factor input may lead to further improvement.

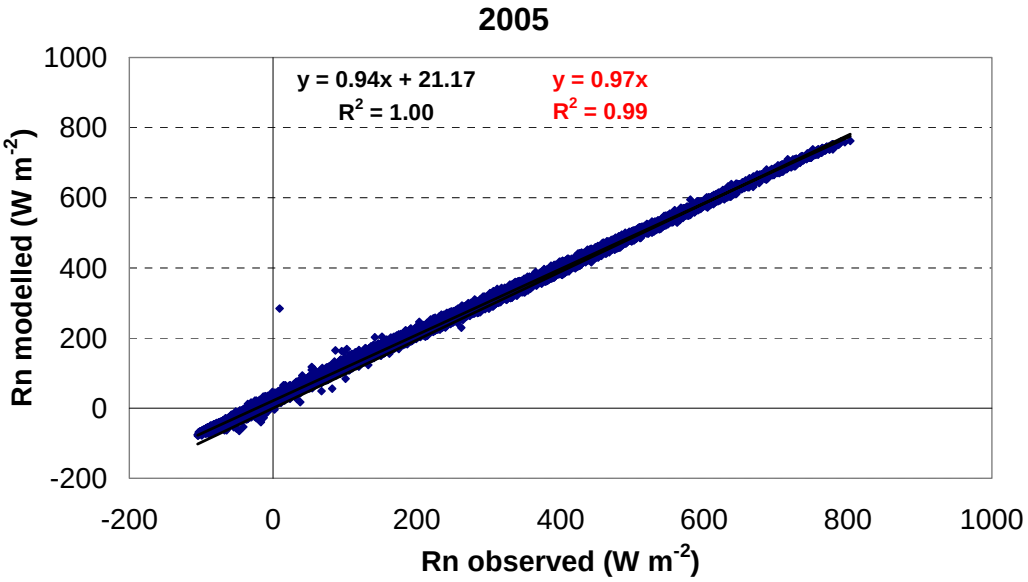

Figure 90. Regression between modelled and measured net radiation flux (Rn) for 2005.

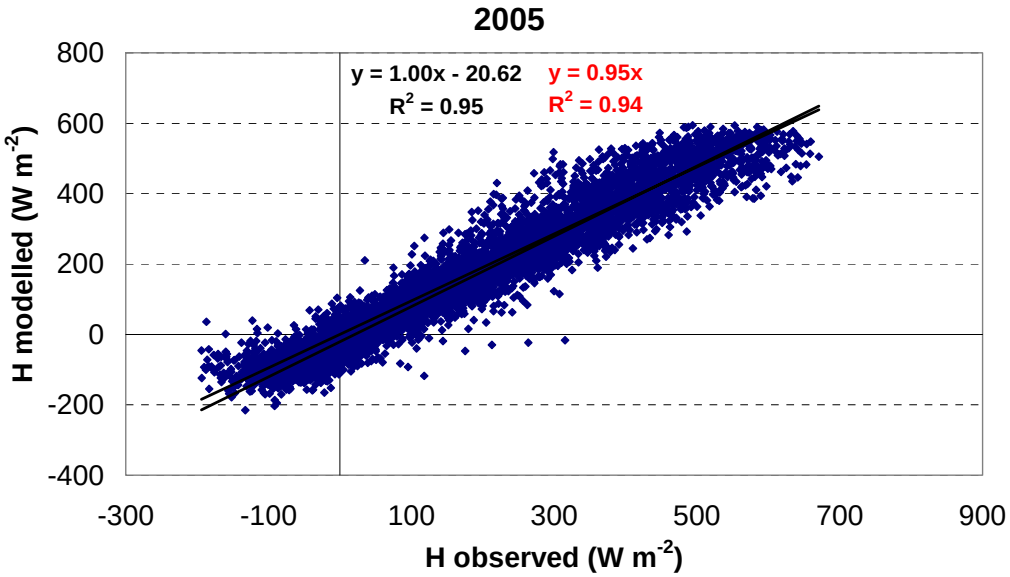

Figure 91. Regression between modelled and measured sensible heat flux (H) for 2005.

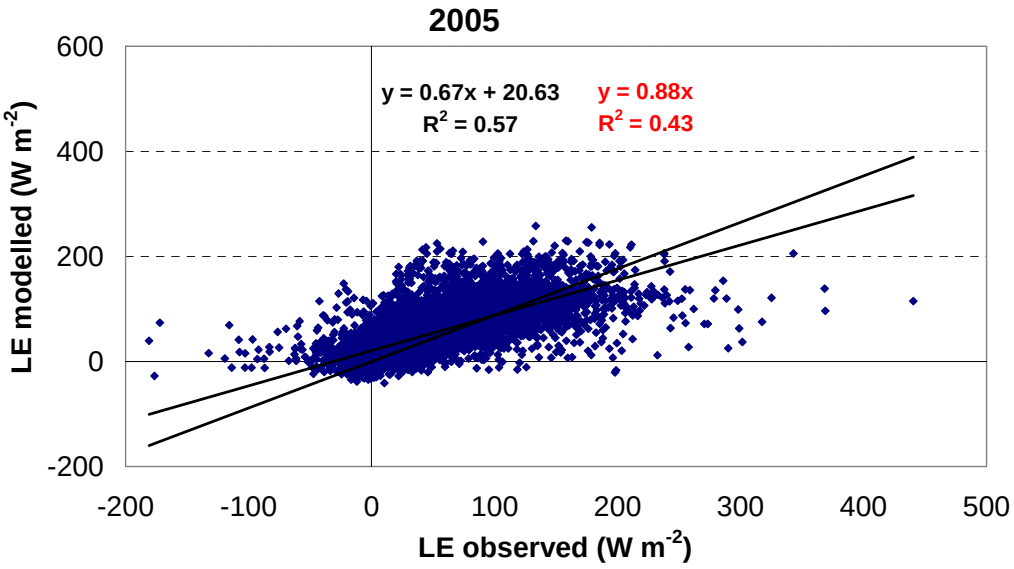

Figure 92. Regression between modelled and measure latent heat flux (LE) for 2005.

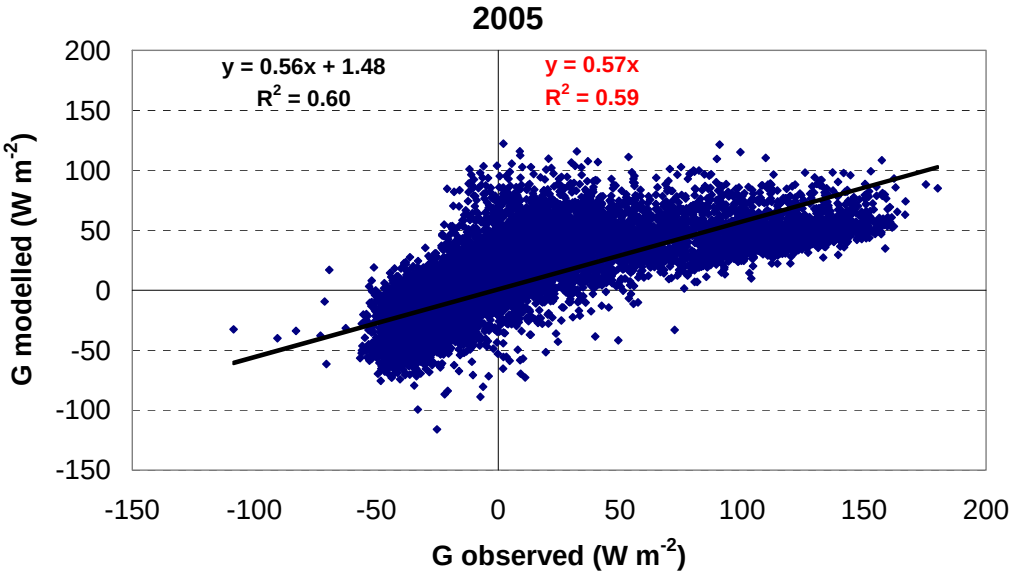

Figure 93. Regression between modelled and measured soil heat flux (G) for 2005.

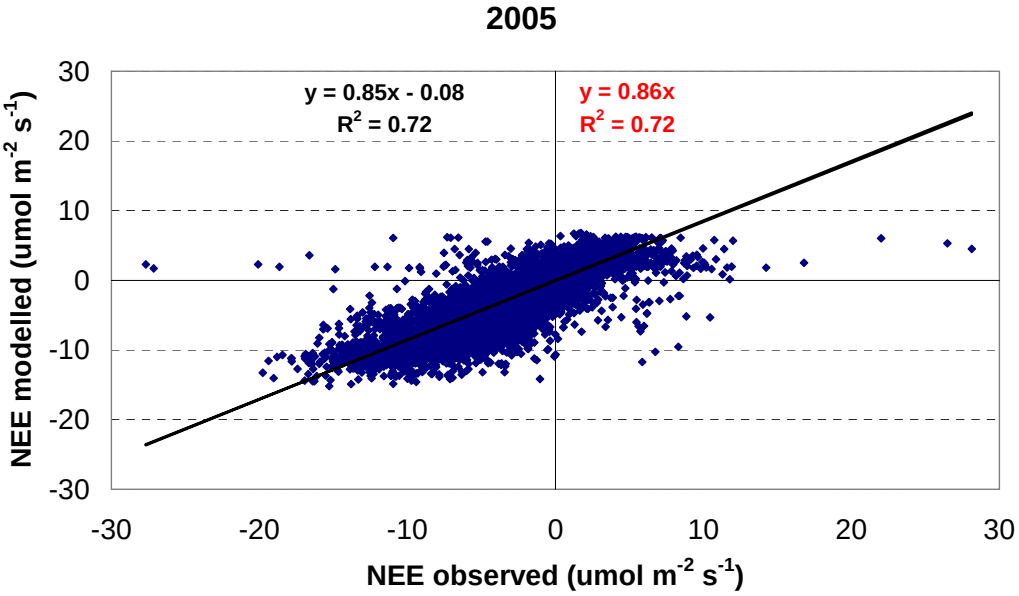

Figure 94. Regression between modelled and measured CO_2 flux (NEE) for 2005.

B) Grape vineyard

2.2.4 Energy budget closure

Energy budget closure was calculated for grapevine using simulated fluxes. In 2005, measurements were taken in two different periods: the first from DOY 179 to 188, and the second period from DOY 213 to 220. The first period was used for model parameterization. The two 2005 measurement periods were considered together for the calculation of energy budget closure with modelled data. ACASA energy budget closure were good with R^2 close to 1 (Figures 95 and 96). Closures obtained with model were higher than those obtained with observed data (Figures 67 and 68). Measured data showed closures with more data dispersion (R^2=0.92) than modelled closures (R^2=0.99-1.00).

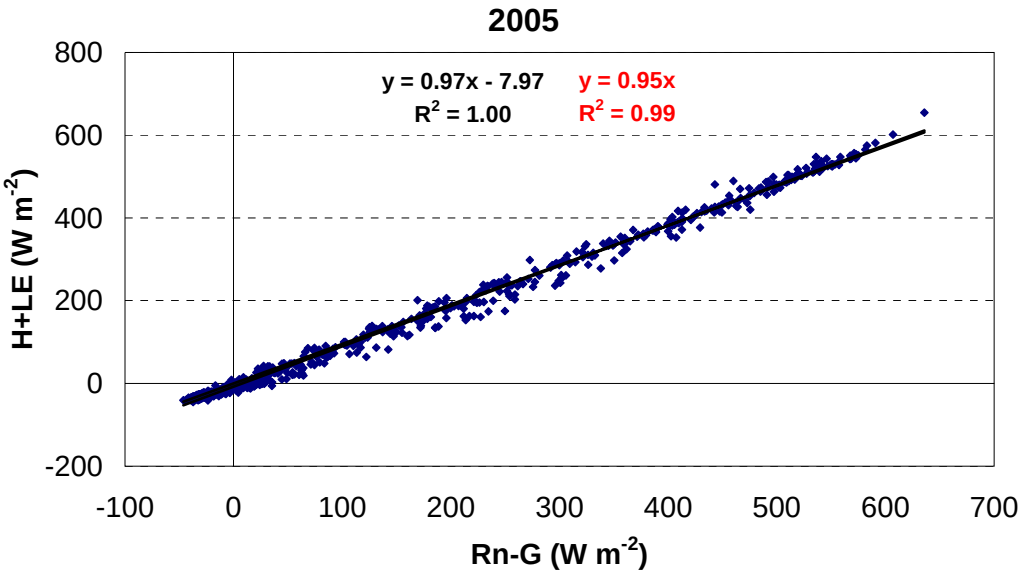

Figure 95. ACASA energy budget closure for the 2005 measurement periods.

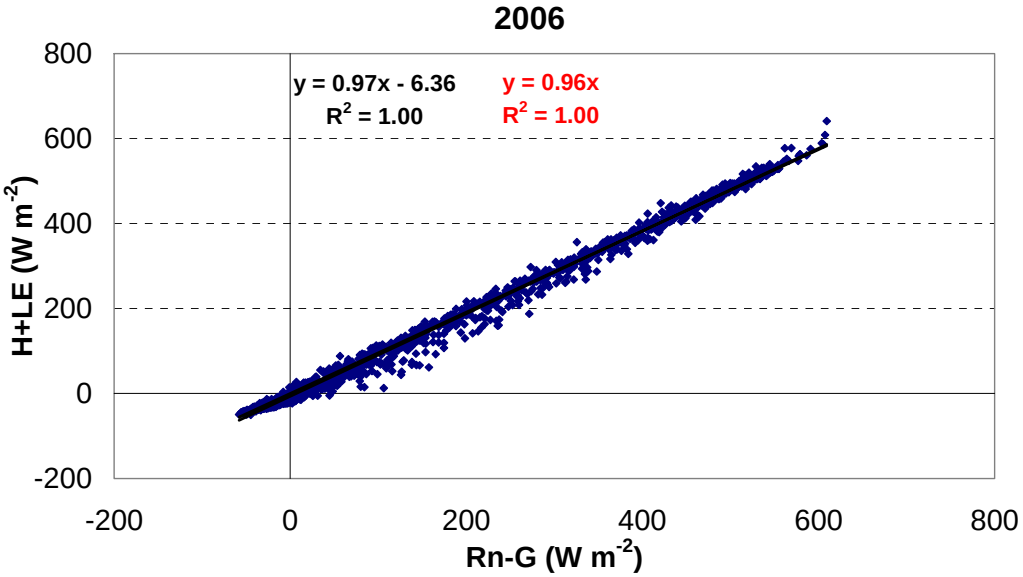

Figure 96. ACASA energy budget closure for June-August 2006.

2.2.5 Fluxes simulations

Simulated energy and mass fluxes during 2005 and 2006 were compared with measurements at half-hourly time steps. Figures 97-102 show the comparison between sensible heat (*H*), latent heat (*LE*), and CO_2 flux (NEE) for each measurement period. Table 12 reports the linear regression parameters and statistics for each measurement period.

During August 2005, *H* simulations were good (Figure 97). In particular, ACASA matches measured data well during the days 216-219. During nighttime, ACASA predicted more negative *H* values. ACASA predicted higher *LE* values than observed during August 2005 (Figure 98). Since the ACASA closure was better and the *H* values were similar for ACASA and observed, it is possible that the observed *LE* was underestimated.

During June-August 2006, simulated *H* values were higher than measured *H* (Figure 99). The ACASA *LE* values were lower than observed for the same period (Figure 100). The discrepancy in *LE* and *H* during July 2006 needs more study. A problem with the Ball-Berry sub model (Eq. C.16), and the plant and soil input file could be the cause. ACASA was able to capture the variation in *LE* flux following rainfall.

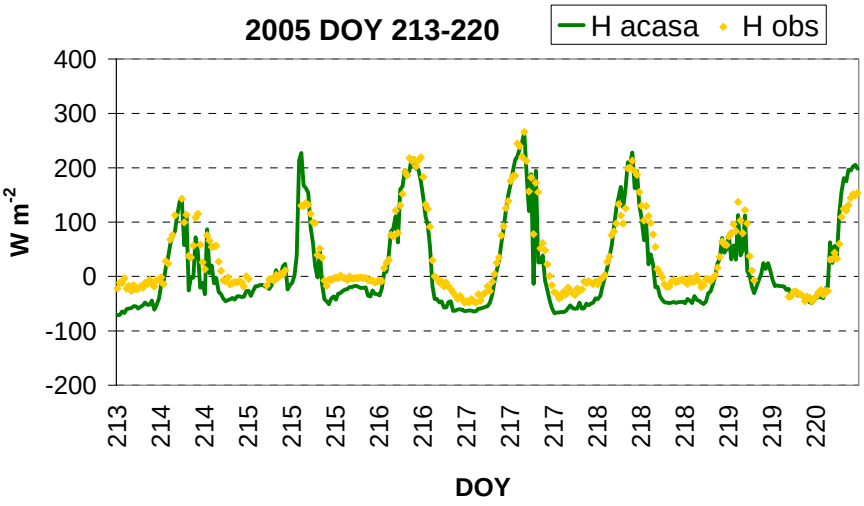

Figure 97. Comparison between simulated and observed sensibile heat flux (H) during August 2005.

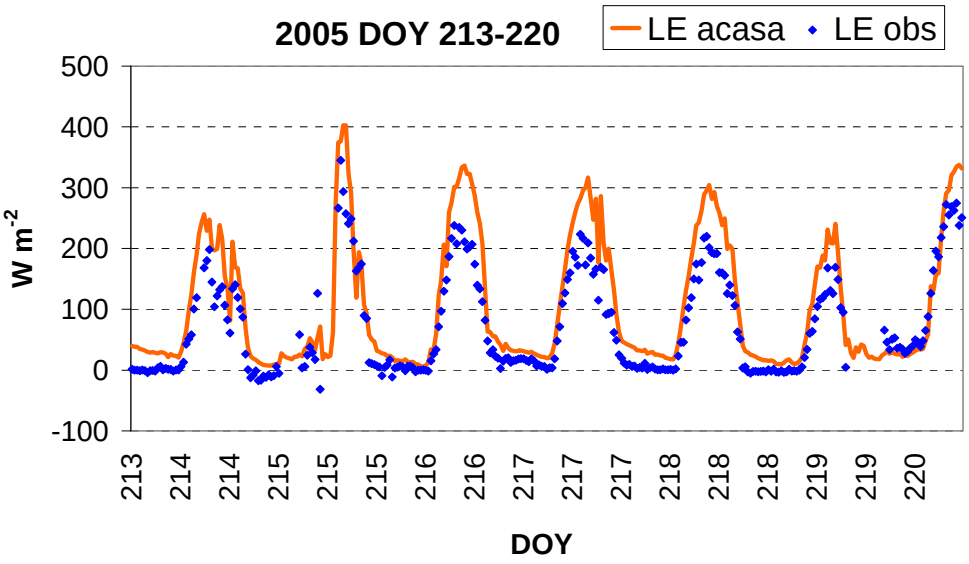

Figure 98. Comparison between simulated and observed latent heat flux (LE) during August 2005.

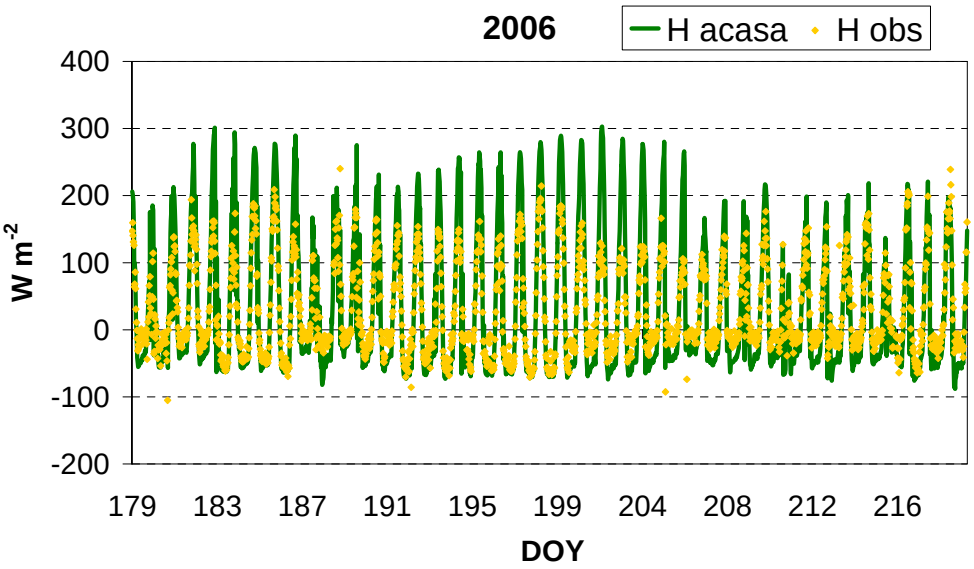

Figure 99. Comparison between modelled (line) and observed (dot) sensible heat flux (H) for 2006.

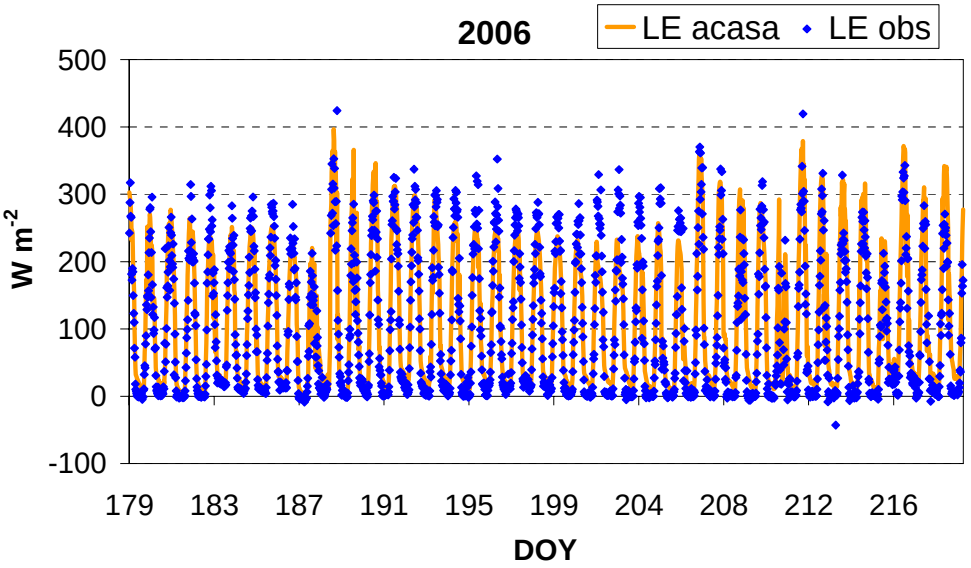

Figure 100. Comparison between modelled (line) and observed (dot) latent heat flux (LE) for 2006.

Table 12. Statistics from the regression (Y=aX+b) of simulated (as Y) on observed (as X) half-hourly energy fluxes (W m^{-2}) and net ecosystem CO_2 flux (μmol m^{-2} s^{-1}) on grapevine ecosystem. (RMSE=root mean squared error; RA=mean absolute error; MBE=mean bias error). Data were from DOY 213-220 in 2005 and from DOY 179-220 in 2006.

Flux	**Year**	**a**	**b**	**R^2**	**RMSE**	**RA**	**MBE**
Rn	2005	0.96	12.01	1.00**	15.2	12.8	6.1
	2006	0.96	13.79	1.00**	15.0	13.4	7.9
H	2005	1.34	-21.81	0.90**	40.5	31.9	-8.5
	2006	1.44	-7.13	0.88**	45.8	32.8	4.4
LE	2005	0.98	25.19	0.91**	38.0	28.7	22.6
	2006	0.93	19.91	0.91**	33.0	23.9	12.9
G	2005	0.93	-9.08	0.55**	28.8	23.9	-9.5
	2006	1.11	-6.51	0.51**	29.7	25.1	-5.9
NEE	2005	0.87	-0.10	0.56**	2.4	1.5	0.1
	2006	0.73	0.81	0.59**	2.6	1.6	1.1

** significant value at 99% probability level.

Figures 101 and 102 show comparisons between simulated and measured CO_2 flux (NEE) during August 2005 and June-August 2006. Better simulations occurred during 2005 (Figure 101). Some days showed simulated respiration flux close to the observations (DOY 217 and 218), while the other days the model predicted higher CO_2 flux (DOY 215 and 220). The days after rainfall events had higher CO_2 flux predictions. Some peaks in simulated respiration occurred during 2006 period, and they were related to precipitation (Figure 102). ACASA, therefore, showed too much sensitivity to rainfall events. Since there was little or no water deficit in 2006, the model prediction was not due to water stress. From day 188 to 205 (between two consecutive rain events), the decrease in simulated photosynthesis may be due to reduced soil water level. As for maquis ecosystem, the CO_2 flux was greatly affected by the maximum carboxilation rate (V_{cmax}). A values of 50 µmol m^{-2} s^{-1} was choosen for grapevine in order to the achievement the best simulations . The selection of this V_{cmax} needs further study.

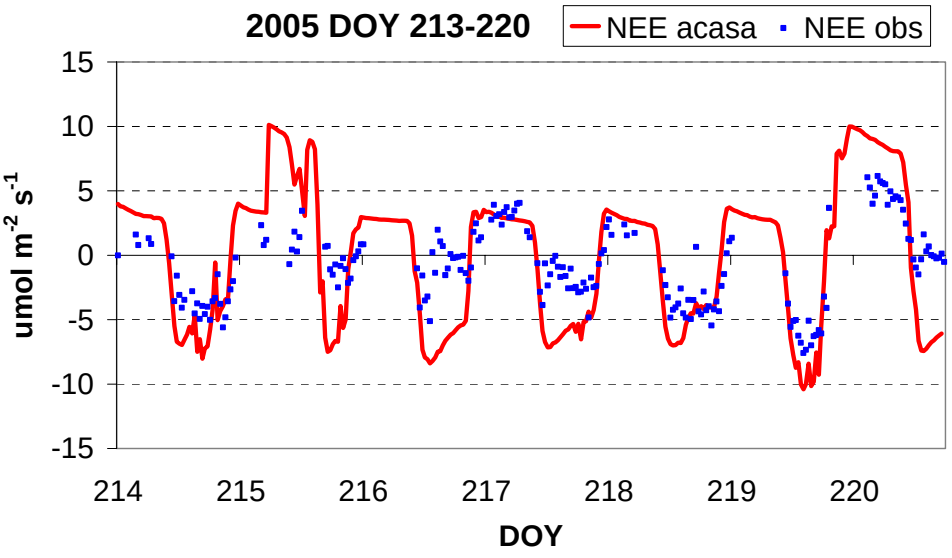

Figure 101. Comparison between modelled (line) and observed (dot) CO_2 flux in August 2005.

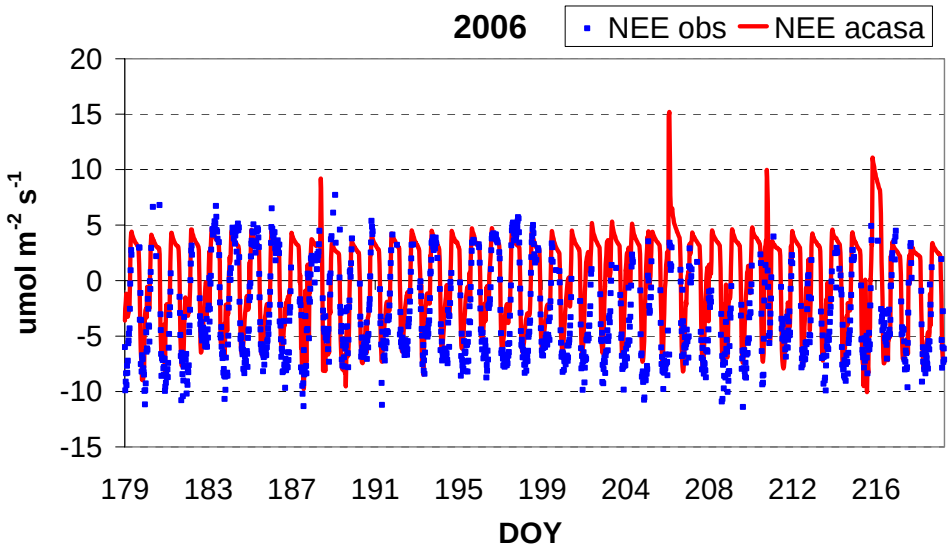

Figure 102. Comparison between modelled (line) and observed (dot) CO_2 flux from June to August 2006.

2.2.6 Statistical analysis

The root mean squared error (RMSE), mean absolute error (RA), and mean bias error (MBE) were used to evaluate model accuracy. Linear regression equations were also calculated. Table 12 reports values of angular coefficient, slope, intercept, and R^2 for linear regressions not passing through the origin for the two measurement periods.

The model explained 100% of half-hourly variance of *Rn*. The RMSE of simulated net radiation had error of about 1.7%, while the RA error was about 1.2%. MBE varied from 0.7 to 0.9%. Error percentage in ACASA *Rn* estimations was low, so the model was able to accurately predict net radiation.

ACASA better estimated observation of *LE* than *H*. The variation in RMSE of simulated sensible heat (*H*) and latent heat (*LE*) were 12% and 8%, respectively. ACASA *H* was overestimated in 2006 (positive value of MBE) and underestimated in 2005 (negative value of MBE). The regression explaind 91% of half-hourly variance of *LE* in each measurement period.

ACASA soil heat flux (*G*) was clearly lower in both measurement periods (negative value of MBE). The regression explained about 53% of half-hourly variance of *G*. The variation in RMSE was about 25%, and the mean variation in the absolute error was about 21%. Grapevine has a sparse canopy, while the model assumes a dense canopy for *G* calculation. Grapevine ecosystem has major exposed soil surfaces, so the model results for soil heat flux estimation were worse than for maquis.

Simulated net ecosystem exchange (NEE) showed lower level of concordance with measured CO_2 flux than maquis. The model explaind 55% of half-hourly variance of NEE, and the RMSE ranged from 2.47 to 2.67 μmol m^{-2} s^{-1} (14%). The comparison had a positive value of MBE although it underpredicted in the period between two consecutive rainfall events in 2006. The mean absolute error was about 8% for each measurement period.

Simulated net radiation (*Rn*), sensible heat (*H*), latent heat (*LE*), soil heat (*G*), and CO_2 (NEE) flux showed significant differences from measured data. ACASA model predictions were in agreement with observed fluxes. This behaviour was similar for each measurement period. Even if some problems occurred in some flux estimation, model results can be generally considered good. Results can be improved by making changes to input parameters and refining the model code to account for ecosystems with sparse canopies.

CONCLUSIONS

Although the ecological role is important, the impact of climate on energy and carbon fluxes in natural and agricultural ecosystems is inadequately investigated. My research contributes to understand the role of Mediterranean natural and agricultural ecosystems in the global carbon cycle, and it shows the importance of models in the study of ecosystem behaviour.

In this research, a Mediterranean maquis and a grapevine ecosystem were monitored using the *Eddy Covariance* technique for estimating energy and carbon exchanges between the vegetation and atmosphere. The ACASA higher-order closure model was used to estimate ecosystem exchanges over the two ecosystems, and the model results were compared with observed data.

The observed data showed that the maquis ecosystem generally acted as a carbon *sink* during the three measurement years (2004-2006). The results of the energy balance closure showed good measurement accuracy. Energy partitioning exhibited distinct seasonal pattern with Bowen ratio (β) clearly increasing during the drought season. The decoupling coefficient (Ω) showed values approaching 0 during the summer in each measurement period, indicating that water vapour flux was largely controlled by vegetation rather than net radiation.

Maquis assimilated CO_2 mainly during the spring and released carbon during the fall. A severe summer drought reduced the carbon uptake in each year. The estimate of the net ecosystem exchange (NEE) showed differences among years depending on drought and temperature conditions. In general, NEE was relatively low compared to other forest ecosystems.

The grape vineyard generally acted as a carbon *sink* during the 2005 and 2006 measurement periods, except in August 2005 when the grapevines was a *source* of carbon due to intense precipitation that increased the ecosystem respiration (Reco). The energy balance closure indicated a good measurement accuracy. In the grapevines, fluxes of *LE* were consistently higher than *H* during each measurement period, while, in the maquis ecosystem, the net radiation was mainly partitioned into *H* during the summer drought season.

Modelled data showed a good energy balance closure for both maquis and grapevines ecosystems. Net radiation (*Rn*) showed the best results when compared with measured values. ACASA's estimates of *H* flux were good with only small

differences between modelled and observed data over maquis. For grapevines, ACASA generally predicted higher *H* and lower *LE* than the observations. The lower *LE* values may be due to the underestimation of stomatal conductance, which is estimated using the Ball-Berry sub model. This phenomena was more pronounced during 2006 measurements. The discrepancy in *LE* and *H* during 2006 needs more study.

The ACASA soil heat flux (*G*) was generally lower than observed in both ecosystems. The model assumes a closed canopy and this may be the reason in the underestimation of the diurnal cycle. Both maquis and grape vineyard ecosystems have a sparse canopy and perhaps the model was unable to perfectly capture exposed soil surfaces. Uncorrected input values for soil conductivity and soil diffusivity can also cause errors in soil heat flux estimates.

Regarding CO_2 flux, the model predictions were good with both positive and negative fluxes well predicted by the model. For both ecosystems, the difference between simulated and observed NEE was low. In maquis, the ACASA model usually was able to capture the seasonal variation in CO_2 flux. NEE showed the typical summer decrease due to drought induced water stress, and the simulations predicted the lower CO_2 flux. Differences between ACASA simulations and observed CO_2 flux data during the dry summer may be due to water stress sensitivity controls in the model. ACASA uses physiological models for non-sclerophyllous plants that have high sensitivity to water stress. Since maquis are sclerophyllous plants, future modifications to the code or inputs might be necessary to allow for the maquis, which can still function at low levels during drought. The comparison with observed data was good, and future adjustment of the stress factor inputs may lead to further improvement. The model was also able to capture the increase in respiration (positive NEE values), which occurred after rainfall events in both ecosystems.

Statistical analysis showed that errors of ACASA predictions were low. Differences between simulated and observed energy and CO_2 fluxes were significant at the 0.001 probability level. The results were similarly good for each measurement period. Future result can be improved by making changes to input parameters and by refining the model code to account for ecosystems with sparse

canopies. In particular, improvements can be made on the response of the model to water stress and on the estimation of *G* and *LE* fluxes.

My research demonstrated how to study ecosystems behaviour and to quantify the energy and carbon exchanges between the vegetation and atmosphere. My work also showed the potential for a higher-order closure model to be used for predicting energy and CO_2 fluxes and to investigate environmental factors affecting the ecosystem behaviour. The ACASA model was tested for the first time over sparse canopy, so the results of this work were important to show the model strong and weak points to identify the changes needed to improve the ACASA model.

ACKNOWLEDGEMENTS

The completation of this dissertation was possible thanks to the contribution of many Institutions and people. Thanks to the national project "*Ecophysiological, healthful and molecular studies for the qualitative valorization and the environmental protection, in viticultural systemsi"* funded by the Italian "Ministry of Education, University and Research" several grapevine experiments were conducted, which contributed information for my dissertation.

My study of the *Eddy Covariance* technique was facilited by a Summer School in Belgium, organized by CARBOEUROPE group, and funded by the PhD Program in "Agrometeorology and Ecophysiology of Agricultural and Forest Systems" in the Department of Economics and Woody Plant Ecosystem (DESA).

The study of ACASA model has been possible thanks to a collaboration with the University of California (Davis) (UCD), Department of Land, Air and Water Resources (LAWR), in which I had the fortune to visit for one year. The scholarship was funded by the Program "Master and Back" of the Sardinia Region.

I really would thanks the Department of Economics and Woody Plant Ecosystem (DESA), expecially the Chair Professor Pietro Deidda who gave me the opportunity to complete my training in Italy and abroad.

A special thank to my advisor Professor Donatella Spano, for the support and precious advice given during these years and for the assistance in preparing the final dreaft of my thesis. I expecially thank her for the knowledge she gave to me and the passion for this work.

I sincerely thank Professor Richard Snyder, who welcomed me in my long period in Davis, and for his friendship, which made my visit pleasant. His advice and suggestions were also absolutely necessary to complete my thesis.

I want to thank Professor Kyaw Tha Paw U and Dr. David R. Pyles (UCD) who developed the ACASA model and, with patience, helped and directed me to comprehend and use the model. I also wish to thank all the LAWR Department staff and collegues who made my work at UCD pleasant.

I can not forget to thank my collegue Dr. Costantino Sirca, for our innumerable and usefull discussions, which made me grow and complete my research project and thesis. He was a constant supporter during these years of work, with his teaching and helping me in everything, either theoretic or practical.

My research was made in collaboration with the CNR-Biometeorology Institute of Sassari, and I want to thank them for helping me with the data collection and analysis. The Institute is directed by Dr. Pierpaolo Duce who I wish to personally thank for his advice and collaboration.

A sincere thank goes to Pierpaolo Zara and Angelo Arca, from the CNR Institute, for their important work in the set up of the micrometeorological stations during the field experiments.

I want to give special thanks to all my friends and collegues from the PhD Program, especially Dr. Michele Salis, Dott.ssa Valentina Bacciu, and Dr. Maurizio Laconi, who shared with me the joy and difficulties during these three years. They really contributed to making a very friendly atmosphere in our office, and I found in them to be special people for sharing experiences and communication.

I really wish to thank the person who is sharing his life with me, my boyfriend Daniele, for the support and the constant presence during these years. His advice, encouragement, incentive, and his continued desire to achieve that in which he believes, was an incentive for me to improve and finish this thesis, overcoming also the difficulty met during this work.

Finally, and must important, all my gratitude is for my family, my mother, my father, and my sister Manuela. Their unconditional trust and their invisible sacrifice let me to follow my dream to work in the difficult world of the research. I would expecially thank my mother, who supported and encouraged me in each difficult period of my life, to have shared the major joy of my life, and to have believed in me and in my work every single moment of her life.

RINGRAZIAMENTI

La realizzazione di questa tesi, per i molti argomenti trattati, è stata possibile grazie al contributo di diversi Istituti o Enti e di molte persone. La raccolta dei dati nel vigneto situato a Montalcino (Toscana) è stata possibile grazie al PRIN *"Studi ecofisiologici, salutistici e molecolari per la valorizzazione qualitativa e la salvaguardia ambientale nei sistemi viticoli nazionali"* finanziato dal Ministero dell'Educazione, dell'Università e della Ricerca.

Lo studio della tecnica *Eddy Covariance* è stato approfondito durante la Summer School tenutasi in Belgio, organizzata dal gruppo CARBOEUROPE, finanziata dal Dipartimento di Economia e Sistemi Arborei (DESA) con i fondi per il Dottorato di Ricerca in "Agrometeorologia ed Ecofisiologia dei Sistemi Agrari e Forestali".

Lo studio del modello ACASA è stato possible grazie alla collaborazione con l'Università della California (Davis) (UCD), Dipartimento di Land, Air and Water Resources (LAWR), nel quale ho avuto la fortuna di effettuare uno stage di un anno. Questo stage è stato finanziato dal Programma "Master and Back" promosso dalla Regione Sardegna.

Vorrei sinceramente ringraziare il Dipartimento di Economia e Sistemi Arborei (DESA), e in particolar modo il direttore Prof. Pietro Deidda, per avermi dato l'opportunità di completare la mia formazione professionale in realtà così diverse tra loro.

Un ringraziamento speciale va al mio docente guida, la Prof.ssa Donatella Spano, per il sostegno e i preziosi consigli dati durante questi anni e per l'aiuto e le correzioni apportate durante la stesura finale di questa tesi. Desidero, inoltre, ringraziarla per tutti gli insegnamenti dati in questo periodo e, soprattutto, per avermi trasmesso la passione per questo lavoro.

Sento di dover sinceramente ringraziare il Prof. Richard Snyder, che mi ha accolto durante il mio lungo periodo a Davis, e che, con la sua amicizia, ha reso più piacevole il periodo dello stage. I suoi consigli e i suoi suggerimenti sono stati, inoltre, assolutamente necessari per completare questa tesi.

Desidero ringraziare anche il Prof. Kyaw Tha Paw U e il Dr. David R. Pyles (UCD), che hanno sviluppato il modello ACASA e che, con pazienza, mi

hanno aiutato e guidato nella comprensione e nell'utilizzo del modello. Desidero inoltre ringraziare tutto lo staff e i colleghi del LAWR Department che hanno reso molto piacevole lavorare in un posto lontano da casa.

Non posso dimenticare di ringraziare il mio collega Dr. Costantino Sirca per le innumerevoli e utili discussioni che hanno fatto crescere e realizzare il progetto di ricerca di questa tesi. E' stata una presenza costante durante questi anni di lavoro, con i suoi insegnamenti e il suo aiuto in ogni cosa, sia teorica che pratica.

Il mio lavoro è stato condotto in collaborazione con il CNR-Istituto di Biometeorologia di Sassari, il cui aiuto è stato prezioso per la raccolta e il trattamento dei dati. L'istituto è diretto dal Dr. Pierpaolo Duce, che desidero ringraziare per i consigli e la collaborazione offerti durante questi anni.

Un sincero ringraziamento va a Pierpaolo Zara e Angelo Arca, i tecnici del CNR, per il loro prezioso lavoro nell'installazione delle stazioni micrometeorologiche durante le campagne sperimentali.

Un ringraziamento particolare a tutti i miei amici e colleghi di dottorato, in particolar modo al Dr. Michele Salis, alla Dott.ssa Valentina Bacciu, e al Dr. Maurizio Laconi, che hanno condiviso con me gioie e difficoltà durante questi tre anni. Grazie a loro si è creata un'atmosfera di amicizia nel nostro ufficio e in loro ho trovato delle persone speciali con cui parlare e condividere diversi interessi.

Uno speciale ringraziamento alla persona che sta condividendo la sua vita con me, il mio fidanzato Daniele, per il sostegno e la costante presenza durante questi anni. I suoi consigli, incoraggiamenti, stimoli, e il suo continuo desiderio di realizzare ciò in cui crede, sono stati per me uno stimolo a migliorare e terminare questa tesi, superando anche le difficoltà incontrate durante questo lavoro.

Infine, perché più importante, tutta la mia gratitudine è per la mia famiglia, mia madre, mio padre e mia sorella Manuela. La loro incondizionata fiducia e il loro invisibile sacrificio mi hanno permesso di seguire il sogno di lavorare nel difficile mondo della ricerca. Vorrei ringraziare in particolar modo mia madre per avermi sostenuto e incoraggiato in ogni periodo difficile della mia vita, per aver condiviso con me le gioie più grandi, e per aver creduto in me e nel mio lavoro ogni singolo istante della sua vita.

REFERENCES

Aber J.D., Melillo J.M., 1991. *Terrestrial Ecosystems*. Saunders College Publishing, Philadelphia - Fort Worth, Chicago, San Francisco, Montreal, Toronto, London, Sydney - Tokio.

Allen R.G., Pereira L.S., Raes D., Smith M., 1998. *Crop evapotranspiration. Guidelines for computing crop water requirements*. FAO Irrigation and Drainage. Paper No. 56, United Nations-FAO, Rome, Italy, pp. 300.

Andrè J.C., De Moor G., Lacarrere P., and Du Vachat R., 1976a. *Turbulence approximation for inhomogeneous flows. I: The clip-ping approximation*. J. Atmos. Sci., 33: 476-481.

Andrè J.C., De Moor G., Lacarrere P., and Du Vachat R., 1976b. *Turbulence approximation for inhomogeneous flows. II: Numerical simulation of a penetrative convection experiment*. J. Atmos. Sci., 33: 482-291.

Andrè J.C., DeMoor G., Lacerure P., Therry G., and DuVachat R., 1978. *Modelling the 24-hour evolution of the mean and turbulent structures of the planetary boundary layer*. J. Atmos. Sci., 35: 1861- 1883.

Anthoni P.M., Knohl A., Rebmann C., Freibauer A., Mund M., Ziegler W., Kolle O., Schulze E.D., 2004. *Forest and agricultural land-use-dependent CO_2 exchange in Thuringia, Germany.* Global Change Biology 10: 2005–2019.

Aubinet M., Grelle A., Ibrom A., Rannik U., Moncrieff J., Foken T., Kowalski A.S., Martin P.H., Berbigier P., Bernhofer Ch., Clement R., Elbers J., Granier A., Grunwald T., Morgenstern K., Pilegaard K., Rebmann C., Snijders W., Valentini R., Vesala T., 2000. *Estimates of the annual net carbon and water exchange of European forests: the EUROFLUX methodology.* Adv. Ecol. Res., 30: 113-174.

Aubinet M., Chermanne B., Vandenhaute M., Longdoz B., Yernaux M., Laitat E., 2001. *Long term carbon dioxide exchange above a mixed forest in the Belgian Ardennes.* Agric. For. Meteor. 108: 293–315.

Aubinet M., Heinesch B., Longdoz B., 2002. *Estimation of the carbon sequestration by a heterogeneous forest: night flux corrections, heterogeneity of the site and inter-annual variability*. Global Change Biology 8: 1053–1071.

Aubinet M., Falge E., Reichstein M., Chojnick B., Di Tommasi P., Dore S., Law B., Leahy P., Longdoz B., Manca G., Marcolla B., Moffat A., Montagnani L., Nagy M., Nagy Z., Njarosz N., Papale D., Rebmann C., Rotenberg E., Sagerfors J., Schelde K., Styles J., Suni T., Weslien P., and Wilkinson, M., 2004. *Minutes of the data gap filling and partitioning workshop*, Viterbo, June 9- 10th, 2004.
Available at: http://gaia.agraria.unitus.it/download/edow.html.

Aubinet M., Berbigier P., Bernhofer Ch., Cescatti A., Feigenwinter C., Granier A., Grünwald Th., Havrankova K., Heinesch B., Longdoz B., Marcolla B., Montagnani L., and Sedlak P. 2005. *Comparing CO_2 storage and advection conditions at night at different Carboeuroflux sites.* Boundary-Layer Meteorology, 116: 63-93.

Baeza P., Ruiz C., Cuevas E., Sotés V., and Lissarrague J.R., 2005. Ecophysiological and Agronomic Response of Tempranillo Grapevines to Four Training Systems. Am. J. Enol. Vitic. 56 (2): 129-138.

Baldocchi D., Hicks B.B., Meyers T.P., 1988. *Measuring biosphere-atmosphere exchanges of biologically related gases with micrometeorological methods.* Ecology, (69): 1331-1340.

Baldocchi D., 1994. *A comparative study of mass and energy exchange over a closed C3 (wheat) and an open C4 (corn) canopy: I. The partitioning of available energy into latent and sensible heat exchange.* Agric. For. Meteor. 67: 191-220.

Baldocchi D., Valentini R., Running S., Oechel W., Dahlman R., 1996. *Strategies for measuring and modelling carbon dioxide and water vapour fluxes over terrestrial ecosystems.* Global Change Biology, (2): 159-168.

Baldocchi D., Vogel C.A., Hall B., 1997. *Seasonal variations of carbon dioxide exchanges rates above and below a boreal jack pine forest.* Agricultural and Forest Meteorology, 83: 147-170.

Baldocchi D., 1997a. *Flux footprint within and over forest canopies.* Boundary Layer Meteor. 85: 273-292.

Baldocchi D., 1997b. *Measuring and modelling carbon dioxide and water vapour exchange over a temperate broad-leaved forest during the 1995 summer drought*. Plant, Cell and Environment, 20:1108-1122.

Baldocchi D., Finnigan J., Wilson K., Paw K.T., Falge E., 2000. *On measuring net ecosystem carbon exchange over tall vegetation on complex terrain.* Boundary-Layer Meteorology, 96: 257-291.

Baldocchi D., Falge E., Gu L., Olson R., Hollinger D., Running S., Anthoni P., Bernhofer Ch., Davis K., Evans R., Fuentes J., Goldstein A., Katul G., Law B.E., Lee X., Malhi Y., Meyers T., Munger W., Oechel W., Paw U K.T., Pilegaard K., Schmid H.P., Valentini R., Verma S., Vesala T., Wilson K., and Wofsy S., 2001. FLUXNET: *A new tool to study the temporal and spatial variability of ecosystem-scale carbon dioxide, water vapour, and energy flux densities.* Bulletin of the American Meteorological Society, 82: 2415–2434.

Baldocchi D., 2003. *Assessing the eddy covariance technique for evaluating carbon dioxide exchange rates of ecosystems: past, present and future.* Global Change Biology 9: 479-492.

Barbero M., Loisel R., Quézel P., 1989. *Perturbations et incendies en région méditerranéenne*. Inst. Est. Pyrenaicos Jaca, (12): 409-419.

Bernhofer C., Aubinet M., Clement R. et al., 2003. *Spruce forests (Norway and Sitka spruce, including Douglas fir): carbon and water fluxes and balances, ecological and ecophysiological determinants.* In: Fluxes of Carbon, Water and Energy of European Forests. Vol. 163. Ecological Studies Series (ed. Valentini R), pp. 99–123. Springer-Verlag, Heidelberg.

Bigot A., Fontaine F., Clément C., Vaillant-Gaveau N., 2007. *Effect of the herbicide flumioxazin on photosynthetic performance of grapevine (Vitis vinifera L.)*. Chemosphere, 67: 1243-1251.

Bullock, P., Le Houerou, H, 1996. *Land degradation and desertification.* In: Climate change 1995. Impacts, adaptations and mitigation of climate change: scientific-technical analyses. Watson R.T., ZINYOWERA, M.C; Moss, R.H. (eds.). Cambridge University Press, Cambridge:. 171-189.

Caspersen J.P., Pacala S.W., Jenkins J.C., Hurtt G.C., Moorcroft P.R., Birdsey R.A., 2000. *Contributions of land-use history to carbon accumulation in US forests*. Science 290:1148–51.

Chapin F.S. III, Matson P.A., Mooney H.A., 2002. *Principles of terrestrial ecosystem ecology*. New York: Springer.

Ceccon P., Borin M., 1995. Elementi di Agrometeorologia e Agroclimatologia. Imprimitur.

Collatz G.J., Ball J.T., Grivet C., and Berry J.A., 1991. *Physiological and environmental regulation of stomatal conductance, photosynthesis and transpiration: a model that includes a laminar boundary layer*. Agric. And For. Meteor., 54 (2): 107-136.

Davies W.J, Zhang J., 1991. *Root signals and the regulation of growth and development of plants in drying soil.* Annual Review of Plant Physiology and Plant Molecular Biology 42: 55–76.

Davis G.W., and Richardson D.M., Eds, 1995 *Mediterranean-Type Ecosystems: The Function of Biodiversity.* Springer, Heidelberg.

Denmead O.T., 1969. *Comparative micrometeorology of a wheat field and a forest of Pinus radiate*. Agric. Meteor. 6: 357-371.

Denmead O.T., and Bradley E.F., 1985. *Flux-gradient relationship in a forest canopy.* In: Hutchison B.A., Hicks, B.B (Eds), The forest-Atmosphere Interaction. D. Reidel Publishers, Dordrecht, pp. 421-441.

Denmead O.T., and Bradley E.F., 1987. *On scalar transport in plant canopies.* Irrig. Sci. 8: 131-149.

Denmead O.T., Dunin F.X., Wong S.C., and Greenwood E.A.N., 1993. *Measuring water use efficiency of Eucalypt trees with chambers and micrometeorological techniques.* Journal of Hydrology, 150 (2): 649-664.

De Pury D.G.G., 1995. *Scaling photosynthesis and water use from leaves to paddocks.* Ph.D. Dissertation. Australian National University. Canberra, Australia.

Desjardins R.L., 1974. *A technique to measure CO_2 exchange under field conditions.* International Journal of Biometeorology, 18: 76-83.

Desjardins R.L., and Lemon E.R., 1974. *Limitations of an eddy covariance technique for the determination of the carbon dioxide and sensible heat fluxes*. Boundary Layer Meteor., 5: 475-488.

Dickinson R.E., Henderson-Sellers A., and Kennedy P.J., 1993. *Biosphere-Atmosphere Transfer Scheme (BATS) Version 1e as coupled to the NCAR Community Climate Model.* NCAR Technical Note NCAR/TN-387+STR, National Center for Atmospheric Research, 72p.

Di Castri F., Goodall D.W., and Specht R.L., eds. 1981. *Ecosystems of the world 11. Mediterranean-type shrublands*. Elsevier Scientific, New York.

Dyer A.J., 1981. *Flow distortion by supporting structures.* Boundary Layer Meteor. 20: 243-251.

Dore S., and Valentini R., 2002. *Fenologia e scambi atmosfera/biosfera. PHENAGRI:* Fenologia per l'agricoltura. Atti del Convegno Nazionale, Roma 5-6 Dicembre: 58-63.

Drexler J.Z., Snyder R.L., Spano D., Paw U. KT., 2004. *A review of models and micrometeorological methods used to estimate wetland evapotranspiration.* Hydrological Processes 18: 2071-2101.

Ek M., and Mahrt L., 1991. OSU 1-D PBL Model User's Guide. *A one-dimensional planetary boundary layer model with interactive soil layers and plant canopy.* Version 1.0.4. March 1991. Available from Dept. of Atmospheric Sciences, Oregon State University.

Falge E., Graber W., Seigwolf R., and Tenhunen J.D., 1996. *A model of the gas exchange response of Picea abies to habitat conditions*. Trees, 10: 277-287.

Falge E., Baldocchi D., Olson R.J., Anthoni P., Aubinet M., Bernhofer C., Burba G., Ceulemans, R., Clement R., Dolman H., Granier A., Gross P., Grünwald T., Hollinger D., Jensen N.O., Katul G., Keronen P., Kowalski A., Ta Lai C., Law B.E., Meyers T., Moncrieff J., Moors E., Munger J. W., Pilegaard K., Rannik Ü., Rebmann C., Suyker A., Tenhunen J., Tu K., Verma S., Vesala T., Wilson K., and Wofsy. S. 2001a. *Gap filling strategies for defensible annual sums of net ecosystem exchange.* Agricultural and Forest Meteorology, 107: 43–69.

Falge E., Baldocchi D., Olson R.J., Anthoni P., Aubinet M., Bernhofer C., Burba G., Ceulemans R., Clement R., Dolman H., Granier A., Gross P., Grunwald T., Hollinger D., Jensen N.O., Katul G., Keronen P., Kowalski A., Lai C.T., Law B.E., Meyers T., Moncrieff J., Moors E., Suyker A., Tenhunen J., Tu K., Verma S., Vesala T., Wilson K and Wofsy S., 2001b. *Gap filling strategies for long term energy flux data sets.* Agricultural and Forest Meteorology, 107: 71–77.

Falkowski P., Scholes R.J., Boyle E., Canadell J., Canfield D., Elser J., Gruber N., Hibbard K., Hogberg P., Linder S., Mackenzie F.T., Moore B., III, Pedersen T., Rosenthal Y., Seitzinger S., Smetacek V., and Steffen W., 2000. *The global carbon cycle: A test of our knowledge of earth as a system.* Science. Vol. 290: 291-296.

Fan S.M., Wofsy S.C., Backwin P.S., andJacob D.J., 1990. *Atmosphere-biosphere exchange of CO_2 and O_3 in the central Amazon forest.* Journal of Geophysical Research, 95: 16851-16864.

FAO, 2002a. *Terrestrial carbon observations: The Ottawa assessment of requirements, status and next steps.* J.Cihlar ed. Food and Agriculture Organization of the United Nations. Environment & Natural Resources report #2, 96 pp. Isbn 92-5-104801-0. Issn 1684-8241.

FAO, 2002b. *Terrestrial carbon observations: The Rio de Janeiro recommendations for terrestrial and atmospheric measurements.* J.Cihlar et al ed. Food and Agriculture Organization of the United Nations. Environment & Natural Resources report #3, 42 pp. Isbn 92-5-104802-9. Issn 1684-8241.

FAO, 2003. *Terrestrial carbon observations: The Frascati report on in situ carbon data and information.* J.Cihlar et al. ed. Food and Agriculture Organization of the United Nations. Environment & Natural Resources report #5, 120 pp. Isbn 92-104844-4. Issn 1684-8241.

FAO, 2007. *Crop Water Requirement*. Irrigation 6th Edition, May 2007 Draft.

Farquhar G.D., and von Caemmerer S., 1982. *Modelling photosynthetic response to environmental conditions.* Encyclopedia of Plant Physiology II,

12b, O.L. Lange, P.S. Nobel, C.B. Osmond, and H. Ziegler, Eds., Springer-Verlag, Berlin, Germany, 747 pp.

Field C.B., Berry J.A., Mooney H.A., 1982. *A portable system for measuring carbon dioxide and water vapour exchanges of leaves.* Plant, Cell and Environment, 5: 179-186.

Finnigan J.J., 1999. *A comment on the paper by Lee (1998) "On micrometeorological observations of surface-air exchange over tall vegetation".* Agricultural and Forest Meteorology, 97: 55–64.

Finnigan J.J., Clement R., Malhi Y., Leuning R., and Cleugh H.A., 2003. *A revaluation of long-term flux measurement techniques Part I: Averaging and coordinate rotation.* Boundary-Layer Meteorology, 107: 1–48.

Flesch T.K. 1996. *The Footprint for Flux Measurements. From Backward Lagrangian Stochasitic Models.* Boundary-Layer Meteorol. 78: 399-404.

Foken Th., and Gerstmann W., 1984. *Eigenschaften des Ultraschallanemometers der Firma Kaijo-Denki auf Grund der Ergebnaisse von 'MESP-81'.* Geod. Geophys. Veroff., R. II, 26: 30-35.

Foken Th., Skeib G. and Richter S.H. 1991. *Dependence of the integral turbulence characteristics on the stability of stratification and their use for Doppier-Sodar measurements.* Z. Meteorol 41:311-315.

Foken Th., Wichura B., 1996. *Tools for quality assessment of surface-based flux measurements.* Agric. For. Meteorol. 78: 83-105.

Foken Th., Jegede O.O., Weisensee U., Richter S.H., Handorf D., Gorsdorf I.J., Vogei G., Schubert L.I., Kirzel H.-J., and Thiermann V., 1997. *Results for the LINEX-96/2 experiment.* Deutscher Wetterdienst, Geschftsbereich Forschung und Entwicklung, Arheitserdebnisse 48, 75 pp.

Foken Th. 1999. *The turbulence experiment FINTUREX at the Neumayer Station/Antartica.* Ber. des Deutschen Wetterdienstes, Berlin.

Foley J.A., Prentice I.C., Ramankutty N., Levis S., Pollard D., Sitch S., Haxeltine A., 1996. *An integrated biosphere model of land surface processes, terrestrial carbon balance, and vegetation dynamics.* Global Biogeochemical Cycles, 10 (4): 603-628.

Frak E., Le Roux X., Millard P., Adam B., Dreyer E., Escuit C., Sinoquet H., Vandame M., and Varlet-Grancher C., 2002. *Spatial distribution of leaf nitrogen and photosynthetic capacity within the foliage of individual trees : disentangling the effects of local light quality, leaf irradiance, and transpiration.* Journal of Experimental Botany, 53 (378): 2207-2216.

Friedlingstein P.J.L., Dufresne P.M., Cox P., Rayner. 2003. *How important is the positive feedback between climate change and the carbon cycle.* Tellus 55B: 692–700.

Fung I.Y., Doney S.C., Lindsay K., and John J., 2005. *Evolution of carbon sinks in a changing climate.* PNAS August 9, 2005, Vol. 102 (32):11201–11206.

Gaim, 1998. *Global net primary productivity. Global analysis, integration and modelling, 1993-1997 report.* 18 pp.

Garratt J.R., 1992. *The Atmospheric Boundary Layer*. Cambridge University Press, 316 pp.

Gash J.H.C. 1986. *A Note on Estimating the Effect of a Limited Fetch on Micrometeorological Evaporation Measurements.* Boundary-Layer Meteorol. 35: 409-415.

Gates D.M., 1980. *Biophysical Ecology*. Springer-Verlag, New York, NY, 611 pp.

Goudriaan J.,. Groot J.J.R and Uithol. P.W.J., 2001. *Productivity of agro-ecosystems.* In: Terrestrial global productivity. Mooney and Roy eds. Academic press.: 301-313.

Goulden M.L, Munger J.W, Fan Song-Miao, Daub B.C., Wofsy S.C., 1996. *Measurements of carbon sequestration by long-term eddy covariance: methods and a critical evaluation of accuracy.* Global Change Biology, 2: 169-182.

Goulden M.L., and Crill P.M., 1997. A*utomated measurements of CO_2 exchange at the moss surface of a black spruce forest.* Tree Physiology, 17: 537-542.

Granier A., Ceschia E., Damesin C., Dufrene E., Epron D., Gross P., Lebaube S., Le Dantec V., Le Goff N., Lemoine D., Lucot E., Ottorini M., Pontailler

J.Y., and Saugier B., 2000. *The carbon balance of a young Beech forest.* Functional Ecology 14: 312-325.

Granier A., Pilegaard K., and Jensen N.O., 2002. *Similar net ecosystem exchange of beech stands located in France and Denmark.* Agr. For. Meteor. 114: 75-82.

Granier A., Reichstein M., Breda N., Janseens I.A., Falge E., Ciais P., Grunwald T., Aubinet M., Berbigier P., Bernhofer C., Buchmann N., Facini O., Grassi G., Heinesch B., Ilvesniemi H., Keronen P., Knhol A., Kostner B., Lagergren F., Lindroth A., Longdoz B., Loustau D., Mateus J., Montagnani L., Nys C., Moors E., Papale D., Peiffer M., Pilegaard K., Pita G., Pumpanen J., Rambal S., rebmann C., Rodrigues A., Seufert G., Tenhunen J., Vesala T., Wang Q., 2007. *Evidence for soil control on carbon and water dynamics in European forests during the extremely dry year:2003*. Agric. For. Meteor. 143: 123-145.

Greco S., and Baldocchi D.D., 1996. *Seasonal variations of CO_2 and water vapour exchange rates over a temperate deciduous forest.* Global Change Biology 2: 183-198.

Grelle A. and Lindroth A., 1996. *Eddy-correlation system for long term monitoring of fluxes of heat, water vapour, and CO_2.* Global Change Biol. 2: 297-307.

Grime J.P., 1977. *Evidence for the existence of three primary strategies in plants and its relevance to ecological and evolutionary theory.* American Naturalist, (111): 1169-1194.

Grunwald T., and Bernhofer C., 2007. *A decade of carbon, water and energy flux measurements of an old spruce forest at the Anchor Station Tharandt*. Tellus 59B: 387-396.

Grunzweig J.M., Lin T.L., Rotenberg E. et al., 2003. *Carbon sequestration in arid-land forest.* Global Change Biology, 9: 791–799.

Hamilton J.G., Thomas R.B., Delucia E.H., 2001. *Direct and indirect effects of elevated CO_2 on leaf respiration in a forest ecosystem*. Plant, Cell and Environmental, 24: 975-982.

Hao Y., Wang Y., Huang X., Cui X., Zhou X., Wang S., Niu H., and Jiang G., 2007. *Seasonal and interannual variation in water vapour and energy exchange over a typical steppe in Inner Mongolia, China.* Agric. For. Meteor. 146: 57-69.

Harley P.C., and Tenhunen J.D., 1991. *Modelling the photosynthetic response of C3 leaves to environmental factors.* In: Modelling Crop Photosynthesis-from Biochemistry to Canopy. American Society of Agronomy. Madison, WI. pp. 17-39.

Harley P.C., Thomas R.B., Reynolds J.F., and Strain B.R., 1992. *Modelling photosynthesis of cotton grown in elevated CO_2.* Plant, Cell Environment. 15: 271-282.

Hastings S.T., Oechel W.C., and Muhlia-Melo A, 2005. *Diurnal, seasonal and annual variation in the net ecosystem CO_2 exchange of a desert shrub community (Sarcocaulescent) in Baja California, Mexico.* Global Change Biology 11: 927-939.

Haszpra L., Barcza Z., Davis K.J., and Tarczay K., 2005. *Long-term tall tower carbon dioxide flux monitoring over an area of mixed vegetation.* Agric. For. Meteorol. 132: 58-77.

Haxeltine A., and Prentice I.C., 1996a. *A general model for the light-use, efficiency of primary production.* Functional Ecology, 10:551-561.

Haxeltine A., and Prentice I.C., 1996b. *BIOME3: An equilibrium terrestrial biosphere model based on ecophysiological constraints, resource availability, and competition among plant functional types.* Global Biogeochemical cycles 10 (4): 693-709.

Haxeltine A., Prentice I.C., and Cresswell I.D., 1996. *A coupled carbon and water flux model to predicte vegetation structure.* Journal of Vegetation Science, 7 (5): 651-666.

Heal, O.W. and Dighton, J., 1986. *Nutrient cycling and decomposition in natural terrestrial ecosystems.* In: Microflora land Faunal Interactions in Natural and Agro-Ecosystems. Ed. M.J. Mitchell & J.P. Nakas, Martinus Nijhoff/Dr. W. Junk: 14-73.

Hinckley T.M., Brooks J.R., Cermak J., Ceulemans R., Kucera J., Meinzer F.c:, and Roberts D.A., 1994. *Water flux in a hybrid poplar stand.* Tree Physiol. 14: 1005-1018.

Hyson P., Garratt J.R., and Francey R.J., 1977. *Algebraic and electronic corrections of measured uw covariance in the lower atmosphere*. Journal of Applied Meteorology 16: 43-47.

Horst T.W. and Weil J.C. 1992. *Footprint Estimation for Scalar Flux Measurements in the Atmospheric Surface Layer.* Boundary-Layer Meteorol. 59:279-296.

Hu W.H., Shi K., Song X.S., Xia X.J., Zhou Y.H., and Yu J.Q., 2006. *Different effects of chilling on respiration in leaves and roots of cucumber (Cucumis sativus)*. Plant Biology and Biochemistry 44: 837-843.

Huglin P., 1978. *Nouveau mode d'évaluation des possibilities héliothermiques d'un milieu viticole.* C.R. Acad. Agric. Fr. 64:1117-1126.

Huglin P., and Schneider C., 1998. *Biologie et écologie de la vigne.* 370 pp. Lavoisier Tec & Doc, Paris.

Huschke, R.E., 1959. *Glossary of Meteorology*. American Meteorol. Soc., Boston. 638 pp.

Iacono F., Buccella A., Peterlungen E., 1998. *Water stress and rootstock influence on leaf of grafted and ungrafted grapevines*. Scientia Horticulturae 75: 27-39.

IPCC 2001. *Climate change 2001*. Cambridge University Press. pp 881

IPCC 2006. *Guidelines for National Greenhouse Gas Inventories.* www.ipcc-nggip.iges.or.jp/public/2006gl/index.htm

Jacobs A.F.G., 1985. *The normal force coefficient on a thin closed fence*. Boundary-Layer Meteorology, 32: 329–335

Jarvis P.G., James G.B., and Landsberg J.J., 1976. *Coniferous forest.* In: Vegetation and the Atmosphere, Vol. 2 (ed Monteith J.J.), pp. 171-240. Academic Press, London.

Jones H.G., 1992. *Plants and microclimate. A quantitative approach to environmental plant physiology.* Cambridge University Press, Cambridge.

Jones G.V., 1997. *A Synoptic Climatological Assessment of Viticultural Phenology*. Dissertation, University of Virginia, Department of Environmental Sciences, 394 pp.

Jones G.V., and Davis R.E., 2000. *Climate Influences on Grapevine Phenology, Grape Composition, and Wine production and Quality for Bordeaux, France.* Am. J. Enol. Vitic., Vol. 51, (3): 249-261.

Ju W., Chen J.M., Black T.A., Barr A.G., Liu J., and Chen B., 2006. *Modelling multi-year coupled carbon and water fluxes in a boreal aspen forest.* Agric. For. Meteor. 140: 136-151.

Jury W.A., Gardner W.R., and Gardner W.H., 1991. *Soil Physics* (5th ed.). John Wiley & Sons, Chichester, UK, 352 pp.

Kaimal J.C., and Haugen D.A., 1969. *Some errors on the measurement of Reynold's stress.* Journal of Applied Meteorology 8: 460-462.

Kaimal J.C., and Wyngaard J.C., 1990. *The Kansas and Minnesota experiments.* Boundary Layer Meteor., 50: 31-47.

Kaimal J.C., and Finnigan J.J., 1994. *Atmospheric Boundary Layer Flows: Their Structure and Measurement*. Oxford-University Press., New York.

Katul G.G., Cava D., Poggi D., Albertson J.D., and Mahrt L., 2004. *Stationarity, homogeneity, and ergodicity in canopy turbulence.* In: Handbook of Micrometeorology: A Guide for Surface Flux Measurements (Eds. Lee X., Massman W., and Law B.). Kluwer Academic Press, pp. 161–180.

Kelliher F.M., Leuning R., Raupach M.R., and Schulze E.D., 1994. *Maximum conductances for evaporation from global vegetation types.* Agric. For. Meteorol., 73: 1-16.

Kim J., and Verma S.B., 1990. *Carbon dioxide exchange in a temperate grassland ecosystem.* Boundary Layer Meteor., 52: 135-149.

Kim M.H., Nakane K., Lee J.T., Bang H.S., and Na Y.E., 2007. *Stem/branch maintenance respiration of Japanese red pine stand.* Forest Ecol. Manage (in press).

Korner Ch., 1994. *Leaf diffusive conductances in major vegetation types of the globe.* In, Ecophysiology of Photosynthesis. (Eds). E.D. Schulze and M.M. Caldwell. Berlin. pp. 463-490.

Kristensen L., and Fitzjarrald D.R. 1984. *The effect of line averaging on scalar flux measurements with a sonic anemometer near the surface.* Journal of Atmospheric and Oceanic Technology 1: 138-146.

Kumagai T., Saitoh T.M., Sato Y., Morooka T., Manfroi O.J., Kuraji K., and Suzuki M., 2004. *Transpiration, canopy conductance and the decoupling coefficient of a lowland mixed dipterocarp forest in Sarawak, Borneo: dry spell effects.* Journal of Hydrol. 287: 237-251.

Landsberg J.J., and Waring R.H:, 1997. *A generalised model of forest productivity using simplified concepts of radiation-use efficiency, carbon balance and partitioning*. Forest Ecology and Management, 95: 209-228.

Launder B.E., 1975. *On the effects of a gravitational field on the turbulent transport of heat and momentum*. J. Fluid Mech., 67: 569-581.

Lauteri M., Monteverdi M.C., Scartazza A., Augusti A., Brugnoli E., Spaccino L., Cherubini M., 1997. *Stable isotopes and forest ecophysiology. Two case studies concerning: a) Adaptation of Castanea sativa Mill to contrasting environments; b) seasonal variations of water use efficiency within and among plant communities of a mediterranean coastland ecosystem.* Atti del I Congresso S.I.S.E.F. "La ricerca italiana per le foreste e la selvicoltura". Legnaro (PD), 4-6 giugno: 303-307.

Leclerc M.Y. and Thurtell G.W. 1990. *Footprint Predictions of Scalar Fluxes Using a Markovian Analysis.* Boundary-Layer Meteorol. 52: 247-258.

Leclerc M.Y., Shen S., and Lamb B. 1997. *Observations and Large-Eddy Simulation Modeling of Footprints in the Lower Convective Boundary Layer.* J. Geophys. Res. 102: 9323-9334.

Lee X., 1998. *On micrometeorological observations of surface-air exchange over tall vegetation.* Agricultural and Forest Meteorology, 91: 39-49.

Lemon E.R., 1960. *Photosynthesis under field conditions. II. An aerodynamic method for determining the turbulent carbon dioxide exchange between the atmosphere and a cornfield.* Agron. J. 52: 697-703.

Leuning R., Denmead O.T., Lang A.R.G., and Ohtaki E., 1982. *Effects of heat and water vapour transport on eddy covariance measurements of CO_2 fluxes.* Boundary §Layer Meteor. 23: 209-222.

Leuning R.F.M., 1990. *Modelling stomatal behavior and photosynthesis of Eucalyptus grandis Aust.* J. Plant Physiology., 17: 159-175.

Leuning R.F.M., Kelliher D., De Pury D.G.G., and Schulze E.D., 1995. *Leaf nitrogen, photosynthesis, conductance and transpiration, scaling from leaves to canopies.* Plant, Cell Environment., 18: 1183-1200.

Li-Cor, 1996. *LI-6262 CO2/H2O Analyzer, Operating and Service Manual.* Li-Cor, Inc., Lincoln, NE, 118 pp.

Lichter J., 1998. *Primary succession and forest development on coastal Lake Michigan sand dunes.* Ecol. Monogr. 68:487–510.

Livingston G.P., and Hutchinson G.L., 1995. *Enclosure-based measurements of trace gas exchange: applications and sources of error.* In: Biogenic Trace Gases: Measuring Emissions from Soil and Water (eds Matson P.A., Harriss R.C.), pp 14-51. Blackwell Science, London.

Lloyd J., and Taylor J.A., 1994. *On the temperature dependence of soil respiration.* Functional Ecology, 8: 315–323.

Lovett G.M., Cole J.J., Pace M.L., 2006. *Is net ecosystem production equal to net ecosystem accumulation?*. Ecosystems 9: 1-4.

Luhar A.K. and Rao K.S. 1994. *Source Footprint Analysis for Scalar Fluxes Measured in Flows Over Inhomogeneous Surface*. In S.V. Gryning and M.M. Millan (eds.), Air Pollution Modelling and Its Application, Plenum Press, New York, pp. 315-323.

Luo H., Oechel W.C., Hastings S., Zulueta R., Qian Y., and Kwon H., 2007. *Mature semiarid chaparral ecosystems can be a significant sink for atmospheric carbon dioxide.* Global Change Biology 13: 386-396.

Manabe S., and Wetherald R.T., 1975. *The effects of doubling the CO_2 concentration on the climate of a general circulation model.* J. Atmos. Sci., 32: 3-15.

Magliulo E., Duce P., Miglietta F., Spano D., 1998. *Carbon dioxide exchange of coast mediterranean macchia during the drought season.* 23rd Conference on Agricultural and Forest Meteorology. Albuquerque, New Mexico, November, 2-6: 103-106.

Marcolla B., Cescatti A., Montagnani L., Manca G., Kerschbaumer G., Minerbi S., 2005. *Importance of advection in the atmospheric CO_2 exchanges of an alpine forest.* Agric. For. Meteorol. 130, 193–206.

Massman W.J., Sommerfield R.A., Mosier A.R., Zeller K.F., Hehn T.J., and Rochelle S.G., 1997. *A model investigation of turbulence-driven pressure pumping effects on the rate of diffusion of CO_2, N_2O, and CH_4 through layered snowpacks.* Journal of Geophysical Research, 102: 18851–18863.

Mateus J., Pita G., and Rodigues A., 2006. *Seasonality and inter-annual forest atmosphere carbon and water exchanges in a Portuguese Eucalyptus plantation (Mediterranean climate)*. 27th Conference ion Agricultural and Forest Meteorology. 25 May 2006.

Matthews M., and Anderson M., 1988. *Fruit ripening in Vitis vinifera L.: Responses to seasonal water deficits.* Am. J. Enol. Vitic. 39:313-320.

McNaughton K.G., and Jarvis P.G., 1983. *Predicting effects of vegetation changes on transpiration and evaporation.* In: Kozlowski, T.T. (Ed.), Water Deficits and Plants Growth, 7: 1-47.

Meinzer F.C., 1993. *Stomatal control of transpiration.* Trends Ecol. Evol. 8: 289-294.

Meyers T.P. 1985. *A simulation of the canopy microenvironment using higher order closure principles.* PhD dissertation. Purdue University, 153 pp.

Meyers T.P., and Paw U K.T., 1986. *Testing of a higher-order closure model for modelling airflow within and above plant canopies.* Boundary Layer Meteorology, 31: 297-311.

Meyers T.P., and Paw U K.T., 1987. M*odelling the plant canopy micrometeorology with higher-order closure principles.* Agric. For. Meteorol., 41: 143-163.

Molina F.D., Valera D.L., Ivarez A.J.A., and Maduen A., 2006. *A wind tunnel study of airflow through horticultural crops: determination of the drag coefficient.* Biosystem Engineering 93 (4): 447-457.

Mooney H.A., Dunn E.L., 1970. *Convergent evolution of Mediterranean climate evergreen sclerophyll shrubs*. Evolution, (24): 292-303.

Moore C.J., and Fisch G., 1986. *Estimating heat storage in Amazonian tropical forest.* Agric. For. Meteor., 38: 147-169.

Moncrieff J.B., Mabli Y. and Leuning R. 1996. *The propagation of errors in long-term measurements of land-atmosphere fluxes of carbon and water*. Global Change Biol. 2: 231-240.

Moncrieff J.B., Valentini R., Greco S., Seufert G., Ciccioli P., 1997 (a). *Trace gas exchange over terrestrial ecosystems: methods and perspectives in micrometeorology*. Journal of Experimental Botany, 48: 1133-1142.

Moncrieff J.B, Massheder J.M, de Bruin H., Elbers J., Friborg T., Heusinkveld B., Kabat P., Scott S., Soegaard H., Verhoef A., 1997 (b). *A system to measure surface fluxes of momentum, sensible heat, water vapour and carbon dioxide.* Journal of Hydrology, 188-189: 589-611.

Monteith J.L., and Szeicz G., 1960. *The CO_2 flux over a field of sugar beets.* Quarterly Journal of the Royal Meteorological Society, 86: 205-214.

Monteith J.L., 1973. *Principles of Environmental Physics*. Arnold, London

Monteith J.L., 1995. *A reinterpretation of stomatal responses to humidity.* Plant Cell Environ. 18: 357-564.

Monteith J.L., Unsworth M.H., 1990. *Principles of Environmental Phisics.* Edward Arnold, London.

Mueller-Starck, G., 1989. *Genetic implications of environmental stress in adult forest stands of Fagus sylvatica L*. In: Scholz, F., Gregorius, H.R. and Rudin, D., (Eds.), Genetic effects of air pollutants in forest tree populations. Springer-Verlag Berlin: 127-142.

Mullins M.G., Bouquet A., and Williams L.E., 1992. *Biology of the Grapevine.* 239 pp. Cambridge University Press, Great Britain.

Norman J.M., 1979. *Modelling the complete crop canopy. Modification of the Aerial Environment of Crops.* B. Barfield and J. Gerber, (Eds)., Amer. Soc. Agric. Eng. Monograph 2, ASAE, St. Joseph, MI., 249-277.

Odum E.P., 1959. *Fundamental of Ecology*. Sanders W.B., Philadelphia.

Oke T.R:, 1987. *Boundary layer climates.* Routledge, London.

Ojeda H., Andary C., Kraeva E., Carbonneau, A., and Deloire A., 2002. *Influence of pre- and post-veraison water deficits on synthesis and*

concentration of skin phenolic compounds during berry growth of Vitis vinifera cv. Shiraz. Am. J. Enol. Vitic. 53:261-267.

Owen K., Tenhunen J., Reichstein M., Wang Q., Falge E., Geyer R., Xiao X.A., Toy P., Ammann C., Farain A., Aubinet M., Aurela M., Bernhofer C., Choinicki B.H., Granier A., Gruenwals T., Hadley J., Heinesch B., Hollinger D., Knhol A., Kutsch W., Lohila A., Meyers T., Moors E., Moureaus C., Pilegaard K., Saigusa N., Verma S., Vesala T., and Vogel C., 2007. *Linking flux network measurements to continental scale simulations: ecosystem carbon dioxide exchange capacity under non-water-stressed conditions*. Global Change Biology 13: 1-27.

Papale D., and Valentini R., 2003. *A new assessment of European forests carbon exchanges by eddy fluxes and artificial neural network spatialization.* Global Change Biology, 9: 525-535.

Papale D., Reichstein M., Canfora E., Aubinet M., Bernhofer C., Longdoz B., Kutsch W., Rambal S., Valentini R., Vesala T., and Yakir D., 2006. *Toward a more harmonized processing of eddy covariance CO_2 fluxes: algorithms and uncertainty estimation.* Biogeosciences Discussions, 3: 961, 992.

Pasquill F., and Smith F.B., 1983. *Atmospheric Diffusion*, 3rd Edition. Wiley, New York, 437 pp.

Paw U K.T., and Gao W., 1988. *Applications of solutions to non-linear energy budget equations*. Agric. For. Meteor., 43: 121-145.

Paw U K.T., 1992. *Development of models for thermal infrared radiation above and within plant canopies.* J. Photogrammetry Remote Sens.,47: 189-203.

Paw U K.T., Baldocchi D., Meyers T.P., and Wilson K.B., 2000. *Correction of eddy-covariance measurements incorporating both advective effects and density fluxes*. Boundary Layer Meteorology, 91: 487-511.

Paw U K.T., Falk M., Suchanek T.H., Ustin S.L., Chen J., Park Y.S., Winner W.E., Thomas C.S., Hsiao T.C., Shaw R.H., King T.S., Pyles R.D., Schroeder M., Matista A.A., 2004. *Carbon Dioxide Exchange Between an Old-growth Forest and the Atmosphere*. Ecosystem 7: 513-524.

Pereira A.R., 2004. *The Priestley–Taylor parameter and the decoupling factor for estimating reference evapotranspiration.* Agric. For. Meteor. 125: 305-313.

Piccini P., Piotto B., 2001. *Il degrado della vegetazione mediterranea.* In: "Propagazione per seme di alberi e arbusti della flora mediterranea". Manuale ANPA.

Pignatti S., 1978. *Evolutionary trends in Mediterranean flora and vegetation.* Vegetatio, (37): 175-185.

Pisanu S., 2005. *Misure indirette dell'indice di area fogliare(LAI) in ecosistemi a macchia mediterranea.* PhD Thesis, Università di Sassari.

Powell T.L., Bracho R., Li J., Dore S., Hinkle C.R., and Drake B.G., 2006. *Environmental controls over net ecosystem carbon exchange of scrub oak in central Florida*. Agr. For. Meteorology 141: 19-34.

Prentice I.C., Cramer W., Harrison S.P., Leemans R., Monserud R.A., and Solomon A.M., 1992. *A global biome model based on plant physiology and dominance, soil properties and climate*. Journal of Biogeography 19:117-134.

Prentice I.C., Heimann M., Sitch S., 2000. *The carbon balance of the terrestrial biosphere: ecosystem models and atmospheric observations*. Ecological Applications, 10: 1553–1573.

Pyles R.D., 2000a. *The development and testing of the UCD Advanced Canopy-Atmosphere-Soil Algorithm (ACASA) for use in climate prediction and field studies*. PhD dissertation, Davis, University of California, pp. 190.

Pyles R.D., Weare B.C., and Paw U K.T., 2000b. *The UCD Advanced Canopy-Atmosphere-Soil Algorithm: Comparison with observations from different climate and vegetation regimes*. Q.J.R. Meteorol. Soc.,126: 2951-2980.

Pyles R.D., Weare B.C., Paw U K.T., and Gustafson W., 2003. *Coupling between the University of California, Davis, Advanced Canopy-Atmosphere-Soil Algorithm (ACASA) and MM5: Preliminary Results for July 1998 for Western –North America*. J Appl. Meteorol. 42: 557-569.

Randerson J.T., Chapin F.S., Harden J.W., Neff J.C., Harmon M.E., 2002. *Net ecosystem production: a comprehensive measure of net carbon accumulation by ecosystems*. Ecol. Appl. 12:937–47.

Rannik Ü., Vesala T., and Keskinen R., 1997. *On the damping of temperature fluctuations in a circular tube relevant to the eddy covariance measurement technique*. Journal of Geophysical Research, 102: 12789-12794.

Raupach M.R., 1989a. *A pratical Lagrangian method for relating concentrations to source distributions in vegetation canopies*. Q.J.R. Meteorol. Soc. 115: 609-632.

Raupach M.R., 1989b. *Applying Lagrangian fluid mechanics to infer scalar source distributions from concentration profiles in plant canopies*. Agric. For. Meteorol. 47: 85-108.

Reichstein M., Falge E., Baldocchi D., Papale D., Aubinet M., Berbigier P., Bernhofer C., Buchmann N., Gilmanov T., Granier A., Grunwald T., Havrankova K., Ilvesniemi H., Janous D., Knohl A., Laurila T., Lohila A., Loustau D., Matteucci G., Meyers T., Miglietta F., Ourcival J.M., Pumpanen J., Rambal S., Rotenberg E., Sanz M., Tenhunen J., Seufert G., Vaccari F., Vesala T., Yakir D., and Valentini R.,. 2005. *On the separation of net ecosystem exchange into assimilation and ecosystem respiration: review and improved algorithm*. Global Change Biology 11: 1424-1439.

Reynolds O., 1895. *On the dynamical theory of incompressible viscous fluids and the determination of criterion.* Philosophical Transactions of Royal Society of London, A174: 935-982.

Renzullo L.J., Blanchfield A.L., Guillermin R., Pwell K.S., and Helpd A.A. 2006. *Comparison of PROSPECT and HPLC estimates of leaf chlorophyll contents in a grapevine stress study*. International Journal of Remote Sensing 27 (4): 817-823.

Rosenberg N.J., Blad B.L., Verma B.S., 1983. *Microclimate. The biological environment*. John Wiley & Sons, New York-Chichester-Brisbane-Toronto-Singapore.

Rossi F., Duce P., Facini O., Georgiadis T., Magliulo E., Miglietta F., Peressotti A., Spano D., 1999. *Vulnerabilità climatica della macchia mediterranea:*

l'esperienza del progetto MEDEFLU. Atti 2 Congresso SISEF. Applicazioni e Prospettive per la Ricerca Forestale Italiana, Bologna, 20-22 ottobre 99: 397-400.

Rossi F., Facini O., Rotondi A., Loreti S., Georgiadis T., 2001. *Optical properties of juniper and lentisk canopies in a coastal Mediterranean macchia shrubland*. Trees 15: 462-471.

Rossi F., Facini O., Georgiadis T., and Nardino M., 2004. *Bilancio energetico, bilancio radiativo e flussi di carbonio in un vigneto ad uva da tavola allevato a tendone.* Quad. Vitic. Enol. Univ. Torino 27, pp.178-199.

Running S.W., Baldocchi D.D., Turner D., Gower S.T., Bakwin P.S., and Hibbard K.A., 1999. *A global terrestrial monitoring network integrating tower fluxes, flask sampling, ecosystem modeling and EOS satellite data*. Remote Sensing Environment 70: 108-127.

Sala A., and Tenhunen J.D., 1994. *Simulations of canopy net photosynthesis and transpiration of Quercus ilex L. under the influence of seasonal drought*. Agric. For. Meteor., 78: 203-222.

Schmid H.P., 1994: *Source areas for scalars and scalar fluxes*. Bound.-Layer Meteor., 67: 293-318.

Schmid H.P., 2002. *Footprint modelling for vegetation atmosphere exchange studies: a review and perspective*. Agric. And For. Meteor. 113: 159-183.

Schmid H.P., Grimmond C.S.B., Cropley F., Offerle B., Hong-Bing Su., 2000. *Measurements of CO_2 and energy fluxes over a mixed hardwood forest in the mid-western United States*. Agricultural and Forest Meteorology, 103: 357-374.

Schotanus P., Nieuwstadt F.T.M., De Bruin, H.A.R., 1983. *Temperature measurement with a sonic anemometer and its application to heat and moisture fluxes*. Boundary-Layer Meteorol., 26: 81-93.

Schuepp P.H., Leclerc M.Y., MacPherson J.I., and Desjardins R.L. 1990. *Footprint Prediction of Scalar Fluxes from Analytical Solutions of the Diffusion Equation*. Boundary-Layer Meteorol. 50: 355-373.

Schulze E.D., and Koch W., 1969. *Measurement of primary productivity with cuvettes*. In: Productivity of Forest Ecosystems, Proceedings of the Brussels Symposium. UNESCO, pp. 141-157.

Schulze ED, Kelliher F.M., Korner C., Lloyd J., and Leuning R., 1994. *Relationships between maximum stomatal conductance, ecosystem surface conductance, carbon assimilation rate and plant nitrogen nutrition., a global exercise*. Annual Rev. Ecological Systematics., 25: 629-660.

Scrase F.J., 1930. *Some characteristics of eddy motion in the atmosphere*. Geophysical memoirs 52: pp 56.Meteorological Office, London.

Seguin G., 1986. *"Terroirs" and pedology of vine growing*. Experientia 42:861-873.

Sitch S., Smith B., Prentice I.C., Arneth A.,. Bondeau A, Cramer W., Kaplan J., Levis S., Lucht W., Sykes M.,. Thonicke K, and Venevski S.. 2003. *Evaluation of ecosystem dynamics, plant geography and terrestrial carbon cycling in the LPJ Dynamic Vegetation Model*. Global Change Biology 9:161-185.

Sivilotti P., Bonetto C., Paladin M., and Peterlunger E., 2005. *Effect of Soil Moisture Availability on Merlot: From Leaf Water Potential to Grape Composition.* Am. J. Enol. Vitic. 56 (1): 9-18.

Sirca C., Asunis C., Spano D., Duce P., 2001. *Measurements of CO_2 and energy fluxes over mediterranean maquis in Sardinia. "The future of the green Mediterranean"*, Euro-Mediterranean Conference, Alghero, 1-2 Giugno: 185-187.

Smart R.E., and Coombe B.G., 1983. *Water relations of grapevines.* In Water Deficits and Plant Growth. Vol. 7. T. Kozlowski (Ed.), pp. 137-196. Academic Press, New York.

Smart R.E., 1985. *Principles of Grapevine Canopy Microclimate Manipulation with Implications for Yield and Quality. A Review.* Am. J. Enol. Vitic. 36 (3): 230-239.

Smart R.E., and Robinson M., 1991. *Sunlight into wine. A Handbook for Winegrape Canopy Management*. Winetitles, Adelaide.

Spano D., Duce P., Snyder R.L., Paw U KT., 2000. *Estimating sensible and latent heat flux densities from grapevine canopies using Surface Renewal*. Agric. and Forest Meteor. 104: 171-183.

Spano D., Snyder R.L. and Cesaraccio C., 2003. *Mediterranean climates.* Chapter 3.2. In: Phenology: An Integrative Environmental Science. Schwartz, M. (Ed.). Kluwer Academic Publishers. Dordrecht, The Netherlands. pp. 139-156.

Spano D., Duce P., Sirca C., and Snyder R.L., 2004. *Valutazione degli scambi di massa ed energia nel sistema vigneto*. Quad. Vitic. Enol. Univ. Torino 27, pp.163-176.

Specht R.L, 1969. *A comparison of the sclerophyllous vegetation characteristics of Mediterranean type climates in France, California, and Southern Australia, (I). Structure, morphology and succession*. Australian J. Bot., (17): 277-292.

Stull R.B., 1988. *An Introduction to Boundary Layer Meteorology*. Kluwer Academic Publishers, Dordrecht, The Netherlands, 666 pp.

Su H.B., Paw U K.T., and Shaw R.H., 1996. *Development of a coupled leaf and canopy model for the simulation of plant-atmosphere interactions.* J. Appl. Meteor., 35: 733-748.

Sun W.Y., and Ogura Y., 1980. *Modelling the evolution of the convective boundary layer*. J. Atmos. Sci., 37: 1558-1572.

Tanner C.B., and Thurtell G.W., 1969. *'Anemoclinometer measurements of Reynolds stress and heat transport in the atmospheric surface layer'*. Research and Development Tech. Report ECOM 66-G22-F to the US Army Electronics Command. Dept Soil Science, Univ. of Wisconsin, Madison, WI.

Tirone G., Manca G., Valentini R., Seufert G., 2003. *Assorbimento di carbonio negli ecosistemi forestali mediterranei: confronto tra una lecceta ed una pineta.* In: De Angelis P., Macuz A., Bucci G., Scarascia Mugnozza G. (Eds.), Alberi e Foreste per il Nuovo Millennio, Atti del III Congresso Nazionale della Societa` Italiana di Selvicoltura ed Ecologia Forestale (SISEF Atti III), IP/Office 2003. Antonini, Viterbo, pp. 99–104.

Ubarana V.N., 1996. *Observation and modelling of rainfall intercepton loss in two experimental sites in Amazonian forest*. Amazon Deforestation and Climate, J. H.C. Gash, C.A. Nobre, J.M. Roberts, and R.L. Victoria, (Eds). John Wiley & Sons, Chichester, UK, 595 pp.

Valentini R., Scarascia Mugnozza G., De Angelis P., Bimbi R., 1991. *An experimental test of the eddy correlation technique over a Mediterranean macchia canopy*. Plant, Cell and Environment, 14: 987-994.

Valentini R., de Angelis P., Matteucci G., Monaco R., Dore S., Scroscia Mugnozza G.E., 1996. *Seasonal net carbon dioxide exchange of the beech forest with the atmosphere*. Global Change Biology 2: 199-208.

Valentini, R., 1998. *La foresta come unità funzionale nelle interazioni tra biosfera e l'atmosfera*. Atti del Convegno"La ricerca italiana per le foreste e la selvicoltura". S.I.S.E.F. Atti 1: 9-13.

Valentini R., Baldocchi D., and Olson R.., 1999. *FLUXNET: a challenge that is becoming reality*. Global Change News letter 37: 15-17.

Valentini R., Matteucci G., Dolman A.J., Schulze E.D., Rebmann C., Moors E.J., Granier A., Gross P., Jensen N.O., Pilegaard K., Lindroth A., Grelle A., Bernhofer C., Grunwald T., Aubinet M., Ceulemans R., Kowalski A.S., Vesala T., Rannik U., Berbigier P., Loustau D., Guamundsson J., Thorgeirsson H., Ibrom A., Morgenstern K., Clement R., Moncrieff J., Montagnani L., Minerbi S., and Jarvis P.G., 2000. *Respiration as the main determinant of carbon balance in European forests*. Nature, 404: 861-864.

Valiente-Banuet, A., Flores-Hernández, N., Verdú, M. and Dávila, P,. 1998. *The chaparral vegetation in Mexico under nonmediterranean climate: the convergence and Madrean-Tethyan hypotheses reconsidered*. American Journal of Botany, (85): 1398-1408.

van Leeuwen C., and Seguin G., 1994. *Incidences de l'alimentation en eau de la vigne, appréciée par l'état hydrique du feuillage, sur le développement de l'appareil végétatif et la maturation du raisin (Vitis vinifera variété Cabernet franc, Saint-Emilion, 1990)*. J. Int. Sci. Vigne Vin. 28 (2):81-110.

van Leeuwen C., Friant P., ChonéX., Tregoat O., Koundouras S., and Dudourdieu D., 2004. *Influence of Climate, Soil and Cultivar on Terroir*. Am J. Enol. Vic., 55 (3): 207-217.

Verma S.B., 1990. *Micrometeorological methods for measuring surface fluxes*. Remote Sensing Reviews, 5: 99-115.

Verma S.B:, Baldocchi D.D., Anderson D.E:, Matt D.R., and Clement R.J., 1986. Eddy *fluxes of CO_2, water vapour, and sensible heat over a deciduous forest.* Boundary Layer Meteor., 36: 71-91.

Verma S.B., Kim J., and Clement R.J., 1989. *Carbon dioxide, water vapour and sensible heat fluxes over a tall grass prairie*. Boundary Layer Meteor., 46: 53-67.

Villagarcia L., Were A., Domingo F., Garcia M., and Alados-Arboledas L., 2007. *Estimation of soil boundary-layer resistance in sparse semiarid stand for evapotranspiration modelling*. Journal of Hydrology, 342: 173-183.

Vose J.M., and Bolstad P.V., 1999. *Challenges to modelling NPP in diverse eastern deciduous forest: species-level comparisons of foliar respiration responses to temperature and nitrogen*. Ecological Modelling 122: 165-174.

Webb E.K., Pearman G.I., Leuning R., 1980. *Correction of flux measurements for density effects due to heat and water vapour transfer*. Quarterly Journal Royal Meteorological Society, 106: 85-100.

Wesely M.L., Cook D.R., and Hart R.L., 1983. *Fluxes of gases and particles above a deciduous forest in wintertime*. Boundary Layer Meteor., 27: 237-255.

Wever L.A., Flanagan L.B., and Carlson P.J., 2002. *Seasonal and inter-annual variation in evapotranspiration, energy balance, and surface conductance in northern temperate grassland*. Agric. For. Meteor. 112: 31-49.

Wichura B., and Foken Th., 1995. *Anwendung integraler Turbulenzcharakteristiken zur Bestimmung von Beimengungen in der Bodenschicht der Atmosphare*. No. 29. DWD, Abteilung Forschung, Arbeitsergeb-nisse, 52 pp.

Wilczak J.M., Oncley S.P., and Stage S.A., 2001. *Sonic anemometer tilt correction algorithms*. Boundary Layer Meteorology, 99: 127–150.

Wilson, W. and Shaw, R.H., 1977. *A higher order closure model for canopy flow*. J. Appl. Meteor. 16: 1 197-1 205.

Wilson J.D., and Sawford B.L., 1996. *Review of Lagrangian stochastic models for trajectories in the turbulent atmosphere*. Boundary Layer Meteorology, 78: 191-210.

Wilson T.B., Norman J.M., Bland W.L., and Kucharik C.J., 2003. *Evaluation of the importance of Lagrangian canopy turbulence formulations in a soil-plant-atmosphere model*. Agric. For. Meteorol. 115: 51-69.

Winkler A., Cook J., Kliewer W, and Lider L., 1974. *General Viticulture*. 710 pp. University of California Press, Berkeley.

Woodwell G.M., Whittaker R.H., 1968. *Primary production in terrestrial ecosystems*. Am. Zoologist. 8:19–30.

Wofsy S.C., Goulden M.L., Munger J.W., Fang S.M., Bakwin P.S. , Daube B.C., Bassow S.L., and Bazzaz F.A., 1993. *Net exchange of CO_2 in a mid-latitude forest*. Science, 260: 1314-1317.

Yamamoto S., Murayama S., Saigusa N., Kondo H., 1999. *Seasonal and interannual variation of CO_2 flux between a temperate forest and the atmosphere in Japan*. Tellus, 51B: 402-413.

Zeman O., and Tennekes H., 1975. *A self contained model for the pressure terms in the turbulent stress equations of the neutral atmospheric boundary layer*. J. Atmos. Sci., 32: 1808-1813.

Zeman O., and Lumley J.L., 1976. *Modelling buoyancy driven mixed layers*. J. Atmos. Sci., 33: 1974-1988.

Zhang W.L., Chen S.P., Chen J., Wie L., Han X.G., and Lin G.H., 2007. *Biophysical regulations of carbon fluxes of a steppe and cultivated cropland in semiarid Inner Mongolia*. Agric. And For. Meteorol. 146: 216-229.

APPENDIX

EC corrections

Raw data screening

Raw data are the data that are recorded at the sampling rate of the data logger. Processed data files, usually, contain half-hour means or total data. Raw data are used for fluxes calculation, but it is necessary to do a raw data screening before calculating fluxes. With the raw data screening, the raw data are classified, and the selected data can be corrected or deleted for fluxes calculation. The raw data screening is a first quality control of the available data. The raw data screening is not an automatic process. It varies with the measurement site and the available instrumentation.

Tests are made on u, v, w, Ts, CO_2 concentration (C), and water vapour concentration (q), and data are classified in three categories:

- *normal data*
- *hard flag*, spikes are present in the data due to problem with instrumentation. Spikes are defined as peaks in the data (i.e., deviation of the data from the mean value).
- *soft flag*, spikes are present due to environmental conditions.

Goulden et al. (1996) and Baldocchi et al. (1997) reported that the main raw data controls are

1. *Spikes*

Spikes are peaks or deviations of the data from the mean value due to several causes. For example, they can be due to electrical malfunctioning of the instruments, presence of water on the open path gas analyzer or on the sonic transducers. To detect spikes is needed to calculate the mean and standard deviation (σ) for a window of known length (e.g., five minutes). If the data value goes over the value of the mean plus 3.5 times the standard deviation value, it is

considered spike and has to be deleted. If five or more consecutive points go over this value, they are not considered spikes and are kept into the dataset. Spikes detected are replaced by linear regression or gap-filling tecniques.

2. *Anomalous data*

Data recorded during bad weather conditions (e.g., rain, high wind speed) have to be deleted. Data from malfunctioning instruments have also to be eliminated. Negative values of CO_2 flux recorded during the night are deleted.

3. *Threshold values*

Data are reliable if they lie in a range of threshold values. Data outside the range are eliminated. Threshold values are different for each variable. For example, CO_2 concentration has to be between 300 to 600 ppm, while H_2O concentration can vary between 3.2 to 48 mmol/mol.

4. *Time lag*

The time lag is the delay time that air takes to cover the distance between the measurement point (near to sonic anemometer) and the chamber of the gas analyzer, along the sample tube. It has been calculated only for closed path system. A right range of time lag for the covariances *wC* and *wq* is inserted in the software. The correct time lag is the time for which the covariance (flux) is maximum (Moncrieff et al., 1997b).

The open path system does not require to calculate the time lag because its value is constant and it is written in the manual.

Coordinate rotation

In ideal conditions, the flux densities are measured across the mean streamlines of the wind. Fluctuations in the longitudinal components of the wind appear as vertical velocity fluctuations, and vice versa. Therefore, the vertical velocity measured by a three dimensional sonic anemometer is not the true atmospheric vertical velocity. Causes of errors are due to improper instrument alignment and distortion of the air streamlines by the underlying surface. As consequence, it is needed a tilt correction for these small deviations of the sonic coordinates. To pass this problem someone aligns the instrument with the geopotential, but it is not correct (Wilczak et al., 2001; Finnigan et al., 2003).

The simple Reynolds' average equation suggests that the mean vertical velocity, w, is zero, which is true near the surface (i.e., vertical motions must go to zero at the ground surface). Over flat land the mean vertical velocity is close to zero, and over long times indeed averages to zero. In the truth, it is often impossible to orient the vertical velocity sensor, so that the mean velocity is nearly zero, or find a perfectly flat experimental site.

Misalignment of the vertical velocity sensor can cause an apparent mean vertical velocity (Kaimal and Haugen, 1969; Hyson et al., 1977; Dyer, 1981). Tilt errors are about 3-4% per degree for scalar fluxes (Verma, 1990), and about 14% per degree for momentum fluxes (Dyer, 1981). For friction velocity the error due to tilt is about 3% (Foken and Gerstmann, 1984). Tilt errors can be minimized by rotating the coordinates of the wind velocity vectors, so the vertical axis is orthogonal to the mean wind streamline. Vertical and lateral velocity components are, hence, equal to zero and turbulent fluxes are calculated perpendicularly to the streamlines (Figure A.1) (Hyson et al., 1977). Coordinate rotation can be applied only on terrain with slope $< \approx$ 8-15% (Baldocchi et al., 1988).

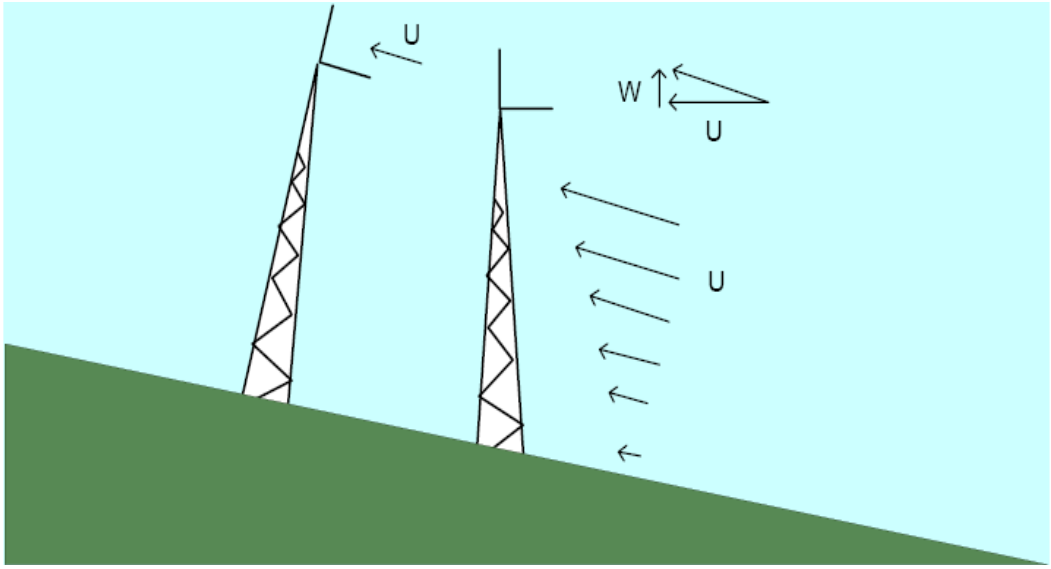

Figure A.1. Scheme on need to rotate coordinates (from Baldocchi lectures).

Three main methods exist to determine the orientation of a sonic anemometer relative to a Cartesian coordinate system aligned along the mean wind: double rotation, triple rotation, and planar fit.

Double and third rotation methods use measured wind to define an orthogonal vector basis for each observational period (e.g., 30 min.) to which all fluxes are transformed. The procedure for double or third rotation is the same. It was first proposed by Tanner and Thurthell (1969), but it was also improved by Kaimal and Finnigan (1994). In the *double rotation*, the first rotation is about the z axis and aligns *u* into the x direction of the x-y plane (Figure A.2 a). The second rotation is about the x axis and aligns *w* into the z direction (Figure A.2 b) yielding a mean value of *w* and *v* equal to 0. The *u* vector is equal to the mean scalar wind speed. In more complex terrain, the covariances $\overline{u'v'}$ and $\overline{v'w'}$ are not equal to zero. A *third rotation* is needed along the z-y plane in order to obtain $\overline{v'w'}$ =0 (Figure A.2 c). Usually, it is not necessary, so it is not made.

Trigonometric values are deduced from the orthogonal wind vectors

$$\cos\alpha = \overline{u} / \left(\overline{u}^2 + \overline{v}^2\right)^{0.5} \quad \text{(A.1)}$$

$$\sin\alpha = \overline{v} / \left(\overline{u}^2 + \overline{v}^2\right)^{0.5} \quad \text{(A.2)}$$

$$\cos\beta = \left(\overline{u}^2 + \overline{v}^2\right)^{0.5} / \left(\overline{u}^2 + \overline{v}^2 + \overline{w}^2\right)^{0.5} \quad \text{(A.3)}$$

$$\sin\beta = \overline{w} / \left(\overline{u}^2 + \overline{v}^2 + \overline{w}^2\right)^{0.5} \quad \text{(A.4)}$$

where u, v, and w are the components velocity measured in the original coordinate system of a 3-D sonic anemometer.

The rotated coordinates u_i, v_i, and w_i, are given by:

$$u_i = u\cos\beta\cos\alpha + v\cos\beta\sin\alpha + w\sin\beta \quad \text{(A.5)}$$

$$v_i = v\cos\alpha - u\sin\alpha \quad \text{(A.6)}$$

$$w_i = w\cos\beta - u\sin\beta\cos\alpha - v\sin\beta\sin\alpha \quad \text{(A.7)}$$

The new equation for covariance calculation is obtained using the new coordinates, and applying the simple Reynolds' average equation to the algebraic sums

$$\overline{w_i c} = \overline{w'c'}\cos\beta - \overline{u'c'}\sin\beta\cos\alpha - \overline{v'c'}\sin\beta\sin\alpha \quad \text{(A.8)}$$

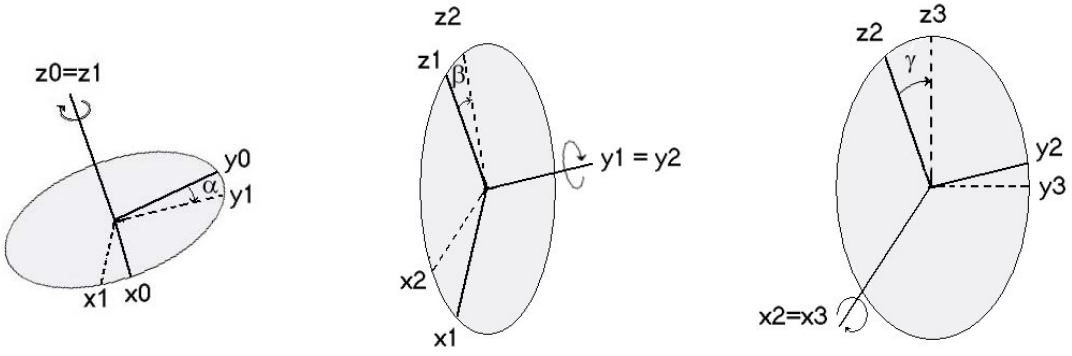

a b c

Figure A.2. Scheme of the first, second and third coordinates rotation.

Planar fit method is a recent method that is more appropriate. It is based on the determination of a fixed plane for the site over a long period (e.g., few months). In detail, the *z* coordinate is fixed over the chosen period, and *x* and *y* axes are variable with time. In this system, the mean vertical wind component can have non zero values during individual 30 min. period, but it averages to zero during longer period (Wilczak et al., 2001; Paw U et al., 2000).

This system can be only applied over period during which there was no change in the anemometer's position relative to the surface. The original coordinate system is rotated to have the horizontal velocity components placed in a plane of the "real" mean horizontal wind (assuming that it is parallel to the surface), and the *u*-component is aligned with the streamline. The orientation of this plane is determined by a least-squares fit of the wind data to the equation

$$\overline{w}_m = b_0 + b_1\overline{u}_m + b_2\overline{v}_m \tag{A.9}$$

where $\overline{w}_m$, $\overline{u}_m$, and $\overline{v}_m$ are the velocity components averaged over a period of 30 minutes, and b_0, b_1, and b_2 are coefficients obtained by multiple linear regression. To calculate tilt angles it is needed to know the periods delimited by known physical changes in the sonic orientation. These angles are α and β (same of the double method). In the planar fit method they are calculate as

$$\sin\alpha = p_0 \tag{A.10}$$

$$\cos\alpha = \sqrt{p_1^{\,2} + p_2^{\,2}} \tag{A.11}$$

$$\sin\beta = \frac{-p_1}{\sqrt{p_1^{\,2} + p_2^{\,2}}} \tag{A.12}$$

$$\cos\beta = \frac{p_2}{\sqrt{p_1^{\,2} + p_2^{\,2}}} \tag{A.13}$$

where $p_0 = \dfrac{-b_1}{\sqrt{b_1^{\,2} + b_2^{\,2} + 1}}$, $p_1 = \dfrac{-b_2}{\sqrt{b_1^{\,2} + b_2^{\,2} + 1}}$, and $p_2 = \dfrac{1}{\sqrt{b_1^{\,2} + b_2^{\,2} + 1}}$.

A first matrix (P) is calculated to rotate data into a coordinate system that has the x-y-plane parallel to the ground.

$$P = \begin{bmatrix} \cos\alpha & 0 & \sin\alpha \\ 0 & 1 & 0 \\ -\sin\alpha & 0 & \cos\alpha \end{bmatrix} \begin{bmatrix} 1 & 0 & 0 \\ 0 & \cos\beta & -\sin\beta \\ 0 & \sin\beta & \cos\beta \end{bmatrix}. \tag{A.14}$$

A second matrix (M) is, hence, calculated to rotate data into the mean wind direction for each run (i.e., $v = 0$).

$$M = \begin{bmatrix} \cos\gamma & \sin\gamma & 0 \\ -\sin\gamma & \cos\gamma & 0 \\ 0 & 0 & 1 \end{bmatrix}, \tag{A.15}$$

where γ is the angle of the third rotation by the new z-axis and it is given by $\gamma = \tan^{-1}\left(\frac{\overline{v}_p}{\overline{u}_p}\right)$.

Using planar fit method, although the vertical velocity averaged over the entire data set is zero, the mean vertical velocity may be non-zero for individual data run, due to mesoscale motions or to sampling limitations. This residual mean vertical velocity is subtracted for each run, so that it does not contribute to the Reynolds' stress. Many data are used to determine the tilt angles with this method, so it is less susceptible to sampling errors, and the compute of the lateral components of the stress is more accurate. Planar fit method, however, requires that many data runs be recorded before the stresses can be computed. In contrast, the double and third rotation methods can be applied in real time to each data run as it is recorded.

Nocturnal fluxes

Ideal conditions are difficult to be met during experimental field. It is important to evaluate the influences of the different terms in the Equation 5.5 (storage, horizontal and vertical advection). During the night, particular problems occur (Katul et al., 2004), and they are emphasized when measuring above high vegetation (Lee, 1998).

During the night, when wind speed is low, the surface layer becomes stable and turbulence is suppressed. In this case, CO_2 flux is underestimated by the EC system (Aubinet et al., 2000). The CO_2 efflux from soil and plants continues at a constant rate, but all the CO_2 is not transported up to the measurement level. The cause is a turbulence reduction. CO_2, hence, accumulates in the air layer close to the surface. Storage term is, therefore, non-zero and the Equation 5.6 is not valid more. The CO_2 flux underestimate during the night comes from a lack of turbulence rather than a varying CO_2 *source* strength. Underestimation of the nighttime CO_2 flux is an example of a selective systematic error, and as such can be a serious problem, particularly when long-term budgets are estimated by integration of short-term flux measurements (Moncrieff et al, 1996; Goulden et al., 1996; Baldocchi et al., 2000).

Opposite situation occurs during the morning, when the awakening turbulence transports air with CO_2 to the measurement level. The turbulent flux observed by the EC system is then greater than the actual NEE at that time, and this should be compensated by a negative storage term in the Equation 5.5. The storage term may be estimated by measuring the CO_2 concentration changes in the air space below the measurement height, typically at few levels inside and above the canopy (Aubinet et al., 2000).

Underestimate of CO_2 flux appears clear when, during the nighttime, there is a correlation between u^* (friction velocity) and CO_2 flux. Friction velocity is a turbulent velocity scale and can be understood as a measure of the turbulence intensity (Stull, 1988). The correlation between u^* and CO_2 flux is in contrast with respiration fluxes that should not depend on turbulence, although during strong winds the pressure pumping effect may accelerate the ventilation of CO_2

from soil pores (Massman et al., 1997). It seems probable that there are some additional, non-turbulent, processes removing CO_2 from the air layer below the measurement height either vertically or horizontally. Aubinet et al., (2000) found that various transport mechanisms (e.g., vertical and horizontal advection, slow diffusion or intermittent turbulence not detected by standard EC) are responsible of these problems in the stably-stratified surface layer.

In complex terrain these phenomena create more problems (Kaimal and Finnigan, 1994). Horizontal advection term (*II*) can be important because of horizontal heterogeneity of surface. Vertical advection term (*III*) can be non-zero in sloping terrain, and the slope can cause drainage of cool CO_2-rich air during stable nights and thus horizontal advection (*II*). It is relatively easy to take the storage term into account, but it is difficult to measure the vertical and horizontal advection, and it is indeed presently unfeasible as a routine measurement (Aubinet et al., 2005). It is important to avoid the double count that occurs when correct nocturnal data and data occurring in the morning are considered at the same time during CO_2 balance calculation.

The u^*-correction is used to correct for flux underestimation during stable nights (Papale et al., 2006). A u^* threshold is determined. It is the value below which the conditions are considered not turbulent enough, and the turbulent fluxes are not representative of the *source* term. All the data corresponding to these conditions are thus discarded from the data set. These data gaps are replaced by the simulated efflux estimated during well-mixed conditions.

Different gap filling methods exists (Aubinet et al., 2004) such as look up table, nonlinear regression or mean diurnal variation (Falge et al., 2001a, b; Reichstein et al., 2005). Papale and Valentini (2003) have also proposed a new method based on statistical approach (e.g., Artificial Neural Networks).

Sensor distance

The sensor distance is an important parameter that has to be considered during the set up of instrumentation. The distance between sonic anemometer and IRGA should be less than the length scale of the smallest eddy to be detected, because the signals of two sensors become increasingly uncorrelated with increasing separation distance. At the same time, a sensor distance too much short leads to air flow distortion measured by anemometer. An equation to calculate maximum distance between two sensors (D) is given by Kristensen and Fitzjarrald (1984)

$$D \leq \frac{(z-d)}{5} \tag{A.16}$$

where z is the measurement height and d is the zero place displacement. This distance is, usually, few centimeters for the measurements of H and momentum flux, but can be 40-60 centimeters for humidity measurements (Foken and Wichura, 1996).

Webb correction

Simultaneous fluxes of heat and water vapour occur in the air causing expansion of the air, and affecting the air constituent's density (e.g., CO_2 and H_2O). Turbulent fluxes of any constituent measured using an EC system require some corrections that accounts for this problem. Fluctuations of CO_2 and H_2O concentrations in the atmosphere are due to heating or cooling phenomena, and fluxes arise from these phenomena instead of air transport. Therefore, the exchange of these entities leads to fluctuations in the density in dry air, which introduces a small but significantly non-zero mean vertical velocity (Webb et al., 1980). Ignoring this effect can result in a substantial error in the *in situ* measurements flux, so it is needed to consider corrections to the measured flux. Fluctuations in air density can be erroneously attributed to fluctuations in CO_2 and

latent heat in sensors, which measure the partial density of CO_2 or H_2O in air. A correction term, called "WPL term", has to be calculated and added to fluxes calculation (Webb et al., 1980). No correction are required if the fluxes are evaluated from measured fluctuations of constituents' *mixing ratio* (dry air component). In this case, the air is pre-dried and brought to a common temperature and pressure, but this is not likely feasible in fast response EC system.

For measurement of the constituent's density fluctuations made *in situ*, the corrections arising from both heat and water vapour are required. Therefore, from Webb et al. (1980) the corrected vertical turbulent CO_2 flux (*Fc*), measured in terms of concentration (*c*) is given by

$$F_c = \overline{w'c'} + 1.61(\overline{c}/\rho_a)E + (1 + 1.61\overline{q})H\overline{c}/(\overline{\rho}_a C_p \overline{T}_k) \qquad \text{(A.17)}$$

where *E* is the mass flux of water vapour, *H* is the sensible heat flux, *Cp* is the specific heat of air, *q* is the specific humidity, and *Tk* is the absolute temperature. *Fc* measurements, therefore, require the measurements of water vapour and sensible heat in each experiment.

Density fluctuation can cause errors as large as 40% in the measurements of CO_2 exchange (Leuning et al., 1982). The correction is not needed for *H* calculation (Webb et al., 1980), and it is generally small for water vapour and other constituents at low concentrations. In practice, the Webb correction for the water vapour flux needs to be only applied if the water vapour pressure is larger than 15-20 hPa. Usually, the correction is applied over a 30 minutes averaged period.

Using a closed path system, the temperature variation may be assumed to vanish in the inlet tube (Rannik et al., 1997), so the Webb correction is not needed. In addition, some gas analyzers (e.g., LI-6262) automatically take the humidity effect into account in internal calculations (Li-Cor, 1996). Using open-path instruments (e.g., LI-7500) the full correction is required.

Data quality control

A quality check needs to be made on corrected fluxes. The main quality controls are three: stationarity test, verify of turbulence integrity, and energy budget closure. In this section a briefly discussion about these topics is presented.

Stationarity test

Stationarity of measurements is one of the assumptions to correctly apply the EC method. Stationarity term is referred to a condition in which statistics do not vary with time (instationarity) and with space (homogeneity). Stationarity test allows the verification of the presence of instationarity conditions (Aubinet et al., 2000; Foken and Wichura, 1996). The procedure is the following

- The measured time series of about 30 min duration will be divided into $n_s/m = 4...\ 8$ intervals of about 5 min.
- The covariance of a measured signal ξ and η (similar algorithm for dispersions with $\xi = \eta$) of the interval l with m = 6000 (6000 measuring values in five minutes for 20-Hz scanning, i.e. n_s = 36 000 in 30 min) is

$$\overline{\xi'\eta'} = \frac{1}{m-1}\left[\sum_{k=1}^{m}\xi_{kl}\eta_{kl} - \frac{1}{m}\left(\sum_{k=1}^{m}\xi_{kl}\right)\left(\sum_{k=1}^{m}\eta_{kl}\right)\right] \qquad \text{(A.18)}$$

- Mean covariance of the n_s/m period is used for the test

$$\overline{\xi'\eta'} = \frac{1}{\eta_s/m}\left[\sum_{l=1}^{\eta_s/m}\overline{\xi'_l\eta'_l}\right] \qquad \text{(A.19)}$$

- The value of the covariance for the full period will be determined according to

$$\overline{\xi'\eta'} = \frac{1}{\eta_s - 1}\left[\sum_{l=1}^{\eta_s/m}\sum_{k=1}^{m}\xi_{kl}\eta_{kl} - \frac{1}{\eta_s}\left(\sum_{l=1}^{\eta_s/m}\sum_{k=1}^{m}\xi_{kl}\right)\left(\sum_{l=1}^{\eta_s/m}\sum_{k=1}^{m}\eta_{kl}\right)\right] \tag{A.20}$$

and it will be compared with the equation A. 18.

If there is a difference of less than 30% between the covariances (or dispersions) determined with equations A. 19 and A. 20, then the measurement is considered to be stationary. This is an initial criterion that characterizes the quality of the measurements. For practical use, all data with differences <30% are of high quality, and those with differences between 30% and 60% have an acceptable quality (Foken et al., 1997).

Verification of turbulence integrity

Variations in turbulence or partial turbulence do not allow the instruments to work adequately. Verify turbulent test gives the possibility to prove the maintenance of integral turbulence with time. Wichura and Foken (1995) defined integral turbulence characteristics of the vertical velocity and the temperature as follow

$$\frac{\sigma_w}{u^*} = a_1\left[\vartheta_m(z/L)\right]^{b_1} \tag{A.21}$$

$$\frac{\sigma_T}{T^*} = a_2\left[(z/L)\vartheta_h(z/L)\right]^{b_2} \tag{A.22}$$

where σ_w and σ_T are the vertical velocity and temperature standard deviations, φ_m is the surface layer similarity function, u^* is the friction velocity, and ξ is the stability parameter defined by $(z–d)/L$, where L is the Obukhov length. The empirical coefficients a and b are obtained with the model of Foken et al. (1991).

The data quality is good if the difference between the measured integral characteristics and the calculated value differs by not more than 20-30%. For

neutral stratification, this test can not be used for scalar fluxes, but it can be used for stable stratification (Foken et al., 1997; Foken, 1999).

Using the turbulence integrity test is possible to discover some typical effects of non-homogeneous terrain. An obstacle will create additional mechanical turbulence, and the measured values of integral characteristics will be significantly higher than modelled values. In addition, measured values will be higher than modelled values for terrain with not homogeneity in surface temperature and moisture conditions, but it will be not for surface roughness not homogeneous (Wichura and Foken, 1995).

Energy budget closure

The energy balance at the Earth's surface is fundamental for the dynamics of the planetary boundary layer. Using the conservation of energy law it is possible to formulate a budget equation for the energy flux at the surface. The general equation of energy budget is

$$Rn = H + LE + G + \Delta S \qquad \text{(A.23)}$$

where Rn is the net radiation measured by net radiometer, H and LE are the sensible heat and latent heat flux density, respectively, measured by EC method, G is the soil heat flux density measured by flux plates, and ΔS is the storage term (due to the sensible and the latent heat flux divergence within the air column and to the energy stored in the biomass). The metabolic term M, which accounts for metabolic processes occurring in the ecosystem, is neglected because it is small.

The closure of the energy balance is a useful parameter to check the plausibility of data sets obtained at different sites. In this approach, the sum of turbulent heat fluxes is compared with the available energy flux (i.e., the net radiative flux density less the storage flux densities in the observed ecosystem, including soil, air and biomass), so that Rn−G = H+LE.

In the reality, it is not simple to reach this balance because of the difficulty to measure with accuracy all components of the energy budget, especially the G

term. A linear regression between the turbulent fluxes and the available energy is forced to pass through the origin, and it allows the verification of the divergence from the theory. If the divergence is about 10-20% data are considered to be of good quality, and *H* and *LE* measurements made with EC are considered reliable (Baldocchi et al., 1988; Moncrieff et al., 1997b). It is possible to obtain higher values of divergence for shorter temporal scale (e.g., 30 min periods).

Measured values of the energy balance components at a specific site depend on many factors, such as the type of surface and its characteristics, geographical location, season, time of the day, and weather. Radiation fluxes and heat storage terms are, therefore, subject to errors (Aubinet et al., 2000). Moreover, under certain meteorological conditions, processes (e.g., melting, freezing or heat conductance to cold intercepted rain) may contribute considerably to the energy balance. They are usually not considered in the budget calculation when using a standard set of meteorological observables. Under these conditions, the closure can not be taken as a plausibility criterion for flux observations. On the other hand, the apparent lack of energy balance closure does not constitute conclusive evidence for erroneous turbulent flux measurement, but might indicate the occurrence of other non-vertical and turbulent fluxes (e.g., advection and subsidence). In terrain with surface not horizontally homogeneous (e.g., regarding roughness elements, moisture, surface temperature) or when fetch is insufficient, the horizontal advection of energy can become significant and it has to be taken in account. More studies, therefore, are needed to investigate the error of this quality check in complex and not ideal terrain (Baldocchi, 2003).